

Roland Balint

**Impacts of Time and
Temperature Gradient
on the Morphology
and Chemical Composition of
Superheater Ash Deposits**





Impacts of Time and Temperature Gradient on the Morphology and Chemical Composition of Superheater Ash Deposits

Roland Balint

Inorganic Chemistry
Faculty of Science and Engineering
Åbo Akademi University
Åbo, Finland, 2024

Supervisors

D.Sc Markus Engblom
Åbo Akademi University

D.Sc Patrik Yrjas
Åbo Akademi University

Prof. Leena Hupa
Åbo Akademi University

Opponent and Reviewer

Prof. Marcus Öhman
Luleå University of Technology

Reviewer

Prof. Kevin J. Whitty
The University of Utah

ISBN 978-952-12-4343-1 (printed)

ISBN 978-952-12-4344-8 (digital)

Painosalama, Åbo, Finland 2024

Preface

The work presented in this thesis was carried out at the research group of High-Temperature Processes and Materials, Åbo Akademi University from 2018 to 2023. The work was funded by the Graduate School of Chemical Engineering (GSCE) and the Fortum Foundation [Application number 20190123]. The work was also partly funded by the Academy of Finland [Decision number 310266 “Understanding the dynamics of intradeposit chemistry and morphology for control of corrosion in high temperature processes”; Decision number 338322 “New insights on the effects of temperature gradients on high temperature corrosion”]. The work was partially carried out within the CLUE (2017-2019), CLUE² (2020-2022) projects. Support from ANDRITZ Oy, Fortum, Valmet Technologies Oy, UPM-Kymmene Oyj, Metsä Fibre Oy, and International Paper Inc. is gratefully acknowledged. The probe measurements were financed by Suomen Soodakattilayhdistys (The Finnish Recovery Boiler Committee) [Contract numbers: 16A0913/S144; 16A0913/S155]. In addition, the financial support from the Åbo Akademi Rector Scholarship is gratefully acknowledged.

I would like to thank everyone at the research group of high High-Temperature Processes and Materials who helped and supported me during the past years to complete this thesis. First, I want to expressly thank my main supervisor D.Sc Markus Engblom for always taking the time to help me with any problem I was facing during the last years. Without your guidance, this thesis would not have been completed. I would also like to thank D.Sc Patrik Yrjas for his support and for making my first stay at Åbo Akademi University possible, which set the path for this thesis. I would also like to thank D.Sc Jonne Niemi for his constant support with carrying out experiments, interpreting results, and dealing with FactSage. A special thanks goes to Tor Laurén and D.Sc Emil Vainio who took the time to travel with me to Rauma to carry out the probe measurements in the kraft recovery boiler. The guidance of Prof. Emerit. Mikko Hupa and him sharing his great scientific knowledge concerning recovery boilers is highly appreciated. Lastly, I would like to thank Prof. Leena Hupa for giving me the opportunity to carry out this thesis work at the group of High-Temperature Processes and Materials.

I am very grateful for the help of Jaana Paananen with anything concerning the experimental equipment in the laboratory and Linus Silvander for operating the SEM/EDXA. Furthermore, I would like to express my gratitude to Daniel Silva da Costa from Celulose Nipo-Brasileira S.A – CENIBRA as well as Jaakko Rautala and Timo Saarinen from Metsä-Fibre Oy for providing the superheater deposits.

I also want to thank my colleagues and friends at the laboratory. Our common lunch breaks, barbecues, board game events, and cross-country skiing in winter were always a lot of fun and made the last years even more enjoyable and provided some distraction from work. A special thanks goes out to D.Sc Juho Lehmusto for giving me the possibility to live in his house during the first

year of my studies. I'm looking forward to many more discussions concerning sports with you in the future. Lastly, I want to thank my family and friends both here in Finland and back home in Germany. Without your continuous support, all of this would not have been possible.

Åbo October 2023

Roland Balint

Abstract

The work presented in this thesis focuses on the effect of a temperature gradient on the local composition and morphology of ash deposits formed on heat exchanger tubes of power boilers. Cross-sections of superheater deposits from a Brazilian and Finnish kraft recovery boiler were analysed using Scanning Electron Microscopy/Energy-Dispersive X-ray Analysis (SEM/EDXA). The data obtained from the Finnish superheater deposits was complemented by deposition probe measurements, that were carried out in the superheater region of the same boiler. In addition, laboratory-scale experiments were carried out using synthetic ash deposits to study the initial melting behaviour of deposits and, by varying the deposit composition, whether the identified deposit ageing mechanisms are also applicable to deposits other than those found in kraft recovery boilers.

In the Brazilian superheater deposits, all three deposit ageing mechanisms identified in previously reported laboratory studies (i.e. temperature gradient zone melting, movement of enriched melt toward the steel, and diffusional transport of alkali chloride vapours toward the steel) were confirmed to also occur in actual superheater deposits. In addition, the movement of a melt and concurrent enrichment in K toward the steel, induced by a temperature gradient, was identified. Due to the local K enrichment in the vicinity of the superheater steel surface, the local first melting temperature of the deposit decreased significantly and reached a minimum where the local K concentration was the highest.

The ageing behaviour of the Finnish superheater deposits differed from the Brazilian deposit samples. Due to the different chemical composition and ergo lower amount of melt, the Finnish deposits formed a skeletal morphology and the dominating ageing mechanism was diffusional transport of alkali chloride vapours toward the steel. Two deposit archetypes were observed.

Type 1 deposits had an innermost layer concurrently enriched in Cl and K. The probe deposits showed that a Cl and K-rich layer was formed also directly on the steel surface, where it subsequently caused corrosion via active oxidation. The local enrichment in alkali chloride was also identified to cause a local decrease in the first melting temperature of the deposit and reached a minimum in the Cl and K-rich layer that was formed directly on the steel surface. Furthermore, the probe deposits showed that over time, an overall enrichment in the average Cl content within the deposit had occurred. Alkali chlorides in the flue gas diffused into the porous deposit, where they subsequently condensed as the local temperature decreased.

Type 2 deposits were characterized by a region enriched in K and S while concurrently depleted in Cl, due to sulphation. A deposit region initially enriched in alkali chloride, was sulphated over time as SO₂ from the flue gas can diffuse into the deposit and subsequently react with alkali chloride.

The initial melting behaviour of synthetic ash deposits was studied on a laboratory scale to identify the parameter determining the change of deposit morphology from skeletal to densely molten. The amount of melt formed in the

deposit was identified to be the parameter determining the final deposit morphology. The transition from a skeletal to a molten deposit morphology is in this thesis suggested to take place at a melt fraction of about 30 wt-%. In deposits with lower melt fractions, the melt was observed to accelerate sintering and the formation of the skeletal morphology.

The identified ageing mechanisms were also observed in synthetic deposit mixtures comprising NaBr-Na₂SO₄ and KBr-K₂SO₄. This implies that the mechanisms are also applicable to other processes than kraft recovery boilers.

Overall, the results of this thesis demonstrate the impact deposit ageing can have on the local chemical composition and morphology of actual superheater deposits. Independently of the final deposit morphology, the local first melting temperature of the deposits was shown to decrease toward the steel, which can promote the formation of melt in the direct vicinity of the steel surface and cause severe melt-induced corrosion. In addition, the formation of a layer of alkali chloride directly on the steel surface can promote corrosion via active oxidation. Furthermore, the results show that deposit ageing is not exclusive to kraft recovery boiler deposits but is also of relevance to deposits in other combustion processes.

Svensk sammanfattning

Arbetet som presenteras i denna avhandling fokuserar på effekten av en temperaturgradient på den lokala sammansättningen och morfologin av askavlagringar som bildas på värmeväxlarrör i kraftverk. Tvärsnitt av askavlagringar från överhettare från en brasiliansk och en finsk sodapanna analyserades med hjälp av ett svepelektronmikroskop utrustat med en energidispersiv röntgenanalysator (SEM/EDXA). De data som erhöles från de finska överhettaravlagringarna kompletterades med resultat från mätningar som utfördes i överhettarområdet i samma panna med en avlagringssond. Dessutom genomfördes laboratorieexperiment med syntetiska askavlagringar för att studera de initiala smälttegenskaperna hos avlagringarna. Genom att variera avlagringssammansättningen studerades det om de identifierade åldringsmekanismerna är tillämpliga även på avlagringar från andra anläggningar än sodapannor.

Gällande de brasilianska överhettaravlagringarna bekräftades det att alla tre tidigare identifierade åldringsmekanismer som observerats i laboriestudier (vilka är temperaturgradientzonsmältning, rörelse av berikad smälta mot stålet, diffusionstransport av alkalikloridångor mot stålet) även förekommer i verkliga överhettaravlagringar. Dessutom identifierades smälttransport, och samtidig berikning av kalium (K), mot stålet, som orsakades av en temperaturgradient. På grund av K-berikningen minskade avlagringens första smälttemperatur betydligt och nådde ett minimum där den lokala K-koncentrationen var som högst.

Åldringsbeteendet för de finska avlagringarna skiljde sig från de brasilianska avlagringar. På grund av den olika kemiska sammansättningen och följaktligen lägre mängd smälta hade de finska avlagringar en skelettformig morfologi. Den dominerande åldringsmekanismen i de finska avlagringarna visade sig basera på diffusion av alkalikloridångor mot stålet. Två typer av avlagringar observerades.

Typ 1-avlagringar hade ett innersta lager som var berikat med klor (Cl) och kalium (K). Sondavlagringarna visade att ett Cl- och K-rikt lager också bildades direkt på stålytan, vilket kan förorsaka korrosion genom aktiv oxidation. Den lokala berikningen av alkaliklorid visade sig också vara en orsak till en minskning av avlagringens första smälttemperatur. Smälttemperaturens minimum nåddes i det Cl- och K-rika lagret som bildades direkt på stålytan. Dessutom visade sondavlagringarna en generell ökning av den genomsnittliga Cl-halten i avlagringen som förorsakats av transport av alkaliklorid från rökgasen. Denna alkaliklorid diffusion med tiden in i den porösa avlagringen, där den sedan kondenserade när den lokala temperaturen sjönk.

Typ 2-avlagringar karakteriserades av ett område som var berikat med K och svavel (S) och utarmat på klor. Detta avlagringsområde var initialt berikat med alkaliklorid, som sulfaterades med tiden när svaveldioxid (SO₂) från rökgasen kunde diffundera in i avlagringen och reagera med alkaliklorid.

De initiala smälttegenskaperna hos syntetiska askavlagringar studerades på laboratorieskala för att identifiera övergången från en skelettformig till en

smält avlagringsmorfologi. Det visade sig att mängden smälta är den avgörande faktorn och att övergången från en skelettformig till en smält avlagringsmorfologi äger rum då smältfraktionen överstiger cirka 30 vikt-%. I avlagringar med lägre smältfraktioner observerades det att smältan accelererade sintring och bildandet av den skelettformiga morfologin.

De identifierade åldringsmekanismerna observerades också med syntetiska avlagringar av $\text{NaBr-Na}_2\text{SO}_4$ och $\text{KBr-K}_2\text{SO}_4$. Resultaten antyder att åldringsmekanismerna är även tillämpliga på avlagringar från andra högttemperaturprocesser än sodapannor.

Sammanfattningsvis visar resultaten från denna avhandling den påverkan som avlagringens åldring kan ha på den lokala kemiska sammansättningen och morfologin hos verkliga överhettaravlagringar. Oberoende av den slutliga avlagringsmorfologin visades det att den lokala första smälttemperaturen för avlagringarna minskade ju närmare stålet man kom, vilket kan gynna bildandet av smälta i direkt närhet till stålytan och orsaka allvarlig smältinducerad korrosion. Dessutom visar resultaten att avlagringens åldring inte är exklusivt för avlagringar från sodapannor utan är också relevanta för avlagringar i andra förbränningsprocesser.

List of publications

This thesis is based on the work contained in the following papers:

- I. **R. Balint**, M. Engblom, J. Niemi, D. Silva da Costa, D. Lindberg, P. Yrjas, L. Hupa, M. Hupa, Temperature gradient induced changes within superheater ash deposits high in chlorine, *Energy* 226 (2021) 120439
- II. **R. Balint**, M. Engblom, J. Niemi, D. Lindberg, T. Saarinen, J. Rautala, M. Hupa, L. Hupa, Morphological and chemical differences within superheater deposits from different locations of a black liquor recovery boiler, *Energy* 267 (2023) 126576
- III. **R. Balint**, M. Engblom, E. Vainio, T. Laurén, J. Niemi, J. Rautala, T. Saarinen, M. Hupa, L. Hupa, Changes in chlorine content over time – Probe deposit sampling in a Finnish kraft recovery boiler, *Fuel* 340 (2023) 127599
- IV. **R. Balint**, M. Engblom, J. Niemi, M. Hupa, L. Hupa, Superheater ash deposit ageing – impact of melt fraction on morphology and chemistry, *Fuel* 359 (2024) 130386
- V. J. Niemi, **R. Balint**, M. Engblom, J. Lehmusto, D. Lindberg, Temperature-Gradient-Driven Aging Mechanisms in Alkali-Bromide- and Sulfate-Containing Ash Deposits, *Energy & Fuels*, 33 (7) (2019) 5883-5892

Contribution of the author

Paper I

Balint prepared the obtained deposit samples for analysis. The analysis results were interpreted together with the co-authors. Balint carried out the FactSage calculations with the support of Lindberg and Niemi. Balint was the main writer of the paper.

Paper II

Balint prepared and analysed the obtained deposit samples. Balint carried out the FactSage calculations with the support of Lindberg and Niemi. Balint was the main writer of the paper.

Paper III

The probe was designed by Balint together with the co-authors. Balint carried out the measurements together with Laurén and Vainio. Balint analysed the deposits and the results were interpreted together with the co-authors. Balint was the main writer of the paper.

Paper IV

The experiments were planned by Balint together with the co-authors. Balint conducted the laboratory experiments and analysed the results. Balint was the main writer of the paper.

Paper V

The measurements were planned by Niemi together with the co-authors. Balint carried out the experimental work. Balint and Niemi analysed the results together. Niemi was the main writer of the paper.

Table of contents

Preface	IV
Abstract	VI
Svensk sammanfattning	VIII
List of publications	X
Contribution of the author	XI
Table of contents	XII
1. Introduction	1
1.1. Motivation	1
1.2. Objective	2
2. Background	3
2.1. The kraft pulping process	3
2.1.1. Black liquor as a fuel	4
2.1.2. The kraft recovery boiler	5
2.2. Ash deposits in the kraft recovery boiler	6
2.2.1. Ash forming matter in black liquor combustion	6
2.2.2. Superheater deposit formation mechanisms	7
2.3. Deposit ageing	9
2.3.1. Temperature gradient zone melting	10
2.3.2. Movement of enriched melt toward steel	11
2.3.3. Diffusional transport of alkali chloride vapours	12
3. Experimental	14
3.1. Kraft recovery boiler superheater deposits	14
3.1.1. Brazilian deposit samples	14
3.1.2. Finnish deposit samples	15
3.2. Full-scale probe deposit sampling	16
3.3. Laboratory temperature gradient experiments	19
3.4. Analysis of deposit samples	22
4. Results and discussion	24
4.1. Full-scale boiler deposits	24
4.1.1. Brazilian boiler deposits	24
4.1.2. Finnish boiler deposits	32
4.2. Impact of amount of melt on deposit ageing	42
4.3. Applicability of results to other combustion processes	47
4.4. Updated understanding of deposit ageing and practical implications ..	51
5. Conclusions	54
References	56
Original publications	60

1. Introduction

1.1. Motivation

On July 29th 2021, the European climate law came into force with the goal of all member states of the European Union to become climate-neutral by 2050 [1]. A key factor in achieving this ambitious goal is the transition from utilising fossil fuels toward renewable sources for heat and power production to reduce net greenhouse gas emissions. In this transition, the combustion of biomass fuels has an important role. Not only will the total amount of biomass used to produce heat and power increase in the future, but also a larger variety of biomasses will be utilized in combustion processes. For some of these biomasses, the content of inorganics can be significantly higher when compared to coal or oil, which can pose additional operational obstacles for a boiler. During combustion, inorganics are released into the flue gas, known to contribute to the formation of ash deposits on heat transfer surfaces.

Ash deposits lower the efficiency of the overall process as they act as a resistor to conductive heat transfer and in some cases, extensive deposit formation can even cause complete blockage of the flue gas duct of a boiler. Furthermore, some of the inorganic compounds found in ash deposits are known to cause severe corrosion of the heat transfer surfaces. Due to these operational challenges, the final steam temperature in boilers utilising biomass fuels is typically kept lower compared to coal-fired plants, resulting in lower electrical efficiencies for combustion processes utilising biomass fuels.

The composition and operational problems caused by ash deposits vary among different fuels. Thus ash and deposit formation has been a main focus point in research over the last decades and has been studied for a variety of biomass fuels. One of these biomass-based fuels is black liquor, a waste stream of the kraft pulping process and one of the largest sources for the production of bioenergy worldwide [2].

The composition of ash deposits and their formation mechanisms in kraft recovery boilers have been studied extensively over the last decades [3–7]. However, more recent laboratory studies showed, that the local composition of such deposits can change significantly over time [8–10]. One key observation in these studies has been the movement and enrichment of corrosive alkali chloride species toward the heat transfer surface, resulting in a non-uniform deposit composition. Similar local enrichment patterns could also be seen in actual boiler deposits, but were typically associated with changes in the deposition mechanisms [4,11].

For boiler operators to efficiently handle deposit-induced issues, such as corrosion and deposit removability, a good understanding of the behaviour of ash-forming elements in the combustion environment is required. This does not only include detailed knowledge of deposit formation and its bulk composition but also the processes taking place within a deposit after it has

formed on a heat transfer surface. Such processes are referred to as deposit ageing, and earlier laboratory experiments have shown that deposit ageing can have a significant impact on the corrosion of heat transfer surfaces and hamper deposit removal. However, these mechanisms have so far only been studied on a laboratory scale, under well-controlled conditions.

1.2. Objective

The objective of this thesis is to get a better understanding of temperature gradient-induced deposit ageing mechanisms. Previously, several ageing mechanisms have been identified during studies of the effect of a temperature gradient on ash deposits under well-controlled laboratory conditions. The focus of this work is to determine whether these earlier identified mechanisms can also be seen taking place in actual superheater deposits obtained from kraft recovery boilers. For this purpose, several deposit samples were obtained from two kraft recovery boilers and analysed regarding morphology and chemical composition. In addition, laboratory-scale experiments utilising synthetic ash deposits were conducted to study deposit ageing mechanisms under well-controlled conditions. The focus of the laboratory experiments was on getting a better understanding of the initial melting behaviour of deposits and the evolution of the deposit morphology. Furthermore, deposit compositions relevant to combustion processes other than kraft recovery boilers were studied regarding their ageing behaviour. The results of the work presented in this thesis aim to shed more light on the underlying fundamental phenomena relevant to operational problems in boilers caused by ash deposits, especially deposit removability and deposit-induced corrosion.

2. Background

2.1. The kraft pulping process

In 2021, a total of 201 million tonnes of wood pulp were produced worldwide, of which 158 million tonnes were produced using the kraft pulping process [12]. Thus the kraft pulping process, sometimes also referred to as sulphate pulping, is the dominating method used for industrial production of pulp. The main advantage of the kraft process over other commercially used methods is the high flexibility of the process regarding the input material as both, soft- and hardwood but also non-woody biomass such as bagasse, straw, or reed can be used [13]. Furthermore, the spent pulping chemicals can be recovered efficiently, with recovery rates of up to 98 % [14], while at the same time heat and power are produced. In the following chapter, the main process steps of the kraft pulping process will be introduced with a focus on the chemical recovery line.

The goal of every pulping process is the liberation of the cellulose fibres from the wood matrix (predominantly lignin). Chemical, mechanical, or biological methods are used to achieve this goal, with the kraft process being a chemical process.

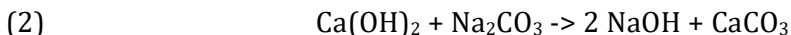
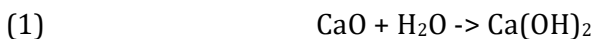
In the kraft process, debarked wood chips are mixed with white liquor, a basic solution of NaOH and Na₂S to delignify the fibres. In the digester, the suspension is heated to temperatures between 160 – 180 °C at an elevated pressure of up to 8 bar [15]. After approximately 2 hours, delignification is complete to a sufficient degree and the mixture is further processed [16]. In the blow tank, the fibres are obtained from the delignified wood chips and subsequently separated from the spent pulping chemicals which now also contain the dissolved lignin fragments [14]. The fibres can then be further processed for end use [17].

The solution of the spent pulping chemicals (Na₂SO₄ and Na₂CO₃) and organic material from the wood is referred to as black liquor. After the blow tank, the black liquor has a dry solids content of around 15 % [16]. In the first step, the dry solids content of the liquor is increased in a multistage evaporator process. After the evaporators, the dry solids content ranges between 65 % and 85 %.

The concentrated black liquor, also called heavy black liquor, is then burned in the recovery boiler. The recovery boiler has a dual role. On the one hand, the spent pulping chemicals are recovered to be reused in the pulping process. On the other hand, through the combustion of the organic material dissolved in the liquor, heat and power are produced [3,14]. At the bottom of the boiler, a smelt bed of inorganic salts forms. The reducing conditions in the bed promote the formation of Na₂S over Na₂SO₄. To avoid the formation of dead zones in the bed, the dry solids content of the black liquor droplets should exceed 58 % [3].

The smelt is then extracted at the bottom of the boiler and dissolved in water. In the causticizer, the aqueous smelt solution is mixed with CaO. In two

steps according to reactions 1 and 2, active NaOH is recovered from Na_2CO_3 [16].



The solid CaCO_3 produced in the causticizer is subsequently removed by filtration, together with additional impurities [16]. In a lime kiln, CaO is recovered from the CaCO_3 produced in the causticizer. The remaining liquid solution after the causticizer contains NaOH and Na_2S , which are reintroduced into the digester [17]. If needed, additional sodium compounds can be added to the solution before introducing it into the digester.

The advantages of the kraft pulping process over other commercially used methods are a relatively high yield and greater strength of the obtained pulp fibres compared to the sulphite method [17]. Furthermore, cooking times are short, independent of the used wood type [17]. The overall process is also highly efficient in terms of regenerating energy and chemicals. The key factor for the efficient recovery of the spent pulping chemicals and generation of heat and power is the recovery boiler, where the concentrated black liquor is combusted.

2.1.1. Black liquor as a fuel

After the digester, approximately 50 % of the used raw wood, around 85 – 93 % of the original lignin and 56-71 % of the original hemicellulose [18] are dissolved to form weak black liquor [2]. Therefore, black liquor is considered a biomass-based fuel, making it the largest biomass-based fuel for power production worldwide [2]. Besides organic material, black liquor contains significant amounts of inorganic compounds from the spent pulping chemicals. Thus, black liquor has unique fuel properties that differ from conventionally used biomasses and impose significant ash-related challenges on the boiler during combustion.

Besides organic matter, additional inorganic compounds from the wood matrix are dissolved in the liquor during pulping. These dissolved inorganics are referred to as non-process elements and comprise mainly P, Si, Al, Mg, Fe, Ca, Cl, K, and Mn [19]. In terms of ash-related issues in the recovery boiler, K and Cl are of the biggest concern. The concentration of non-process elements in black liquor can vary significantly among different pulp mills [20]. The variations are due to differences in process design but also due to different wood types used as raw material [21]. In northern Europe and North America, softwoods such as spruce or pine are most commonly used as pulping wood. Whereas in South America the dominating wood type used is eucalyptus. Besides the wood species, the environment of the harvesting location affects the inorganic content of wood as well. For example, trees harvested in a coastal region contain larger fractions of chlorine compared to the same species

harvested inland [3,22]. Thus the composition of the inorganics dissolved in the black liquor can vary significantly and depends on various parameters. In Table 1, typical compositions for North European, North American, and South American liquors are summarized [13].

Table 1: Typical compositions of virgin black liquor from northern Europe, North America, and South America [13]

Element	Northern Europe	North America	South America
C, %	32-37	32-37.5	33-37
H, %	3.2-3.7	3.4-4.3	2.7-3.9
N, %	0.06-0.12	0.06-0.12	0.1-0.6
O, %	33-36	32-38	33-39
Na, %	18-22	17.3-22.4	16.2-22.2
K, %	1.5-2.5	0.3-3.7	0.4-9.2
S, %	4-7	2.9-5.2	2.4-7.0
Cl, %	0.1-0.8	0.1-3.3	0.1-3.3
Inert, %	0.1-0.3	0.1-2.0	0.2-3.0

From Table 1 it can be seen that the sum of Na, K, and S is high in all liquors, which causes the average higher heating value of black liquor (13.4-15.5 MJ/kg) [3] to be significantly lower compared to other biomass fuels such as dry spruce (18.2-20.5 MJ/kg) [23] or dry wheat straw (16.2-20.8 MJ/kg) [23]. Furthermore, due to the high content of inorganics in black liquor, the ash content is significantly higher compared to other conventionally used fuels. Thus, black liquor is a rather unattractive and challenging fuel for the sole purpose of heat and power production. However, as already indicated above, the purpose of the recovery boiler is not only the combustion of black liquor for heat and power production but also the recovery of the spent pulping chemicals.

2.1.2. The kraft recovery boiler

Due to the dual purpose of the recovery boiler and the complexity of black liquor as a fuel, the boiler design requires a high degree of engineering, with the focus being on maximizing boiler availability rather than high energy efficiency [2]. The recovery boiler is designed to achieve the contradictory goals of creating a reducing environment to recover Na_2S from Na_2SO_4 while at the same time achieving complete combustion of the organics dissolved in black liquor [3]. In modern recovery boilers, the amount of heat and power generated is sufficient to supply the whole mill [14].

The concentrated black liquor with a dry solids content of up to 85 % is introduced as a spray to produce millimetres sized droplets in the lower part of the boiler [3,14]. The combustion air is introduced separately from the fuel, at three to four levels [2]. Primary and secondary airports are located

underneath the liquor guns and the tertiary air is introduced above the liquor guns. The fourth air level is controlling NO_x emissions [2]. The multiple air level system ensures complete combustion of the organics, a high reduction efficiency, and low emission levels [13].

The combustion of a black liquor droplet can be divided into four stages: drying, devolatilization, char combustion, and smelt formation [3,14]. As the droplets are sprayed into the boiler, they are subjected to high heating rates resulting in the onset of drying and subsequent devolatilization in flight. In each droplet a local temperature gradient prevails, thus the various combustion stages can occur simultaneously. During devolatilization, organic compounds decompose into light hydrocarbons and gases, causing the droplet to swell significantly. Depending on various operational parameters, swelling can increase the droplet volume by 20 to 50 times [3]. In an ideal case, the particles reach the bottom of the furnace after devolatilization where they form a char bed. The ongoing char combustion provides a reducing environment for the smelt underneath to avoid reoxidation of Na₂S that has already been formed during char combustion [3,14]. The smelt is then extracted from the bottom of the boiler through smelt spouts. Primary and secondary air is used to control the shape and height of the bed. In addition, secondary air is also maintaining a constant temperature above the bed, reducing emissions, and guaranteeing a high reduction efficiency [14].

The high degree of swelling of the black liquor droplets during devolatilization imposes an increased risk for particles being entrained in the flue gas and carried to the convective heat transfer zone of the boiler. On the other hand, if the droplets are too large, they could reach the bed while still wet, which can cause a decrease in bed temperature or even local blackouts in the bed. Thus the droplet size is of utmost importance to achieve a constant bed temperature and ideal combustion conditions. However, between different recovery boilers, the composition of the black liquor, dry solids content, and the operating conditions of the boiler can vary significantly. Thus, no generalized guideline for an ideal droplet size can be found in the literature.

2.2. Ash deposits in the kraft recovery boiler

The generated heat of combustion is utilised to produce superheated steam. The hot flue gases are entrained in the combustion air and move toward the upper section of the boiler, where the superheaters are located. Superheaters are bundles of vertically aligned steel tubes. Convective heat transfer heats the steam inside the tubes, as the hot flue gases pass through the superheater region. The superheated steam can then subsequently be used in a steam turbine to generate power.

2.2.1. Ash forming matter in black liquor combustion

Besides the organic combustion products, a considerable portion of inorganics is released during devolatilisation and char combustion of black liquor

droplets. The amount and composition of the released inorganics depend on various parameters and thus vary among different recovery boilers. The main inorganic elements released however do not change and comprise Na, K, Cl, S, and C [24]. These elements are mainly responsible for the formation of ash deposits on the superheater tubes. Compared to other industrial combustion processes for power production, the amount of fly ash in the recovery boiler is significantly higher, due to its high inorganic content.

The deposits consist almost entirely of water-soluble alkali compounds: Na_2SO_4 , Na_2CO_3 , NaCl, and their K counterparts [6,25]. Besides these main compounds, traces of various other non-process elements, e.g. Si, Ca, or Mg can be found in the deposits as well [14,25].

In a recovery boiler, particles are classified into three size fractions. Fume particles typically have an average diameter of less than $1\text{ }\mu\text{m}$ [14]. Vapourisation of alkali salts and subsequent homogeneous condensation in the gas phase cause the formation of fume particles. The main constituent of fume is Na_2SO_4 , but it also contains Cl, K and CO_3 [24,26]. The majority of the ash particles entrained in the flue gas of recovery boilers are fume [14].

The second particle size fraction is called intermediate-sized particles (ISP) and the diameter ranges between $1\text{--}100\text{ }\mu\text{m}$ [27]. They are either entrained particles of burning droplets or char, or particles broken off from already deposited material via sootblowing [28]. The composition of ISPs is slightly more complex and cannot easily be generalized and depends on the formation pathway of the respective particle. Re-entrained, sintered fume particles typically do not differ significantly in their composition from ESP ash. In some cases, however, the Cl content is significantly lower due to sulphation [28]. Furthermore, mineral impurities contained in the black liquor can be released and entrained in the flue gases and form ISPs [28].

The largest particle size fraction in the flue gas of a recovery boiler is called carryover. Carryover particles are swollen black liquor droplets entrained in the flue gas with diameters up to several millimetres [27]. Depending on whether the droplets are already fully combusted or not when they reach the bullnose, the composition of carryover particles varies. Particles that were still burning contain a significant share of unburnt carbon, whereas particles where all carbon is burnt can contain large amounts of Na_2S [14].

2.2.2. Superheater deposit formation mechanisms

All three particle size fractions contribute to the formation of ash deposits on the superheater tubes of a boiler. Ash deposits lower the boiler efficiency as they act as thermal resistance to heat transfer from the hot flue gases to the steam [6]. Deposits can also cause severe corrosion of the superheater steel, causing eventual failure of the tube [29]. Extensive deposit formation can even cause complete blockage of the flue gas path [3]. In the worst case, deposit-induced problems can cause severe operational issues requiring a shutdown of the boiler, which is connected to an extensive financial loss [30]. Hence, a good understanding of deposit formation and the mechanisms causing operational

problems are required when dealing with deposit-induced challenges during boiler operation to avoid an unscheduled shutdown of the mill.

Due to differences in particle diameter and shape, deposits form via various mechanisms, concurrently taking place during boiler operation [3]. In the following chapter, the governing mechanisms of deposit formation and the general properties of kraft recovery boiler superheater deposits will be discussed. The discussed deposit formation mechanisms are not exclusive to kraft recovery boilers but apply also to other types of boilers.

Condensation contributes to deposit formation in regions where the flue gases are still sufficiently hot to contain inorganic vapours. The flue gas temperature decreases continuously after exiting the furnace and throughout the convective pass of the boiler. The saturation pressures of volatile compounds entrained in the flue gas are temperature-dependent and decrease with decreasing temperature. If the concentration of a volatile compound in the flue gas exceeds its saturation pressure, it condenses [24,31].

Condensation can be distinguished between homogeneous and heterogeneous condensation [24,32]. Heterogeneous condensation describes the condensation of a vapour either on a cold steel surface [33] or on a particle entrained in the flue gas [32]. The heterogeneous condensation of alkali compounds on the clean steel surface is often described to be the initiator of deposit formation [33,34]. Already the presence of a thin layer of condensate increases the stickiness of the surface and promotes deposition and adherence of larger particles [31,32].

Besides heterogeneous condensation, vapours can also condense homogeneously if the concentration of the inorganic vapour exceeds its saturation pressure significantly [32]. Homogeneous condensation causes the formation of small fume particles [6,32]. Fume particles, typically smaller than 1 μm in diameter [27,35], subsequently deposit on heat transfer surfaces mainly via thermophoresis [36] and also via eddy impaction [35]. Thermophoresis describes the temperature gradient-driven movement of small particles toward the colder temperature regime. Furthermore, smaller particles with diameters up to 100 μm [28] get caught in eddies that form as the flue gas flows around the superheater tube. The particle trajectory is changed toward the tube surface by the eddies, resulting in deposit build-up [35]. For deposits that form on the side of the superheater tube (surface parallel to the direction of the flue gas flow), eddy impaction is the governing deposition mechanism [28]. Deposition via heterogeneous condensation and thermophoresis can be observed around the whole circumference of a superheater tube, as these mechanisms are driven by the temperature difference between the hot flue gas and the colder steel surface, independent of the location along the steel tube.

Larger ISPs and carryover particles deposit via inertial impaction. If a particle has too much inertia, it no longer follows the streamlines of the flue gas around the superheater tube, but instead deposits upon impaction [35]. Thus inertial impaction is exclusive to the tube side facing the opposite

direction of the flue gas flow (wind side). Hence, the deposits on the wind side consist predominantly of large ISPs and carryover particles.

Not all particles that reach the steel surface also stick to it. Larger particles may rebound after impactation. Smaller fume particles may detach from the superheater surface and get re-entrained into the flue gas [35]. The sticking propensity of particles depends on various parameters [31], of which the amount of melt has been identified to be crucial.

Ash deposits formed in a kraft recovery boiler are a multi-component system, and deposits melt over a larger temperature interval. The melting behaviour is thereby determined by the chemical composition of the deposit. The most important elements in terms of deposit melting are Cl and K. For superheater deposits in a kraft recovery boiler, the melting behaviour can be summarized as the following: An increase in K decreases the first melting temperature (T_0) [37], while an increase in Cl results in an increase in the amount of melt that is formed at the T_0 [5]. For melt fractions between 15 and 70 wt-%, kraft recovery boiler deposits are considered to be sticky, hence they adhere to the heat transfer surface and further deposit growth is possible [14]. If the melt fraction of a deposit exceeds 70 wt-%, gravitational forces will cause the mostly liquid deposit to flow off the heat transfer surfaces.

However, due to the different particle size fractions and deposition mechanisms, ash deposits in a kraft recovery boiler are not uniform in terms of their composition and morphology. Thus predicting the composition and morphology of a deposit that forms on a superheater tube is challenging. Furthermore, the composition of a deposit can also change over time due to the evaporation of volatiles initially present in the formed deposit [4], or chemical reaction with gaseous species from the flue gas. A typical reaction between deposits and the flue gas in the recovery boiler is the sulphation of alkali chlorides and carbonates in the deposit [4,30].

2.3. Deposit ageing

After their formation, deposits undergo physical and chemical changes such as sintering or (partial) melting. During sintering, bridges form between single particles resulting in a higher degree of interconnection between the single particles [38] which impedes the removal of a deposit [35]. Furthermore, several studies can be found in the literature that identified local differences in the composition of deposits obtained from actual power boilers [11,39–41]. These local differences are commonly associated with changes in the deposition mechanism, such as the formation of an initial deposit layer consisting of fume which enables subsequent deposition of larger particles via inertial impactation [40]. Another common explanation found in the literature for local differences in deposit composition is the diffusion of vapours from the flue gas into the porous deposit and subsequent condensation on particle surfaces or reaction with the solid deposit [4].

More recent studies at Åbo Akademi University, however, showed that the local composition of deposits can also change due to processes taking place

within the deposit, after its initial formation [8–10,42]. Such processes are referred to as deposit ageing. Deposit ageing describes physical and chemical mechanisms that take place in a deposit over time, after it has formed on a heat transfer surface, affecting the local deposit chemistry and morphology. Temperature gradients over deposits were identified to be connected to several deposit ageing mechanisms. Due to the temperature difference between the colder steam inside the superheater tube and the hotter flue gases, a temperature gradient develops over the deposit in its radial direction. The temperature gradient changes with time, as the deposit grows in thickness. Furthermore, morphological changes due to melting or sintering result in changes in the deposit temperature gradient. Depending on the porosity of a deposit, the thermal conductivity, hence the temperature gradient over the deposit cross-section changes [43]. Thus, the steepness of the temperature gradient is not uniform over the deposit cross-section.

To get a better understanding of how the temperature gradient affects the local chemistry and morphology of superheater ash deposits, Lindberg et al. [8,9] exposed synthetic ash deposits to a temperature gradient. They showed that the majority of the obtained deposits could be divided into three distinct regions. In each of these regions, characteristics specific to a particular deposit ageing mechanism were identified. These three deposit ageing mechanisms will be introduced in more detail in the following sections.

2.3.1. Temperature gradient zone melting

Temperature gradient zone melting (TGZM) describes the transport of a melt droplet through a solid medium induced by the temperature gradient the system is exposed to. The driving force for the transport is the temperature-dependency of the liquid phase composition. The solubility of the primary crystallising phase in the liquid phase increases with increasing temperature. Thus, a concentration gradient develops over the melt droplet in the direction of the temperature gradient. The concentration gradient causes diffusional transport in the melt resulting in the dissolution of the surrounding solid phase at the hot end of the droplet. Simultaneously, the primary crystallising phase recrystallises at the cold end of the droplet. By this, TGZM causes an overall movement of the liquid phase toward the hotter temperature [8,44].

In the outermost region of the synthetic deposits, where local temperatures were the highest, a region depleted in alkali chlorides was observed. For exposure times of 24 h or more, the outermost layer had a dense morphology consisting of alkali sulphate (primary crystallising phase). In all experiments, the furnace temperature exceeded the T_0 of the used synthetic deposits, thus the dense deposit morphology was the result of (partial) melting [8,9]. In the samples of shorter exposure times, the outer layer had a similar morphology. However, channels of alkali chloride perpendicular to the steel surface were identified within the outermost layer [8].

The channels of alkali chloride were oriented in the same direction as the temperature gradient and formed as a result of temperature gradient zone

melting [8]. For the synthetic deposits used in these earlier studies, the composition of the formed melt is temperature-dependent. With alkali sulphate as the main compound in the original mixture, the primary crystallising phase is pure alkali sulphate. The corresponding melt contains all Cl present within the original salt particles and a certain share of sulphate, which is temperature-dependent. With increasing temperature, the solubility of alkali sulphate in the melt increases [8].

As the local temperature in the outer deposit region exceeds the T_0 , the melt accumulates in the void areas of the originally porous deposit, forming melt pockets [9,45]. Due to the exposure to a temperature gradient, the equilibrium composition of the melt, even for a small melt droplet, is not uniform in the radial direction. The region of the droplet closer to the steel, thus at a lower local temperature, is enriched in alkali chloride compared to the region further away from the steel. The local differences in the melt composition cause diffusional transport of alkali chloride from the colder to the hotter region inside the melt droplet [8].

As the alkali chloride concentration in the colder region of the melt droplet decreases, alkali sulphate begins to recrystallize for the melt to reach its equilibrium composition. Simultaneously, the local increase in the Cl content at the hotter part of the droplet causes dissolution of the surrounding solid alkali sulphate. This continuous process of concurrent recrystallisation and dissolution, induced by the internal diffusion of alkali chlorides in the melt droplet causes alkali chlorides to move toward the outer deposit surface with time [8].

After the alkali chlorides have reached the outer deposit surface, they evaporate into the furnace [8], leaving behind an outer deposit region depleted in alkali chloride, which has a characteristic sharp border to the chloride-rich region below, closer to the steel [8]. Due to the recrystallisation of alkali sulphate, TGZM causes densification of the outer deposit layer.

2.3.2. Movement of enriched melt toward steel

Besides the movement of melt toward the hot part of the deposit due to TGZM, the formed melt was also seen to move toward the steel. A melt that forms in the outer region of a deposit, where local temperatures are above the T_0 , moves toward the steel due to capillary and gravitational forces. As the melt moves toward the steel, the local deposit temperature experienced by the melt decreases and the primary crystallising phase begins to solidify. Thus, despite the decreasing local temperature, the remaining melt remains liquid and can move even closer toward the steel.

In the synthetic deposits, below the Cl-depleted region, a second dense deposit layer was observed. The two dense layers are separated by a sharp border, which coincides with T_0 [8,9]. The chemical composition of this second dense layer approached the composition of the eutectic point [8,9].

The formation of this “eutectic region” is due to partial melting of the deposit at temperatures above the T_0 . Due to capillary and gravitational forces, the

formed melt subsequently moves toward the steel [8,9]. As the local deposit temperature decreases, the primary crystallising phase begins to solidify. In the case of binary NaCl-Na₂SO₄ and KCl-K₂SO₄ mixtures with alkali sulphate as the main component, sulphate is the primary crystallising phase. Consequently, the remaining melt enriches in alkali chloride, as the composition follows the liquidus line. Hence, with decreasing temperature, the composition of the remaining melt approaches the eutectic point. If the melt, which is now at the eutectic composition due to the continuous enrichment in Cl, moves even further toward the steel, complete solidification takes place as the local deposit temperature reaches the T_0 . Due to the low cooling rate of the melt, as it moves toward the steel, the typical labyrinth-like distribution of alkali chlorides and alkali sulphate can develop [8]. In several of these earlier experiments, the movement of melt toward the steel was identified and a labyrinth-like eutectic solidification pattern was observed between original, sharp-edged particles [9]. This was a clear indication that melt moved toward the steel and filled voids in the deposit at colder temperatures.

The movement of melt toward the steel causes densification of the deposit, similar to TGZM. In addition, the movement of melt enriches the deposit in alkali chloride toward the steel. Experiments carried out in an entrained flow reactor, where synthetic KCl-K₂SO₄ and NaCl-Na₂SO₄ deposits were fed into the system subsequently showed that mixing of the alkali compounds promotes the melt to move even closer toward the steel. Due to the mixing of the alkali compounds, melt with a T_0 lower than that of the respective binary salts formed [10].

2.3.3. Diffusional transport of alkali chloride vapours

The third deposit ageing mechanism identified is the diffusional transport of alkali chloride vapours toward the steel. The diffusional transport is temperature gradient induced and connected to the temperature-dependence of the alkali chloride vapour pressures. With increasing temperature, the vapour pressure of both NaCl and KCl increases exponentially. Therefore, a concentration gradient for alkali chloride vapours develops over the gas phase of the porous deposit region in the radial direction [8]. At higher local temperatures, further away from the steel, the vapour pressures of alkali chlorides are higher.

Hence, in the air gap between two distinct particles located at different temperatures, the concentration of alkali chloride vapours is higher at the steel-facing side of the hotter particle compared to the furnace-facing side of the cooler particle. Thus a concentration gradient of alkali chloride vapours develops over the air gap between the two particles. Alkali chloride vapours then subsequently diffuse toward the steel due to the concentration gradient. As the alkali chloride vapour concentration on the surface of the cooler particle increases, alkali chloride condenses on the cooler particle surface to maintain saturation concentration. At the same time, additional alkali chloride evaporates from the inside of the hotter particle, as the vapour concentration

at the hotter particle surface tends to decrease due to diffusional transport toward the cooler deposit region [8,9].

The diffusional transport of alkali chloride vapours toward the steel was seen in the region of the deposit where local temperatures did not exceed the T_0 and the distinct particles retained their original shape and no melt was formed during the experiment.

This continuous process of evaporation, diffusion, and condensation results in the build-up of alkali chloride layers on the furnace-facing side of particles over time. Simultaneously, the steel-facing side of the original salt particles was observed to deplete in alkali chloride, leaving behind a skeleton of alkali sulphate [8,9].

In addition to the furnace-facing side of particles, alkali chloride layers formed directly on the steel surface [8,9]. However, closer to the steel surface, where local temperatures were lower, the thickness of the formed layers decreased [8,9]. As the vapour pressure increases exponentially with increasing temperature, the concentration gradient is steeper at higher temperatures, thus the diffusion flux is greater and the alkali chloride layer thickness increases with distance from the steel [8]. The formation of an alkali chloride layer directly on the steel surface implies an increased risk for alkali chloride-induced corrosion.

3. Experimental

In this thesis, deposit ageing mechanisms in ash deposits obtained directly from the superheater tubes of kraft recovery boilers were studied. In addition, probe measurements were carried out in the superheater region of a kraft recovery boiler. To complement the full-scale data, a laboratory setup was used in which temperature gradient-induced changes on synthetic ash deposits were studied under well-controlled conditions.

The morphology and chemical composition of all deposit samples were analysed using scanning electron microscopy (SEM) and energy dispersive X-ray analysis (EDXA). Thermodynamic modelling was utilised to calculate the melting behaviour of the deposits, the composition of the formed molten phase, and the vapour pressures of alkali halides.

3.1. Kraft recovery boiler superheater deposits

A major part of this thesis concerns deposit ageing in actual superheater ash deposits from kraft recovery boilers. Deposit samples were obtained from the superheater tubes of two different kraft recovery boilers.

3.1.1. Brazilian deposit samples

The deposit samples presented in Paper I were obtained from a kraft recovery boiler located in Belo Oriente, Brazil. The boiler has a maximum firing capacity of 2700 tons of dry solids per day. The deposits were removed directly from the superheater tubes, after 6 months of continuous boiler operation. The samples were taken by the boiler operator, during a shut-down of the boiler, from where they were then shipped to Finland for detailed analysis.

A total of three samples were taken from different locations along the convective pass of the boiler (secondary superheater tube, screen tube, and tertiary superheater tube). The sampling locations are indicated in the schematic drawing of the convective pass of the boiler shown in Figure 1.

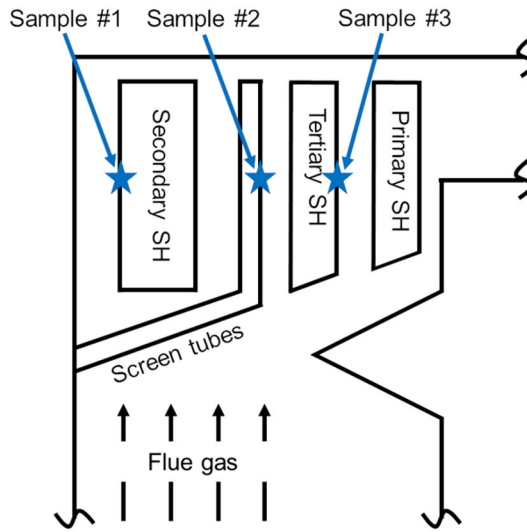


Figure 1: Sampling locations of superheater deposits obtained from Brazilian kraft recovery boiler. Reprinted with permission from Paper I under a CC-BY-4.0 license. Copyright © 2021 Elsevier

The superheater tubes were accessed through manholes in the boiler wall. The deposits were manually removed from the superheater tubes. A loss of material during sampling, especially of the innermost deposit layer, could not be ruled out as some of the deposit material either remained attached to the superheater tube or got destroyed during sampling and transportation.

No information on the flue gas temperature at the sampling locations was available. However, typical flue gas temperatures in recovery boilers are around 900 °C at the entrance to the convective pass [28] and 700 – 800 °C at the exit of the tertiary superheater tubes [28]. The steam temperature at the respective sampling locations was 420 °C at sampling point 1, 290 °C at sampling point 2, and 460 °C at sampling point 3.

3.1.2. Finnish deposit samples

A second batch of deposit samples was obtained from a kraft recovery boiler in Rauma, Finland with a maximum firing capacity of 3200 tons of dry solids per day (Paper II). Analogous to the Brazilian deposits, the boiler was accessed through openings in the boiler wall and the deposits were manually removed from the superheater tubes by the boiler operator. The sampling locations are indicated in the schematic in Figure 2.

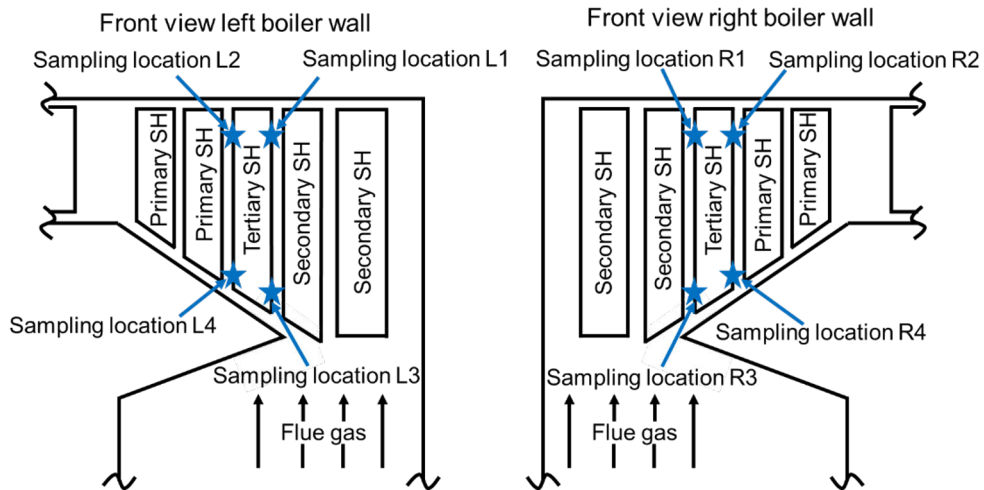


Figure 2: Sampling locations of superheater deposits obtained from Finnish kraft recovery boiler. Reprinted with permission from Paper II under a CC-BY-4.0 license. Copyright © 2023 Elsevier

The deposits were obtained after a continuous boiler operation of approximately one month. Four sampling locations were located close to the boiler roof, similar to the Brazilian boiler. In addition, samples were taken from the lower part of the tertiary superheater, close to the bullnose. Deposits were taken from a total of 8 different sampling locations, as the superheaters were accessed from both boiler side walls. The steam temperature in the tertiary superheater tubes averaged 480 °C. No data on the flue gas temperature was available. However, flue gas temperature measurements during separate probe sampling campaigns showed flue gas temperatures in the upper superheater region (Sampling location R1) to range between 550 – 650 °C.

3.2. Full-scale probe deposit sampling

Besides actual superheater deposits, a new sampling probe was designed to carry out long-term deposit sampling campaigns in actual recovery boilers. The design of the probe and measurement results are discussed in Paper III. All probe measurements were carried out at Sampling location R1 (Figure 2) of the Finnish kraft recovery boiler.

The deposit sampling probe consists of two steel tubes made from P235GH steel (a carbon steel). The outer diameter of the probe is 5 cm. The main features of the probe design are shown in Figure 3.

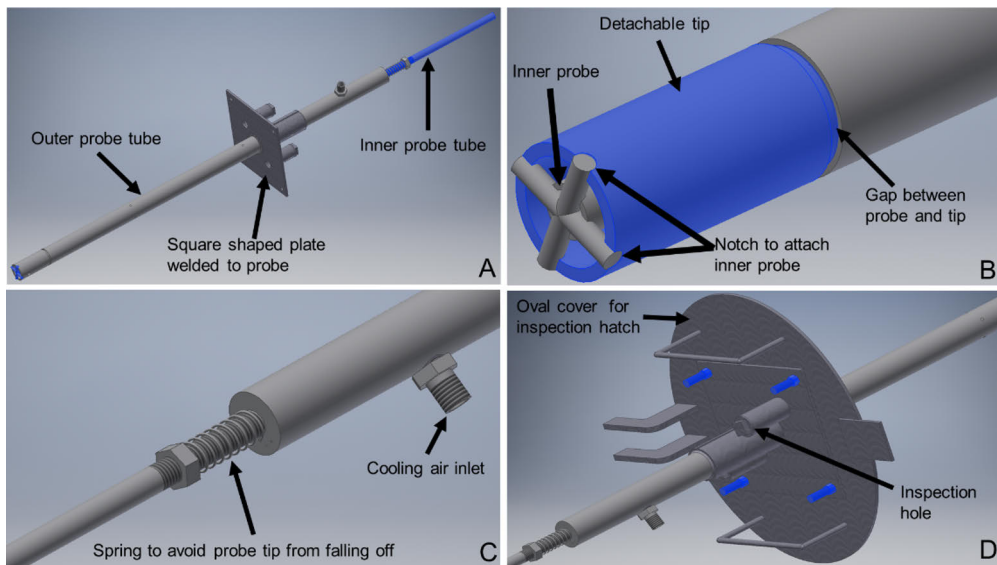


Figure 3: Main design features of full-scale deposit sampling probe: A) Fully assembled probe; B) Removable tip; C) Back end of probe; D) Custom made manhole cover; Reprinted with permission from Paper III under a CC-BY-4.0 license. Copyright © 2023 Elsevier

In image A of Figure 3 the fully-assembled probe is shown. The square-shaped plate is attached to the boiler wall, thus dividing the probe into two parts: the part to the left of the plate, with a total length of 85 cm, is located inside the boiler during the experiment. The part to the right of the plate remains outside of the boiler. The main probe is welded to the squared metal plate, to avoid any rotation during the measurement, enabling differentiation between various locations along the probe's circumference when analysing the obtained deposit sample. Two inspection holes are drilled into the squared plate, which can be used to remove deposit material from the inside boiler wall before removing the probe. For the whole duration of the experiment, a thermocouple was inserted directly into the boiler through one of the inspection holes, measuring the flue gas temperature.

The deposit sample is collected on a removable tip, 10 cm in length, highlighted in image B. The removable tip allows analysis of the collected deposit, while still attached to the probe surface. During the experiment, the tip is held in place by a second steel tube, located inside the probe. A metal cross is welded to the tip of the inner tube, fitting into the grooves of the outer tip and preventing it from falling off the probe during the experiment. Additional grooves are located at the contact area between the main probe and the tip, preventing the tip from rotating during the experiment. After longer

exposure times, the tip could no longer be removed from the main probe due to extensive corrosion. Therefore, a small gap between the tip and the main probe can be seen in image B. It is possible to cut off the tip at this gap, without damaging the probe or the deposit on the sampling tip.

The sampling tip is cooled to a designated temperature using pressurized air. During the exposure, two thermocouples are placed inside the sampling tip, one of which is connected to a PID controller adjusting the flow of cooling air inside the probe thus maintaining a constant steel temperature. The second thermocouple logs the steel temperature. The cooling air enters the probe at its back end, indicated in image C, and passes through the probe in the space between the inner and outer tube from where it is then blown into the boiler, exiting the probe at its tip.

At the back of the probe shown in image C, a spring is used to build up force for the inner tube to keep the tip in place during the measurement. By using a spring, differences in the thermal expansion of the inner and outer tube can be compensated while at the same time exerting sufficient force for the tip to remain attached to the probe during the whole duration of the experiment.

An oval metal plate was manufactured, exactly fitting the opening in the boiler wall and onto which the probe can be attached. A square opening in the oval plate with an edge length of 15 cm ensures the removal of the probe from the boiler without damaging the deposit. Four bolts are used to attach the squared metal plate to the oval plate covering the boiler wall opening.

Before inserting the probe in the boiler, the sampling tip was preheated to temperatures above 100 °C to avoid immediate condensation of water vapour on the blank steel surface. After the experiment, the flow of cooling air was increased to achieve fast cooling of the sample. The cool deposit was then cast in epoxy resin, while still attached to the sampling tip.

At the sampling location, three sootblowers were located in the direct vicinity of the probe. The locations of the three sootblowers in relation to the

probe are shown in Figure 4 together with the nomenclature for distinct points along the probe's circumference.

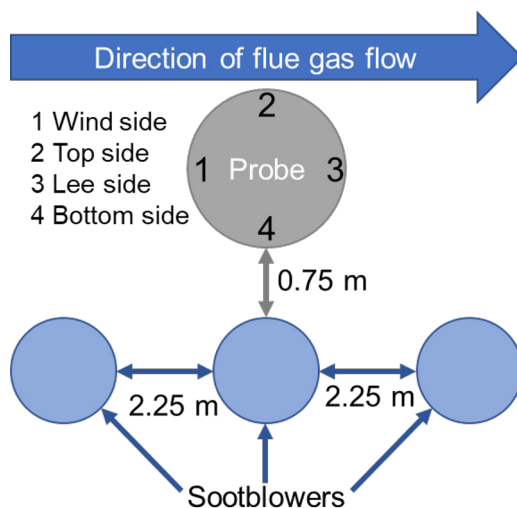


Figure 4: Nomenclature of distinct points around probe circumference and location of nearest sootblowers during probe measurement. Adapted with permission from Paper III under a CC-BY-4.0 license. Copyright © 2023 Elsevier

The side of the probe facing the flue gas stream directly is referred to as the wind side and the opposite part of the probe is the lee side. The top side was facing upward during the experiment. The bottom side, which was directly exposed to the closest sootblower at a distance of 0.75 meters, faced downward. Two more sootblowers were located 2.25 meters to the left and right, on the same level as the one directly underneath the probe.

3.3. Laboratory temperature gradient experiments

Deposit ageing was also studied on a laboratory scale (Papers IV and V). Synthetic ash deposits were exposed to a temperature gradient by placing an air-cooled probe in a tube furnace. Images of the laboratory probe setup are shown in Figure 5.

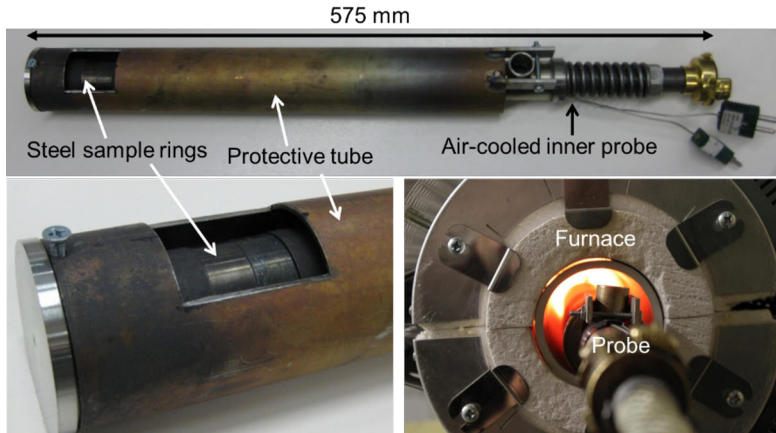


Figure 5: Laboratory temperature gradient probe with two removable steel sample rings on which the synthetic deposits were placed on. Reprinted with permission from Lindberg et al. [9] Copyright © 2016 Elsevier.

The probe itself consists of 2 concentric steel tubes. Synthetic ash deposits are placed on two steel sample rings at the tip of the inner tube. Cooling air, recirculating inside the probe, is used to maintain a constant steel temperature during the experiment. The outer tube is used to minimize the cooling effect the inner tube has on the furnace and at the same time reduce the flow of cooling air. The deposits are exposed to the furnace through a small opening in the outer tube. More stable furnace temperatures during the experiments are ensured by this design.

During the exposure, the synthetic ash deposits are held in place by moulds of fire-sealant paste. This prevents molten salts from flowing off the probe during the experiment. In each of the steel rings, a thermocouple is placed to control the cooling airflow and log the steel temperature, respectively. A third thermocouple logs the furnace temperature just above the outer deposit surface. In Paper IV, the temperature measured at the outer deposit surface is used to calculate the maximum amount of melt formed in the deposit during an experiment.

The preparation of the synthetic deposits used in the laboratory scale experiments consisted of the following steps: the single compounds are weighed, mixed, and melted for homogenization. After cooling to room temperature, the solidified melt is crushed and sieved to a particle size of 53 – 250 μm . The initial compositions of the synthetic deposits (pre-melting) used in this thesis are summarized in Table 2. After melting and crushing, the final compositions of the synthetic deposits were analysed using electron dispersive X-ray analysis.

Table 2: Compositions and calculated T_0 of synthetic ash deposits used in laboratory temperature gradient experiments

Name	Na [wt-%]	K [wt-%]	Cl [wt-%]	SO ₄ [wt-%]	Br [wt-%]	T ₀ [°C]
86-Na ₂ SO ₄	33	-	4	63	-	626
77-K ₂ SO ₄	-	46	5	49	-	690
69-K ₂ SO ₄	-	46	8	46	-	690
1K 1Cl	32	1	1	66	-	615
10K 1Cl	25	10	1	64	-	556
10K 10Cl	26	10	10	54	-	557
1K 10Cl	33	1	10	56	-	613
NaBr-Na ₂ SO ₄	29	-	-	46	25	622
KBr-K ₂ SO ₄	-	40	-	33	27	670

Besides the deposit composition, other parameters varied in the laboratory experiments were the exposure time (0-336 h), furnace temperature (780-980 °C), and probe temperature (400-500 °C). The laboratory setup was used to study deposit ageing in synthetic deposits relevant to kraft recovery boilers (Cl-containing salts) as well as deposits relevant to other processes, e.g. waste combustion, by replacing Cl with Br in some of the salts (Paper V).

In Paper IV, deposit compositions containing Na and K concurrently (ternary reciprocal systems) were studied. The ternary reciprocal deposits are closer to the composition of actual recovery boiler superheater deposits compared to the earlier studied binary salts. Furthermore, the initial melting behaviour of deposits was studied in experiments with short exposure times (Paper IV). The shortest exposure time to investigate the initial melting behaviour of deposits was zero minutes. Temperature profiles of the probe and furnace temperature during a zero-minute experiment are shown in Figure 6.

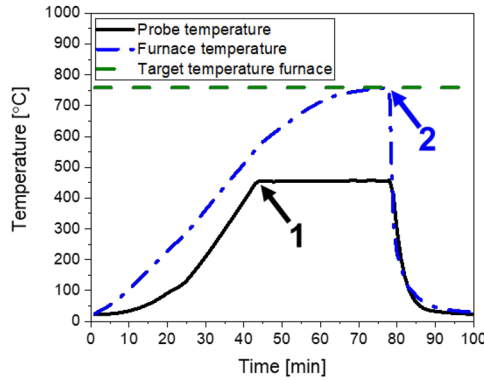


Figure 6: Probe and furnace temperature of zero-minute laboratory probe experiment. Reprinted with permission from Paper IV under a CC-BY-4.0 license. Copyright © 2023 Elsevier

The probe was placed in the cold furnace and heating of the furnace was started (0 minutes on the X-axis in Figure 6). As soon as the probe reached its designated temperature (Point 1 in Figure 6), cooling of the probe started. From this point on, the probe temperature remained stable at its set temperature. At the same time, the furnace was further heated up to its designated temperature. At point 2 in Figure 6, the furnace reached its target temperature, marking the starting point of the experiment. In the case of a zero-minute experiment shown in Figure 6, point 2 concurrently marks the endpoint of the experiment. After the experiment, the probe was removed from the tube furnace and the flow of cooling air inside the probe was increased to cool the deposit samples to room temperature. Before removing the steel sample rings from the probe, the deposit samples are cast in epoxy resin to minimize the risk of damaging the deposit when removing the steel rings from the probe.

3.4. Analysis of deposit samples

The same analysis method was used for all samples in this thesis, independent of it being a superheater deposit, boiler probe deposit, or laboratory probe deposit. First, the samples were cast in epoxy resin. By this, the probe deposits remained attached to the steel surface and the loss of deposit material during further process steps was prevented. The cured samples were then cut to obtain a cross-section. The cross-sections were ground using different grades of SiC grinding paper to obtain a smooth surface. A water-free lubricant was used for polishing to avoid the dissolution of any deposit material. The polished deposits were cleaned using petroleum ether and subsequently carbon coated.

The morphology of the cross-sections was analysed using scanning electron microscopy (SEM). The chemical composition of the cross-sections was analysed using energy-dispersive X-ray analysis (EDXA). The EDXA data were further used to create elemental maps of the cross-sections and to calculate

concentration profiles of certain elements and the molar $K/(Na+K)$, $Cl/(Na+K)$, and $S/(Na+K)$ ratios throughout the cross-section. Furthermore, the deposit melting behaviour and local T_0 were calculated using FactSage 8.1[46] and the FTPulp database containing data relevant to deposits forming in kraft recovery boilers [47].

4. Results and discussion

4.1. Full-scale boiler deposits

Deposits from superheater tubes of two different kraft recovery boilers, one located in Brazil (Paper I) and one located in Finland (Paper II) were analysed regarding their morphology and chemical properties to identify deposit ageing mechanisms. In addition, long-term probe deposit measurements were carried out in the Finnish boiler (Paper III). As shown in Table 1, the composition of the fired black liquor can be significantly different, depending on the wood type used in the pulping process. Due to these compositional differences in the fired liquors, the Brazilian and Finnish deposits will be discussed in separate sections.

4.1.1. Brazilian boiler deposits

Three deposits from different locations along the convective pass of the Brazilian boiler were analysed in Paper I. No significant differences in the bulk chemical composition of the single deposits were observed. In Figure 7 the

cross-section of one of the obtained deposits is shown, with the three identified deposit ageing mechanisms highlighted on the right.

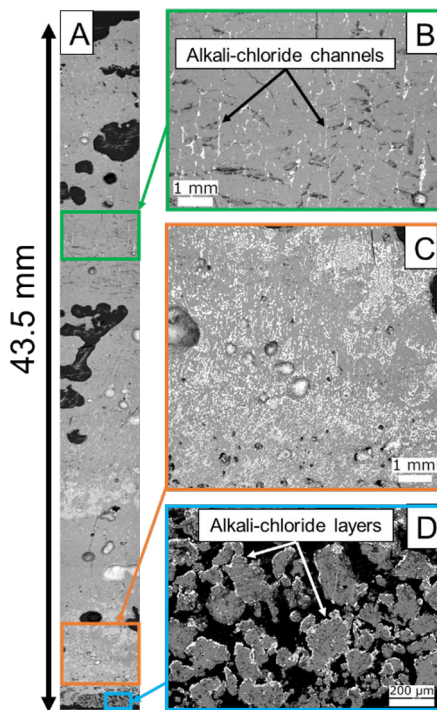


Figure 7: (A) SEM cross-section of Brazilian superheater deposit; (B) Channels of alkali chloride rich melt perpendicular to steel surface; (C) Molten region enriched in K and Cl closest to steel; (D) Alkali chloride layers on furnace facing side of particles within porous region of deposit. Adapted with permission from Paper I under a CC-BY-4.0 license. Copyright © 2021 Elsevier

For all backscatter images of deposit cross-sections in this thesis, the white colour corresponds to alkali halides, darker shades of grey are alkali sulphate and carbonate, and black represents voids within the deposit. In all deposits, the bottom of the image was located closest to the steel surface.

The majority of the deposit cross-section shown in Figure 7 A was of a dense morphology, indicating the presence of large amounts of melt during boiler operation. Closest to the steel, at the bottom of the image, the deposit had a porous region of distinct particles. Characteristics of three deposit ageing mechanisms, previously identified on a laboratory scale using synthetic ash deposits [8–10,42], were also observed in the Brazilian superheater deposits.

In the outer region of the deposit, furthest away from the steel surface, channels of alkali chloride perpendicular to the steel surface were seen (Figure 7 B), a clear indicator for temperature gradient zone melting. During partial melting of the outer deposit region, the melt formed within the originally porous deposit accumulates in void areas. As the deposit is exposed to a temperature gradient, the local temperature within the formed melt pockets is

not constant. The temperature gradient over the melt pockets causes the alkali chloride-rich melt to move toward the outer deposit surface over time. A more detailed explanation of the mechanism can be found in Chapter 2.3.1 of this thesis and Paper V.

Different stages of temperature gradient zone melting were observed in the same deposit sample. For larger melt pockets, the majority of the melt was still within the pocket and a Cl-rich channel led from the upper part of the melt pocket toward the outer deposit surface. For smaller pockets, TGZM already progressed further, leaving behind spherical voids, depleted of alkali chloride.

In Paper I, TGZM was for the first time observed to take place in actual superheater deposits. Compared to synthetic laboratory deposits, where TGZM has been observed earlier in the context of deposit ageing, actual superheater deposits are significantly more complex regarding their melting behaviour. However, analogous to the synthetic binary deposits used in the earlier laboratory studies, the composition of the melt formed in the superheater deposits is temperature-dependent. Thus, the driving force for the movement of melt in the actual superheater deposits remains the same as for the synthetic deposits utilised in the laboratory scale studies. For the Brazilian recovery boiler deposits, most Cl present in the deposit will be incorporated in the molten phase as soon as the T_0 is reached. With increasing temperature, a larger share of alkali sulphate and carbonate is dissolved in the molten phase. Hence the alkali chloride diffusion is directed toward the outer deposit surface, analogous to the laboratory deposits.

Closer to the steel, within the molten region of the deposit, local enrichment in Cl was seen (Figure 7 C). The melt, formed within the deposit, moves toward the steel due to capillary forces. As the local temperature decreases, solid phases precipitate and the remaining melt is enriched in Cl. The visual appearance of the enriched region at the interface between the molten and porous region was similar to that of a eutectic melt. Local enrichment in Cl within a molten region of deposits has also been observed in laboratory experiments, where the enriched region approached a composition close to that of the eutectic point [8,9].

The region closest to the steel (Figure 7 D) consisted of distinct particles, which did not sinter during boiler operation. On the furnace-facing side of these particles, layers of alkali chloride were formed. These layers form as alkali chloride vapours evaporate from the original deposit particles and diffuse toward the steel surface. Analogous to the laboratory experiments using binary salt mixtures, the driving force of the vapour diffusion is the alkali chloride concentration gradient in the gas phase induced by the temperature gradient. This mechanism has been studied extensively under well-controlled laboratory conditions using synthetic binary ash deposits [8,9,42]. The Brazilian superheater deposits gave proof for the mechanism to be also of relevance for actual superheater deposits.

Within the molten region of the deposit closest to the steel, local enrichment in K was observed. SEM-EDXA maps of the innermost region of the deposit are shown in Figure 8.

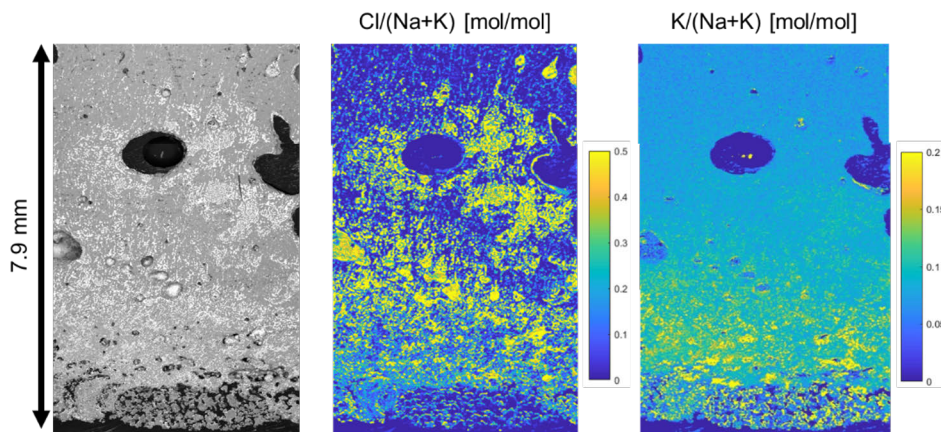


Figure 8: Cross-sectional backscatter SEM image, molar $\text{Cl}/(\text{Na}+\text{K})$ ratio, and molar $\text{K}/(\text{Na}+\text{K})$ ratio (left to right) of innermost region of Brazilian superheater deposit. Adapted with permission from Paper I under a CC-BY-4.0 license. Copyright © 2021 Elsevier

The molar $\text{K}/(\text{Na}+\text{K})$ ratio showed a gradual increase in the K content toward the steel. A maximum was reached at the interface between the porous and molten regions. Throughout the K-enriched region, Cl was more or less evenly distributed but enriched compared to the outer deposit region.

A similar gradual element enrichment has not been observed in earlier laboratory temperature gradient experiments. These earlier laboratory experiments have been carried out using synthetic ash deposits containing only one alkali metal, either K or Na. Therefore, the development of an alkali metal concentration gradient in the melt was not possible in these experiments.

The composition of actual recovery boiler superheater deposits is more complex, as the deposits contain K and Na concurrently. The enrichment in K toward the steel is a consequence of the above-described movement of melt toward the steel due to capillary forces. As the local temperature within the deposit decreases, the melt solidifies partially. The primary solidifying compounds for the Brazilian kraft recovery boiler deposits are Na_2SO_4 and Na_2CO_3 . Hence, K and Cl enrich in the molten phase with decreasing temperature. The K enrichment in the remaining melt affects further solidification. For kraft recovery boiler deposits, an increase in the K content results in a decrease in the T_0 . Therefore, the remaining melt solidifies at a temperature well below the T_0 of the deposit bulk composition. The melting behaviour of the Brazilian deposits and subsequent solidification of the formed melt was calculated using FactSage 8.1. In Figure 9, the gradual K enrichment in the remaining melt during solidification is shown.

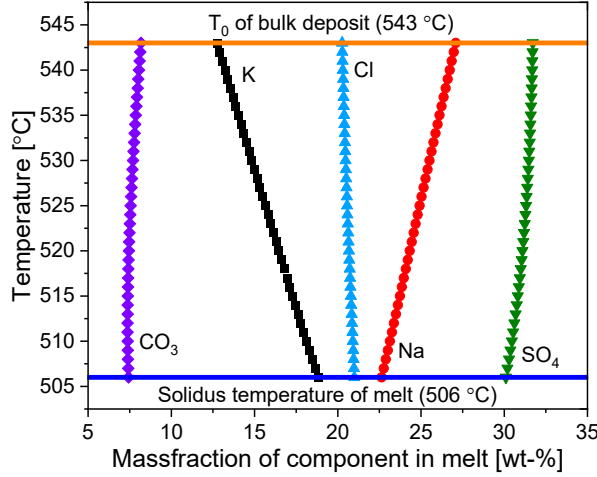


Figure 9: Change of melt composition during solidification of melt initially formed at the deposit bulk T_0 of the Brazilian deposit. Adapted with permission from Paper I under a CC-BY-4.0 license. Copyright © 2021 Elsevier

The local deposit temperature is plotted on the Y-axis of the graph in Figure 9. The bulk T_0 of the deposit was at 543 °C with the following melt composition: 27 wt-% Na; 20 wt-% Cl; 12 wt-% K; 32 wt-% SO_4 ; and 9 wt-% CO_3 . A decrease in temperature results in partial solidification of the melt. As mentioned above, the solidifying phase consists predominantly of Na_2SO_4 and Na_2CO_3 . Therefore, with decreasing temperature, the remaining melt enriched in K. Furthermore, the graph shows that melt, initially formed at the bulk T_0 solidifies over a large temperature range of almost 40 °C. The final solidification temperature was at 506 °C, due to the continuous enrichment of K in the remaining molten phase, as the temperature decreases. At its final solidification temperature (506 °C), the remaining melt consisted of 23 wt-% Na; 21 wt-% Cl; 18 wt-% K; 30 wt-% SO_4 ; and 8 wt-% CO_3 .

Based on the temperature-dependent change in the melt composition as it moves closer toward the steel, a mechanistic explanation of the observed K enrichment was developed. The four main steps of the proposed mechanism are shown in Figure 10.

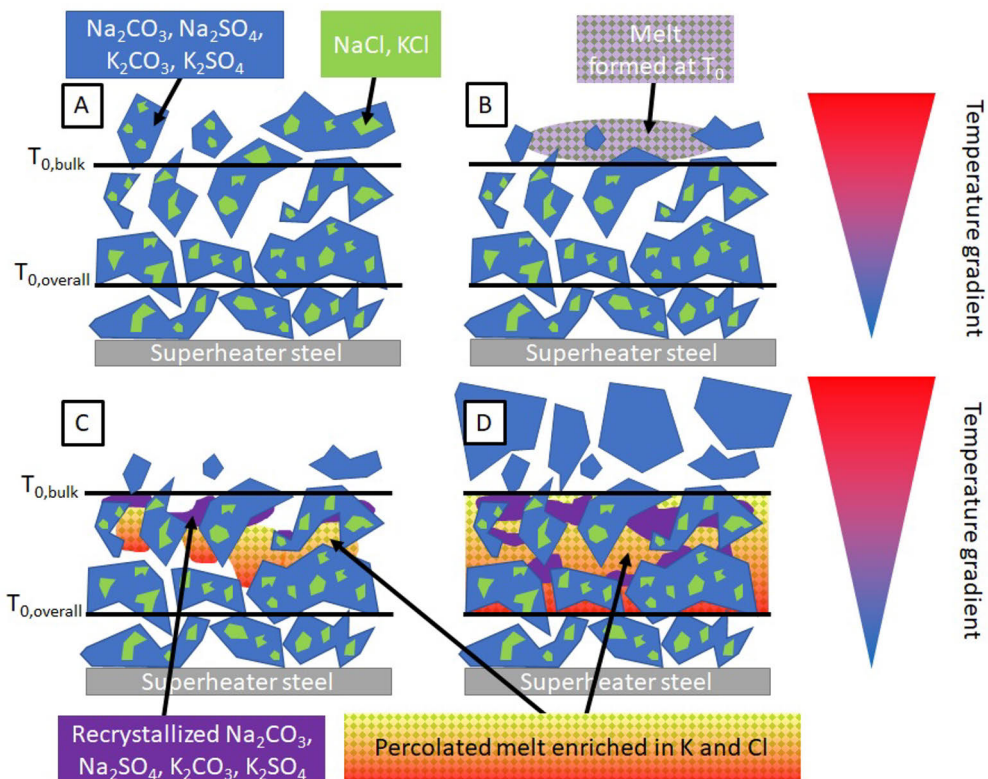


Figure 10: Stepwise illustration of melt enrichment mechanism in a deposit containing NaCl , Na_2SO_4 , Na_2CO_3 , KCl , K_2SO_4 , and K_2CO_3 . A) Outer region of porous deposit exceeds the bulk T_0 ; B) Initial formation of melt at the T_0 ; C) Movement of melt toward the steel and partial solidification; D) Additionally formed melt on outer deposit surface fills remaining voids in porous deposit at temperatures between the $T_{0,bulk}$ and $T_{0,overall}$. Reprinted with permission from Paper I under a CC-BY-4.0 license. Copyright © 2021 Elsevier

In the early phase of deposit build-up on the superheater tube, cooling from the steel is sufficient and the deposited particles do not melt. The local deposit temperature in the region closest to the steel is below the bulk T_0 . Over time additional particles deposit, increasing the deposit thickness. At a certain deposit thickness, cooling from the superheater tube is no longer sufficient and the temperature in the outer deposit region exceeds the T_0 of the bulk deposit composition.

In Figure 10 A, the particles at the outer deposit surface are exposed to temperatures above the bulk T_0 . Hence these particles melt partially. Most of the Cl present in the originally deposited particles will be in the molten phase as soon as the particles reach the T_0 and a melt is formed (Figure 10 B). Due to capillary forces, the melt formed at the outer deposit surface moves toward the steel. As the local temperature decreases toward the steel, the melt solidifies partially. In the case of the Brazilian deposits, the recrystallizing phase consists

of alkali sulphate and carbonate, predominantly Na compounds, whereas almost all chloride remains in the molten phase as well as a large share of K (Figure 10 C).

At the same time, as the melt moves toward the steel, additional material deposits on the outer deposit surface. The newly deposited material is also exposed to local temperatures above the T_0 . Hence additional melt forms at the outer deposit surface which subsequently moves toward the steel following the same mechanisms as described for the melt initially formed. At some point, the melt reaches local temperatures equal to the global T_0 of the system. The process continues until all pores of the deposit, where local temperatures are above the global T_0 , are filled with melt (Figure 10 D). This results in the dense deposit morphology with local enrichment in Cl and K seen in the Brazilian boiler deposits.

The described mechanism of melt moving towards the steel coupled with enrichment in K was shown to affect the local first melting temperature of the deposit. The EDXA data was utilized to analyse to what extent the observed enrichment in K affects the T_0 of the deposit locally. The part of the deposit enriched in K was divided into several sections, as shown in Figure 11.

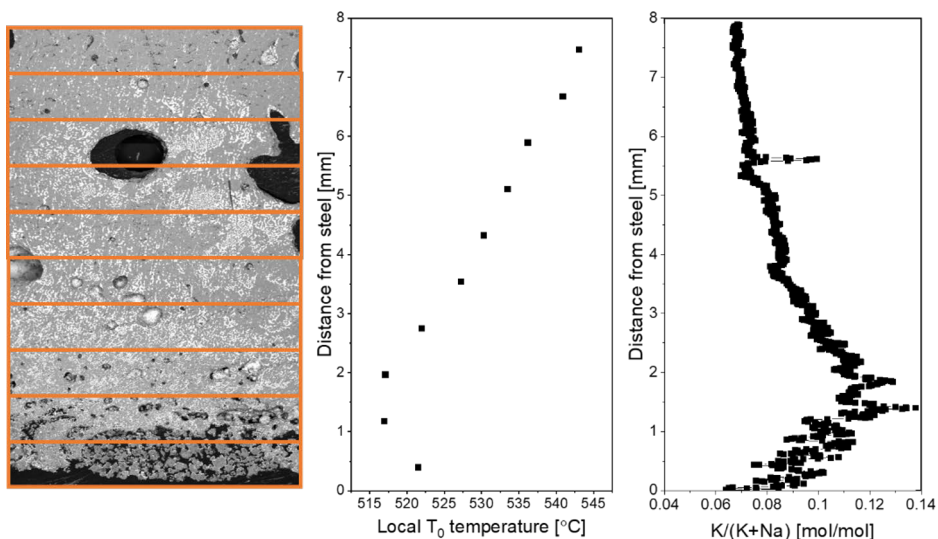


Figure 11: Innermost region of Brazilian superheater deposit divided into several sections (left); Local first melting temperature of the deposit for each corresponding section (middle); molar K/(Na+K) ratio (right). Adapted with permission from Paper I under a CC-BY-4.0 license. Copyright © 2021 Elsevier

The average composition was calculated for each section the deposit was divided into and subsequently used to determine the local T_0 with FactSage. As shown in Figure 11, the local T_0 within the K and Cl-rich region decreased toward the steel. A minimum was reached at the interface of the molten and porous layer, where the K concentration reached a maximum. The profile of the local average T_0 represents a mirrored image of the molar K/(Na+K) ratio as

shown in the right-hand figure in Figure 11. The first melting temperature of recovery boiler deposits depends predominantly on the K content: the first melting temperature decreases with increasing K. Thus the calculations of the average local first melting temperatures were in line with the general understanding of the melting behaviour of superheater deposits in a kraft recovery boiler.

The movement of melt toward the steel coupled with K enrichment was also seen in the laboratory experiments. In Paper IV, synthetic deposits concurrently containing K- and Na-salts were exposed to a temperature gradient. For deposits containing Na- and K-salts, melt was observed significantly closer to the steel compared to earlier experiments where binary salt mixtures had been used. The presence of a melt in the direct vicinity of the steel is directly connected to the local decrease in the T_0 due to the K enrichment. Hence the proposed melt enrichment mechanism poses an increased risk for melt-induced corrosion of superheater tubes.

4.1.2. Finnish boiler deposits

Superheater deposits (Paper II) and probe deposits (Paper III) were obtained from a Finnish kraft recovery boiler. The samples complemented each other very well and are therefore presented together. The Finnish deposits showed significant differences in morphology and chemical composition when compared to the Brazilian superheater deposits. In addition, major morphological differences were observed among individual Finnish deposits. No molten layer formed in the hotter regions of the deposits, due to the low Cl content in the Finnish liquor compared to the Brazilian liquor. Selected cross-sectional SEM images of the Finnish superheater deposits are presented in Figure 12.

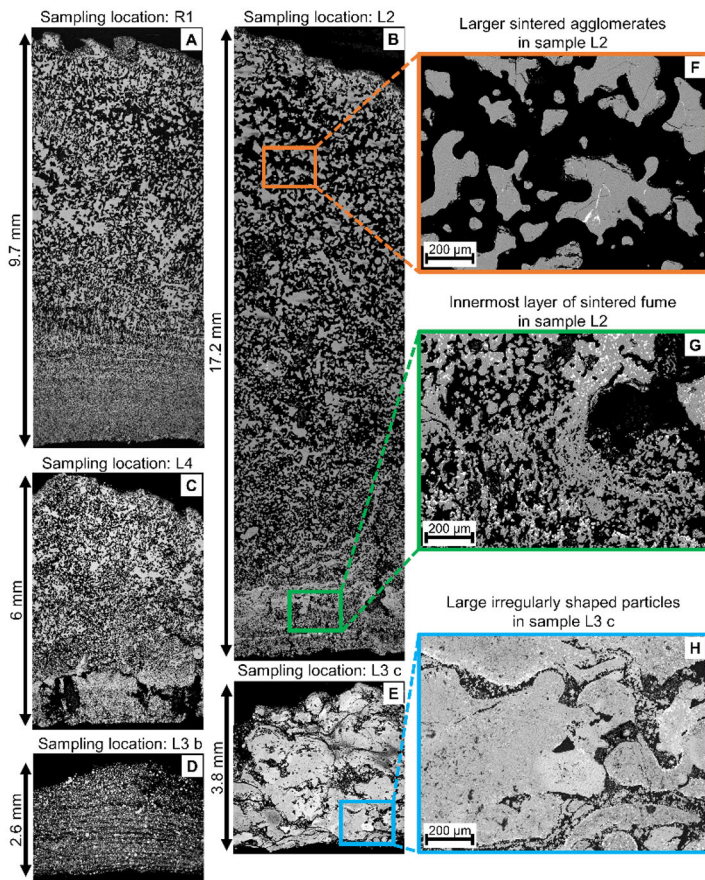


Figure 12: A-E) SEM images of superheater deposit cross-sections obtained from various sampling locations in the Finnish kraft recovery boiler; F) Outer deposit region consisting of larger sintered agglomerates; G) Innermost deposit region of sintered network of sub-micrometre sized particles; H) Large irregular shaped structures; Reprinted with permission from Paper II under a CC-BY-4.0 license. Copyright © 2023 Elsevier

Deposits A and B in Figure 12 were obtained from the upper region of the superheaters, and deposits C, D, and E from the lower region, close to the bullnose. The morphologies of deposit C and the upper superheater deposits (A and B) were very similar, while D and E differ significantly.

The large variations in morphology among the deposits from the lower superheater region are currently not fully understood. A possible explanation for the morphological features of the lower superheater deposits is the increased deposition of carryover particles with a high melt fraction. The shape and size of the particles seen in deposit E indicate the deposition of carryover particles, which were partially molten in flight. As these particles hit the superheater tube, they deform and solidify subsequently, resulting in the irregularly shaped melt-like particles in Figure 12 E. Furthermore, deposit morphologies similar to that in Figure 12 E were also seen at the bottom side of the probe deposits, which were directly facing the sootblower. Thus, the proximity of sootblowers to the sampling location is another possible explanation for the morphology of the deposits obtained from the lower superheater region.

Due to the large variations among the deposits from the lower superheater region, the detailed analysis of the Finnish superheater deposits focused on samples from the upper superheater region. This also ensured better comparability to the deposits from the Brazilian boiler as these deposits were also taken from the upper superheater region. Furthermore, the probe measurements were also carried out in the upper superheater region.

Most of the deposits from the upper superheater could be divided into two distinct regions: An innermost layer consisting of sintered fume particles (Figure 12 G) followed by a layer consisting of larger sintered agglomerates toward the outer deposit surface (Figure 12 F). Some of the analysed cross-sections lacked this inner layer of sintered fume. As the deposits were scraped off the superheater tubes, the risk of particles being lost during sampling was high and the lack of the innermost region of sintered fume particles was believed to be a sampling artefact. By carrying out probe measurements, the risk of material loss could be eliminated as the deposit samples were analysed while still attached to the probe surface.

Due to the lack of a dense molten layer in the Finnish deposit samples, the ageing behaviour differed significantly from the Brazilian deposits. Movement of melt toward the steel and temperature gradient zone melting were not observed within the Finnish deposits, as these mechanisms require larger amounts of melt. However, alkali chloride layers were observed on the furnace-facing side of particles within the porous deposit structure. Hence, diffusional transport of alkali chloride vapours toward the steel took also place in the Finnish deposit samples.

Two different enrichment patterns were identified in the EDXA data. “Type 1” deposits were characterized by a region enriched in K and Cl closest to the steel. An example of a “Type 1” deposit is given in Figure 13.

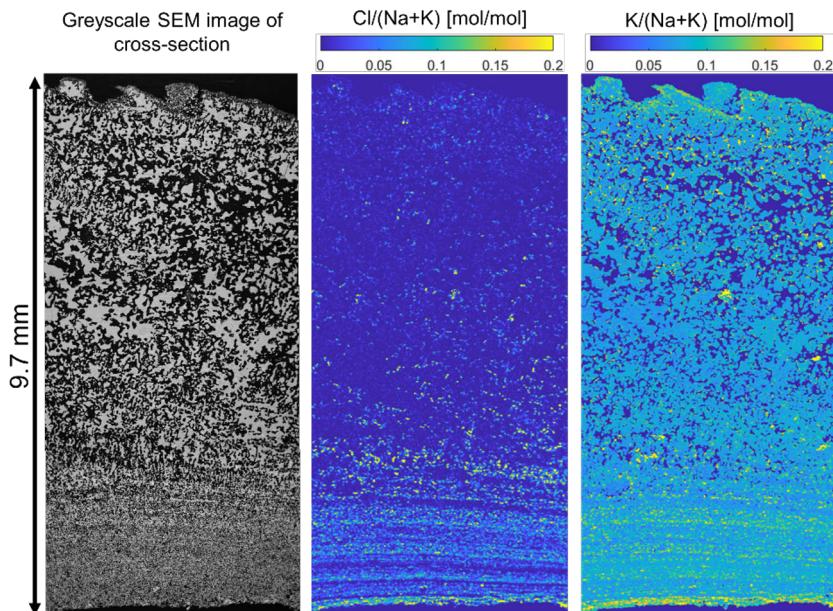


Figure 13: Greyscale cross-sectional SEM image of a Type 1 deposit (left); molar Cl/(Na+K) ratio (middle); molar K/(Na+K) ratio (right); Adapted with permission from Paper II under a CC-BY-4.0 license. Copyright © 2023 Elsevier

In the images depicting the molar Cl/(Na+K) and K/(Na+K) ratios, layered enrichment in Cl and K is seen. A more detailed analysis of the enriched region did not show any significant formation of alkali chloride layers on the individual particles. Therefore, the enrichment visible in Figure 13 was concluded to be the result of fume particles forming an initial deposit layer on the superheater tube. The initial deposit layer subsequently facilitated the deposition of larger particles. Fume particles contain larger amounts of alkali chlorides compared to intermediate-sized and carryover particles [26], thus the innermost region showed enrichment in alkali chloride. After the initial layer of fume particles has formed on the superheater tube, the deposition probability for larger particles, which contain less alkali chloride than fume, is increased [31,32].

The probe deposit measurements gave some additional insights into the deposit ageing behaviour of the Finnish deposits. Three long-term probe experiments were carried out with exposure times of 1, 5, and 8 weeks respectively. Detailed analysis of the chemical composition of the probe deposits was carried out at four selected areas on the wind, lee, top, and bottom sides of each sample. The exact analysis locations are indicated in Figure 14.

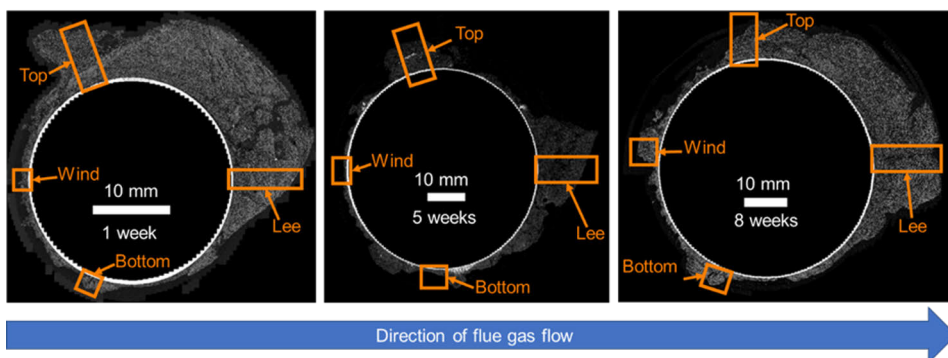


Figure 14: Panorama cross-sectional SEM images of probe deposit samples of exposure times of 1, 5, and 8 weeks from left to right. Locations of EDX analysis along probe circumference indicated by squares. Reprinted with permission from Paper III under a CC-BY-4.0 license. Copyright © 2023 Elsevier

The probe deposits were analysed, while still attached to the steel surface they initially formed on. This eliminated the risk of losing the innermost deposit region. The three deposits were the thickest on the lee side, indicating that eddy impaction and thermophoresis were the governing deposition mechanisms. On the wind side, the deposits were significantly thinner. The measurement location was located between the secondary and tertiary superheater bundles and the main share of the larger particles entrained in the flue gas deposited already on the superheater tubes upstream of the probe. The probe measurements were carried out at the same location from which the superheater deposit sample shown in Figure 13 was obtained. Therefore, the probe deposits strengthened the conclusion that the superheater deposits consisted predominantly of fume particles, which resulted in the observed enrichment in Cl and K within the innermost region of the deposit.

For each of the areas indicated in Figure 14, the average Cl content of the respective deposit cross-section was determined using EDXA data. Figure 15 gives a summary of the average deposit Cl content over time.

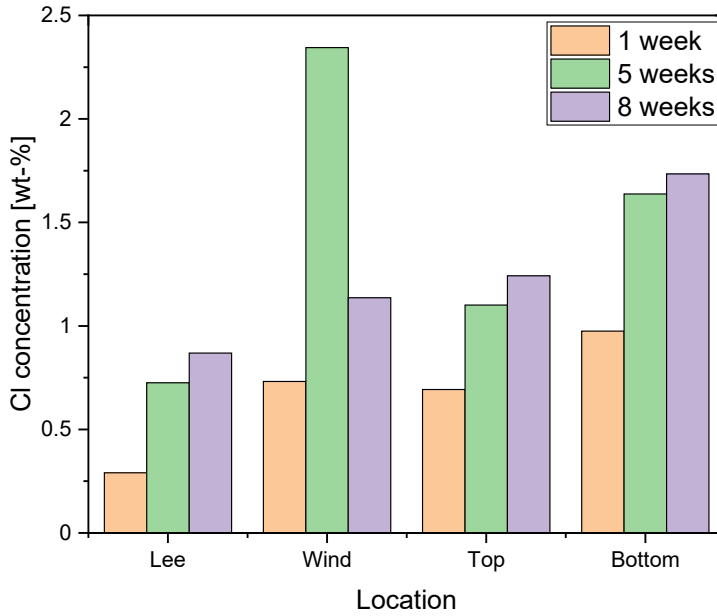


Figure 15: Average Cl content at analysis locations of probe deposit samples with increasing exposure time. Reprinted with permission from Paper III under a CC-BY-4.0 license. Copyright © 2023 Elsevier

With increasing exposure time, the average relative deposit Cl content increased. The enrichment was seen in all analysis locations along the probe's circumference. Due to the porous deposit morphology, alkali chloride vapours present in the flue gas can diffuse into the deposit. As the local temperature within the deposit decreases, the Cl vapours condense within the deposit resulting in the observed increase in the average deposit Cl content with time. The increase in average deposit chlorine content is concentration gradient driven, analogous to the intra-depositional Cl vapour diffusion mechanism. Due to the higher temperature in the flue gas, the concentration of alkali chloride in the bulk flue gas is higher than within the deposit structure which results in the diffusion of additional alkali chloride into the porous deposit.

For the 5- and 8-week probe deposits, local differences in the chemical composition of the deposits were observed. Analogous to the superheater deposits, a region enriched in K and Cl was observed closest to the steel. Throughout the cross-section, Cl layers were observed on the furnace-facing side of the particles. In addition, a Cl and K-rich layer formed directly on the steel surface. In Figure 16, the backscatter SEM image and EDXA maps of a

probe deposit with local Cl and K enrichment in the vicinity of the steel surface are shown.

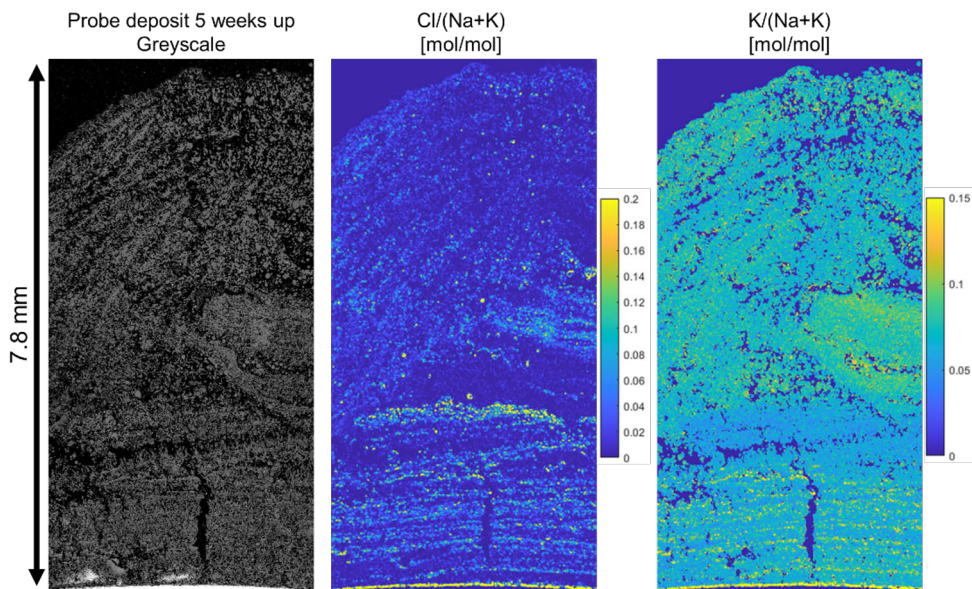


Figure 16: 5-week top-side probe deposit: Greyscale SEM image, molar $\text{Cl}/(\text{Na}+\text{K})$ ratio, and $\text{K}/(\text{Na}+\text{K})$ ratio from left to right. Adapted with permission from Paper III under a CC-BY-4.0 license. Copyright © 2023 Elsevier.

The formation of a Cl layer directly on the probe surface is a clear indicator for temperature gradient-induced vapour diffusion of alkali chlorides toward the steel and subsequent condensation. A similar Cl-layer has previously also been observed in laboratory experiments [8,9,42]. Throughout the Cl and K-rich region of the deposit, alkali chloride layers were also observed on the furnace-facing side of the particles. The results from the probe measurements confirmed that a layer of alkali chlorides can form directly on the steel surface as a result of deposit ageing. After an exposure time of one week, no Cl-layer was observed on the probe surface, thus the Cl layer on the steel surface is suggested to have formed as a result of deposit ageing. The results obtained from the probe samples help to better understand the formation of the K and Cl-enriched region in “Type 1” deposits. The layered Cl and K enrichment closest to the steel is a combination of the innermost deposit layer consisting of Cl and K-rich fume particles and additional temperature gradient-induced diffusion of alkali chlorides toward the steel.

As already mentioned above, a second enrichment pattern was observed among the Finnish boiler deposits. Two examples of “Type 2” deposits, one superheater deposit and one probe deposit, are shown in Figure 17.

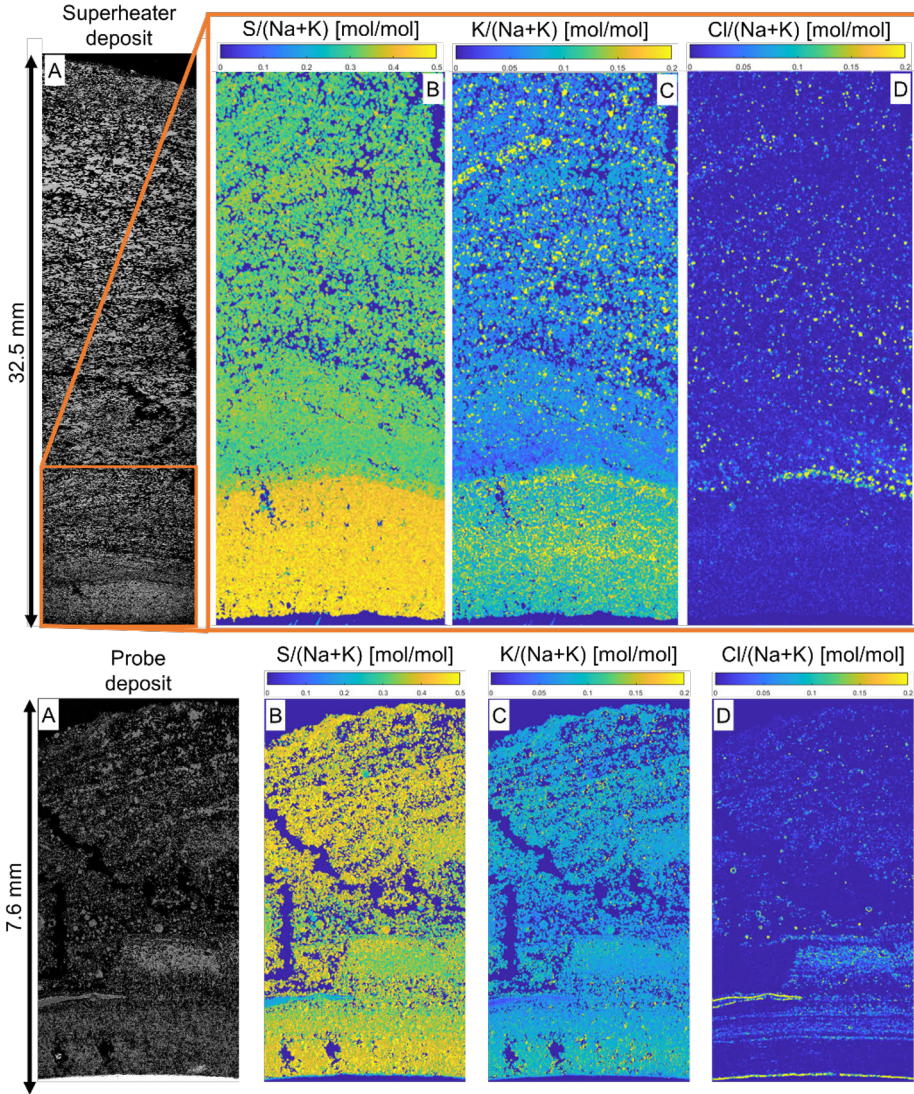


Figure 17: SEM images of “Type 2” superheater deposit (top row) Adapted with permission from Paper II under a CC-BY-4.0 license. Copyright © 2023 Elsevier and probe deposit (bottom row) Adapted with permission from Paper III under a CC-BY-4.0 license. Copyright © 2023 Elsevier; A) Greyscale SEM image; B) molar S/(Na+K) ratio; C) molar K/(Na+K) ratio; D) molar Cl/(Na+K) ratio

“Type 2” deposits are characterized by a region enriched in S and K while being concurrently depleted in Cl, as seen in the region closest to the steel in the two

deposits shown in Figure 17. The depletion in Cl and concurrent enrichment in S indicates sulphation of alkali chlorides. Due to the porous deposit morphology, SO₂ can diffuse from the flue gas into the deposit and subsequently react with alkali chlorides. As described above, the innermost deposit layer consists predominantly of fume particles and, hence is enriched in alkali chloride compared to the outer deposit regions. Therefore, sulphation was most pronounced in the innermost region of the deposit. Image D in the bottom row of Figure 17 shows the molar Cl/(Na+K) ratio of the probe deposit. A distinct chloride layer was seen on the steel surface, indicating enrichment in alkali chloride via vapour diffusion preceding the sulphation. Hence, for the obtained deposits, the sulphation can be divided into two steps. First, the deposit is enriched in alkali chlorides by diffusional transport of alkali chloride vapours toward the steel. Second, the Cl and K enriched region is sulphated by SO₂ from the flue gas. The preceding enrichment in alkali chloride also explains the observed K enrichment within the sulphated region of the deposit, as the K content is not affected by the sulphation reaction.

Sulphation was more pronounced in the superheater deposit (top row of Figure 17) compared to the probe deposit (bottom row of Figure 17). The probe deposits were obtained during regular boiler operation. In contrast, the superheater deposits started to form during the start-up phase of the boiler. During boiler start-up, heavy fuel oil is co-fired to accelerate the heating of the boiler, causing significantly higher concentrations of SO₂ in the flue gas. Therefore, sulphation was more pronounced in the superheater deposits when compared to the probe deposits. However, the probe deposit samples proved that sulphation is also of relevance during regular boiler operation, as sulphated regions were observed in the 5 and 8-week probe deposits.

When comparing the 5-week probe deposit with the 8-week probe deposit, differences in the location of the sulphated region were observed. After an exposure time of 8 weeks, the sulphated region was seen closest to the steel. Whereas after an exposure time of 5 weeks, the sulphated region was seen mid-deposit, at some distance from the steel surface. The SO₂ concentration has been measured in the flue gas stack during both probe sampling periods. Analysis of the data showed that the SO₂ concentration was elevated for a short period for both experiments, but was otherwise essentially zero. A period of elevated SO₂ concentration in the flue gas stack was identified 11 days after the 5-week exposure was started, and 5 days after the 8-week exposure was started. Therefore, the probe deposit of 8 weeks exposure time was sulphated closer to the steel than the probe deposit obtained after 5 weeks.

Besides the differences in the location of the sulphated region within the probe deposits, differences in the chemical composition of the Cl layer that formed directly on the steel surface were observed. For the 5-week probe sample shown in Figure 16, the layer on the steel surface was concurrently enriched in Cl and K. For the 8-week probe deposit shown in Figure 17, no enrichment in K was observed within the Cl-rich layer on the steel surface. The differences in the chemical composition of the Cl layer are caused by corrosion

[48]. The governing corrosion mechanism is active oxidation. Alkali chlorides (NaCl and KCl) attack the steel surface and form FeCl_2 , whereas alkali metals form volatile hydroxides, which can subsequently react with the oxide layer and form alkali ferrates. The formation of $\text{Na}_2\text{Fe}_2\text{O}_4$ is favoured over the formation of $\text{K}_2\text{Fe}_2\text{O}_4$ [48], thus the majority of the formed KOH diffuses away from the steel surface. Hence no enrichment in K is observed within the Cl layer adjacent to the steel surface. The probe measurements proved that a corrosive alkali chloride layer can form directly on the steel surface under boiler conditions due to deposit ageing.

Analogous to the Brazilian deposits, the impact of the different enrichment patterns on the local T_0 of the Finnish deposits was analysed. In Figure 18, three deposits are shown together with their corresponding molar $\text{Cl}/(\text{Na}+\text{K})$, $\text{K}/(\text{Na}+\text{K})$, $\text{S}/(\text{Na}+\text{K})$ ratios, and T_0 profile.

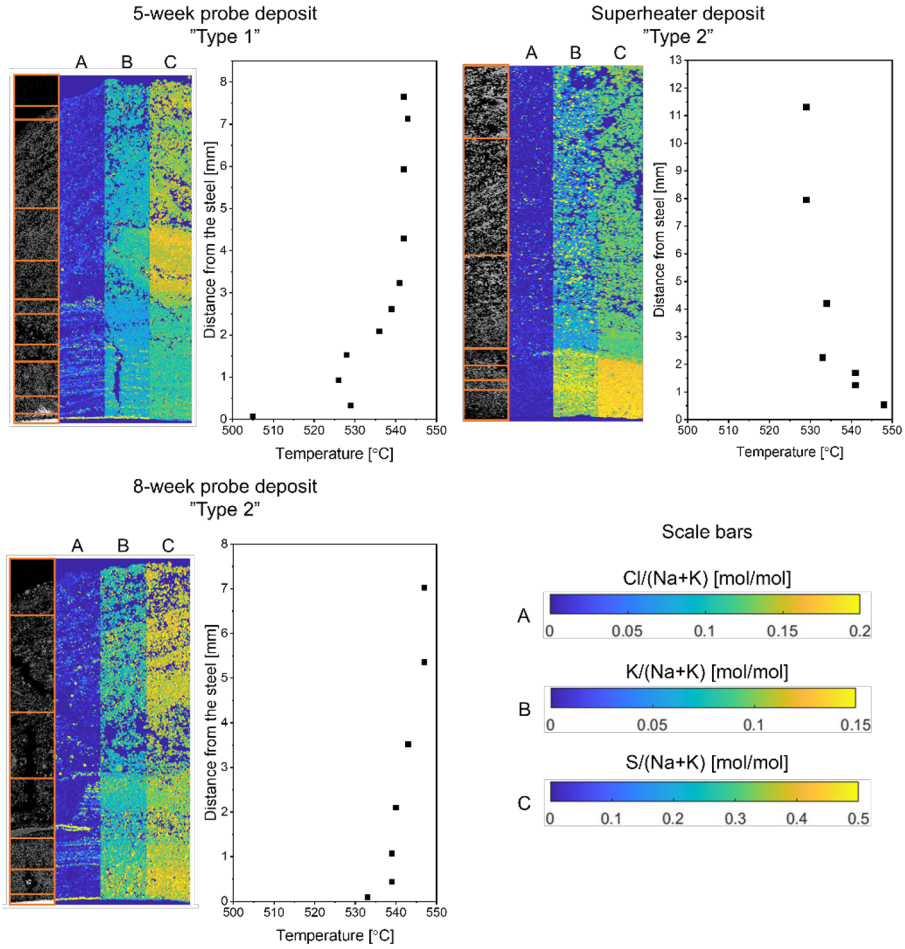


Figure 18: Local T_0 profiles and corresponding molar Cl/(Na+K), K/(Na+K), and S/(Na+K) profiles of Finnish boiler deposits. "Type 1" 5 week probe deposit (top left); "Type 2" superheater deposit (top right); "Type 2" 8 week probe deposit (bottom left). Adapted with permission from Paper II and Paper III under a CC-BY-4.0 license. Copyright © 2023 Elsevier

The probe deposit in the top left corner of Figure 18 is of "Type 1" and a Cl and K layer was found on the steel surface. The calculated local T_0 throughout the Cl and K-rich region was lower compared to the outer part of the deposit. The observed decrease in the T_0 is in line with the observations made in the Brazilian deposits. In kraft recovery boiler deposits an increase in the K-content lowers the T_0 . The local T_0 reached a minimum in the Cl and K-rich layer adjacent to the steel surface and reached almost the global minimum of the K, Na, Cl, SO_4 , and CO_3 system (501 °C) [47].

The innermost region of the superheater deposit in the top right corner of Figure 18 was sulphated with concurrent enrichment in K. The local T_0 within the sulphated region was higher as compared to the outer parts of the deposit,

despite the local enrichment in K. However, with the molar $\text{Cl}/(\text{Na}+\text{K})$ ratio throughout the sulphated region being below 0.015, the K enrichment does not cause any decrease in the T_0 [7]. Furthermore, the enrichment in S increases the SO_4/CO_3 ratio, causing the observed increase in the T_0 throughout the sulphated region.

The innermost region of the probe deposit in the bottom left corner of Figure 18 was sulphated but to a lesser extent compared to the superheater deposit. Furthermore, a layer of Cl was found on the steel surface. A slight decrease in the local T_0 was seen in the Cl layer directly on the steel surface. However, for the Cl and K-rich layer in the 5-week probe deposit on the top left corner of Figure 18, the T_0 reached a significantly lower temperature. An increase in the local Cl content without concurrent K enrichment does not cause a significant decrease in the T_0 [5,26,37], as the deposit K content has a greater impact on the T_0 . Hence the Cl and K-rich layer reached significantly lower T_0 values. However, the lack of K in the Cl layer of the 8-week probe deposit is the result of corrosion via active oxidation. Corrosion products that form during the reactions can lower the T_0 significantly to values well below the steel temperature [49], causing even more severe melt-induced corrosion. The calculated T_0 profiles did not consider elements other than K, Na, Cl, S, C, and O. Hence the impact of formed corrosion products such as FeCl_2 on the T_0 was not considered in the presented T_0 profiles.

For the sulphated region of the 8-week probe deposit, no increase in the local T_0 was seen, as sulphation did not proceed to the same extent as for the superheater deposits. An increase in the local T_0 due to sulphation was not observed in any of the probe deposit samples.

4.2. Impact of amount of melt on deposit ageing

Significant morphological differences were seen between the Brazilian and Finnish boiler deposits, also affecting the ageing behaviour of the deposit. The Brazilian deposits had a dense morphology and transport of a K-Cl-rich melt toward the steel had taken place. In contrast, the Finnish deposits remained porous and did not show any signs of melt movement toward the steel. The amount of melt formed in the deposits was considered as the potentially important parameter resulting in these differences.

To get a better understanding of the initial melting behaviour of ash deposits, short-term laboratory experiments using synthetic ash deposits were carried out. The goal was to identify the parameter determining the final deposit morphology and a threshold value for when the deposit morphology changes.

Analogous to the boiler deposits, two archetype morphologies emerged from the laboratory experiments. The final deposit morphology of the laboratory experiments was strongly connected to the initial Cl content in the synthetic salts, hence the amount of melt formed during the experiment. The maximum amount of melt formed within the laboratory deposit was calculated using FactSage 8.1. During the experiment, a thermocouple located just above

the outer deposit surface was continuously recording the temperature. The measured temperature was defined to be equal to the outer surface temperature of the deposit. Based on the initial composition of the synthetic deposit, the amount of melt formed at the highest temperature recorded during the experiment was calculated.

A total of 33 cross-sections comprising short and long-term laboratory deposits as well as boiler deposits were analysed regarding their morphology. Based on the SEM images of the cross-sections the samples were categorized as skeletal or molten, corresponding to the porous Finnish deposits and the dense Brazilian deposits, respectively. The graph shown in Figure 19 gives a summary of the morphologies of the analysed deposits.

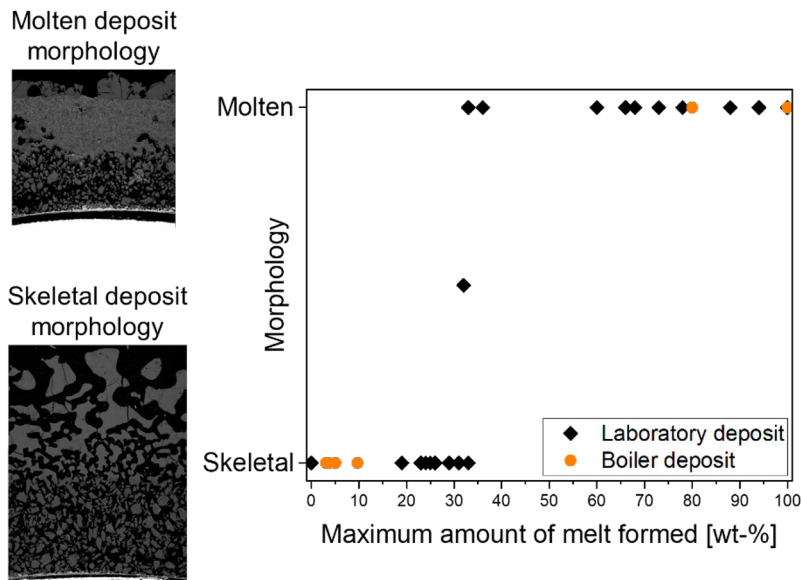


Figure 19: Classification of final deposit morphology into skeletal or molten as a function of maximum amount of melt formed. Adapted with permission from Paper IV under a CC-BY-4.0 license. Copyright © 2023 Elsevier

In the graph, the final deposit morphology is plotted as a function of the maximum amount of melt formed at the outer deposit surface during the exposure. The transition from a skeletal to molten deposit morphology takes place at about 30 wt-% melt. It should be noted that the amount of melt referred to in Figure 19 is based on the temperature measured at the outer deposit surface. As the deposit is exposed to a temperature gradient during the whole exposure, the highest temperature within the cross-section prevails at the outer surface furthest away from the steel. The local deposit temperature decreases toward the steel surface, hence the amount of melt decreases and is not constant throughout the whole cross-section.

Among the boiler deposits included in the graph, a skeletal morphology was exclusively observed for Finnish deposit samples and a molten morphology exclusively for Brazilian deposits. The higher Cl content in the Brazilian

deposits caused the formation of larger amounts of melt during boiler operation, enabling the formation of a molten morphology. For the boiler deposits, the temperature at the outer deposit surface was assumed to be equal to the estimated flue gas temperature at the deposit sampling location.

The suggested threshold of 30 wt-% melt for a molten layer to form is in good agreement with reference values found in the literature. For liquid phase sintering, approximately 30 vol-% liquid is required to efficiently fill the pores of a porous medium [45]. Further, the average porosity of random packings is within the range of 26 vol-% to 36 vol-% [50].

Besides the identification of a threshold value for the formation of a molten layer, additional observations were made when analysing the laboratory deposits. A better understanding of the formation of a skeletal deposit morphology was obtained from short-term laboratory experiments. A magnified image of the skeletal region of a 0-minute experiment is shown in Figure 20.

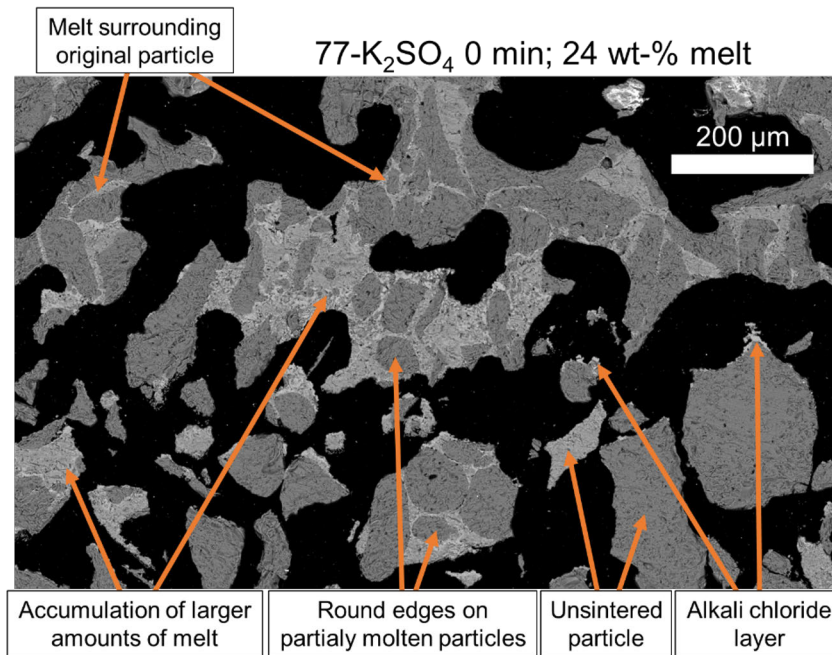


Figure 20: Skeletal region of a synthetic deposit of 0-minute exposure time highlighting its main characteristics. Reprinted with permission from Paper IV under a CC-BY-4.0 license. Copyright © 2023 Elsevier

Accumulations of larger amounts of melt (white areas) are seen in the skeletal region of the deposit. The SEM images of the short-term experiments clearly show that melt was formed in the skeletal structure of the deposits. The amount of melt was not sufficient to initiate pore filling for a molten morphology to form. However, as the melt was predominantly found at contact areas of distinct particles, it was identified to accelerate the formation of the skeletal structure. The round edges and the lack of alkali chloride within the particles

surrounded by melt further indicated partial melting of these particles. In general, sintering processes are known to be accelerated significantly by the presence of a melt [45] and without the presence of a melt, no skeletal layer would have been formed during the short-term experiments as solid-state sintering processes are significantly slower.

For skeletal deposits of longer exposure times, the alkali chlorides tend to evaporate and diffuse either into the furnace or toward the steel and the skeletal region is depleted in alkali chloride. Also, within the 0-minute experiment shown in Figure 20, some of the alkali chlorides have evaporated and diffused toward the steel, resulting in the formation of the alkali chloride layers on the furnace-facing side of particles at lower local temperatures.

With an increasing amount of melt in the deposits, larger agglomerates were observed. Of the analysed cross-sections, one sample could neither be classified on an either-or basis into skeletal or molten and was therefore categorized to be of intermediate morphology. A greyscale SEM image of the cross-section of the sample in question is shown in Figure 21.

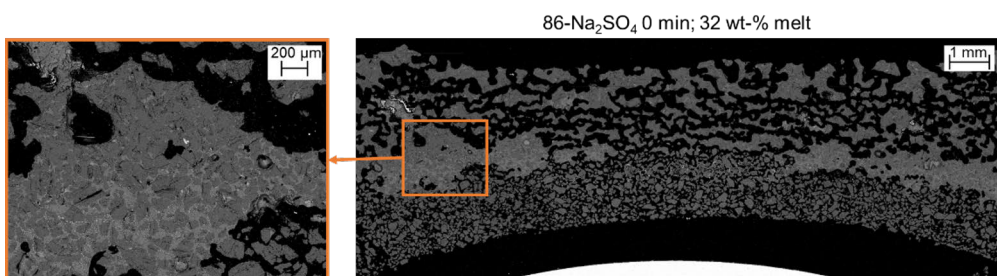


Figure 21: Cross-sectional SEM image of morphological intermediate and magnification of molten agglomerate mid-deposit (left). Adapted with permission from Paper IV under a CC-BY-4.0 license. Copyright © 2023 Elsevier

The outer region of the deposit formed a skeletal morphology. Mid-deposit, larger agglomerates and the onset of the formation of a molten layer are seen. Further, the close-up image of the molten region on the left of Figure 21 shows the formation of two distinct layers. The outer layer of the molten region (toward the furnace) is depleted in Cl compared to the layer closer to the steel. The enrichment in Cl toward locally lower temperatures indicated melt moving toward the steel according to the mechanism described in 2.3.2.

The formation mechanism of the observed morphology can be explained as follows: Melt initially forms in the outermost regions of the deposit, from where it subsequently moves toward the steel due to gravitational and capillary forces. This leaves behind the skeletal structure at the outer deposit surface. As the melt moves toward the steel it accumulates and starts to form the observed larger agglomerates mid-deposit. In the present case, the amount of melt is not sufficient to cover the whole cross-section with a molten layer, hence larger accumulations of melt are only seen at the outer edges of the deposit.

When further increasing the melt fraction, the deposit morphology changes to that of molten deposits. Three molten deposits are shown in Figure 22 illustrating the development of the molten layer with increasing melt fractions.

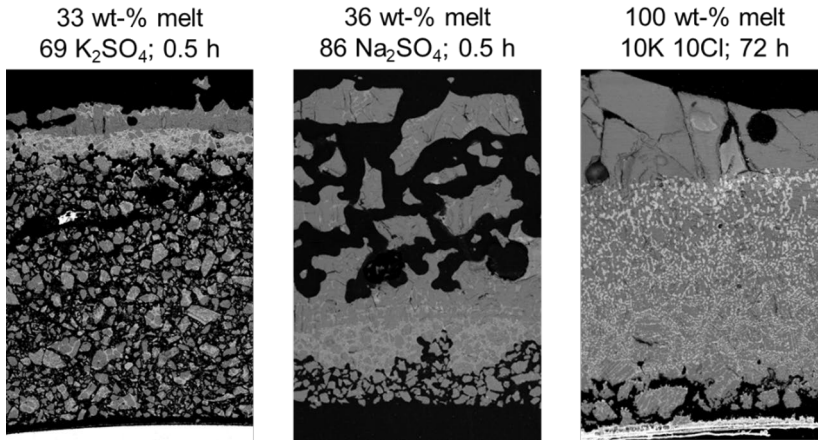


Figure 22: Cross-sectional SEM images of selected laboratory deposits of molten morphology with increasing maximum amount of melt formed at the outer deposit surface from left to right. Adapted from Paper IV under a CC-BY-4.0 license. Copyright © 2023 Elsevier

The image on the left shows the molten deposit with the lowest melt fraction. The molten layer is located at the outer deposit surface, and no movement of melt toward the steel was seen in the cross-section. However, similar to the morphological intermediate shown in Figure 21, two distinct layers were identified in the molten region. The outer layer of the molten region was depleted in Cl (dense, grey layer), as the Cl-rich melt moved toward the steel (dense, white layer).

The salt that was used for the morphological intermediate in Figure 21 was also used for the deposit shown in the middle of Figure 22. For the deposit in the middle of Figure 22, the temperature measured at the outer deposit surface was slightly higher, resulting in the maximum amount of melt having been 4 wt-% higher compared to the morphological intermediate in Figure 21. The small increase in melt fraction, due to the higher temperature at the outer deposit surface, was sufficient for the molten layer to cover the whole cross-section. Analogous to the morphological intermediate, the molten layer is found in the middle of the cross-section, indicating that a large share of the melt had initially formed at the outer deposit surface, from where it subsequently moved toward the steel where it accumulated and formed the molten layer.

Differences in the melting behaviour of the 69- K_2SO_4 and 86- Na_2SO_4 salts resulted in molten layers at different locations, although the melt amounts were nearly equal. The 69- K_2SO_4 salt forms 30 wt-% melt at a T_0 of 690 °C. As the maximum amount of melt formed in that deposit was 33 wt-% at a temperature at the outer deposit surface of 731 °C, only the outermost region of the deposit reached temperatures above the T_0 . Hence, the formed melt

could not move toward the steel. The 86- Na_2SO_4 salt on the other hand forms 20 wt-% melt at a T_0 of 626 °C, and the maximum melt fraction formed during the experiment was 36 wt-%, at an outer deposit temperature of 725 °C, which is 100 °C above the salt's T_0 . This implies that a larger region of the outer part of the deposit reached temperatures above the T_0 , and melt could move closer toward the steel before solidifying. Therefore, for the 86- Na_2SO_4 deposit, melt was formed over a larger area of the cross-section and the formed melt moved toward the steel, where it subsequently accumulated in the middle of the deposit forming the molten layer seen in Figure 22.

The deposit shown on the right of Figure 22 consisted of a ternary reciprocal salt. In this sample, the melt has moved significantly closer toward the steel than initially expected. Analysis of the elemental composition of the molten region showed enrichment in K toward the steel, analogous to the superheater deposits from the Brazilian kraft recovery boiler. The local enrichment in K of the melt caused a decrease in the T_0 of the melt compared to the T_0 of the initial deposit composition. This enabled the presence of a melt significantly closer to the steel, almost reaching the steel surface. The results of the ternary reciprocal systems gave additional validation for the laboratory temperature gradient set up to replicate conditions in actual superheater deposits reasonably well, as the results are in good agreement with observations made in the full-scale boiler deposits presented in Chapter 4.1.

4.3. Applicability of results to other combustion processes

The results presented so far focused on deposit ageing in the context of kraft recovery boilers. In Paper V, laboratory temperature gradient experiments were carried out to study whether the so far identified deposit ageing mechanisms are also applicable to ash deposits of compositions other than those found in kraft recovery boilers. Therefore, synthetic deposits consisting of $\text{NaBr-Na}_2\text{SO}_4$ and $\text{KBr-K}_2\text{SO}_4$ were utilised.

In combustion processes, bromides can be found in processes utilizing solid waste-derived fuels. Bromide is a constituent of flame retardants used for wood and plastics [51,52]. In nature, the sea is the largest reservoir for bromide. Thus, plants in coastal regions have been observed to be enriched in bromine compared to their inland counterpart [53]. Furthermore, some marine algae species have been identified to accumulate bromine [53].

Alkali bromides were chosen due to their similarity to alkali chlorides in molecular structure, melting behaviour and chemistry. Bromides also form volatile compounds with alkali metals [51]. The Br-containing mixtures can be used to identify whether the observed deposit ageing mechanisms are exclusive to alkali chlorides or if the mechanisms are general and also applicable to deposits of other compositions.

In the laboratory experiments, synthetic deposits were exposed to a temperature gradient for 2, 4, and 8 hours. An SEM backscatter image of a deposit cross-section after an exposure time of 4 h is shown in Figure 23.

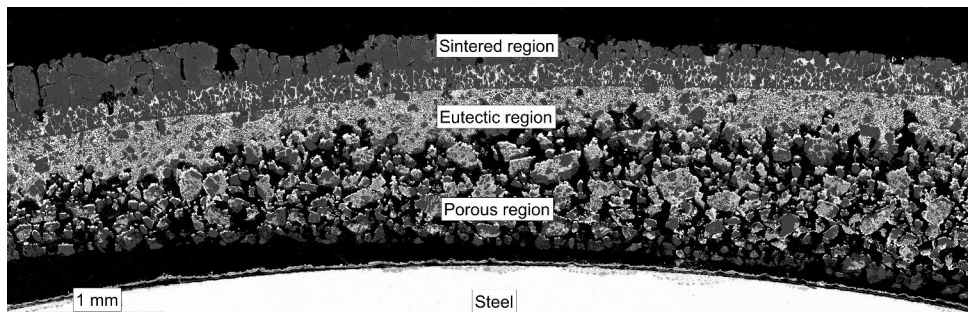


Figure 23: SEM backscatter image of synthetic $\text{NaBr-Na}_2\text{SO}_4$ deposit after an exposure time of 4 h. Reprinted with permission from Paper V under a CC-BY-4.0 license. Copyright © 2019 American Chemical Society

The overall morphological features seen in the cross-section of the Br-containing deposit were similar to those identified in the synthetic Cl-containing deposits. Three distinct layers were also identified for the cross-sections of the synthetic Br deposits. The outer region had a molten morphology and vertical channels of alkali bromide were observed in this region. After 8 hours, the outer part of the deposit was depleted in bromide and contained only alkali sulphate. The Br-rich channels perpendicular to the steel surface and the depletion in Br over time are indicators for temperature gradient zone melting. Due to the temperature gradient and the temperature dependence of the composition of the melt, alkali bromide-rich melt moves toward the outer deposit surface.

Closer to the steel, within the molten region of the deposit, a region enriched in Br compared to the initial composition was observed. The Br-rich region had a composition close to the eutectic composition. Analogous to the Brazilian superheater deposits and previously presented laboratory experiments with alkali chloride-containing deposits, the formed melt moved toward the cooler steel and was enriched in alkali bromide. As the used binary salts are eutectic systems, the composition of the melt follows the liquidus line and approaches the eutectic point as the local temperature decreases. The first melting temperature of the remaining melt of the used binary salts is not affected by compositional changes and the T_0 is equal to the system's eutectic temperature.

In the deposit region where local temperatures did not exceed the T_0 , the deposit particles retained their original shape. On the furnace-facing side of the particles, layers of alkali bromide formed. Alkali bromides, both NaBr and KBr, evaporate from the original particles and subsequently diffuse toward the steel, where the vapours condense on the surface of cooler particles. Analogous to earlier experiments with alkali chloride deposits, the driving force for the diffusional transport is the concentration gradient for alkali bromides in the

gas phase. The vapour pressures of NaBr and KBr are temperature-dependent and increase exponentially with increasing temperature. Hence a concentration gradient for NaBr and KBr vapours prevails in the gas phase. In addition, alkali bromides were also observed to have deposited directly on the steel surface. On the steel surface iron and chromium bromides formed due to corrosion of the steel sample ring, initiated by the alkali bromide layer.

The results from Paper V show that deposit ageing, and especially mechanisms observed earlier in kraft recovery boiler deposits, are also of relevance to deposits other than those found in kraft recovery boilers. Volatile compounds were identified to diffuse toward the steel by Fickian diffusion and causing corrosion of the steel sample. Furthermore, movement of melt and element enrichment within the melt, and temperature gradient zone melting were identified in the alkali bromide-containing deposits.

However, when comparing the measured halide layer thickness on the particles in the porous region of the Cl-containing deposit with the Br-containing deposits significant differences were observed. After an exposure time of 4 hours using the NaBr-Na₂SO₄ salt, layer thicknesses comparable to those of a 24-hour experiment using a NaCl-Na₂SO₄ salt [8] were observed. The measured average layer thicknesses of these two experiments and the calculated vapour pressures of alkali chloride and bromide are shown in Figure 24.

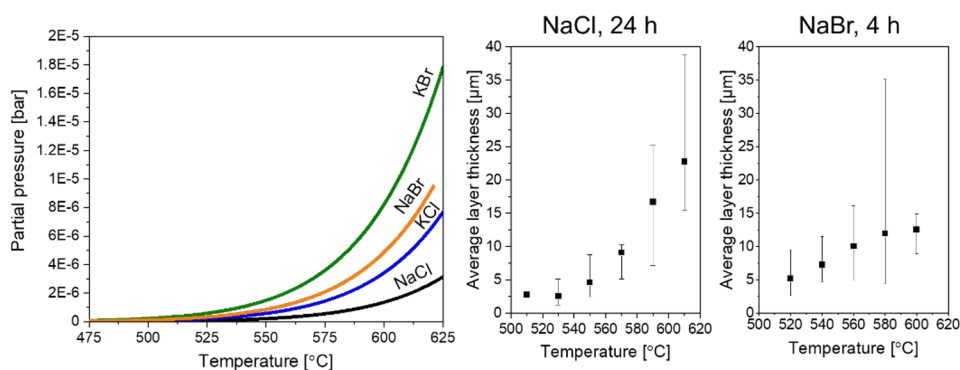


Figure 24: Vapour pressures of NaCl, KCl, NaBr, and KBr and measured average thickness of alkali halide layers on particles in the porous deposit region for NaCl after an exposure time of 24 h [8] and NaBr after an exposure time of 4 h. The error bars resemble the maximum and minimum layer thickness measured for the respective temperature interval.

Alkali bromides have higher vapour pressures compared to alkali chlorides, as the vapour pressure increases with increasing size of the anion or cation. Furthermore, the partial pressure increases exponentially with increasing temperature, and thus the concentration gradient for alkali bromide is larger than for alkali chloride for the same temperature interval. Based on the first Fickian law of diffusion, the diffusion flux increases linearly with increasing concentration gradient. Hence the diffusion flux for alkali bromides is higher

than for alkali chlorides at the same temperature and temperature gradient. The observations from the bromide deposits gave further confirmation that the layer formation is the result of concentration gradient-induced diffusion of alkali halides toward the steel due to a temperature gradient.

4.4. Updated understanding of deposit ageing and practical implications

The work presented in this thesis provides new insights into deposit ageing mechanisms. Furthermore, the obtained boiler deposits confirmed that deposit ageing mechanisms also occur under operating boiler conditions. Previously, these mechanisms were identified and studied only under well-controlled laboratory conditions. Figure 25 gives a summary of the current understanding of deposit ageing.

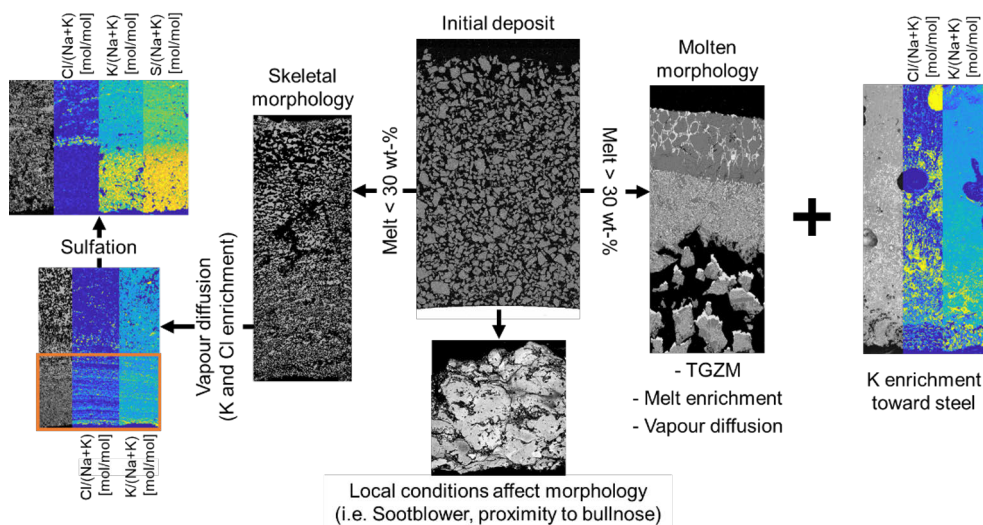


Figure 25: Summary of current understanding of deposit ageing in kraft recovery boilers based on the results obtained in this thesis

Based on the deposit composition and the surrounding temperatures, deposits form either a skeletal or molten morphology. The final deposit morphology is mainly influenced by the maximum amount of melt formed in the deposit. If the maximum amount of melt formed in the deposit exceeds about 30 wt-%, a molten deposit morphology is formed. For molten deposits, the three governing deposit ageing mechanisms are temperature gradient zone melting, movement of melt toward the steel coupled with concurrent element enrichment in the melt, and diffusional transport of alkali chloride vapours toward the steel.

If the amount of melt formed in the deposit does not exceed 30 wt-%, a skeletal deposit morphology develops. Due to the lack of a molten layer, the only deposit ageing mechanism identified in skeletal deposits was diffusional gas phase transport of alkali chloride vapours toward the steel. The porous deposit morphology enables alkali chloride vapours to diffuse through the outer region of the deposit and condense within the deposit at regions closer to the steel, where local temperatures are lower. Furthermore, sulphation of the deposit regions originally enriched in alkali chlorides was observed.

For some of the analysed deposits, significant differences in the overall deposit morphology were observed. The direct vicinity of the sampling location to a sootblower or proximity to the bullnose can affect the deposition behaviour, deposit morphology, and consequently the ageing behaviour.

Overall, the results presented in this thesis show that deposit ageing is of relevance in actual kraft recovery boiler superheater deposits obtained from industrial boilers. The results emphasize that accurate knowledge of the bulk deposit composition is not sufficient when dealing with deposit-induced operational issues. Due to deposit ageing, the local composition of a deposit can change significantly, affecting deposit corrosiveness and removability. The boiler deposits also verified that the temperature gradient probe set-up used for laboratory scale studies is a suitable method for studying deposit ageing mechanisms under well-controlled conditions.

The local enrichment in K and Cl toward the steel due to the movement of melt or gas phase diffusion was shown to locally affect the T_0 . Both mechanisms lowered the local T_0 to values close to the global T_0 of the chemical system. When designing a boiler, the maximum steam temperature is typically set to be well below the bulk T_0 of the fuel ash, to avoid the presence of a melt directly on the steel surface. However, the results of this work showed that the deposit T_0 locally can reach values significantly lower than the T_0 of the bulk ash composition, due to deposit ageing. Hence, element enrichment through deposit ageing significantly increases deposit corrosiveness by locally lowering the T_0 and thus increasing the risk for melt-induced corrosion.

The results of this thesis also provide more fundamental explanations for observations made in earlier deposit studies. Costa et al. [11] reported severe corrosion of the hottest superheater tubes in a kraft recovery boiler. Deposit samples obtained from these tubes confirmed enrichment in K and Cl toward the steel-facing side of the deposit resulting in a lower T_0 . The superheater deposits from a Brazilian recovery boiler presented in this thesis were obtained from the same boiler. The detailed analysis of these deposits provided a fundamental explanation of the underlying mechanisms resulting in the observed enrichment in K and Cl toward the steel.

Reeve et al. [40] have observed local element enrichment in an 800 h probe deposit obtained from a kraft recovery boiler. The deposits were enriched in K and Cl toward the steel and the outer deposit surface, resulting in a concentration minimum in the middle of the deposit. The observations were explained by the deposit formation mechanisms, where an initial layer of fume forms an inner layer enriched in K and Cl. The results presented in this thesis showed, however, that the local enrichment in K and Cl toward the steel can also be contributed by deposit ageing mechanisms. Further, the enrichment in K and Cl toward the outer deposit surface can be due to temperature gradient zone melting, in case the probe deposit obtained by Reeve et al. was of a molten morphology.

The superheater deposits also showed the connection between their morphology and the observed ageing mechanisms. A porous morphology

enables flue gases to diffuse into the formed deposit and interact with the deposit as either additional vapours condense within the deposit or react with already deposited material. For deposits of a molten morphology, the dense outer layer prevents flue gases from diffusing into the deposit and thus also hinders any subsequent reactions from taking place.

The suggested threshold value of about 30 wt-% melt required for a molten morphology to form can help in identifying the relevant deposit ageing mechanisms for a specific process. Furthermore, the results can help in estimating the deposit removability based on the final morphology, and thus the sootblowing frequencies can be optimised.

In the laboratory experiments in which synthetic deposits of NaBr-Na₂SO₄ and KBr-K₂SO₄ were used, the same deposit ageing mechanisms as for Cl-containing deposits were identified. The results imply that the underlying mechanisms of deposit ageing are not specific to certain elements, such as alkali chlorides. Hence the results are also applicable to systems other than kraft recovery boiler deposits.

5. Conclusions

In this thesis, temperature gradient-induced changes in the morphology and chemical composition of ash deposits were studied. Cross-sections of superheater deposits from a Brazilian and Finnish kraft recovery boiler were analysed. Further, probe deposit samples were obtained from the Finnish boiler, enabling analysis of deposits of different ages, while still attached to the metal surface they formed on. In addition to the full-scale data, laboratory experiments were carried out using synthetic ash deposits. The objective of the work was to get a better understanding of the local changes in deposit morphology and chemical composition over time, also referred to as deposit ageing.

In earlier work, three deposit ageing mechanisms have been identified in laboratory-scale experiments using synthetic ash deposits. These three deposit ageing mechanisms were now also identified to take place in actual superheater ash deposits. The kraft recovery boiler deposits analysed in this work confirmed that deposit ageing is also of relevance in actual boiler deposits. Furthermore, the results verified that the laboratory setup is suitable for studying deposit ageing mechanisms and the impact of a temperature gradient on synthetic deposits under well-controlled conditions.

For molten deposits with a sufficiently high K content, local enrichment in K toward the steel was observed in the molten region of the deposit. The melt, formed in the outer regions of the deposit, had a lower first melting temperature than the bulk deposits. Hence, the formed melt can move toward the steel due to capillary forces. The local deposit temperature decreases toward the steel, and the melt solidifies partially. In the analysed kraft recovery boiler deposits, the primary crystallising phase consists predominantly of Na_2SO_4 and Na_2CO_3 , thus the remaining melt is enriched in K. As a consequence of the local K enrichment, the deposit T_0 decreases locally and a minimum is reached for the highest K-concentration. Depending on the operating conditions of the boiler, the local decrease in the T_0 can allow the presence of a melt adjacent to the steel surface which would result in severe melt-induced corrosion of the heat transfer surface.

The probe deposit samples of exposure times of 1, 5, and 8 weeks showed enrichment in the average Cl content over time. Due to the porous deposit morphology, alkali chloride vapours from the flue gas diffused into the deposit, driven by the temperature-gradient induced vapour concentration difference between the hot flue gas and the cooler steel surface. The alkali chloride vapours then subsequently condensed at lower temperatures, resulting in the observed increase in the Cl content over time. The enrichment in bulk deposit Cl follows the same underlying mechanism as the intra-depositional vapour diffusion in the porous region of the deposit. The probe measurements could also show the formation of a corrosive Cl-layer with concurrent enrichment in K directly on the steel surface, which also caused a significant decrease in the local T_0 compared to the bulk deposit T_0 .

Since a significantly lower T_0 was observed, the maximum steam temperature in the superheater tubes should not simply be determined based on the T_0 of the bulk deposit but also local deposit conditions should be considered. The results obtained in this thesis imply that the T_0 can locally reach values as low as the global minimum of the chemical system.

In addition, short-term laboratory experiments were carried out in this thesis to identify the parameter determining the final deposit morphology. The analysed superheater deposits showed significant differences in their ageing behaviour, depending on their final morphology. In the molten deposits from the Brazilian boiler, all three deposit ageing mechanisms identified earlier were observed. In the skeletal deposits from the Finnish boiler, only vapour diffusion was observed. A molten morphology was identified to form when the amount of melt formed within the deposit exceeds about 30 wt-%. Molten and skeletal deposit morphologies were already observed in samples of very short exposure time. For skeletal morphologies, small amounts of melt were seen to accumulate at contact points of the original deposit particles, accelerating the sintering of the outer deposit region.

Additionally, laboratory experiments with different deposit compositions showed that the three deposit ageing mechanisms were identified regardless of composition and that the mechanisms are not exclusive to Cl-containing deposits. The underlying mechanisms are based on the thermodynamic and physical deposit properties. Hence the identified deposit ageing mechanisms are also applicable to processes other than kraft recovery boilers and can be predicted with proper understanding of the chemical system and process details.

References

- [1] European Commission. European Climate Law n.d.
https://climate.ec.europa.eu/eu-action/european-green-deal/european-climate-law_en (accessed June 22, 2023).
- [2] Vakkilainen EK. Chapter 11 Recovery Boiler. *Steam Generation from Biomass*, Elsevier; 2017, p. 237–59. <https://doi.org/10.1016/B978-0-12-804389-9.00011-3>.
- [3] Adams TN, Frederick WJ, Hupa M. *Kraft Recovery Boilers*. New York (NY) : Atlanta (GA) : American Forest & Paper Association ; Tappi Press 1997; 1997.
- [4] Tran HN, Reeve DW, Barham D. Formation of Kraft Recovery Boiler Superheater Fireside Deposits. *Pulp and Paper Canada* 1983;84:36–41.
- [5] Reeve DW, Tran HN, Barham D. The effluent-free bleached kraft pulp mill - Part XI Morphology, chemical and thermal properties of recovery boiler superheater fireside deposits. *Pulp & Paper Canada* 1981;82:T315–20.
- [6] Leppänen A, Tran H, Taipale R, Välimäki E, Oksanen A. Numerical modeling of fine particle and deposit formation in a recovery boiler. *Fuel* 2014;129:45–53. <https://doi.org/10.1016/j.fuel.2014.03.046>.
- [7] Tran H. Recovery boiler fireside deposits and plugging prevention. *TAPPI Kraft Recovery Course* 2007 n.d.;2:537–72.
- [8] Niemi J, Lindberg D, Engblom M, Hupa M. Simultaneous melt and vapor induced ash deposit aging mechanisms – Mathematical model and experimental observations. *Chemical Engineering Science* 2017;173:196–207. <https://doi.org/10.1016/j.ces.2017.07.041>.
- [9] Lindberg D, Niemi J, Engblom M, Yrjas P, Laurén T, Hupa M. Effect of temperature gradient on composition and morphology of synthetic chlorine-containing biomass boiler deposits. *Fuel Processing Technology* 2016;141:285–98. <https://doi.org/10.1016/j.fuproc.2015.10.011>.
- [10] Niemi J, Lindberg D, Engblom M, Tran H. A Fundamental Study on the Change in Composition of Fireside Deposits with Time in Kraft Recovery Boilers. *Journal of Science and Technology for Forest Products and Processes* 2018;7:45–52.
- [11] Costa A, Silva D, Abelha F, Cenibra CNSA. EXPERIENCE OF RECOVERY BOILER SUPERHEATER CORROSION AT CENIBRA. *International Chemical Recovery Conference - ICRC*, Halifax, Canada: 2017.
- [12] Food and Agriculture Organization of the United Nations n.d.
<https://www.fao.org/faostat/en/#data/FO> (accessed June 15, 2023).
- [13] Tikka P. *Papermaking Science and Technology / 6. Chemical Pulping. Part 2: Recovery of Chemicals and Energy*. 2., totally updated ed. Helsinki: Paperi ja Puu Oy; 2008.
- [14] Vakkilainen EK. *Kraft recovery boilers - Principles and practice*. Suomen Soodakattilayhdistys r.y.; 2005.
- [15] Biermann CJ. *Handbook of pulping and papermaking*. 2nd ed. San Diego: Academic Press; 1996.

- [16] Smook GA. Handbook for pulp & paper technologists. 2nd ed. Vancouver: Angus Wilde Publications; 1992.
- [17] Gullichsen J, Fardim P, Paulapuro H, Suomen Paperi-Insinöörien Yhdistys, editors. Fibre chemistry and technology. Second edition, totally updated version. Helsinki: Paper Engineers' Association; 2011.
- [18] Hubbe MA, Alén R, Paleologou M, Kannangara M, Kihlman J. Lignin Recovery from Spent Alkaline Pulping Liquors Using Acidification, Membrane Separation, and Related Processing Steps: A Review. *BioResources* 2019;14:2300–51.
- [19] Karlemo C. Non-process elements in the recovery cycle of six Finnish Kraft pulp mills. Master's Thesis. Åbo Akademi University, 2019.
- [20] Karlemo C, Engblom M, Vakkilainen E. Non-process elements in the recovery cycle of six Finnish kraft pulp mills. *TJ* 2023;22:184–92. <https://doi.org/10.32964/TJ22.3.184>.
- [21] Cardoso M, Oliveira ÉD de, Passos ML. Chemical composition and physical properties of black liquors and their effects on liquor recovery operation in Brazilian pulp mills. *Fuel* 2009;88:756–63. <https://doi.org/10.1016/j.fuel.2008.10.016>.
- [22] Tran HN. How does a kraft recovery boiler plugged? *Tappi Journal* 1986;69:102–6.
- [23] TNO Biobased and Circular Technologies. Phyllis2, database for (treated) biomass, algae, feedstocks for biogas production and biocha n.d. <https://phyllis.nl/Browse/Standard/ECN-Phyllis> (accessed June 5, 2023).
- [24] Mikkani P. Fly ash particle formation in kraft recovery boilers. 2000.
- [25] Mao X, Tran H. Formation of blue deposits in kraft recovery boilers. *PEERS Conference 2015: Sustainable Solutions for Our Future* 2015;2:1255–65. <https://doi.org/10.32964/TJ15.3.195>.
- [26] Frederick WJ, Vakkilainen EK. Sintering and Structure Development in Alkali Metal Salt Deposits Formed in Kraft Recovery Boilers. *Energy and Fuels* 2003;17:1501–9. <https://doi.org/10.1021/ef034012s>.
- [27] Kochesfahani, S.H., Tran, H., Jones, A.K., Grace, T.M., Lien, S.J., Schmidl, W. Particulate Formation During Black Liquor Char Bed Burning. *Journal of Pulp and Paper Science* 2000;26:180–7.
- [28] Mikkani P, Jokiniemi JK, Kauppinen EI, Vakkilainen EK. Coarse ash particle characteristics in a pulp and paper industry chemical recovery boiler. *Fuel* 2001;80:987–99. [https://doi.org/10.1016/S0016-2361\(00\)00195-2](https://doi.org/10.1016/S0016-2361(00)00195-2).
- [29] Mikkani P, Kauppinen EI, Pyykönen J, Jokiniemi JK, Aurela M, Vakkilainen EK, et al. Alkali salt ash formation in four Finnish industrial recovery boilers. *Energy and Fuels* 1999;13:778–95. <https://doi.org/10.1021/ef980189o>.
- [30] Zbogor A, Frandsen F, Jensen PA, Glarborg P. Shedding of ash deposits. *Progress in Energy and Combustion Science* 2009;35:31–56. <https://doi.org/10.1016/j.pecs.2008.07.001>.

- [31] Kleinhans U, Wieland C, Frandsen FJ, Spliethoff H. Ash formation and deposition in coal and biomass fired combustion systems: Progress and challenges in the field of ash particle sticking and rebound behavior. *Progress in Energy and Combustion Science* 2018;68:65–168. <https://doi.org/10.1016/j.pecs.2018.02.001>.
- [32] Jokiniemi JK, Pyykonen J, Mikkanen P, Kauppinen EI. Modeling fume formation and deposition in kraft recovery boilers. *TAPPI JOURNAL* 1996;79:171–81.
- [33] Wang Y, Tan H. Condensation of KCl(g) under varied temperature gradient. *Fuel* 2019;237:1141–50. <https://doi.org/10.1016/j.fuel.2018.10.046>.
- [34] Broström M, Enestam S, Backman R, Mäkelä K. Condensation in the KCl-NaCl system. *Fuel Processing Technology* 2013;105:142–8. <https://doi.org/10.1016/j.fuproc.2011.08.006>.
- [35] Sinquefield SA. Deposition of sub-micron and micron-sized particles from combustion of black liquor. PhD thesis. Oregon State University, 1998.
- [36] Cameron JH, Goerg-Wood K. Role of thermophoresis in the deposition of fume particles resulting from the combustion of high inorganic containing fuels with reference to kraft black liquor. *Fuel Processing Technology* 1999;49–68.
- [37] Tran H, Gonsko M, Mao X. Effect of composition on the first melting temperature of fireside deposits in recovery boilers. *TAPPI Journal* 1999;82:93–100.
- [38] Tran HN, Barham D, Reeve DW. Sintering of Fireside Deposits and Its Impact on Plugging in Kraft Recovery Boilers. *Tappi Journal* 1988;71:109–13.
- [39] Jensen PA, Frandsen FJ, Hansen J, Dam-Johansen K, Henrisken N, Hörlyck S. SEM investigation of superheater deposits from biomass-fired boilers. *Energy and Fuels* 2004;18:378–84. <https://doi.org/10.1021/ef030097l>.
- [40] Reeve DW, Tran HN, Barham D. Superheater Fireside Deposits and Corrosion in Kraft Recovery Boilers. *Tappi* 1981;64:109–13.
- [41] Hansen LA, Nielsen HP, Frandsen FJ, Dam-Johansen K, Hörlyck S, Karlsson A. Influence of deposit formation on corrosion at a straw-fired boiler. *Fuel Processing Technology* 2000;64:189–209. [https://doi.org/10.1016/S0378-3820\(00\)00063-1](https://doi.org/10.1016/S0378-3820(00)00063-1).
- [42] Lindberg D, Engblom M, Yrjas P, Laurén T, Lindholm J, Hupa M. Influence of deposit aging on superheater corrosion. 2014 International Chemical Recovery Conference, Tampere, Finland: Finnish Recovery Boiler Committee; 2014, p. 101–13.
- [43] Zbogor A, Frandsen FJ, Jensen PA, Glarborg P. Heat transfer in ash deposits: A modelling tool-box. *Progress in Energy and Combustion Science* 2005;31:371–421. <https://doi.org/10.1016/j.pecs.2005.08.002>.
- [44] Rettenmayr M. Melting and remelting phenomena. *International Materials Reviews* 2009;54:1–17. <https://doi.org/10.1179/174328009X392930>.

- [45] German RM, Suri P, Park SJ. Review: Liquid phase sintering. *Journal of Materials Science* 2009;44:1–39. <https://doi.org/10.1007/s10853-008-3008-0>.
- [46] Bale CW, Bélisle E, Chartrand P, Decterov SA, Eriksson G, Gheribi AE, et al. FactSage thermochemical software and databases, 2010-2016. *Calphad: Computer Coupling of Phase Diagrams and Thermochemistry* 2016;54:35–53. <https://doi.org/10.1016/j.calphad.2016.05.002>.
- [47] Lindberg D, Backman R, Chartrand P. Thermodynamic evaluation and optimization of the (NaCl + Na₂SO₄+ Na₂CO₃+ KCl + K₂SO₄+ K₂CO₃) system. *The Journal of Chemical Thermodynamics* 2007;39:1001–21. <https://doi.org/10.1016/j.jct.2006.12.018>.
- [48] Karlsson S, Pettersson J, Johansson L-G, Svensson J-E. Alkali Induced High Temperature Corrosion of Stainless Steel: The Influence of NaCl, KCl and CaCl₂. *Oxid Met* 2012;78:83–102. <https://doi.org/10.1007/s11085-012-9293-7>.
- [49] Jonsson T, Folkesson N, Svensson J-E, Johansson L-G, Halvarsson M. An ESEM in situ investigation of initial stages of the KCl induced high temperature corrosion of a Fe–2.25Cr–1Mo steel at 400°C. *Corrosion Science* 2011;53:2233–46. <https://doi.org/10.1016/j.corsci.2011.03.007>.
- [50] Berryman JG. Random close packing of hard spheres and disks. *Phys Rev A* 1983;27:1053–61. <https://doi.org/10.1103/PhysRevA.27.1053>.
- [51] Vainikka P, Enestam S, Silvennoinen J, Taipale R, Yrjas P, Frantsi A, et al. Bromine as an ash forming element in a fluidised bed boiler combusting solid recovered fuel. *Fuel* 2011;90:1101–12. <https://doi.org/10.1016/j.fuel.2010.11.032>.
- [52] Vainikka P, Bankiewicz D, Frantsi A, Silvennoinen J, Hannula J, Yrjas P, et al. High temperature corrosion of boiler waterwalls induced by chlorides and bromides. Part 1: Occurrence of the corrosive ash forming elements in a fluidised bed boiler co-firing solid recovered fuel. *Fuel* 2011;90:2055–63. <https://doi.org/10.1016/j.fuel.2011.01.020>.
- [53] Vainikka P. Occurrence of bromine in fluidised bed combustion of solid recovered fuel. PhD thesis. VTT, 2011.

Original publications

R. Balint, M. Engblom, J. Niemi, D. Silva da Costa, D. Lindberg, P. Yrjas, L. Hupa,
M. Hupa (2021)

**Temperature gradient induced changes within superheater ash deposits
high in chlorine.**

Energy



Temperature gradient induced changes within superheater ash deposits high in chlorine

Roland Balint ^{a,*}, Markus Engblom ^a, Jonne Niemi ^{a,b}, Daniel Silva da Costa ^c,
Daniel Lindberg ^{a,b}, Patrik Yrjas ^a, Leena Hupa ^a, Mikko Hupa ^a

^a Laboratory of Molecular Sciences and Engineering, Faculty of Science and Engineering (FNT) Åbo Akademi University, Åbo, Finland

^b Department of Chemical and Metallurgical Engineering, Aalto University, Espoo, Finland

^c Departamento de Fabricação – DEFAB, Celulose Nipo-Brasileira S.A. – CENIBRA, Belo Oriente, Brazil

ARTICLE INFO

Article history:

Received 20 November 2020

Received in revised form

17 February 2021

Accepted 18 March 2021

Available online 22 March 2021

Keywords:

Superheater deposit

Temperature gradient

Ageing mechanism

Melt enrichment

ABSTRACT

Cross-sections of kraft recovery boiler superheater deposits were analyzed using scanning electron microscopy (SEM) and energy dispersive X-ray analysis (EDX). The observed deposit morphology can be explained by temperature gradient induced time-dependent processes such as diffusional transport of alkali chloride vapours, temperature gradient zone melting, formation of melt enriched in Cl and K, and movement of this enriched melt towards the steel. These processes have recently been identified on a laboratory scale under well-controlled conditions, and are now for the first time identified to take place also in actual boiler superheater deposits. The identified processes alter the local deposit composition and melting behaviour close to the steel. The local first melting temperature (T_0) close to the steel is lower by 30 °C compared to that of the deposit bulk T_0 . The observations made in this work give new insight into the melting and ageing behaviour of superheater deposits, relevant for superheater corrosion.

© 2021 The Authors. Published by Elsevier Ltd. This is an open access article under the CC BY license (<http://creativecommons.org/licenses/by/4.0/>).

1. Introduction

Most of the modern, commercially operated pulping processes are based on the kraft recovery cycle. In this process, a suspension with a high solids fraction of up to 85 wt-% is fired in the kraft recovery boiler [1]. The main components of the fired suspension are spent pulping chemicals, organic material, mainly lignin, from wood, and water [2]. This liquid is called black liquor. With approximately 50 wt-% of the raw wood used in the process being combusted, the kraft recovery process is the largest industry sector to utilize biomass as fuel. Contributing by around 25% to the total amount of biomass annually utilized for heat and power production in the world [1].

Ash deposition and deposit related problems such as corrosion can cause major problems in kraft recovery boilers. Non-process elements such as Cl and K are incorporated in the wood, thus making their way into the process. Also, Cl can enter the process via

make-up chemicals and process water used in the bleaching process [3]. The non-process elements Cl and K tend to accumulate in the chemicals recovery cycle, and particularly in the fly ash (called recovery boiler dust).

Ash deposits and deposit induced corrosion have been crucial research areas for kraft recovery boilers as well as combustion processes in general. Over the last decades, research within this area focused on understanding the mechanisms causing superheater deposit formation and how operational parameters can affect deposit build-up [4–9]. Deposits formed in kraft recovery boilers contain mainly Na_2CO_3 , Na_2SO_4 , and NaCl as well as the corresponding potassium counterparts [5,8]. Two major particle size fractions contribute to the formation of superheater deposits. Fine fume particles with diameters of up to 1 μm form via nucleation of vapours. These particles then deposit predominantly through thermophoresis. Furthermore, vapours also condense directly on superheater steel surfaces. The other size-fraction contains larger particles in the range of 100 μm up to a few mm. These larger particles originate from entrained black liquor droplets and deposit predominantly via inertial impact on the wind side of superheater tubes [10,11].

Despite the advanced knowledge of deposit formation

* Corresponding author. Laboratory of Molecular Sciences and Engineering Faculty of Science and Engineering (FNT) Åbo Akademi University Biskopsgatan 8 Åbo, FI-20500, Finland.

E-mail address: roland.balint@abo.fi (R. Balint).

mechanisms, time-dependent changes that occur within the deposit after its formation are less extensively studied. Deposit related research has mainly focused on the sintering behaviour of deposits [2,12,13], but recent studies have shown that deposits undergo more structural changes, besides sintering, after they form on the superheater steel. Superheater deposits are constantly exposed to a temperature gradient due to the temperature difference between the hot flue gas and the colder superheater steel. Recent studies at Åbo Akademi University have identified several so-called temperature gradient induced deposit ageing mechanisms [14–18]. The studies were carried out on a laboratory scale using synthetic salt mixtures under well-controlled conditions and could identify three ageing mechanisms caused by the temperature gradient. In the porous region of the deposit, closest to the steel, alkali halides evaporate, diffuse as vapours toward the steel, and condense on colder surfaces resulting in an enrichment of alkali halide (chloride and bromide) toward and onto the superheater steel surface. In addition, partial melting of the deposit has been identified to result in transport of alkali halide enriched melt toward the steel, resulting in local enrichment of alkali chloride. Further, toward the outer parts of the deposit, a process called “temperature gradient zone melting” has been identified to take place, resulting in transport of alkali halide enriched melt toward the outer surface of the deposit.

It can be expected that deposit ageing mechanisms may occur also in actual boiler deposits, having an impact on the corrosiveness of boiler deposits. So far, temperature gradient induced deposit ageing mechanisms were studied only under well-controlled laboratory conditions using synthetic salts. To this point, it is unclear to what extent ageing mechanisms lead to changes within the local chemical composition and morphology of actual superheater deposits and how this might affect design and operation of boilers. The continuous presence of alkali chloride vapours in direct vicinity to the superheater steel as a result of diffusional transport processes favours corrosion. Furthermore, the possibility of Cl and K enriched melt being transported toward the steel increases corrosion rates significantly [2].

Data on deposit ageing under full scale conditions is rare. In the literature, a few publications point in the direction that deposit ageing processes identified in the laboratory could also take place in full scale deposits. In one study kraft recovery boiler deposits obtained using an air-cooled probe showed Cl-enrichment toward the cool probe surface and an area depleted in chloride located mid-deposit [11]. The authors reasoned that some kind of time-dependent enrichment process, most likely via the gas phase, was responsible. Another study deals with deposit induced corrosion on superheater tubes in a kraft recovery boiler [19]. Heavy corrosion was observed on several superheater tubes although the steam temperature was well below the calculated first melting point of the fly ash (carryover and fume). Analysis of superheater deposits showed local enrichment of K and Cl close to the steel, corresponding to a local first melting temperature that was lower than the first melting temperature of the bulk fly ash. It was concluded that this local enrichment of Cl and K toward the steel was connected to alkali chloride diffusion from the flue gas, through the deposit, toward the steel. In a third study, cross-sections of several mature superheater deposits collected from two Danish straw fired boilers were analyzed [20]. The analyzed deposits had a multi-layered structure, where the intermediate layer was depleted in Cl, followed by a layer of KCl when moving toward the steel. This depletion of Cl has been argued to be a result of reactions involving KCl, Si, and Ca taking place within the deposit, where Cl is released in gaseous form as one of the reaction products. The mature deposit samples were also compared to short term probe measurements. The deposits obtained from the probe measurements did not

contain an intermediate layer depleted in Cl and the innermost KCl layer was observed to be significantly thinner in the probe deposits. The observed differences when comparing the mature deposits with probe measurements of shorter exposure times could also be caused by temperature gradient induced aging processes. KCl evaporates within the intermediate layer and subsequently diffuses toward the colder steel surface, resulting in a similar deposit structure as described by Jensen et al. [20].

The data published so far provides first indications of time-dependent changes taking place in superheater deposits, including local enrichment of alkali chlorides toward the steel. However, a systematic study using cross-sectional images of superheater deposits focusing on the identification of deposit ageing mechanisms has so far not been carried out.

The objective of the present study is to obtain a better understanding of deposit ageing mechanisms in actual boiler superheater deposits. Careful analysis of full scale deposits from the superheater tubes of a kraft recovery boiler was carried out. The deposits were analyzed regarding their morphology and chemical composition to identify temperature gradient induced ageing mechanisms. This study gives insight into processes taking place in the analyzed deposits and points out the effect these observed mechanisms can have on corrosiveness emanating from the deposit.

2. Methods

Three superheater ash deposits were analyzed in this study. The deposits were collected from superheater tubes of a pulp mill kraft recovery boiler with a maximum firing capacity of 2700 tons of dry solids per day, located in Belo Oriente, MG, Brazil. The boiler in question has earlier faced severe superheater corrosion problems related to local enrichment of K and Cl within the deposit [19]. In the present study, samples were collected during a boiler shutdown after approximately six months of continuous operation. The deposits were collected by hand, without the use of further tools. The convective pass of the boiler was accessed through manholes located between two superheater panels. Therefore the sampling locations are limited by the possible access points determined by the location of suitable manholes. Samples from different locations were collected by the boiler operator to cover a wider flue-gas and steam temperature range. The three sampling locations along the flue gas path are indicated in the schematic in Fig. 1.

The sampling points were located i) at the inlet (windward) to the secondary superheater (Sample #1), ii) at the outlet (leeward) of the superheater screen, located between the secondary and tertiary superheater (Sample #2), iii) and at the outlet (leeward) of the tertiary superheater (Sample #3).

No dedicated analysis of the fired black liquor has been carried out during the time the deposit samples were collected. Data on the composition of the black liquor fired in the kraft recover boiler of the present study are available for the years 2007 and 2015 [19]. The available data are summarized in Table 1. Besides typical values for black liquor compositions for kraft pulp mills in Brazil [21] and northern Europe [22] are presented in Table 1.

The mill uses eucalyptus in the pulping process, resulting in a black liquor containing higher amounts of Cl compared to pulp mills located in northern Europe.

Steam temperatures at the sampling points were on average 420 °C in the secondary superheater (Sample #1), 290 °C in the screen tubes (Sample #2), and 460 °C in the tertiary superheater (Sample #3). Data regarding the flue gas temperature in the superheater area of the boiler was not available. However, the flue gas temperatures in this region of a boiler were estimated to range from 900 °C at the secondary superheater inlet to 700–800 °C [6] or even as low as 600 °C after the tertiary superheater.

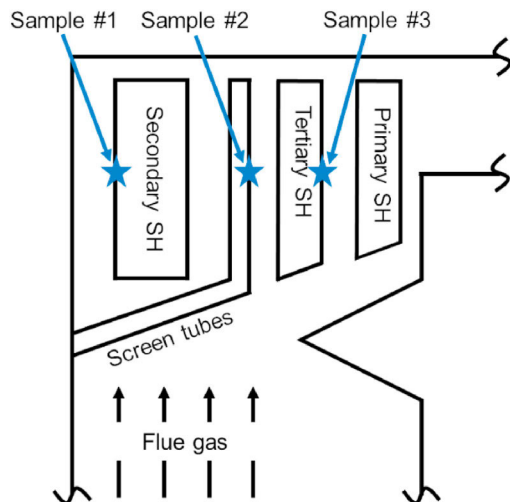


Fig. 1. Schematic drawing of the superheater area indicating the locations of sampling points.

The deposit samples were first cut into smaller pieces using a hand saw while being fixed in a bench vice. All deposits analyzed in the present study appeared robust toward mechanical processing and the overall deposit structure has not been damaged. Afterwards, the deposits were cast in epoxy resin to retain their initial structure and prevent loss of material during further preparation steps. The cast deposits were then cut a second time using a hand saw to obtain a cross-section and polished using SiC grinding paper. During cutting and polishing of the samples, no lubricants were used to avoid dissolution of water-soluble deposit material and to simplify sample preparation. The polished cross-sections were then carbon-coated and analyzed using scanning electron microscopy and energy dispersive X-ray analysis (SEM/EDX) (LEO Gemini 1530 equipped with a ThermoNORAN Vantage X-ray analyzing system manufactured by Thermo Scientific). Elemental maps were taken, enabling analysis of the distribution of elements within the deposits. The molar potassium to alkali ratio ($K/(K+Na)$) and chlorine to alkali ratio ($Cl/(K+Na)$) was calculated from the cross-sectional elemental maps. In addition, one-dimensional profiles of elements and their ratios as functions of distance from steel were

calculated from the two-dimensional cross-sections. For the profiles in the vertical direction of the two-dimensional cross-sectional images, the average molar concentration of each element was calculated along each horizontal line of pixels.

3. Results and discussion

3.1. Deposit structure

When comparing the cross-sections of the deposits from different sampling points, they differ in their appearance when examined visually. These differences are seen in Fig. 2.

In Fig. 2, Sample #1 on the left appears to be more porous, containing several bigger cavities and a partly lamellar structure. Sample #2, on the other hand, appears to be very dense and has a layered structure.

Both samples show regions with blue colour. However, in Sample #1, the blue colour is seen throughout the deposit's cross-section, while in Sample #2, the blue colour is limited to a relatively thin layer inside the deposit sample. During further analyses of the cross-sections of the two samples, only minor differences in their chemical compositions were identified. Blue colouration of kraft recovery boiler deposits has been connected to the sampling position and local flue gas temperatures. Small amounts of Mn in the deposit in combination with the presence of carbonate can lead to a blue colouration of the deposit under oxidizing conditions at sufficiently high temperatures. However, the colouration does not change the properties of the deposit in a way that would further affect boiler operation [23]. Sample #1 was collected on the wind side of the secondary superheater where the local flue gas temperature is higher than in the sampling location of Sample #2. Higher temperatures, above 700 °C, are required for blue deposits to form [23]. Traces of Mn are always present in kraft recovery boiler deposits, but their concentrations are too low to be detected by SEM/EDX.

Apart from the macroscopic differences in the deposit structures seen in Fig. 2, no major differences between the deposit samples concerning their chemical composition and structures could be identified under the electron microscope. Therefore, Sample #2 is used in further discussion, representing the general chemical and morphological characteristics of the deposits collected within this work. Table 2 summarizes the average bulk composition of the three analyzed deposits and the corresponding first melting temperature. The Na, K, Cl, and S content of the deposit is obtained from SEM/EDX analysis. The carbon content is then calculated, by zeroing the charge balance. It is assumed that all sulfur is present as sulfate, even though in carry-over particles some of the sulfur can

Table 1

Composition of the black liquor fired in the kraft recovery boiler of the present study from the years 2007 and 2015 together with typical values for black liquor compositions in Brazilian and north European kraft pulp mills.

Element	Black liquor from pulp mill of present study 2007	Black liquor from pulp mill of present study 2015 [19]	Typical black liquor of Brazilian pulp mills [21]	Typical black liquor of north European pulp mills [22]
C [wt-%]	29.4	n.a.	30–35	34.6
H [wt-%]	3.7	n.a.	3–4	3.5
N [wt-%]	0.2	n.a.	0–0.04	—
S [wt-%]	3.2	n.a.	3–5	4.8
Na [wt-%]	20.8	18.5	18–24	19.9
K [wt-%]	1.5	1.8	1.5–2	1.0
Cl [wt-%]	0.5	1.7	2–5	0.1

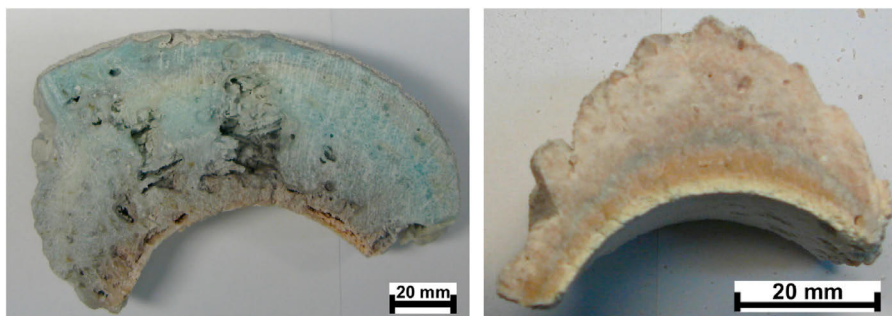


Fig. 2. Deposit cross-section of Sample #1 (left) and Sample #2 (right) before casting in epoxy resin.

Table 2

Bulk deposit compositions of the analyzed deposits and corresponding first melting temperatures (T_0).

Sample	Na [wt-%]	K [wt-%]	Cl [wt-%]	SO ₄ [wt-%]	CO ₃ [wt-%]	T_0 [°C]
Sample #1	35.71	2.57	1.52	34.43	25.78	543
Sample #2	32.83	3.95	4.74	44.25	14.23	543
Sample #3	32.32	4.04	3.76	47.37	12.51	546

also be present in the form of sulfide. The first melting temperatures listed in Table 2 were calculated using the thermodynamic software FactSage version 7.3 and the FTPulp thermodynamic database, relevant for alkali salts in kraft recovery boiler conditions [24]. The bulk deposit composition represents the average value of each element determined by elemental analysis of the whole cross-section of the deposit using SEM/EDX.

The overall bulk compositions of deposit Sample #2 and Sample #3 do not vary much. Only Sample #1 shows a higher concentration of carbonate and a lower chlorine concentration. This difference is most likely due to the sampling location. Sample #1 has been obtained from the windward side of the secondary superheaters, which are facing the flue-gas stream first, as shown in Fig. 1. Thus, the probability for inertial impaction of carry-over material containing unburnt carbon is higher for Sample #1 compared to the other two sampling locations. This difference does not affect the estimated first melting temperature of the deposit. A cross-sectional SEM image of Sample #2 is shown in Fig. 3. Cross-sectional SEM images of Sample #1 and Sample #3 can be found in Appendix A and B.

In Fig. 3, a SEM panorama image (A) of the cross-section of the sample is shown on the left. The three images on the right side of Fig. 3 are magnifications of selected areas of the deposit to highlight the deposit's essential features. All images in Fig. 3 are oriented in the same direction. The deposit-steel interface is located at the bottom of the image and the flue gas facing side of the deposit on top.

Three distinct areas were identified within all deposits. The hotter region of the deposit, toward the flue gas, seemed to have been in a fully or partially molten state during boiler operation and therefore has a dense morphology. This part consists mainly of alkali sulfate and carbonate (grey colour in SEM images) and is interveined by vertical alkali chloride channels (white colour in SEM images) (Fig. 3 B). Similar radially oriented channels of alkali halides were observed in previous laboratory experiments using synthetic ashes of binary systems [15,17]. This topic will be discussed in detail in section 3.2.

When moving closer toward the steel surface, the morphology of the deposit does not change significantly. The chemical composition of the deposit, on the other hand, changes. All analyzed deposits show similar regions with a dense morphology that is enriched in potassium and chloride close to the superheater steel (Fig. 3 C). A more detailed description of this region within the deposit structure can be found in section 3.3.

Closest to the superheater steel, the deposit morphology changes from dense to porous. For one of the analyzed samples, this porous layer is missing. It is not clear whether the deposit-steel interface of this deposit was not porous, or whether the porous layer had detached from the deposit either during sampling or during transportation. The change in morphology is an indication that the local temperature within the deposit was below the first melting temperature T_0 . At temperatures below T_0 , no melt-induced-pore-filling can occur, and as a result, this region of the deposit remains porous. On the furnace facing side of particles within the porous region, layers of pure alkali chloride form (Fig. 3 D). A more detailed description of the porous region of the deposit can be found in section 3.4.

3.2. Temperature gradient zone melting

In the hotter deposit regions toward the flue gas, the dense morphology indicates presence of melt during boiler operation. In this region, radial channels of alkali chloride were observed. These channels are currently believed to be caused by temperature gradient zone melting (TGZM) [17]. The mechanism of TGZM describes the movement of a liquid phase through a solid phase of a different bulk-composition when the system is exposed to a temperature gradient [25,26]. The mechanism was first brought up in connection with deposit ageing by Niemi et al. [18]. They observed similar vertically oriented channels of alkali chloride and alkali bromide to form in the hotter region of artificial, binary deposits under laboratory conditions. With time, these channels moved further away from the steel, transporting alkali halides and in some cases also corrosion products [17] to the outer deposit surface where they subsequently evaporated into the furnace. The present study represents a more complex system in terms of deposit composition, which affects the general melting behaviour of the salt. Furthermore, external influences such as sootblowing or continuous deposition of new material, are possibly affecting the mechanism during boiler operation. Nevertheless, all of the analyzed samples in the present study exhibit signs of temperature gradient zone melting. This observation gives further proof for the relevance of the TGZM mechanism regarding deposit ageing not

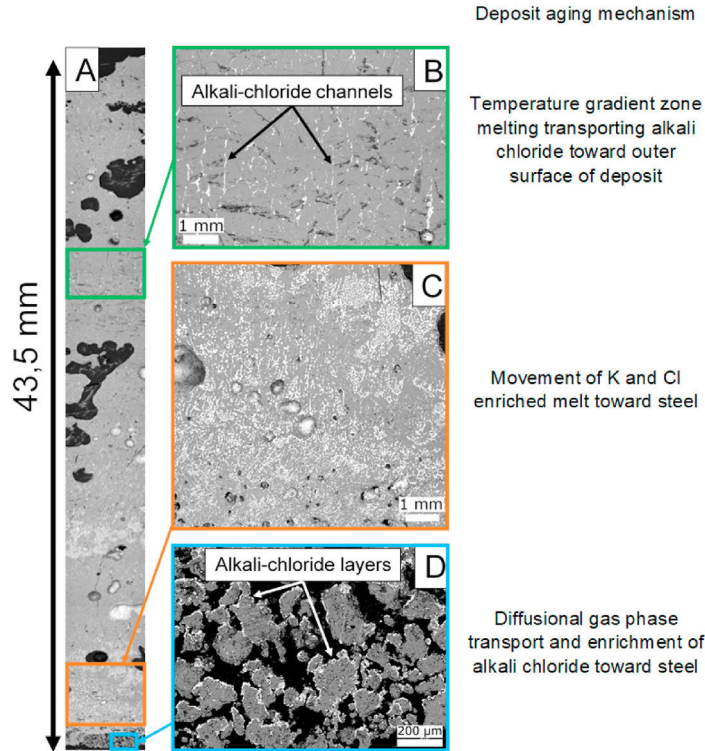


Fig. 3. SEM cross-section images of Sample #2. The light grey/white colour corresponds to alkali chloride, the dark grey to alkali sulfate and carbonate, and the black to the surrounding epoxy-resin. A) Panorama image of the whole cross-section. B) Vertical alkali chloride channels in outer deposit. C) Area enriched in Cl and K toward the superheater steel. D) Porous region of deposit, closest to the steel with alkali chloride layers on top of particles. (For interpretation of the references to colour in this figure legend, the reader is referred to the Web version of this article.)

only on laboratory scale but also in actual full scale superheater deposits.

With increasing deposit thickness on the superheater tube, the local temperature within the deposit increases. At a certain deposit thickness, the outer surface reaches a temperature equivalent to T_0 . At this point, the newly depositing particles, which are partially molten do not solidify after deposition but remain in a partially molten state. This melt subsequently accumulates in void areas between particles forming melt-pockets. Overall this leads to a densification of the deposit and a change in the local composition. The change in the local deposit composition can affect the melting behaviour of the deposit and result in additional melt formation. Calculations of the melting behaviour of the deposit using the thermodynamic software FactSage were conducted. The calculations showed that melt, which is formed at temperatures close to T_0 contains almost all Cl present in the bulk material together with a certain share of sulfate and carbonate. The amount of alkali sulfate and carbonate soluble in the formed melt is temperature-dependent. With increasing temperature, the solubility of sulfate and carbonate increases. This means that the melt is enriched in Cl compared to the bulk and the surrounding solid phase contains mainly alkali sulfate and carbonate. This temperature dependence of the melt composition together with the effect of the temperature

gradient in the deposit leads to concentration differences within the melt-pockets. The hotter region of the melt-pocket contains higher amounts of sulfate and carbonate, thus a percentual lower amount of Cl compared to the colder region of the melt-pocket. These concentration differences lead to diffusional transport of Cl toward the hotter region in the melt and transport of sulfate and carbonate in the opposite direction. Subsequently, the increased amount of Cl in the hotter region of the melt enables further dissolution of sulfate and carbonate in that region. In the cooler region of the melt, sulfate and carbonate crystallize as the local chlorine concentration decreases and with that, the solubility of carbonate and sulfate decreases. These continuous processes result in movement of the melt through the solid phase toward the hotter region of the deposit. A graphical illustration of the mechanism within binary deposits can be found elsewhere [17]. Fig. 4 shows examples of TGZM within the deposit analyzed in the present study at two different stages of progress.

The image on the left of Fig. 4 shows a melt-pocket that still contains most of the solidified melt. On the upper part of the spherical pocket, first signs of movement due to TGZM can be observed. The melt begins to move toward the hotter region of the deposit (top of image). In the right image, the process has advanced to a point, where the Cl rich melt has left the pocket, leaving behind

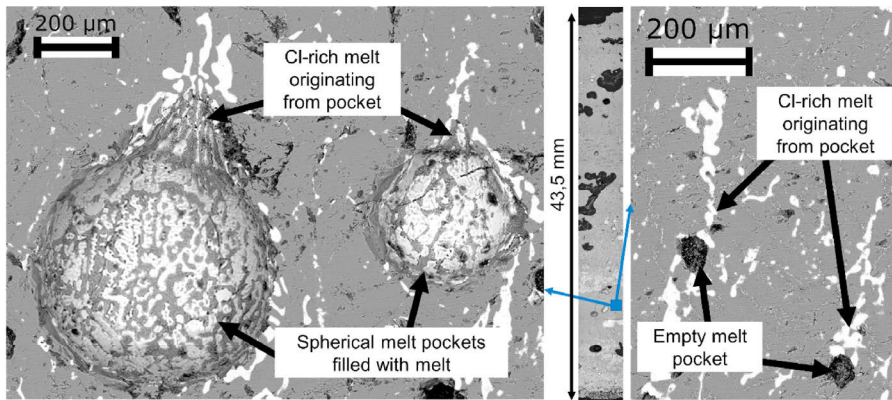


Fig. 4. SEM images of melt pockets in different stages: Melt-pockets filled with Cl-rich melt in the initial stage of TGZM (left); empty melt-pockets with Cl-rich melt in channels above, moving toward the hotter region of deposit (right).

a void sphere in the deposit. The two images of melt-pockets in different stages of TGZM shown in Fig. 4 were found within the same region of the deposit, thus at similar temperature conditions. The possibility for melt pockets being in different stages of TGZM at similar thermodynamic conditions is possibly related to the basic mass transport processes and kinetics of the TGZM process in combination with the size of the formed melt pocket. As mentioned earlier, Cl is transported from the colder region within the melt-pocket toward the hot region via diffusion. This leads to dissolution of sulfate and carbonate in the hotter region of the melt. These two mechanisms strongly affect the overall speed of the process.

In larger melt-pockets, the overall speed of the TGZM process is limited by the diffusional transport of Cl through the melt, whilst in small pockets, the speed of the process is governed by dissolution kinetics [27]. Furthermore, rates of diffusional mass transport due to TGZM are in general slow and not affected by the size of melt pockets [28]. This implies that the exposure time may have been sufficient for the melt to leave small pockets but too short to fully empty larger pockets.

Besides size, the melt pockets location relative to the steel surface might affect the TGZM mechanism as well. Deposit build-up over time affects the internal temperature gradient and local temperature within the deposit during boiler operation. With increasing deposit thickness the local temperature and the steepness of the temperature gradient decreases. In particular in regions close to the steel surface, thus of generally lower temperature, the local temperature can drop below the melt's solidification temperature. This can lead to melt solidifying and being enclosed in the originally formed melt-pocket, as seen on the left of Fig. 4. Nevertheless, larger melt pockets, still containing all or a large share of the melt were found throughout the whole deposit, also in regions that are expected to not have dropped to a temperature below T_0 during boiler operation. This would suggest, that the overall speed of TGZM mechanisms in kraft recovery boiler deposits is governed by dissolution and diffusion.

The images in Fig. 4 indicate clearly that TGZM is relevant as an ageing mechanism in kraft recovery boiler superheater deposits. Compared to previous research with synthetic deposits on laboratory scale [17] the presented data of kraft recovery boiler deposits represents a more complex salt system. Besides the main elements Na, S, O, and C, deposits can contain various non-process elements

[23], of which K and Cl make up the greater part and corrosion products [17,29] which affect the melting properties. Furthermore, the temperature gradient in boiler deposits changes with time due to deposition of new material, sootblowing, and general temperature fluctuations in the convective pass of the boiler. Nevertheless, clear indication for the process taking place within kraft recovery boiler superheater deposits was found in all deposit samples.

3.3. Formation of K and Cl enriched melt close to steel

All analyzed cross-sections showed, to some extent, a region enriched in K and Cl right above the porous layer (Fig. 3C). In Fig. 5, the greyscale image of the deposit is shown together with images visualizing Cl/(K+Na) and K/(K+Na) ratios within the enriched region. In addition, calculated profiles of both ratios are plotted against the distance from the steel. Both graphs contain reference values for the respective ratio based on elemental analysis of the deposit bulk composition and the ESP-ash. The profiles as a function of distance from the steel in Fig. 5 B and D have been calculated from the cross-sectional images by averaging over each horizontal line of pixels.

In Fig. 5, the porous layer closest to the steel (bottom of images in Fig. 5 A, B, and D) extends to a distance of about 1 mm from the steel. Within the porous layer, the gas phase transport of alkali chlorides toward the steel takes place, as discussed in more detail in section 3.4.

At a distance of 1–6 mm from the steel, the deposit is enriched in chlorine and potassium compared to the bulk composition of the deposit and ESP ash. The very dense structure of this region indicates that the deposit has been at least partially molten during boiler operation. The chlorine enrichment is seen to be relatively constant in the 1–6 mm region. In contrast, the potassium enrichment has a maximum in the porous-dense layer interface located at a distance of about 1 mm from the steel. From there on the K content within the deposit decreases almost linearly with increasing distance from the steel. The enrichment of chlorine and potassium in the 1–6 mm region of the deposit is believed to be the result of a chlorine and potassium enriched melt percolating toward the inner parts of the deposit. Similar behaviour has been observed in laboratory and pilot scale experiments [15,16,18].

Differences in the K and Cl distribution within the enriched melt

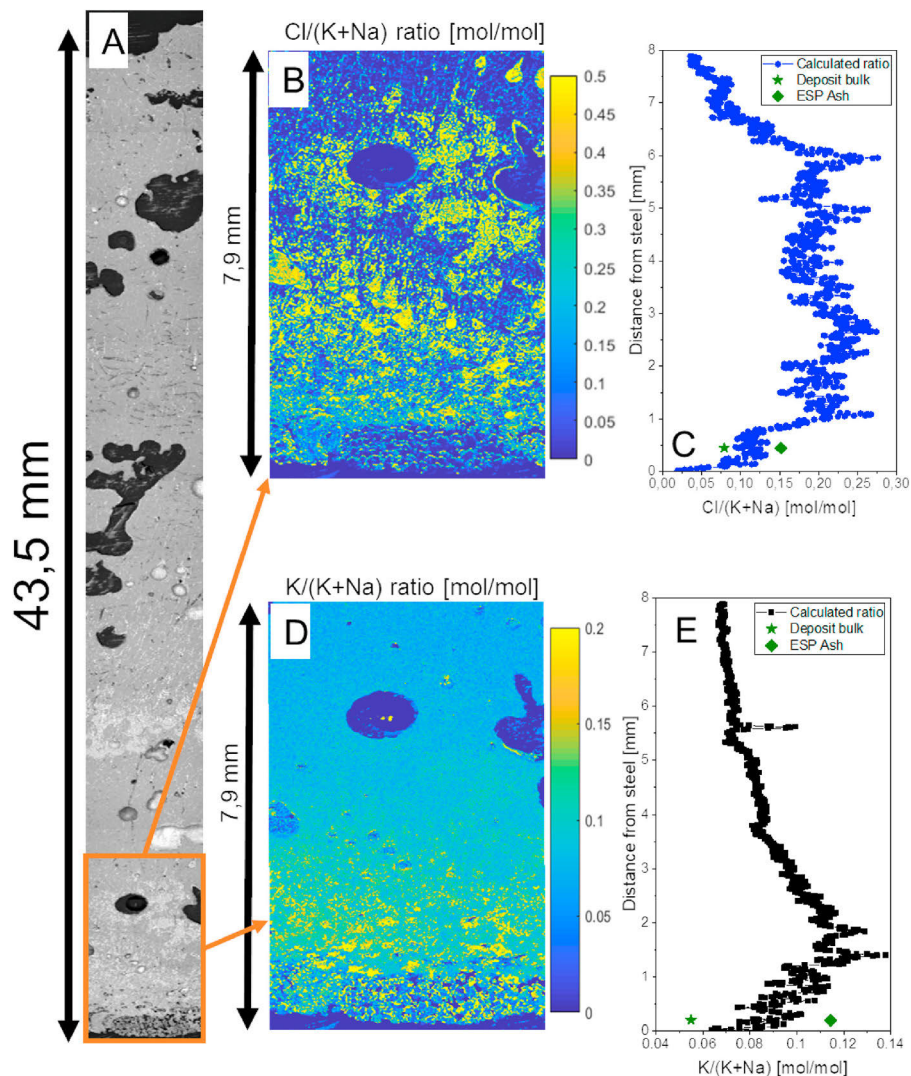


Fig. 5. A) Greyscale image of the whole deposit from the steel to the outer surface. B) An image describing the molar $\text{Cl}/(\text{K}+\text{Na})$ ratio in the deposit. C) The calculated $\text{Cl}/(\text{K}+\text{Na})$ ratio as a function of the distance from the steel. D) An image describing the molar $\text{K}/(\text{K}+\text{Na})$ ratio in the deposit. E) The calculated $\text{K}/(\text{K}+\text{Na})$ ratio as a function of the distance from the steel.

can be connected to the deposit melting behaviour and subsequent solidification of the initially formed melt. Calculations of the melting properties were carried out using the thermodynamic software FactSage version 7.3 and the FTPulp thermodynamic database for alkali salts in kraft recovery boiler settings [24]. As input for these calculations, the bulk composition of the deposit discussed here was used. For a better picture of the deposit's melting behaviour, a calculation consisting of two steps was conducted. First, the composition of melt, which was formed at T_0 of

the bulk deposit composition was calculated. The formed melt in question was then considered separately. The melt composition was used in the second step as input to calculate the composition of the remaining melt during precipitation, thus with decreasing temperature. The input values and calculation procedure are shown in Fig. 6, together with the elemental composition, $\text{K}/(\text{Na}+\text{K})$ ratio, and $\text{Cl}/(\text{Na}+\text{K})$ ratio of the remaining melt during precipitation.

The calculated absolute values of the $\text{K}/(\text{Na}+\text{K})$ and $\text{Cl}/(\text{Na}+\text{K})$ ratios shown in Fig. 6 are higher than the measured values within

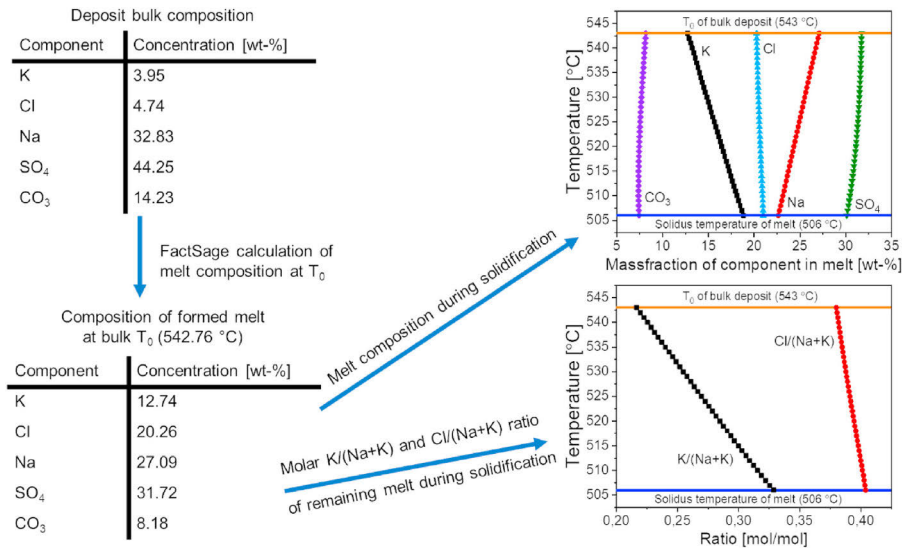


Fig. 6. The applied systematic approach of FactSage calculation to simulate precipitation of melt formed at T_0 of the deposit bulk composition. The mass fractions of components in the melt during precipitation (top right) and the K/(Na+K) and Cl/(Na+K) ratios in the melt during precipitation (bottom right).

the enriched region of the deposit, as shown in Fig. 5. These observed differences between calculated and measured values could be the result of two mechanisms related to temperature gradient induced melt enrichment. Initial melt formation of the bulk material takes place at 542 °C. This initially formed melt then solidifies over the temperature interval from 542 °C to 506 °C, along the path shown in Fig. 6. The implication is that melt can percolate, because of capillary forces, toward the steel through the porous deposit until the local temperature of 506 °C is reached, thus complete solidification takes place. This results in the presence of melt at temperatures below T_0 of the bulk material (542 °C). Thus, the percolating melt fills the voids between solid particles of the porous layer. Consequently, the composition of the deposit in the region where the local temperature is in the interval between 542 °C and 506 °C represents a mixture of melt, enriched in Cl and K, and solid particles with the composition of the original bulk material. Therefore, the measured K/(Na+K) and Cl/(Na+K) ratios in Fig. 5 are lower than the calculated values of the pure melt in Fig. 6, due to dilution of enriched melt with original solid particles. Furthermore, the calculation presented in Fig. 6 does not consider the presence of a solid phase during the solidification process, thus interactions between the enriched melt and solid particles of the porous layer are not taken into account. In reality, interactions between these two phases can be expected to take place at temperatures below 542 °C. These interactions could alter the solidification and enrichment process and therefore contribute to the observed differences between measured and calculated values of K/(Na+K) and Cl/(Na+K). Currently, interactions between the melt and the solid phases in the temperature interval between 542 °C and 506 °C are not taken into account. Fig. 7 illustrates, what is believed to be the main steps of the described melt enrichment.

The melt enrichment is believed to occur during deposit build-up. As the deposit grows onto the superheater tube, its thickness increases. In the early stages of the build-up process, cooling from the superheater tubes is sufficient to prevent formation of melt.

With increasing deposit thickness, the deposit surface temperature increases up to a point where the local temperature on the deposit surface reaches T_0 of the bulk deposit material (Fig. 7 A). At temperatures above the first melting point, particles start to melt partially (Fig. 7 B). As long as the local deposit temperature stays below the temperature of complete melting, parts of the original deposit particles remain in solid-state. These remaining particles contain mainly Na₂CO₃, Na₂SO₄, and their potassium counterparts. The formed melt contains almost all the chlorine present in the original particles together with a certain share of Na₂CO₃, Na₂SO₄, K₂CO₃, and K₂SO₄. The melt that is formed in the outermost parts of the deposit can move toward the inner parts due to capillary forces [18]. During the movement process, parts of the melt gradually solidify as the local deposit temperature decreases toward the steel. The solidifying melt consists mainly of Na₂SO₄ and Na₂CO₃ resulting in enrichment of Cl and K in the remaining melt compared to the bulk material (Fig. 7C). Especially enrichment of K in the remaining melt is connected to a further decrease of the melt's final solidification temperature. Calculations with FactSage showed that the final global solidification temperature for the presented K–Na–Cl–CO₃–SO₄ system is located at about 505 °C. Most likely, in the early stage of the melt movement process, the amount of melt that has had time to form is small. Re-solidification of melt while moving toward the cooler steel leads to a further decrease in the amount of melt. At some point, the melt fraction present within the deposit is not high enough for further movement toward the steel. However, with time, more particles deposit on top of the deposit (Fig. 7 D), increasing its thickness and providing new material for more melt to form. Due to the increasing deposit thickness, the local temperature, at which this additional melt is formed might be higher than in the previous step. This higher temperature affects mainly the solubility of alkali sulfate and carbonate, as almost all Cl available is already incorporated in the melt at temperatures close to T_0 of the deposit bulk material. The additional melt subsequently moves toward the steel increasing the amount of

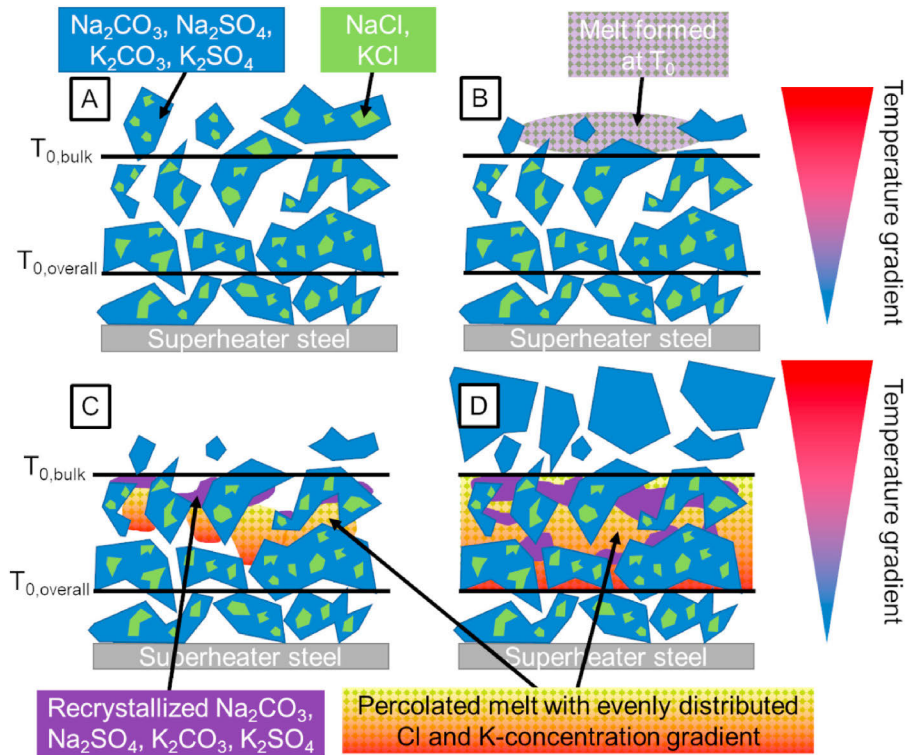


Fig. 7. An illustration of the believed melt enrichment mechanism: A) A deposit in which the local temperature at the outermost part is above T_0 ; B) The formation of a first melt in the outermost part of the deposit; C) The melt moves down toward the steel during which partial solidification takes place, leaving a melt high in Cl and K to move further toward the steel; D) Continued deposition leads to more melt transport toward the steel until all voids become filled.

melt present at lower temperatures within the deposit. A higher amount of melt present enables further moving of melt toward the steel until the local temperature reaches T_0 of the overall system. This can lead to a situation, where all void areas in the temperature region between T_0 of the bulk and the overall T_0 of the system are filled with a melt that was formed at temperatures above T_0 of the bulk material (Fig. 7 D).

It should be noted that the proposed mechanism includes several simplifications. Melt-solid interactions are not considered. Additionally, in a boiler environment, the temperature profile of the deposit is constantly affected by various external and internal changes. Sootblowing, can change the deposit thickness significantly and increase the local temperature in the cooler parts of the deposit. Furthermore, the continuous deposit growth does not only provide a source for more melt to form but the growth also alters the temperature profile within the deposit. The current knowledge is not sufficient to quantitatively estimate how much the listed factors contribute to the time-dependent changes.

3.4. Porous region close to the steel

The region of the deposit closest to the steel is porous and consists of discrete particles. The $\text{Cl}/(\text{Na}+\text{K})$ ratio in Fig. 3 D shows

the characteristic round shapes of alkali chloride layers formed predominantly on the furnace facing side of particles within this porous region closest to the steel. These alkali chloride layers can also be seen in Fig. 5 B as shapes resembling “inverted cups”. Similar layers were previously detected when studying the ageing behaviour of synthetic deposits on a laboratory scale. During the laboratory experiments, alkali chloride layers built-up on top of particles within the porous region of the deposit, close to the steel [14,16–18]. The laboratory experiments could prove that these layers are the result of a temperature gradient induced deposit ageing mechanism.

The driving force for this layer build-up was shown to be the temperature dependence of the alkali chloride vapour pressures [16]. Alkali chloride evaporates from particles within the porous region of the deposit. With increasing local temperature the partial pressure of alkali chloride, thus the local concentration of alkali chloride in the gas phase, increases, and a concentration gradient develops across the porous deposit layer. Vapours of alkali chloride diffuse toward the cold steel surface due to concentration gradients in the gas phase, and subsequently condense either on top of particles at lower temperatures or directly on the superheater tube, as the saturation pressure of the vapours decreases with decreasing temperature [16–18].

As the diffusional transport is directed toward the steel, characteristic alkali chloride layers predominantly build-up on the furnace facing side of particles within the porous layer. Another observation connected to this mechanism besides the formation of alkali chloride layers is the depletion of alkali chloride within the particles in the porous region. These particles serve as sources for continuous evaporation of alkali chloride. Most of the particles within the porous layer of the superheater deposits analyzed in this work showed signs of alkali-chloride depletion, confirming the evaporation-condensation mechanism to take place in actual superheater deposits. Fig. 8 shows a part of the porous region of the deposit within which layers of alkali chloride, as well as particles depleted in alkali chloride, can be seen.

Under operational boiler conditions, the flue-gas contains additional chloride vapours. These vapours could also penetrate the deposit and result in the formation of observed layers within the porous region of the deposit. However, the dense deposit structure in the hotter regions of the deposit complicates diffusion of alkali chloride vapours through the outer deposit region. Furthermore, particles within the porous region being depleted in alkali chloride strengthen the assumption of the described mechanism, first proposed by Lindberg et al. [14], being responsible for the observed formation of alkali chloride layers.

Generally, the observations made in the present study are in line with the laboratory data found in the literature [14,16–18]. This provides substantial evidence, that the evaporation-condensation mechanism takes place within the porous region of actual superheater deposits and that the mechanism can affect the local deposit composition within the porous region, close to the steel.

3.5. Deposit first melting temperature T_0

A deposit T_0 profile depending on location and therefore on local

composition was calculated by dividing the cross-sectional image closest to the steel into sections. For each section, the bulk composition was determined from SEM/EDX data, and T_0 was calculated using FactSage. The results of these calculations are presented in Fig. 9.

The profile shown in Fig. 9 indicates significant changes in T_0 close to the steel (bottom of the image) compared to the bulk composition. T_0 decreases toward the steel to a minimum of 517 °C at the porous-dense interface of the deposit, at a distance of about 1 mm from the steel. This decrease is the result of Cl–K-enriched melt percolating toward the inner parts of the deposit and the steel, as discussed in Section 3.3. T_0 shows a slight increase within the porous layer, but the calculated value is still significantly lower than T_0 of the bulk deposit.

In addition to the bulk deposit, the composition of particles within the porous layer was determined and T_0 of the original particles calculated. The centres of several particles that seemed to have remained at their original composition were analyzed. The inner parts of the particles were assumed to have not been affected by ageing mechanisms. T_0 of the overall bulk deposit and the original particles within the porous part of the deposit differed by 2 °C. The calculated value of T_0 of the bulk composition of the porous layer is well below that of the individual original particles. The deposit ageing mechanisms within the porous region, other than melt enrichment also affect the local deposit composition and therefore also the local first melting temperature within the deposit. Note that the calculated value of T_0 for the porous region as illustrated in the SEM image in Fig. 9 does not exclusively represent the porous layer. On the left-hand side of the image, the deposit seems to have been molten at some point. The presence of melt affects the overall composition of this area of the deposit. Accordingly, the calculated value of T_0 in the porous layer is affected. Nevertheless, as seen from Fig. 5 D there is a local enrichment of K

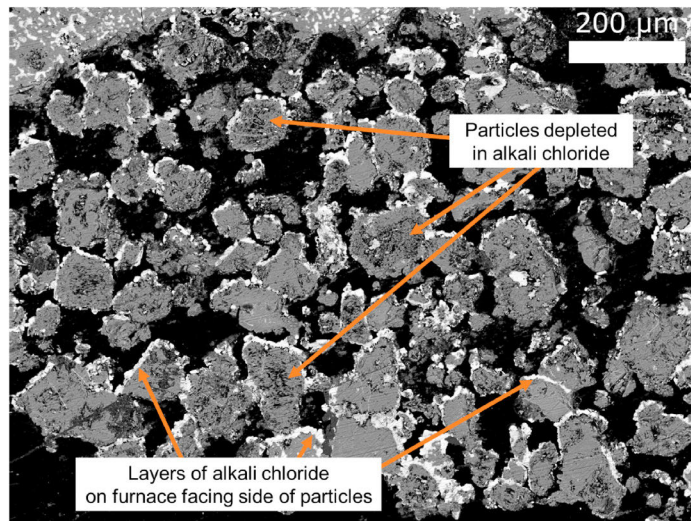


Fig. 8. The porous region of the deposit showing formation of alkali chloride layers (white colour) on the furnace facing sides of particles and alkali chloride depleted particles. (For interpretation of the references to colour in this figure legend, the reader is referred to the Web version of this article.)

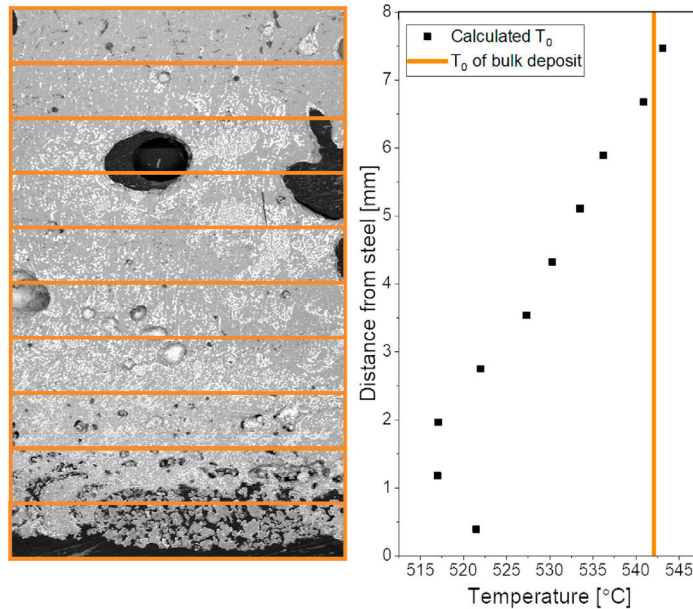


Fig. 9. The local first melting temperatures of the deposit's area enriched in K and Cl.

in the porous layer, mainly on the top of particles. Likely, this enrichment is caused by temperature gradient induced diffusional transport of alkali chloride vapours within the porous layer. The local enrichment of K and Cl within the porous layer can also be a remnant from initial deposition mechanisms. In the early stages of deposit build-up predominantly alkali chloride condenses on top of the cool superheater tubes. This initial condensation of alkali chlorides would result in higher concentrations of Cl and K in the region of the deposit close to the steel [5].

The observations made within the present study also provide additional information concerning superheater corrosion in the same boiler that was reported earlier. A higher concentration of K and Cl in the inner part of the deposit, facing the steel compared to the outer part of the deposit was observed [19]. The results presented in the present study help to understand the mechanisms behind the previously observed enrichment of these elements toward the steel and verify the conclusion made in the earlier publication, that observed corrosion is connected to the presence of melt at the steel surface.

4. Conclusions

This study focuses on investigating the local enrichment of Cl and K within kraft recovery boiler superheater deposits with high

concentrations of Cl. The deposits showed similar characteristics to those previously seen on a laboratory scale [14–18]. These characteristics have been identified to be caused by the temperature gradient across the deposit. Three mechanisms were identified to contribute to changes in the chemistry and morphology of the boiler superheater deposits: 1) in the hotter outer region of the deposit, temperature gradient zone melting transports alkali chlorides away from the superheater steel; 2) in the inner parts of the deposit, enrichment of K and Cl in the melt toward the superheater steel takes place; 3) in the porous region closest to the superheater steel, alkali chlorides vaporize and condense toward the steel.

The changes in deposit chemistry, leading to enrichment in chlorine and potassium toward the steel with time are likely to increase the risk of chlorine and melt induced corrosion. The local first melting temperature T_0 of the deposit was estimated to be about 30 °C lower in the vicinity of the steel as compared to the T_0 of the bulk deposit.

Currently, a common practice for choosing the final steam temperature in the hottest superheater tubes is based on T_0 corresponding to the composition of the fly ash or the composition of a bulk deposit. The present study shows that melt can be present at temperatures significantly lower than the bulk T_0 of the fly ash, as the local composition of the deposit changes due to temperature

gradient induced ageing mechanisms and melt gets transported through the deposit toward the superheater steel. The calculated first melting temperature in the Cl and K enriched region was close to the global minimum of the first melting temperature of the K–Na–Cl–SO₄–CO₃ system at about 505 °C.

More work is needed to better understand the mechanism of melt enrichment toward the steel. The proposed mechanism in the present study can be seen as a first attempt at describing the melt enrichment process. A complete quantitative description of the melt enrichment process is a subject for future work. The results imply that a relatively high amount of melt in the deposit is needed for the melt enrichment mechanism to occur. In practice for kraft recovery boilers, this means that a relatively high content of Cl is needed to enable the melt enrichment toward the steel. It is possible that in kraft recovery boilers with lower chlorine (e.g. in Scandinavia and North America) an insufficient amount of melt for melt enrichment in the deposit is formed at T₀.

As many biomass-based fuels contain large amounts of Cl, these findings can be relevant for a variety of biomass-based fuels. The results presented in this study can serve as a base to better understand processes that can cause severe superheater corrosion.

Credit author statement

Roland Balint: Investigation, Data Curation, Writing – Original Draft, Visualization, Markus Engblom: Supervision, Project administration, Writing – Review & Editing, Conceptualization, Methodology, Investigation, Validation, Jonne Niemi: Methodology, Validation, Investigation, Writing – Review & Editing, Daniel Silva da Costa: Resources, Daniel Lindberg: Validation, Funding acquisition, Writing – Review & Editing, Patrik Yrjas: Writing – Review & Editing, Funding acquisition, Leena Hupa: Writing – Review & Editing, Funding acquisition, Mikko Hupa: Writing – Review & Editing.

Declaration of competing interest

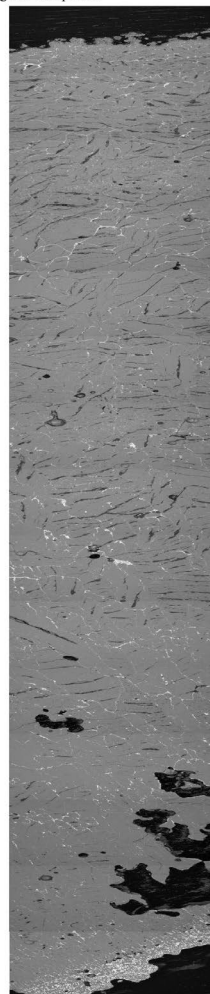
The authors declare that they have no known competing financial interests or personal relationships that could have appeared to influence the work reported in this paper.

Acknowledgements

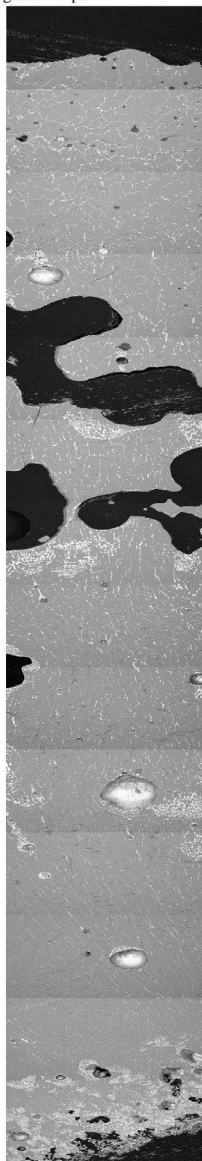
The financing through a research grant awarded by the Fortum Foundation (Application 20190123) is highly acknowledged. This work is part of the project Clean and efficient utilization of demanding fuels (CLUE), with support from the industrial partners: ANDRITZ, Fortum, International Paper, UPM-Kymmene Corporation, and Valmet Technologies Oy, as part of the activities of the Åbo Akademi University Johan Gadolin Process Chemistry Centre. Additional support from the Academy of Finland project “Understanding the dynamics of intradeposit chemistry and morphology for control of corrosion in high temperature processes” (Decision 310266) is highly appreciated. We want to thank Linus Silvander for carrying out SEM/EDX analyses.

Appendix

A) Cross-sectional SEM image of Sample #1



B) Cross-sectional SEM image of Sample #3



References

- [1] Vakkilainen EK. Recovery boiler. Steam gener. From biomass. Elsevier; 2017. p. 237–59. <https://doi.org/10.1016/B978-0-12-804389-9.00011-3>.
- [2] Adams TN, Frederick WJ, Hupa M. Kraft recovery boilers. New York (NY) : Atlanta (GA): American Forest & Paper Association ; Tappi Press; 1997.
- [3] Hupa M. Recovery boiler chemical principles. TAPPI Kraft Recover Course 2007;2:462–88.
- [4] Vakkilainen EK. Predicting ash properties in recovery boilers. Int Chem Recover Conf 2010;2:237–45.
- [5] Tran HN, Reeve DW, Barham D. formation of kraft recovery boiler superheater fireside deposits. Pulp Pap Canada 1983;84:36–41.
- [6] Mikkonen P, Jokiniemi JK, Kauppinen EI, Vakkilainen EK. Coarse ash particle characteristics in a pulp and paper industry chemical recovery boiler. Fuel 2001;80:987–99. [https://doi.org/10.1016/S0016-2361\(00\)00195-2](https://doi.org/10.1016/S0016-2361(00)00195-2).
- [7] Baxter LL. Ash deposit formation and deposit properties. 2000. <https://doi.org/10.2172/760515>.
- [8] Mikkonen P. Fly ash particle formation in kraft recovery boilers. 2000.
- [9] Lapuerta M, Acosta A, Pazo A. Fouling deposits from residual biomass with high sodium content in power plants. Energy Fuels 2015;29:5007–17. <https://doi.org/10.1021/acs.energyfuels.5b00356>.
- [10] Backman R, Skrifvars BJ, Hupa M, Siiskonen P, Mäntyniemi J. Flue gas and dust chemistry in recovery boilers with high levels of chlorine and potassium. J Pulp Pap Sci 1996;22.
- [11] Reeve DW, Tran HN, Barham D. Superheater fireside deposits and corrosion in kraft recovery boilers. TAPPI (Tech Assoc Pulp Pap Ind) 1981;64:109–13.
- [12] Duhaivel M, Tran H, Frederick WJ. The sintering tendency of recovery boiler precipitator dust. Tappi J 2004;3:25–30.
- [13] Frederick WJ, Vakkilainen EK. Sintering and structure development in alkali metal salt deposits formed in kraft recovery boilers. Energy Fuels 2003;17:1501–9. <https://doi.org/10.1021/ef034012s>.
- [14] Lindberg D, Engblom M, Yrjas P, Laurén T, Lindholm J, Hupa M. Influence of deposit aging on superheater corrosion. Int. Chem. Recover. Conf. 2014; 101–13.
- [15] Niemi J, Lindberg D, Engblom M, Tran H. A fundamental study on the change in composition of fireside deposits with time in kraft recovery boilers. J Sci Technol For Prod Process 2018;7:45–52.
- [16] Lindberg D, Niemi J, Engblom M, Yrjas P, Laurén T, Hupa M. Effect of temperature gradient on composition and morphology of synthetic chlorine-containing biomass boiler deposits. Fuel Process Technol 2016;141:285–98. <https://doi.org/10.1016/j.fuproc.2015.10.011>.
- [17] Niemi J, Balint R, Engblom M, Lehmusto J, Lindberg D. Temperature-gradient-driven aging mechanisms in alkali-bromide- and sulfate-containing ash deposits. Energy Fuels 2019;33:5883–92. <https://doi.org/10.1021/acs.energyfuels.8b04199>.
- [18] Niemi J, Lindberg D, Engblom M, Hupa M. Simultaneous melt and vapor induced ash deposit aging mechanisms – mathematical model and experimental observations. Chem Eng Sci 2017;173:196–207. <https://doi.org/10.1016/j.ces.2017.07.041>.
- [19] Costa A, Silva D, Abella F, Cenibra CNSA. Experience OF recovery boiler superheater corrosion at cenibra. In: Int. Chem. Recover. Conf.; 2017. https://www.researchgate.net/publication/319964133_EXPERIENCE_OF_RECOVERY_BOILER_SUPERHEATER_CORROSION_AT_CENIBRA.
- [20] Jensen PA, Frandsen FJ, Hansen J, Dam-Johansen K, Henriksen N, Hörlyck S. SEM investigation of superheater deposits from biomass-fired boilers. Energy Fuels 2004;18:378–84. <https://doi.org/10.1021/ef030097l>.
- [21] Cardoso M, de Oliveira ED, Passos ML. Chemical composition and physical properties of black liquors and their effects on liquor recovery operation in Brazilian pulp mills. Fuel 2009;88:756–63. <https://doi.org/10.1016/j.fuel.2008.10.016>.
- [22] Vakkilainen EK. Kraft recovery boilers - principles and practice. Suomen Soodakattilayhdistys r.y.; 2005.
- [23] Mao X, Tran H. Formation of blue deposits in kraft recovery boilers. PEERS Conf 2015 Sustain Solut Our Futur 2015;2:1255–65. <https://doi.org/10.32964/TJ15.3.195>.
- [24] Bale CW, Bélisle E, Chartrand P, Decterov SA, Eriksson G, Gheribi AE, et al. FactSage thermochemical software and databases, 2010–2016. Calphad Comput Coupling Phase Diagrams Thermochem 2016;54:35–53. <https://doi.org/10.1016/j.calphad.2016.05.002>.
- [25] Pfann WG. Zone Melting - this technique offers unique advantages in purification and in control of composition in various substances. Science 1962;135(80-):1101–9. <https://doi.org/10.1126/science.135.3509.1101>.
- [26] Rettenmayr M. Melting and remelting phenomena. Int Mater Rev 2009;54:1–17. <https://doi.org/10.1179/174328009X392930>.
- [27] Lozovskii VN, Popov VP. Temperature gradient zone melting. Prog Cryst Growth Char 1983;6:1–23. [https://doi.org/10.1016/0146-3535\(83\)90022-9](https://doi.org/10.1016/0146-3535(83)90022-9).
- [28] Lograsso TA, Hellawell A. Temperature gradient zone melting: approach to steady state. J Cryst Growth 1984;66:531–40. [https://doi.org/10.1016/0022-0248\(84\)90151-9](https://doi.org/10.1016/0022-0248(84)90151-9).
- [29] Lagerbom J, Lepistö T, Backman R, Hupa M. Behavior of alkaline sulfate-chloride salts in temperature gradient corrosion test furnace. VTT Symp 2001;541–51.

[1] Vakkilainen EK. Recovery boiler. Steam gener. From biomass. Elsevier; 2017.

R. Balint, M. Engblom, J. Niemi, D. Lindberg, T. Saarinen, J. Rautala, M. Hupa,
L. Hupa (2023)

**Morphological and chemical differences within superheater deposits
from different locations of a black liquor recovery boiler.**

Energy



Morphological and chemical differences within superheater deposits from different locations of a black liquor recovery boiler

Roland Balint^{a,*}, Markus Engblom^a, Jonne Niemi^a, Daniel Lindberg^b, Timo Saarinen^c, Jaakko Rautala^c, Mikko Hupa^a, Leena Hupa^a

^a Johan Gadolin Process Chemistry Centre, Åbo Akademi University, Turku, Finland

^b Department of Chemical and Metallurgical Engineering, Aalto University, Espoo, Finland

^c Metsä-Fibre Oy, Rauma, Finland

ARTICLE INFO

Handling Editor: Henrik Lund

Keywords:

Superheater deposits
Temperature gradient
Ageing mechanism
Local melting behaviour

ABSTRACT

The effects of two deposit ageing mechanisms were identified by analysing superheater ash deposits from a kraft recovery boiler. Local differences in deposit morphology and chemical composition were identified under the electron microscope. Temperature-gradient-induced diffusion of alkali chloride vapours toward the steel was evident. Two deposit types were identified, based on local chemical compositions: “Type 1” deposits had an innermost porous layer of fine, sintered fume particles enriched in K and Cl, that deposited after homogeneous condensation in the gas phase. “Type 2” deposits formed via sulfation of initially deposited fume particles rich in K and Cl. Thus the innermost layer was enriched in K and S, while concurrently depleted in Cl. Differences in the local first melting temperature (T_0) within the innermost regions of the two deposit types were identified. T_0 reached a minimum within the innermost region of Type 1 deposits, implying an increased risk for melt formation and corrosion. Whereas for Type 2 deposits, T_0 was increased closest to the steel, reducing the risk for melt formation and superheater corrosion. The presented results provide a better understanding of intra-depositional changes taking place after initial deposition, helping assess risks of deposit-related operational problems in the boiler.

1. Introduction

About 90% of chemical pulp worldwide is produced via the kraft pulping process, making it the most used process in the industry [1]. A pulp fibre yield of up to 55% can be achieved, by dissolving wood in an aqueous solution of Na_2S and NaOH [1]. The mixture of spent pulping chemicals, dissolved organic matter from the wood, and water is referred to as black liquor. In large-scale industrial steam boilers, the kraft recovery boilers, black liquor is burned to produce heat and power but also to recover the spent pulping chemicals. Recovery rates of the spent pulping chemicals reach values of up to 98%, eliminating the need for new chemicals almost completely [2]. At the same time, the power produced in a modern kraft recovery boiler typically exceeds the mill's energy needs [2]. In Finland, the pulp and paper industry is a vital part of both economy and national energy supply, as 86% of the country's land area is covered by forest [3]. In 2020 renewable energy was the largest energy source in Finland, supplying 40% of the country's energy

demand [3], whereof around one-third is produced from black liquor combustion [3].

Compared to other biofuels, black liquor contains higher amounts of inorganic compounds originating mainly from pulping chemicals, but also raw wood [4]. During combustion, parts of these inorganic compounds are released into the gas phase, forming ash deposits on heat exchanger surfaces in the colder parts of the boiler. Such deposits contain predominantly Na_2SO_4 , Na_2CO_3 , NaCl , Na_2S and their K counterparts [5]. Na and S originate mainly from the pulping chemicals, while K and Cl originate mainly from wood [4]. Thus, the composition of ash deposits in kraft recovery boilers is affected by the wood type used in the pulping process. Both K and Cl can cause severe operational issues in the boiler, affecting the melting behaviour of ash deposits significantly [5,6]. An increased K content lowers the first melting temperature (T_0) of a deposit [5], while an increase in deposit Cl increases the amount of melt formed at T_0 [6].

The initial formation and build-up of ash deposits in recovery boilers

* Corresponding author. Laboratory of Molecular Science and Engineering, Faculty of Science and Engineering (FNT), Åbo Akademi University, Henriksgatan 2, Åbo, FI-20500, Finland.

E-mail address: roland.balint@abo.fi (R. Balint).

<https://doi.org/10.1016/j.energy.2022.126576>

Received 18 July 2022; Received in revised form 8 November 2022; Accepted 27 December 2022

Available online 29 December 2022

0360-5442/© 2023 The Authors. Published by Elsevier Ltd. This is an open access article under the CC BY license (<http://creativecommons.org/licenses/by/4.0/>).

have been studied thoroughly over the last decades and are well understood by now [7,8]. Three particle size fractions have been identified to contribute to the formation of deposits in kraft recovery boilers [9]. The first layer of superheater deposits formed in kraft recovery boilers consists of submicron-sized fume particles, typically enriched in K and Cl, forming a sticky deposit layer and enabling deposition of larger intermediate-sized and carry-over particles, accelerating the deposit growth rate.

More recent experimental data have shown ash deposits to undergo changes in their local chemical composition and morphology, after their initial formation, referred to as deposit ageing [10–12]. These processes are less understood and over the last years, deposit ageing mechanisms have been studied under well-controlled conditions on a laboratory scale at Åbo Akademi University [10–12]. Three different deposit ageing mechanisms have been identified when exposing synthetic ash deposits to a temperature gradient [10,11]. Deposit ageing has been identified to cause densification of ash deposits, increasing the tensile adhesion strength [13], thus hampering removal via sootblowing. Furthermore, local enrichment of corrosive compounds toward the steel has been identified to take place via several pathways [11,12].

Despite ash deposition, and operational problems connected to it, have been studied extensively over the last decades, no data on systematic deposit ageing studies of actual superheater deposits can be found in the literature. A change from laboratory experiments to full-scale deposit studies provides additional valuable information. Not only do full-scale data help in confirming earlier findings from laboratory experiments, carried out under well-controlled conditions. But scaling up to actual boiler conditions also provides additional information on other experimental parameters, which have not been possible to be simulated in the laboratory. Among these parameters are e.g. the impact of sootblowers, reactions between the formed deposit and the flue gas, or continuous deposition of new material and concurrently occurring deposit ageing reactions.

Studies utilising full-scale deposits focused mainly on deposit sintering [14,15], or the initial deposit build-up by carrying out short-term probe measurements [16,17]. However, a few examples indicating deposit ageing to be also of relevance for actual ash deposits in steam power boilers were found in the literature [18,19]. Several studies reported the formation of a layered deposit structure, which typically has been associated with changes in the operating conditions of the boiler or governing deposition mechanisms [8,18,20,21]. Reeve et al. [8] have analysed deposits collected on an air-cooled probe and identified local enrichment in K and Cl within the deposit, toward the steel surface. The observed enrichment has been concluded to be the result of alkali chloride vapours in the flue gas penetrating the outer sintered deposit layer through cracks and subsequently condensing in the inner parts of the deposit. Other studies have identified the local enrichment in S due to sulfation of alkali chlorides [7] and carbonates [22] to be of relevance for kraft recovery boiler deposits, causing melt formation due to compositional changes within the deposit. Sulfation of deposits has also been identified in several straw-fired boilers [18] after the deposits had formed on the superheater tubes. A more recent study carried out in a Brazilian kraft recovery boiler [20] has identified clear enrichment in Cl and K within the region of the deposit closest toward the steel, resulting in a local decrease in the first melting temperature of the deposit and severe melt-induced corrosion of the superheater tubes. In a separate study, deposit samples of this same Brazilian boiler have been analysed in more detail regarding their deposit ageing behaviour [23]. All three ageing mechanisms previously seen within laboratory experiments have also been identified within these actual superheater deposits. Furthermore, a local decrease in T_0 due to local K enrichment connected to deposit ageing has been identified within these deposits [23]. However, more work is needed to better understand and possibly predict deposit ageing mechanisms in actual superheater deposits of boilers.

The objective of the present work was to shed more light on the role of temperature gradient-induced deposit ageing by detailed

characterization of deposit samples from a Finnish kraft recovery boiler. Deposit samples were collected from eight locations within the superheater region during a shutdown of the boiler. Cross-sections of the deposit samples were analysed using scanning electron microscopy and energy dispersive X-ray analysis (SEM/EDX). Several differences in deposit morphology, chemistry, and local melting behaviour among the analysed samples were observed, and different deposit types were identified. These differences are expected to affect the deposit's corrosiveness and removability to different extents.

2. Methods

The present study analysed kraft recovery boiler superheater deposits using SEM/EDX. The deposits were obtained directly from tertiary superheater tubes of a kraft recovery boiler located in Rauma, Finland. The boiler's maximum firing capacity is 3200 tonnes of dry solids per day. The superheater tubes were accessed through eight manholes in the boiler wall, four on each side of the boiler. The exact sampling locations are shown in Fig. 1.

Four sampling locations (L1, L2, R1, and R2) were situated in the upper region of the superheater, close to the boiler roof, and four sampling locations (L3, L4, R3, and R4) were situated in the lower region of the superheater tubes, close to the bull-nose. Deposits were directly scraped off the superheater tubes during a boiler shutdown in September 2019. However, the exact orientation of the analysed deposits concerning their direction to the flue gas stream (wind-side, lee-side, or somewhere between) was not known. Before the shutdown, the boiler had been operating continuously for about 30 days. The fired black liquor had a dry solids content of 74%. The composition of the as-fired black liquor and reference values for a black liquor composition typical for northern Europe are given in Table 1. The oxygen content shown in the table is determined by closing the mass balance.

The steam temperature in the tertiary superheater of the boiler in question averages 480 °C during regular operation. The recovery boiler is not equipped to measure the flue gas temperature in the superheater region from which the samples were obtained. Flue gas temperatures in the region of the boiler the samples were taken from typically range between 600 and 650 °C.

For a detailed analysis of the local chemical composition, the deposit samples were cast in epoxy resin to prevent any loss of deposit material during further processing of the samples. The cast deposits were then cut to obtain a cross-section, which was polished using SiC polishing paper. No additional lubricants were used during sample preparation to avoid the dissolution of the water-soluble deposit. The polished deposit cross-sections were cleaned using petroleum ether, and subsequently carbon-coated. The general morphology and chemical composition throughout the deposit cross-sections were analysed using scanning electron microscopy (SEM) and energy dispersive X-ray (EDX) analysis (LEO Gemini 1530 equipped with a ThermoNORAN Vantage X-ray analysing system manufactured by Thermo Scientific), operated at an accelerating voltage of 20 kV and a working distance of 13 mm. Backscatter SEM images were used to obtain morphological information and EDX data was used to analyse the chemical composition of the deposits. The molar fractions of Na, K, Cl, and S were obtained directly from EDX analysis. The C content of the deposits was subsequently calculated by closing the charge balance. The O content was calculated by assuming all C was present as carbonate and all S as sulfate.

Based on the results from SEM/EDX analysis, the local first melting temperature of the deposits was calculated. Each cross-sectional SEM image was divided into various sections, based on local differences in the chemical composition. For each of these sections, the average composition was calculated, which was then utilised to calculate the respective T_0 of the section. T_0 calculations were carried out using FactSage Version 8.1 [25] and the FTPulp thermodynamic database [26], containing data relevant for salt mixtures containing NaCl, KCl, Na₂SO₄, K₂SO₄, Na₂CO₃, K₂CO₃, Na₂S, and K₂S typical for deposits occurring in

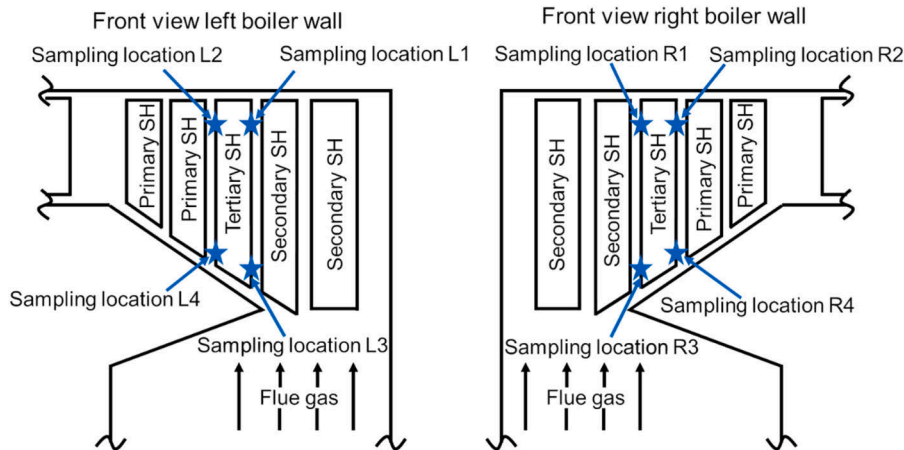


Fig. 1. Schematic front view drawing of left and right side of the superheater area of the boiler with the deposit sampling locations at the tertiary superheater tube bundle indicated.

Table 1
Composition of the black liquor “as-fired” utilised in the present study and reference values of typical black liquor composition in northern Europe.

Element [wt-%]	Black liquor fired in present study	Typical black liquor composition in northern Europe [24]
C	32.8	29.4
H	3.7	3.7
N	0.1	0.2
S	5.7	3.2
Na	20.4	20.8
K	2.8	1.5
Cl	0.3	0.5
O	34.1	40.5
Others	0.1	0.2

kraft recovery boilers. The following phases were considered in the calculation: Liquid phase (designated as FTpulp-MELTA in FactSage); high-temperature, hexagonal alkali sulfate-carbonate solid solution (FTpulp-Hexa); several low-temperature alkali sulfate-carbonate solid solutions (FTpulp-KCO; FTpulp-NKCB; FTpulp-NKCA; FTpulp-OrtA; FTpulp-OrtB); alkali chloride solid solution (FTpulp-ACL); alkali sulfide solid solution (FTpulp-NAKS); and glaserite ($K_3Na_2(SO_4)_2$ -based solid solution, FTpulp-Gsrt). In all calculated cases, only the hexagonal phase and alkali chloride were the solid phases stable at T_0 of the system. Using this method, the impact of local elemental enrichment on the deposit’s local first melting temperature was studied.

3. Results and discussion

3.1. General deposit characteristics

A total of 13 deposits were analysed regarding their chemical composition and morphology. Morphological differences between individual deposits were identified. The main morphological features are presented in the following paragraph. Fig. 2 shows SEM images of selected deposit cross-sections from various sampling locations.

All SEM images of deposit cross-sections shown in Fig. 2 and the following figures are oriented in the same way. The deposit surface at the bottom of the image was closest to the superheater steel during boiler operation while the deposit surface at the top of the image was facing the flue gas. Thus the local temperature throughout the deposit

cross-section increases from the bottom of the image toward the top, due to the temperature difference between the cool superheater steel and the hotter flue gas. However, the orientation of the images in Fig. 2 does not correspond to the actual orientation in the boiler, as the superheater tubes are vertically aligned in the boiler.

As shown in Fig. 2, all analysed deposits were sintered but to a varying degree of porosity. The Cl content suggests that the amount of melt formed in the deposits during boiler operation was relatively low. Thus, the deposits remained porous as the amount of melt was not sufficient for liquid phase sintering, not even toward the outer deposit surface where the local temperatures were the highest. Clear morphological differences between deposits from sampling points 1 and 2 (Fig. 2 A and B), close to the boiler roof, and deposits from sampling points 3 and 4 (Fig. 2C, D, and E), close to the bullnose, were identified.

Deposits from the upper superheater region can be divided into two distinct regions. The innermost layer typically consisted of small particles that sintered into a well-connected skeletal network (Fig. 2 G). With increasing distance to the steel, the deposit morphology changed and the sintered agglomerates increased in size (Fig. 2 F). A more detailed description of these two layers and their underlying formation mechanisms are presented in the further course of the text.

Deposits from the lower superheater region typically contained irregularly shaped particles, significantly larger than the sintered agglomerates on the outer region of deposits from sampling locations one and two (Fig. 2H). The originally deposited particles could still be identified. Deposits from the lower superheater region did not form a skeletal structure. The exact formation mechanism of the deposits from the lower superheater region is not fully understood. However, the morphological features suggest formation via deposition of larger carryover particles, which were partially molten in flight, thus adhered on the superheater tubes, and solidified after impaction. The proposed deposition mechanism accounts for the low porosity of deposits from the lower superheater region. As the deposits did not form a dense molten layer but contained gaps between the single particles, liquid phase sintering was ruled out to have taken place within deposits from the lower superheater region.

Also among samples from the same sampling point, especially the lower superheater region, significant differences in deposit morphology were seen (Fig. 2 D and E). The exact formation mechanisms resulting in the seen morphological differences are currently not understood, and further research is needed.

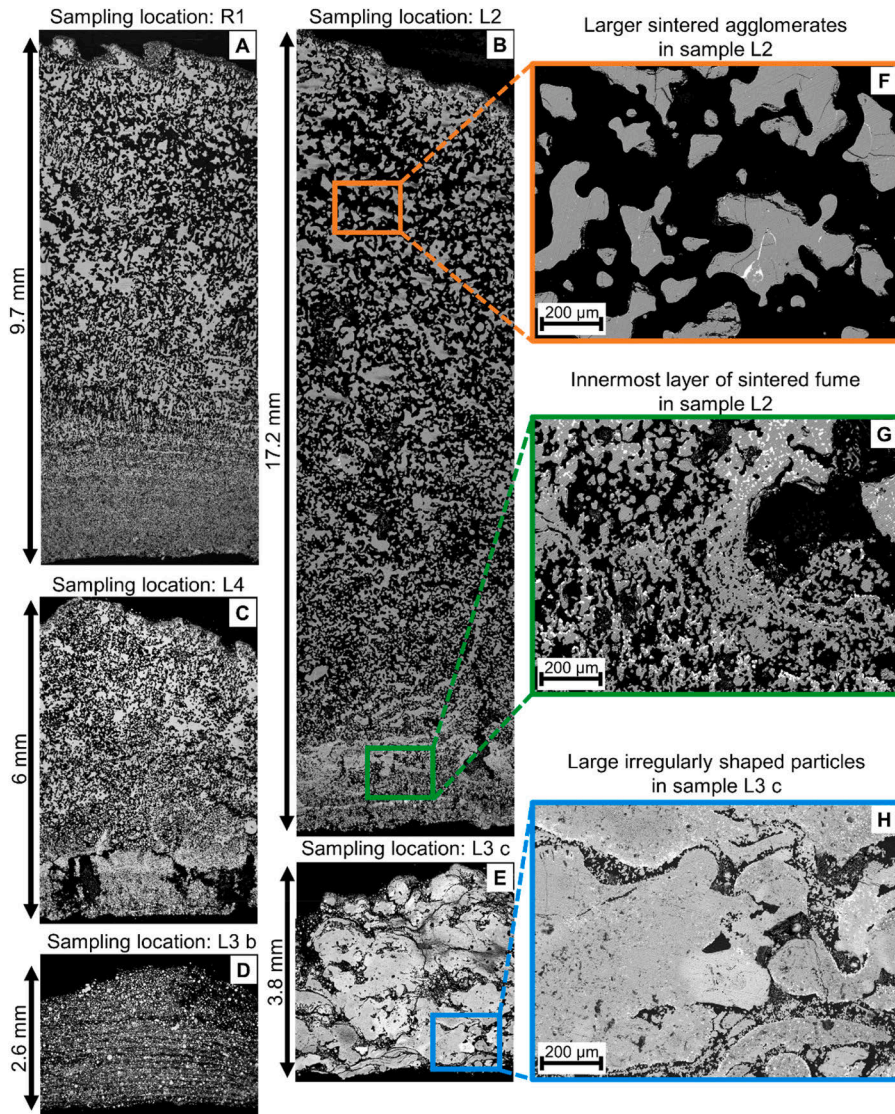


Fig. 2. Selected SEM images of deposit cross-sections from upper superheater region (A and B) and lower superheater region (C, D, and E); zoomed images (F, G, and H) highlighting the main morphological differences between samples; different shades of grey representing the deposit material and black regions corresponding to gas phase (epoxy resin). (For interpretation of the references to colour in this figure legend, the reader is referred to the Web version of this article.)

Besides morphological differences, the deposits from the lower superheater region were typically thinner, with an average thickness of 5.9 mm, compared to deposits from the upper superheater region with an average thickness of 19.6 mm. Multiple parameters can have an impact on the deposit thickness during boiler operation. The distance to the closest sootblower and frequency of sootblowing can account for significant differences within the final deposit thickness as well as the particle load in the flue gas. The bulk of the flue gas enters the upper

superheater region after exiting the furnace, resulting in a higher particle load within the region of the upper superheater tubes (sampling points 1 and 2) compared to the lower superheater region (sampling points 3 and 4) close to the bull-nose. It has been shown for the deposition rate increases linearly with increasing particle load [27]. Thus, the deposit build-up rate was expected to be higher in the upper superheater region compared to the lower superheater region.

For further detailed analysis in the present report, only deposits

collected from the upper superheater region were utilised. This allowed for easier comparison between the present deposit samples and superheater deposits from the upper superheater region of a Brazilian kraft recovery boiler, presented elsewhere [23].

Despite the differences in deposit morphologies seen in Fig. 2, no significant variations in the bulk composition among all analysed deposits were observed. The calculation of the average bulk deposit composition of all analysed deposits was based on EDX data of the cross-sections. In Table 2, the mass-based average bulk deposit composition of all obtained deposits is shown.

The bulk deposit composition in Table 2 was calculated by assuming that all sulfur was bound as sulfate. The carbonate content was calculated by closing the charge balance. The main constituents of the deposits were Na and SO_4 , making up almost 78 wt-% of the deposit, while Cl made up 0.7 wt-% on average. The Cl content in the Finnish deposit samples was lower compared to Brazilian superheater deposits [23]. In general, superheater deposits from Scandinavian and also North American kraft recovery boilers have a lower Cl content than deposits from South America due to the wood type used in the pulping process [4]. This difference in deposit Cl content is thought to be mainly responsible for the differences in deposit morphology between the Finnish and Brazilian deposits.

Due to the low deposit Cl content, no significant melt formation was expected within the deposits at the prevailing flue gas temperatures. The calculated melting curve based on the average deposit composition (Table 2) also suggested a low amount of melt to form at the expected maximum flue gas temperature as shown in Fig. 3.

The amount of melt formed at T_0 was very low, 2 wt-%, and did not increase significantly with increasing temperature. Up to 675 °C, i.e., above the estimated maximum flue gas temperature at the sampling location, the amount of melt within the deposit remained below 10 wt-%. Only at temperatures above 725 °C, well above temperatures relevant for the present deposit samples, the formed amount of melt began to increase more steeply.

Even though no significant differences in the average deposit composition between single samples were seen, local enrichment of elements such as Cl, K and S were observed in SEM/EDX analyses. Two main enrichment patterns were identified, thus the deposits were classified into two main deposit types based on their local chemical composition in the region closest to the steel. In the following, the main characteristics of the two deposit types from the upper superheater region are presented.

3.2. Initial deposit layer of fume enriched in K and Cl – “type 1” deposit

The first deposit type, “Type 1”, can be divided into three distinct regions as shown in Fig. 4.

Closest to the steel (Fig. 4 A), the deposit consisted of a porous layer of a network of fine, sintered particles. A similar morphology has also been identified in laboratory studies investigating the condensation of alkali chloride vapours from hot flue gases onto cold steel tubes [28,29], as well as in deposition experiments burning black liquor in an entrained flow reactor [30]. The observed morphology of fine sintered particles was suggested to have resulted from homogeneous condensation of alkali chlorides in the gas phase. The condensation products were then

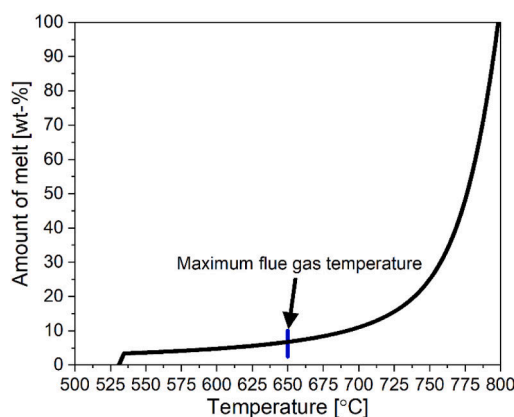


Fig. 3. Melting behaviour of average bulk deposit composition given in Table 2. Estimated maximum flue gas temperature at the sampling location indicated.

transported to the steel surface through the thermal boundary layer via thermophoresis and subsequently deposited on the cold steel surface [28,29].

In the context of recovery boilers, condensation products forming in the flue gas are called fume, typically forming an initial sticky deposit layer on the superheater tubes. Fume particles are of sub-micrometre size and enriched in alkali chlorides [15]. During black liquor combustion, inorganic compounds are released into the flue gas, with alkali chlorides having higher vapour pressures compared to alkali carbonate, sulfate, and sulfide. Therefore, larger amounts of alkali chloride vaporise and enrich in the flue gas. In the superheater region, the inorganic vapours condense as the temperature decreases. These condensation products are not only enriched in Cl due to the higher volatility of alkali chlorides but additionally, enrichment in K is typically observed, as the volatility of KCl is higher compared to NaCl [31].

Fig. 4 D and E show the molar $\text{Cl}/(\text{Na} + \text{K})$ and $\text{K}/(\text{Na} + \text{K})$ ratios within the deposit cross-section. The innermost layer of “Type 1” deposits was enriched in K and Cl compared to the outer regions. Layers enriched in K and Cl parallel to the steel surface were observed throughout the enriched region. However, a more detailed analysis did not show any significant formation of alkali chloride layers on the furnace-facing side of particles, typical for temperature gradient-induced diffusional transport of alkali chloride. Currently, the layered enrichment in alkali chloride is believed to have formed predominantly during initial deposit formation via the above-mentioned condensation mechanism.

Besides differences in the local chemical composition, the particle size within the innermost deposit layer of “Type 1” deposits was significantly smaller compared to the outer regions, as mentioned above. A more detailed analysis of the particle size showed the particle diameter of the innermost layer was slightly below 1 μm on average, implying the main constituent of this region was fume particles [15]. Fume concentration in recovery boiler flue gas streams typically ranges between 10 and 35 g/Nm^3 , while the concentration of larger carry-over particles ranges between 2 and 4 g/Nm^3 [24]. Furthermore, the sampling location favours the formation of an initial deposit layer via fume deposition. Carry-over particles deposit via inertial impaction [18]; thus, most larger particles are expected to not reach the tertiary superheater tubes but instead deposit already on the secondary superheater tubes [32]. Therefore, the analysed deposit morphology, chemical composition, and the general understanding of deposit formation in kraft recovery boilers verified the suggested condensation mechanism yielding the innermost

Table 2
Mass-based average bulk composition of all deposits obtained in wt-%.

Component	Mass fraction [wt-%]
Na	31.9
K	4.6
Cl	0.7
SO_4	45.7
CO_3	17.1

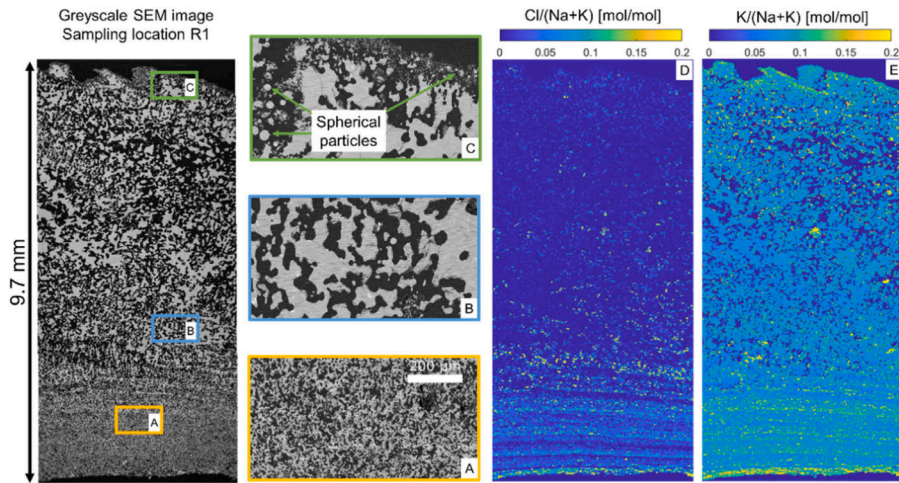


Fig. 4. SEM image of “Type 1” deposit with A) region of fine sintered particles enriched in K and Cl; B) bulk of larger sintered agglomerates; C) layer of spherical particles on outer deposit surface; D) molar Cl/(Na + K) ratio; and E) molar K/(Na + K) ratio.

layer of “Type 1” deposits.

No indications of melt formation within this innermost region of the deposit during boiler operation were found. Closest to the steel, the local deposit temperature was the lowest and expected to remain below T_0 during boiler operation. The steel temperature of the superheaters is kept at temperatures well below T_0 of the bulk deposit to avoid any melt getting in direct contact with the steel. Even deposits from different boilers, with higher Cl concentrations and higher amounts of melt formed during boiler operation, have been shown to contain a porous layer closest to the steel due to the low local temperatures [23].

It is worth mentioning that, in a few cases, the innermost deposit layer of fine, sintered particles was missing, indicating material loss. As the deposits were mechanically removed from the superheater tubes, it is not clear if material was lost during sampling. Thus, it cannot be ruled out that the innermost layer of fine, sintered particles of some deposit samples was damaged during sampling and transportation, resulting in the lack of the innermost deposit layers. Especially, as the region of fine sintered particles appeared to be more fragile than the remaining deposit toward the hotter outer deposit surface, the lack of the innermost deposit layer is currently believed to be a sampling artefact.

The porous layer consisting of fine, sintered particles seen in Region A in Fig. 4 is followed by a second sintered layer consisting of larger agglomerates (Region B). Within Region B, the local temperature was higher compared to Region A due to the temperature gradient in the deposit. The smooth edges on the irregularly shaped particles indicated the local deposit temperature having been above T_0 during boiler operation, resulting in initial melt formation. However, as shown in Fig. 3, the amount of melt formed was below 10 wt-% throughout the deposit as the flue gas temperature at the sampling location did not exceed 650 °C. The amount of melt was thus insufficient to form a dense molten layer. Similar results have been observed in synthetic deposit samples studied in the laboratory [10–12].

The alkali chloride layers on the furnace-facing side of particles in Region B were more pronounced than in Region A. The gap size between two distinct particles was larger in Region B than in Region A, causing larger temperature differences between two distinct particles in Region B. Subsequently, the concentration gradient of alkali chloride in the gas phase increased, resulting in higher diffusional transport rates. Similar observations of the air gap size affecting the rate of diffusional alkali

chloride transport have been reported in laboratory experiments [12]. Thus, the change in deposit morphology was believed to contribute to the increased alkali chloride layer thickness with increasing distance from the steel. Furthermore, higher local temperatures increase the alkali chloride vapour pressure, resulting in a larger concentration gradient of alkali chloride in the gas phase. In comparison to laboratory experiments, the Cl layers were thinner in actual boiler deposits. The observed difference is due to the temperature gradient in the boiler deposits being smaller, resulting in slower transport rates of alkali chloride vapours compared to the laboratory experiments. Furthermore, the boiler deposits contained less alkali chloride, thus the layers could not reach an equal thickness. However, the underlying mechanism of diffusional vapour transport resulting in the formation of such alkali chloride layers is not expected to be further affected when comparing the laboratory set-up to the boiler environment.

Within several of the analysed deposit samples, alkali chloride-rich regions were not exclusively observed on the furnace-facing sides of particles but also within larger sintered agglomerates. The small amount of melt within the deposit is highly enriched in Cl compared to the original deposit. Melt tended to accumulate at contact points between distinct particles, favouring liquid phase sintering [33]. The increased size of sintered agglomerates within Region B compared to Region A (Fig. 4) was due to the capability of already small amounts of melt to accelerate sintering processes [34]. For all deposits obtained from the upper superheater region, a layer with a morphology similar to Region B in Fig. 4 was observed. This morphology accounts for the bulk of the deposits.

A thin layer of small, spherical particles was seen at the outermost part of the deposit (Fig. 4C). These particles were thought to represent newly deposited material, for which the residence time in the deposit was not sufficient to undergo more pronounced sintering during boiler operation. It is not clear to what extent these spherical particles represented the actual deposit material during regular boiler operation. The boiler shut-down before the samples were taken likely affected the flue gas conditions within the convective pass of the boiler. Hence, the composition of the deposited particles may differ from that of particles deposited during regular boiler operation.

Based on the average particle size of 20 μm , the spherical particles on the outer deposit surface are intermediate-sized particles (ISP) [31].

Local enrichment in K on the outer deposit surface was seen in Fig. 4 E. The cause for this enrichment is currently unknown. A thin layer of spherical particles and local enrichment in K was seen on the outer surface of all deposits originating from the upper region of the superheater tubes.

Local enrichment in certain elements within a deposit, especially in direct vicinity to the steel, as seen in Fig. 4 D and E, can have a significant impact on deposit-induced superheater corrosion. Furthermore, changes within the local composition of the deposit affect the local melting behaviour. In an earlier study, deposit ageing mechanisms resulting in local enrichment of K and Cl have decreased the local first melting temperature of kraft recovery boiler superheater deposits toward the steel [23]. The impact of local differences in the deposit composition on the first melting temperature T_0 was studied in detail. For this, the “Type 1” deposit of Fig. 4 was divided into several sections and T_0 was calculated for each section. The local first melting temperature profile as a function of distance from the steel and the sections the deposit was divided into are shown in Fig. 5. The figure also shows the molar $\text{Cl}/(\text{Na} + \text{K})$, $\text{K}/(\text{Na} + \text{K})$ and $\text{S}/(\text{Na} + \text{K})$ ratios.

The local first melting temperature had its minimum in the innermost section closest to the steel, where the molar $\text{Cl}/(\text{Na} + \text{K})$ and $\text{K}/(\text{Na} + \text{K})$ ratios were the highest. Throughout the region enriched in K and Cl, local T_0 values were lower than in the three regions furthest away from the steel, which showed no local elemental enrichment and corresponded to the bulk of the deposit. As the Cl content of the deposit was below 5 wt-% on average, also enrichment in Cl, besides enrichment in K, caused a local decrease in the deposit first melting temperature [6]. The enrichment in Cl and K within the “Type 1” deposit was not thought to be exclusively caused by alkali chloride vapour transport within the already formed deposit. Some alkali chloride enrichment close to the steel likely took place during deposit build-up. However, layers of alkali chloride were seen within the Cl and K enriched region of the deposit as well, thus diffusional gas-phase transport of alkali chloride most likely contributed to the observed decrease in T_0 to some degree. The deposits of the present work were sampled after about 30 days of boiler operation. Whether alkali chloride enrichment would be similar in deposits after 12–18 months of operation, an interval typical between scheduled boiler shut-downs is unclear.

Above the region enriched in K and Cl, the deposit local T_0 and

chemical composition remained fairly constant over a large region. The increased formation of alkali chloride layers within this deposit region did not cause any significant differences in the local chemical composition; thus, local T_0 values did not change significantly. Already minor variations in the local deposit composition, which are within the measurement error of the EDX analysis, result in changes in the calculated local first melting temperature of around 3 °C. Therefore, variations in the local first melting temperature of less than 5 °C were considered too small to assess whether calculated local variations in T_0 were caused by intra-depositional mechanisms altering the local deposit composition.

At the outermost layer of the deposit, the local T_0 value was the highest, despite being enriched in K. Besides K, the outermost deposit layer was also enriched in S, as seen in Fig. 5, while no enrichment in Cl was observed. An increasing K content does not affect the first melting temperature in deposits if the molar $\text{Cl}/(\text{Na} + \text{K})$ ratio remains below 0.015 [9], which applied to the “Type 1” deposit shown in Fig. 5. Furthermore, the simultaneous enrichment in S locally increased the molar SO_4/CO_3 ratio on the outer deposit surface, resulting in the observed increase in the local first melting temperature. These observations are in line with experimental results carried out by Frederick and Vakkilainen [15], and the general understanding of the melting behaviour of deposits formed in a kraft recovery boiler [26]. In terms of corrosiveness, the outer deposit region is of little interest due to the increased distance from the steel surface. In addition, the flue gas composition and the composition of the outermost deposit layer might have been affected by the boiler shut-down. Thus, the outermost layer of the deposit will not be discussed in any more detail within the present report.

3.3. Innermost layer enriched in S and K – “type 2” deposit

An example of a “Type 2” deposit with SEM/EDX maps highlighting the main characteristics is shown in Fig. 6.

The outer region of the “Type 2” deposits did not differ from that of the “Type 1” deposit in morphology and chemical composition and will therefore not be further discussed. However, the chemical composition of the innermost deposit region of “Type 2” deposits differed significantly from “Type 1”.

Closest to the steel the deposit was enriched in potassium and sulfur

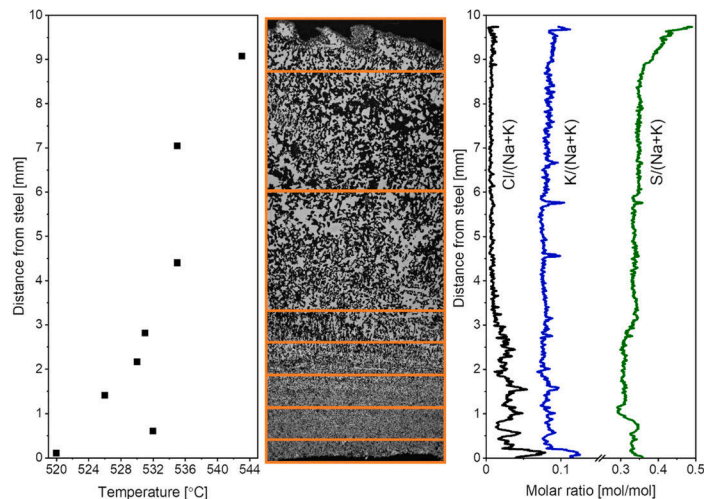


Fig. 5. Local first melting temperature of “Type 1” deposit and molar $\text{Cl}/(\text{Na} + \text{K})$, $\text{K}/(\text{Na} + \text{K})$, and $\text{S}/(\text{Na} + \text{K})$ ratios as functions of distance from the steel.

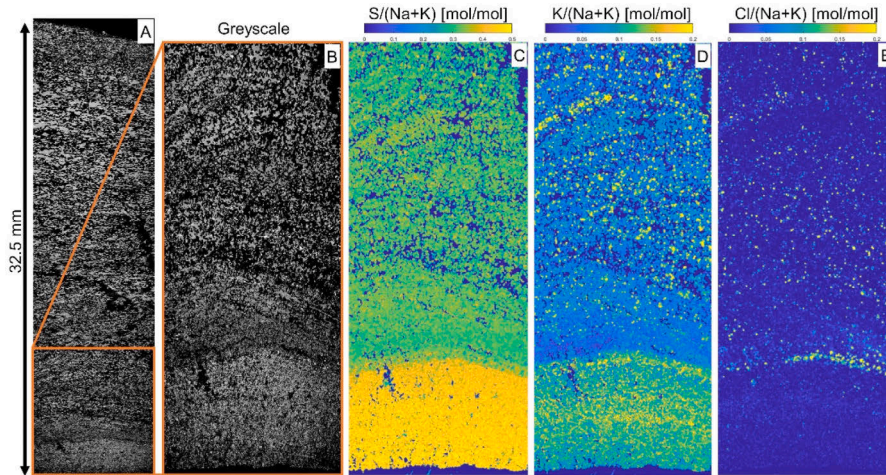


Fig. 6. A) Greyscale image of “Type 2” deposit; B) close-up of the region closest to the steel; C) molar S/(Na + K) ratio; D) molar K/(Na + K) ratio; E) molar Cl/(Na + K) ratio.

(Fig. 6C and D), while at the same time depleted in chlorine (Fig. 6E). The innermost region of “Type 2” deposits consisted of a dendritic structure of fine sintered particles, similar to “Type 1” deposits and was therefore believed to have formed via the same condensation mechanism.

The chemical composition of the innermost layer was believed to have formed via sulfation, whereby the initial deposit layer, originally enriched in K and Cl, reacted with SO_2 from the flue gas. Several studies in the literature have indicated that sulfation of alkali chlorides is of relevance in kraft recovery boilers [7,35] and especially toward the innermost region of deposits [7].

To further investigate whether the sulfation reaction serves as a plausible explanation for the observations made within “Type 2” deposits, the SO_2 concentration measured in the flue gas stack was analysed. Significantly higher SO_2 concentrations of 184 mg/Nm^3 on average with maximum peaks up to 690 mg/Nm^3 were recorded during the first five days of boiler operation. For the remaining operating time of the boiler, corresponding to normal operation, the measured SO_2 concentration in the flue gas stack was essentially zero. During boiler start-up, heavy fuel oil was used, known to cause higher SO_2 emissions. In addition, lower furnace temperatures during start-up as compared to normal boiler operation promoted SO_2 emission [32]. Thus, the measured SO_2 concentrations supported the hypothesis of alkali chloride sulfation to result in the analysed innermost layer composition of “Type 2” deposits.

With increasing distance from the superheater steel surface, the local chemical composition of the deposit changed. The K and S enriched region was followed by a layer enriched in Cl compared to the deposit bulk, while also slightly being enriched in K. A layer enriched in Cl but varying in thickness was analysed within all “Type 2” deposits. For the majority of samples, the Cl-enriched region did not show any enrichment or depletion in either K or S. Also, within the deposit shown in Fig. 6, the Cl-rich layer above the sulfated part of the deposit was not enriched in S, possibly due to the lack of SO_2 in the flue gas after the first five days of boiler operation. Also, regions further away from the steel had a shorter residence time in the deposit, not sufficiently long to undergo substantial sulfation.

However, sulfation of alkali chlorides alone does not explain the concurrent enrichment in K within the innermost region of the “Type 2”

deposits. Currently, the K enrichment is believed to be a remnant of the initial deposit layer, originally enriched in K and Cl as seen in the “Type 1” deposit (Fig. 4). The sulfation reaction does not affect the K content within the deposit, therefore the sulfated region of the deposit remained enriched in K. However, it cannot be ruled out that some other mechanism caused the observed K enrichment. Furthermore, no definite explanation for why the S-rich layer wasn’t seen within all deposit samples can be provided. Based on the analysis results, an asymmetric flue gas flow was believed to have caused local differences in the SO_2 concentration in the flue gas and therefore, not all deposit samples showed signs of sulfation. The lower boiler load during boiler start-up, compared to regular boiler operation, typically amplifies asymmetric flue gas conditions. Further research is needed to better understand the underlying mechanism(s) causing the observed local enrichment in K and S within “Type 2” deposits.

Also for the “Type 2” deposit, the local melting behaviour was analysed in more detail. The sections the deposit was divided into are shown in Fig. 7 together with the local T_0 profile and the molar K/(Na + K), Cl/(Na + K), and S/(Na + K) ratios.

The local first melting temperature within the innermost K and S enriched region of the deposit shown in Fig. 7, was increased by almost 20°C compared to the outer deposit region, an observation made for most of the analysed “Type 2” deposits despite the locally increased K content. The local increase in T_0 resulted from the enrichment in S on one hand, and the depletion in Cl, on the other hand. These observations are in line with the general understanding of the well-studied melting behaviour of ash deposits forming in kraft recovery boilers [26]. Similar to the outer deposit surface, the local increase in the SO_4/CO_3 ratio increased T_0 . Similar observations have been made by Frederick and Vakkilainen, who have identified sulfation of deposits to cause an increase in the first melting temperature [15]. In the present samples, the K increase did not affect T_0 , as the molar Cl/(Na + K) ratio remained below 0.015 throughout the K-enriched region [9].

3.4. Summary of observations and proposed deposit formation and ageing mechanisms

The analysed deposits from the upper superheater region were classified into two main types based on differences in their chemical

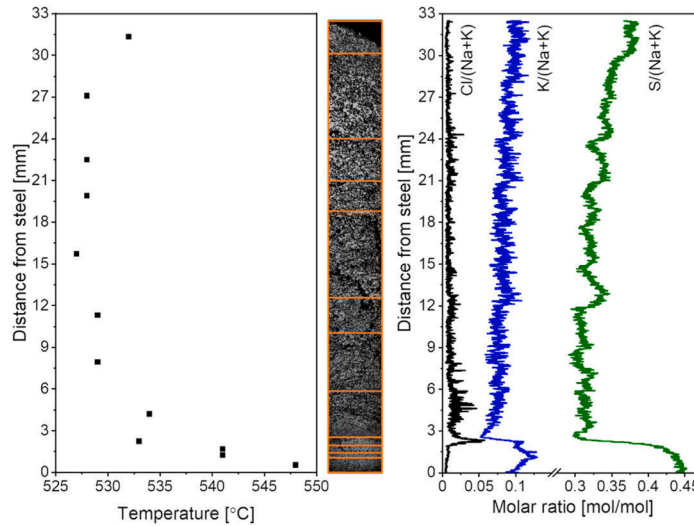


Fig. 7. Local melting behaviour and molar $\text{Cl}/(\text{Na} + \text{K})$, $\text{K}/(\text{Na} + \text{K})$, and $\text{S}/(\text{Na} + \text{K})$ ratios as functions of distance from the steel of innermost region of “Type 2” deposit with locally increased T_0 close to the steel.

composition closest to the steel. In addition, some of the deposits had a morphology and chemical composition differing from these two main types. Fig. 8 summarizes all deposit types observed and puts forward an explanation for how these deposit types can be linked.

The deposits obtained from the upper superheater region were divided into two distinct regions, based on their morphological features. Closest to the steel, the deposits consisted of a porous layer of sub-

micron-sized fume particles. Further away from the steel, the morphology changed to that of larger sintered agglomerates. Temperature gradient-induced diffusion of alkali chloride toward the steel was assumed the governing deposit ageing mechanism in both deposit regions.

The initial deposit layer built up as alkali chloride-rich fume particles, formed via homogeneous condensation in the flue gas, deposited on

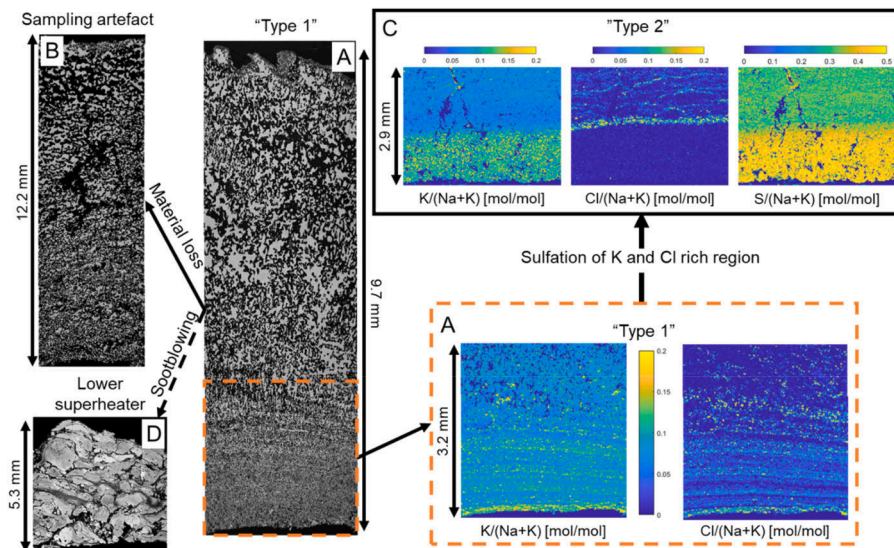


Fig. 8. Summary of identified deposit types: A) “Type 1” deposit with innermost layer of fine sintered particles enriched in K and Cl; B) Sampling artefact lacking innermost layer of fine sintered particles; C) “Type 2” deposit with innermost layer enriched in K and S while concurrently depleted in Cl; D) Thin deposit of large irregularly shaped dense particles from lower superheater region.

the superheater steel resulting in local enrichment in K and Cl closest toward the steel ("Type 1", Fig. 8 A). Local T_0 values were lower within the region enriched in K and Cl as compared to the outer regions of the deposit.

The innermost layer of "Type 1" deposits consisting of fine, sintered particles was more fragile than the outer parts of the deposit. Thus, some of the analysed samples lacked this innermost layer of fine particles (Fig. 8 B) as it presumably got lost during deposit sampling. In general, material loss during sampling could not be ruled out for any of the analysed deposit samples.

The second main deposit type had an innermost layer enriched in K and S while concurrently depleted in Cl ("Type 2", Fig. 8C), believed to have formed via sulfation of the innermost layer initially enriched in K and Cl. Local T_0 values increased within the K and S-rich layer of "Type 2" deposits due to the high S content and concurrent lack of Cl within this region.

Several deposits from the lower superheater region showed significant deviation in morphology (Fig. 8 D) compared to deposits from the upper superheater region. The underlying mechanisms causing the observed densification are currently not known.

4. Conclusions and implications

Ash deposits collected from the tertiary superheater tubes of a Finnish kraft recovery boiler were analysed regarding their chemical composition and morphology using SEM/EDX. The main findings can be summarized as the following.

- The melt fraction formed within deposits did not exceed 10 wt-%, thus the aged deposits from the upper superheater region formed a two-layered skeletal morphology. The governing deposit ageing mechanism was diffusional transport of alkali chloride vapours toward the steel, induced by the temperature gradient the deposits were exposed to.
- Type 1 deposits had an innermost layer enriched in K and Cl, formed via deposition of K and Cl-rich fume particles and additional deposit ageing. Furthermore, the local T_0 of the deposits had a minimum within the K and Cl-rich region, increasing the risk of melt formation in the direct vicinity of the steel and hampering deposit removal via sootblowing. The high Cl concentrations close to the steel and local decrease in T_0 were believed to increase the corrosiveness of the deposits.
- Type 2 deposits had an innermost layer enriched in K and S while concurrently depleted in Cl, formed via sulfation. The innermost deposit layer originally enriched in K and Cl reacted with SO_2 from the flue gas forming alkali sulfate whereas HCl was released into the gas phase. The local T_0 was shown to be increased within the sulfated region compared to the outer regions of the deposits due to the lack of Cl and concurrent increase in the SO_4/CO_3 ratio. Thus sulfation potentially reduces the risk of deposit-induced superheater corrosion.
- More research is needed to better understand the underlying cause for the observed morphological differences between deposit samples from the upper and lower superheater regions. Furthermore, a better understanding of what resulted in the concurrent presence of the two main types of deposits is needed.

CRedit author statement

Roland Balint: Investigation, Data Curation, Writing – Original Draft, Visualization. Markus Engblom: Supervision, Project administration, Writing – Review & Editing, Investigation, Validation. Jonne Niemi: Validation, Investigation, Writing – Review & Editing. Daniel Lindberg: Validation, Funding acquisition, Writing – Review & Editing. Timo Saarinen: Resources. Jaakko Rautala: Resources. Mikko Hupa: Validation, Writing – Review & Editing. Leena Hupa: Writing – Review &

Editing, Funding acquisition.

Declaration of competing interest

The authors declare that they have no known competing financial interests or personal relationships that could have appeared to influence the work reported in this paper.

Data availability

Data will be made available on request.

Acknowledgements

The financing through a research grant awarded by the Fortum Foundation [Application number 20190123] is highly acknowledged. This work has been partly carried out within the Åbo Akademi CLUE² Research Consortium (2017–2022). Support from ANDRITZ Oy, Valmet Technologies Oy, UPM-Kymmene Oyj, Metsä Fibre Oy, and International Paper Inc. is gratefully acknowledged. Additional support from the Academy of Finland projects "Understanding the dynamics of intradeposit chemistry and morphology for control of corrosion in high temperature processes" [Decision number 310266] and "New insights on the effects of temperature gradients on high temperature corrosion" [Decision number 338322] is highly appreciated. We want to thank Linus Silvander for carrying out SEM/EDX analyses.

References

- [1] Alén R. Pulp mills and wood-based biorefineries. In: Industrial biorefineries & white biotechnology. Elsevier; 2015. p. 91–126. <https://doi.org/10.1016/B978-0-444-63453-5.00003-3>.
- [2] Valkilainen EK. Chapter 11 recovery boiler. In: Steam generation from biomass. Elsevier; 2017. p. 237–59. <https://doi.org/10.1016/B978-0-12-804389-9.00011-3>.
- [3] Vaahtera Eeva. Metsätalustilallinen vuosikirja - Finnish statistical yearbook of forestry 2021. Helsinki: Luke Metsätalustilallinen vuosikirja; 2021.
- [4] Karlemo C. Non-process elements in the recovery cycle of six Finnish Kraft pulp mills. Master's Thesis. Åbo Akademi University; 2019.
- [5] Tran H, Gonsko M, Mao X. Effect of composition on the first melting temperature of fireside deposits in recovery boilers. TAPPI J 1999;82:93–100.
- [6] Reeve DW, Tran HN, Barham D. The effluent-free bleached kraft pulp mill - Part XI Morphology, chemical and thermal properties of recovery boiler superheater fireside deposits, vol. 82. Pulp & Paper Canada; 1981. p. T315–20.
- [7] Tran HN, Reeve DW, Barham D. formation of kraft recovery boiler superheater fireside deposits. Pulp Pap Can 1983;84:36–41.
- [8] Reeve DW, Tran HN, Barham D. Superheater fireside deposits and corrosion in kraft recovery boilers. TAPPI (Tech Assoc Pulp Pap Ind) 1981;64:109–13.
- [9] Tran H. Recovery boiler fireside deposits and plugging prevention, vol. 2. TAPPI Kraft Recovery Course; 2007. p. 537–72.
- [10] Lindberg D, Niemi J, Engblom M, Yrjas P, Laurén T, Hupa M. Effect of temperature gradient on composition and morphology of synthetic chlorine-containing biomass boiler deposits. Fuel Process Technol 2016;141:285–98. <https://doi.org/10.1016/j.fuproc.2015.10.011>.
- [11] Niemi J, Lindberg D, Engblom M, Hupa M. Simultaneous melt and vapor induced ash deposit aging mechanisms – mathematical model and experimental observations. Chem Eng Sci 2017;173:196–207. <https://doi.org/10.1016/j.ces.2017.07.041>.
- [12] Niemi J, Engblom M, Laurén T, Yrjas P, Lehmusto J, Hupa M, et al. Superheater deposits and corrosion in temperature gradient – laboratory studies into effects of flue gas composition, initial deposit structure, and exposure time. Energy 2021; 228. <https://doi.org/10.1016/j.energy.2021.120494>.
- [13] Laxminarayan Y, Nair AB, Jensen PA, Wu H, Frandsen FJ, Sander B, et al. Tensile adhesion strength of biomass ash deposits: effect of the temperature gradient and ash chemistry. Energy Fuel 2018;32:4432–41. <https://doi.org/10.1021/acs.energyfuels.7b03114>.
- [14] Skrifvars B-J, Hupa M, Hyöty P. Composition of recovery-boiler dust and its effect on sintering. TAPPI J 1991;74:185–9.
- [15] Frederick WJ, Valkilainen EK. Sintering and structure development in alkali metal salt deposits formed in kraft recovery boilers. Energy Fuel 2003;17:1501–9. <https://doi.org/10.1021/ef034012s>.
- [16] Li X, Fakourian S, Moyer B, Wendt JO, Fry A. Ash aerosol and deposit formation from combustion of coal and its blend with woody biomass at two combustion scales: Part 2—Tests on a 471 MWe full-scale boiler. Energy Fuel 2021;36:565–74. <https://doi.org/10.1021/acs.energyfuels.1c03522>.
- [17] Zhang H, Yu C, Luo Z, Li Y. Investigation of ash deposition dynamic process in an industrial biomass CFB boiler burning high-alkali and low-chlorine fuel. Energies 2020;13:11. <https://doi.org/10.3390/en13051092>.

- [18] Jensen PA, Frandsen FJ, Hansen J, Dam-Johansen K, Henriksen N, Hörlyck S. SEM investigation of superheater deposits from biomass-fired boilers. *Energy Fuel* 2004; 18:378–84. <https://doi.org/10.1021/ef030097l>.
- [19] Furugaki T, Takahashi H, Hayashi S. Effect of temperature gradient in ash on high-temperature corrosion of super-heater material in a waste power generation boiler. *Oxid Met* 2022. <https://doi.org/10.1007/s11085-022-10135-1>.
- [20] Costa A, Silva D, Abelha F, Cenibra CNSA. Experience of recovery boiler superheater corrosion at CENIBRA. Halifax, Canada: International Chemical Recovery Conference - ICRG; 2017.
- [21] Liu X, Chen Q, Long L, Meng X, Lv G, Huang Q, et al. In-situ sampling investigation of deposition and corrosion of convective heating surfaces in a grate type municipal solid waste incineration plant: a case study. *Waste Dispos Sustain Energy* 2021;3:299–308. <https://doi.org/10.1007/s42768-021-00087-8>.
- [22] Tran H, Brown CA, Jones AK. Effects of so2 on superheater fouling in kraft recovery boilers. *Tappi J* 2008;7:11–7.
- [23] Balint R, Engblom M, Niemi J, Costa DS da, Lindberg D, Yrjas P, et al. Temperature gradient induced changes within superheater ash deposits high in chlorine. *Energy* 2021;226:120439. <https://doi.org/10.1016/j.energy.2021.120439>.
- [24] Vakkilainen EK. Kraft recovery boilers - principles and practice. Suomen Soodakattilayhdistys r.y.; 2005.
- [25] Bale CW, Bélisle E, Chartrand P, Decterov SA, Eriksson G, Gheribi AE, et al. FactSage thermochemical software and databases, 2010-2016. *Calphad Comput Coupling Phase Diagrams Thermochem* 2016;54:35–53. <https://doi.org/10.1016/j.calphad.2016.05.002>.
- [26] Lindberg D, Backman R, Chartrand P. Thermodynamic evaluation and optimization of the (NaCl + Na2SO4 + Na2CO3 + KCl + K2SO4 + K2CO3) system. *J Chem Therm* 2007;39:1001–21. <https://doi.org/10.1016/j.jct.2006.12.018>.
- [27] Laxminarayan Y. PhD thesis. In: Formation, sintering and removal of biomass ash deposits. Technical University of Denmark; 2018.
- [28] Broström M, Enestam S, Backman R, Mäkelä K. Condensation in the KCl-NaCl system. *Fuel Process Technol* 2013;105:142–8. <https://doi.org/10.1016/j.fuproc.2011.08.006>.
- [29] Wang Y, Tan H. Condensation of KCl(g) under varied temperature gradient. *Fuel* 2019;237:1141–50. <https://doi.org/10.1016/j.fuel.2018.10.046>.
- [30] Baxter L, Hatch G, Sinquefeld SA, Frederick WJ. An experimental study of the mechanisms of fine particle deposition in kraft recovery boilers. In: International chemical recovery conference. vol. 1. Charleston: Tappi Press; 2004. p. 393–412. 2004.
- [31] Kochesfahani SH, Tran H, Jones AK, Grace TM, Lien SJ, Schmidl W. Particulate Formation during black liquor char bed burning. *J Pulp Pap Sci* 2000;26:180–7.
- [32] Adams TN, Frederick WJ, Hupa M. Kraft recovery boilers. New York (NY) : Atlanta (GA): American Forest & Paper Association ; Tappi Press; 1997. 1997.
- [33] German RM, Suri P, Park SJ. Review: liquid phase sintering. *J Mater Sci* 2009;44: 1–39. <https://doi.org/10.1007/s10853-008-3008-0>.
- [34] Kingery WD. Densification during sintering in the presence of a liquid phase. I. Theory. *J Appl Phys* 1959;30:301–6. <https://doi.org/10.1063/1.1735155>.
- [35] Boonsongsup L, Iisa K, Frederick WJ. Kinetics of the sulfation of NaCl at combustion conditions. *Indus Eng Chem Res* 1997;5885:4212–6. <https://doi.org/10.1021/ie9603225>.

R. Balint, M. Engblom, E. Vainio, T. Laurén, J. Niemi, J. Rautala, T. Saarinen,
M. Hupa, L. Hupa (2023)

**Changes in chlorine content over time – Probe deposit sampling in a
Finnish kraft recovery boiler.**

Fuel



Changes in chlorine content over time – Probe deposit sampling in a Finnish kraft recovery boiler

Roland Balint^{a,*}, Markus Engblom^a, Emil Vainio^a, Tor Laurén^a, Jonne Niemi^a,
Jaakko Rautala^b, Timo Saarinen^b, Mikko Hupa^a, Leena Hupa^a

^a Johan Gadolin Process Chemistry Centre, Åbo Akademi University, Turku, Finland

^b Metsä-Fibre Oy, Rauma, Finland

ARTICLE INFO

Keywords:

Ash deposits

Probe sampling

Temperature gradient

Aging mechanisms

ABSTRACT

Probe deposit samples of 1, 5, and 8 weeks exposure time were collected from the superheater area of a Finnish kraft recovery boiler. Deposit cross-sections were analysed regarding their morphology and chemical composition using SEM/EDXA. Morphological differences along the probe's circumference were observed due to different prevailing deposition mechanisms. Overall enrichment in the deposit Cl content with increasing exposure time was observed. The Cl enrichment proceeds via diffusion of Cl-vapours from the flue gas into the deposit. Two deposit ageing mechanisms were identified within the deposit samples. First, alkali chloride layers formed on the furnace-facing side of deposit particles and also directly on the steel surface as a result of deposit ageing. Second, within the 5 and 8-week probe samples, sulfation of alkali chloride within the inner regions of the deposits was observed. Analysis of the local first melting temperature of the deposits showed a significant decrease within the Cl and K-rich layer adjacent to the steel surface, implying an increased risk for melt formation, and thus corrosion, in the direct vicinity of the steel.

1. Introduction

Finland and Sweden are Europe's main producers of pulp and paper, together accounting for almost 60 % of the annual production in 2021 [1]. The dominating process used is the kraft pulping process, where a solution of NaOH and Na₂S is used to extract the pulp fibres from raw wood. The aqueous solution of spent pulping chemicals (Na₂SO₄ and Na₂CO₃) and organic material, mainly lignin originating from the wood, is called black liquor. The black liquor is burned in the recovery boiler, into which it is sprayed as droplets. These droplets dry, pyrolyze, and start to burn in flight. The process is designed in such a way that the burning droplets reach the bottom of the boiler, where a char bed is formed [2,3]. For an efficient boiler operation, the droplets must not reach the bed while still wet, as this would lower the bed temperature and result in undesired growth of the bed. Due to the reducing atmosphere within the bed, Na₂SO₄ present in the droplets is reduced to Na₂S by reacting either with char carbon or reducing gases [2]. The remaining smelt of incombustible inorganics, predominantly Na₂CO₃ and the reduced Na₂S, exits the boiler at the bottom, flowing into a dissolving

tank forming green liquor. The green liquor is further processed in a causticizer to recover NaOH from Na₂CO₃ [2]. The recovery boiler has two main purposes in the pulping process: through combustion the recovery of the spent pulping chemicals, therewith almost eliminating the need for new process chemicals is enabled [4]. At the same time heat and power are generated through combustion of the organic material dissolved in the black liquor. The energy produced by a modern recovery boiler is sufficient to supply the whole mill [4].

However, ash deposition on superheater tubes and therewith associated operational problems such as reduced heat transfer and corrosion of superheater tubes still pose a major problem for boiler operators. A significant share of sodium but also other inorganic compounds dissolved in the fired black liquor release into the gas phase [3]. Furthermore, occasionally black liquor droplets are entrained in the flue gas and form deposits on heat transfer surfaces [3]. Similar deposit-related obstacles also arise for other combustion processes utilising biomass-based fuels. Compared to coal, biomass fuels generally contain larger amounts of inorganic compounds, causing severe slagging, fouling, and corrosion issues in combustion processes, resulting in a lower boiler-efficiency and

* Corresponding author at: Laboratory of Molecular Sciences and Engineering, Faculty of Science and Engineering (FNT), Åbo Akademi University, Henriksgatan 2, Åbo FI-20500, Finland.

E-mail address: roland.balint@abo.fi (R. Balint).

<https://doi.org/10.1016/j.fuel.2023.127599>

Received 4 November 2022; Received in revised form 3 January 2023; Accepted 22 January 2023

Available online 26 January 2023

0016-2361/© 2023 The Author(s). Published by Elsevier Ltd. This is an open access article under the CC BY license (<http://creativecommons.org/licenses/by/4.0/>).

limiting the maximum steam temperature in the hottest superheaters.

In recovery boilers, Cl and K-containing compounds are mainly causing corrosion-related operational issues. Cl originates from the wood, but makeup and bleaching chemicals or process water provide additional sources for Cl to enter the process. K originates from the raw wood and is dissolved in the liquor in the pulping process [5]. The main compounds of recovery boiler superheater deposits are NaCl, Na₂SO₄, Na₂CO₃, Na₂S, and their K counterparts [6].

The formation mechanisms of superheater deposits have been studied thoroughly over the last decades [2,6]. Particles contributing to deposit build-up in a kraft recovery boiler are divided into three main groups [2,7]. The smallest particles, referred to as fume, are sub-micrometre sized and deposit predominantly via condensation or thermophoresis on the lee-side of superheater tubes. Fume particles are rich in alkali sulfate and contain high amounts of alkali chlorides [2,6]. The particles in the second fraction are called intermediate-sized particles (ISP), typically within the range of 1–100 µm in diameter. ISP particles deposit predominantly via inertial impaction on the wind side of the superheater tubes [2,6]. The formation of ISP is not fully understood, but it is believed that these particles form during char bed burning as small char particles are ejected from the bed and entrained in the flue gas. Thus, ISPs contain only small amounts of Cl and high amounts of carbonate and sulfate [6,7]. The largest particle fraction is called carryover; such particles can reach up to a few millimetres in diameter. Carryover particles are (partially) unburnt (fragments of) black liquor droplets entrained in the flue gas [7], thus containing high amounts of carbonate and sulfate [6]. Due to their large size, a big share of carryover particles deposits already on the first rows of superheater tubes via inertial impaction [6].

However more recently, local changes in the deposit composition occurring after the initial deposit formation have been observed. These changes were shown to affect the local deposit composition and thus corrosiveness, removability, and melting behaviour of deposits [8–11]. Such intra-depositional changes taking place after the initial deposit formation are referred to as deposit ageing. Due to the temperature difference between the hot flue gas and the cooler superheater tubes, deposits are exposed to a temperature gradient, which has been shown to cause deposit ageing mechanisms. Diffusional transport of alkali chloride vapours toward the steel and subsequent condensation of these vapours at lower local temperatures result in the formation of alkali chloride layers on the furnace-facing side of particles within the deposit and also directly on the steel surface [10,11]. Furthermore, temperature gradient-induced movement of Cl and K-enriched melt toward the steel has been identified within deposits [8].

Both deposit ageing mechanisms described above increase the local Cl and K content of the deposits toward the steel, directly affecting the deposit's local melting behaviour. An increase in Cl increases the amount of melt that is formed at the first melting temperature T_0 [12], while an increase in K lowers T_0 [13]. Therefore, deposit ageing increases the risk of melt getting in direct contact with the steel surface, resulting in severe corrosion. Deposit ageing mechanisms have been predominantly studied on laboratory scale using synthetic ash deposits [9–11,14], but have also been verified in actual deposits directly collected from the superheater tubes of kraft recovery boilers [8,15]. Within the superheater deposits, a direct impact of these deposit ageing mechanisms on the local first melting temperature of a deposit could be shown, as T_0 has been significantly lower within the Cl and K-enriched region close to the steel compared to the outer regions of the deposit [8,15]. Several deposit samples have been obtained directly from the superheater tubes of the boiler, in which the probe deposit measurements of the present article were carried out. Within these superheater deposit samples, local enrichment in Cl and K toward the steel due to deposit ageing has been observed to result in a local decrease in T_0 within several samples [15]. In other superheater deposit samples, obtained during the same sampling campaign but from different superheater tubes, a sulfated region closest to the steel has caused an increase

in the local T_0 [15].

However, a systematic study on how actual superheater deposits change in their local chemical composition and morphology with time poses some challenges. Actual superheater deposits can only be obtained during a boiler shutdown. Thus, the duration for the deposit to build up and age cannot be chosen freely. Furthermore, deposits have to be removed from the superheater tube they adhered to during boiler operation, resulting in the loss of valuable information from the innermost deposit layer directly attached to the superheater tube. Therefore, a sampling probe has been designed to obtain and analyse deposits still attached to the steel surface they originally formed on during regular boiler operation. Furthermore, the exposure time of the deposit can be controlled, enabling a systematic study of time-dependent processes taking place within a deposit.

The objective of the present study was to obtain a better understanding of deposit ageing under full-scale conditions. Deposits attached to the steel surface they initially had formed on are obtained using a sampling probe. With this method, the deposit steel interface could be studied in more detail. Furthermore, differences in deposit ageing processes depending on the exact location along the probe's circumference, such as wind or lee side, were identified. The measurements aimed to shed more light on the timeframe within which deposit ageing takes place under actual boiler conditions, as measurements with varying exposure times were carried out. Deposit ageing mechanisms were identified within all of the obtained probe samples. Furthermore, a general increase in deposit Cl with time as well as sulfation of the deposits were identified, as a result of the initially formed deposit interacting with the surrounding flue gas. Deposit ageing significantly lowered the local T_0 closest to the steel surface.

2. Materials and methods

Probe deposit measurements were carried out in the superheater region of a kraft recovery boiler with a maximum firing capacity of 3200 tonnes dry solids per day, located in Rauma, Finland. All measurements were carried out in the upper superheater region, between the secondary and tertiary superheater bundles. The closest sootblower was located 0.75 m below the probe, with two more sootblowers located 2.25 m to the left and right, as shown in Fig. 1.

For the discussion of the obtained results, the following nomenclature for selected locations along the circumference of the probe is used: The part of the probe directly facing the flue gas stream is referred to as the “wind side” deposit, while the region shielded off from the flue gas flow by the probe is called the “lee side”. The region between the “wind side” and “lee side”, directly facing the sootblower, is referred to as the “bottom side” and the region on the opposite is referred to as the “top side”.

The sampling probe has been designed and built at Åbo Akademi University. Several short-term experiments were carried out, and the probe design was refined. The main features of the final probe design are presented in Fig. 2.

The design consists of two concentric tubes made from P235GH steel with an outer diameter of 51 mm (A). The part of the probe inserted into the boiler during the experiment is 0.85 m long, including the 0.1 m long detachable tip on which the deposit sample was collected. Before inserting the probe into the boiler, the sampling tip was preheated to temperatures above 100 °C to avoid condensation of water vapour onto the cold steel surface. The sampling tip was mounted to the outer tube of the probe and held in place by the inner tube (B). On the part of the probe located outside the boiler (C), a spring was used to build up sufficient force for the inner tube to keep the detachable tip in place and prevent it from falling off the probe at any time during the experiment.

A custom-made oval plate, exactly fitting the manhole through which the superheater region was accessed, was used to attach the probe to the boiler wall (D). The probe is welded onto a smaller square-shaped plate (A) that can be attached to the larger oval plate during the

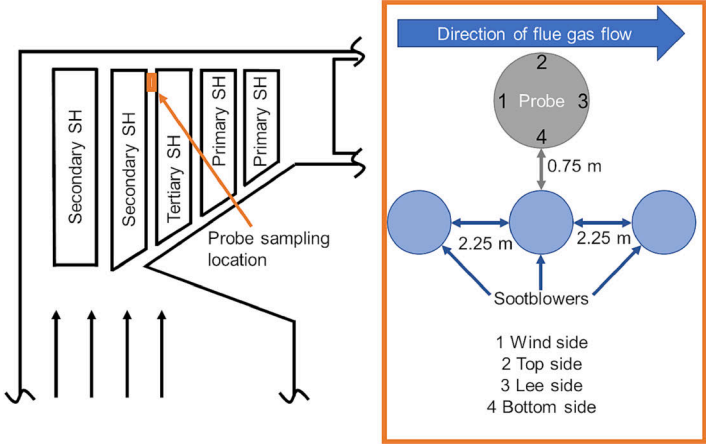


Fig. 1. Probe sampling location in the upper superheater region of the boiler, location of closest sootblowers and sample nomenclature.

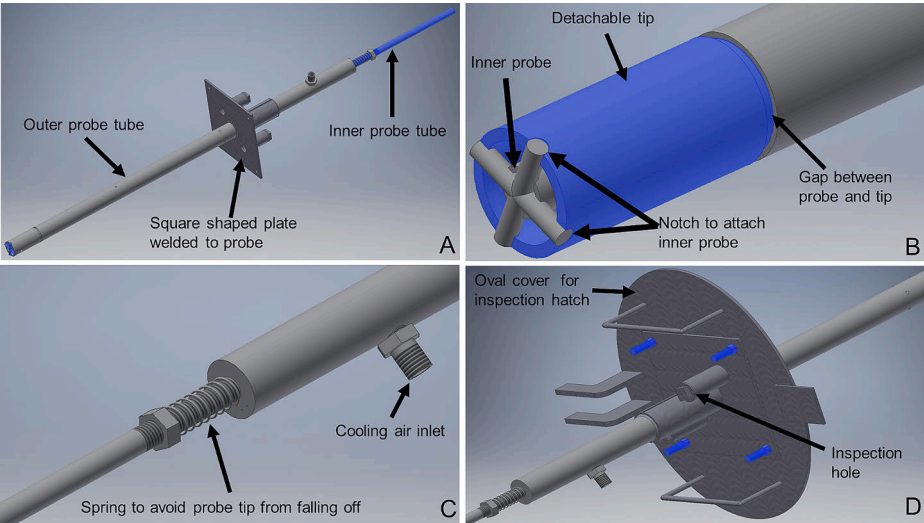


Fig. 2. Main features of probe design: A) Main probe; B) Detachable sampling tip; C) Part located outside of boiler during the experiment; D) Oval manhole cover plate.

experiment, using four bolts highlighted in Fig. 2D. The whole design aims to avoid any rotation of the measurement equipment during the experiment. This design enables differentiation between the probe's wind, lee, bottom, and top sides and identification of location-specific deposition and ageing mechanisms. Two inspection holes are drilled into the squared plate. A thermocouple can be inserted through one of these holes directly into the boiler to measure and log the local flue gas temperature near the probe.

After the experiment, the inner tube was removed first, followed by the tip. Fig. 2B shows a small gap between the detachable tip and the main probe, which helped to remove the tip. Due to corrosion, the tip could not be separated from the probe after longer exposure times. Thus, the tip was cut off using a metal saw without destroying the main probe

or the collected deposit.

Pressurised air entering the probe on the part located outside of the boiler (C) was used to cool the sampling tip and ensure a constant steel temperature during the experiments. Two thermocouples were placed within the detachable tip to control and log the steel temperature throughout the experiment. After passing the probe between the inner and outer tubes, the cooling air exited the probe at the tip and was blown directly into the boiler. Each measurement point of the logged steel and flue gas temperature represents the average temperature over a five-minute interval.

After the experiment, the probe was removed from the boiler and the airflow through the probe was increased to ensure fast cooling of the sample to be able to be cast in epoxy resin. The sample was then cut to

obtain a cross-section. The cross-sections were polished using SiC polishing paper and water-free lubricant to avoid deposit dissolution. The polished cross-sections were cleaned using petroleum ether and carbon-coated before the analysis. Scanning electron microscopy (SEM) and energy dispersive X-ray analysis (EDXA) (LEO Gemini 1530 equipped with a ThermoNORAN Vantage X-ray analysing system manufactured by Thermo Scientific) were utilised to study the deposit morphology and chemical composition in detail.

Based on the SEM/EDXA data, molar $\text{Cl}/(\text{Na} + \text{K})$, $\text{K}/(\text{Na} + \text{K})$, and $\text{S}/(\text{Na} + \text{K})$ ratios were calculated for the analysed cross-sections. In addition, the local first melting temperature (T_0) of the deposits was calculated. The deposit was divided into several sections whereby the average composition for each of these sections was calculated. Subsequently, the local T_0 value was calculated based on the average composition of each section, using FactSage Version 8.1 [16] and the FTPulp database, containing data relevant for deposits forming in kraft recovery boilers [17].

3. Results and discussion

3.1. Morphology and local chemical composition of probe deposits

Deposit sampling experiments with exposure times of 1, 5, and 8 weeks were carried out. The steel temperature at the sampling tip of the probe was set to 450 °C, representing actual steel temperatures of the tertiary superheater tubes in the boiler. The flue gas temperature during the experiments averaged 550 °C, measured with a thermocouple in the vicinity of the probe. Fluctuations in the measured flue gas temperature were observed, occasionally reaching values as high as 650 °C.

Three panorama images of deposit cross-sections obtained from the three experiments are presented in Fig. 3. In addition, locations on the wind, lee, bottom, and top side of the probe deposit samples, where the morphology and chemical composition was analysed in more detail, are indicated.

It should be mentioned that the probe diameter of the one-week experiment shown in Fig. 3 is smaller compared to the five and eight-week experiments. The probe design was changed after the one-week experiment, including an increased probe diameter. However, the overall shape of the obtained deposits shown in Fig. 3, as well as the morphological features of the three deposits, were similar despite the difference in probe diameter. Hence, the modified probe design did not affect the results of the experiments.

All deposits obtained were porous and appeared the thickest at the lee and top sides of the probe, while the bottom and wind sides were significantly thinner. The bottom part of the probe was affected the most by the sootblower it was directly facing, located 0.75 m below the probe.

Therefore, the bottom side deposit was thinner than other locations along the probe's circumference. Differences in deposit thickness between the wind and lee sides were caused by differences in the prevailing deposition mechanisms at those two locations. As the measurements were carried out between the secondary and tertiary superheater, the deposits built up predominantly from sub-micrometre-sized fume particles. A major share of the larger intermediate-sized and carryover particles tended to deposit via inertial impaction already on the secondary superheater tubes. Only small amounts of larger particles were expected to reach the measurement location [18]. Sub-micrometre-sized fume particles start to form in the measurement region either via homogeneous condensation in the gas phase or heterogeneous condensation directly on the steel surface; thus, fume particles contributed the most to the deposit building up on the probe [6]. The governing deposition mechanism for fume particles on the sampling tip appeared to be eddy impaction, predominantly depositing on the lee side of the probe [19], resulting in the deposit shape seen in Fig. 3, with the maximum deposit thickness at the lee side. In general, no significant differences in deposit morphology were identified when comparing probe deposit samples of different exposure times from the same location along the probe's circumference. This suggests good reproducibility of the results obtained from the probe measurements.

For all three deposits, the average deposit Cl content has been determined at the four locations indicated in Fig. 3. The average mass-based Cl concentration of the three deposits at the respective analysis location is shown in Fig. 4.

The average Cl content of the deposits increased with exposure time in all four locations along the probe's circumference. A significant increase in deposit Cl content was seen when increasing the exposure time from one to five weeks. In contrast, the deposit Cl content increased to a lesser extent when increasing the exposure time from five to eight weeks.

It is worthwhile to mention that a period of almost three years lay between the 1-week and the sequentially carried out 5- and 8-week experiments; thus, changes in the operating conditions of the boiler possibly affecting the Cl content in the flue gas cannot be ruled out. However, no significant differences in the chemical composition of the black liquor fired during the 1-week experiment and the 5- and 8-week experiments were identified. Therefore, the enrichment in probe deposit Cl with increasing exposure time was believed to be representative of the time-dependent chlorine enrichment of actual superheater deposits. The overall deposit Cl content increased over time as alkali chloride vapours, present in the flue gas, diffused through the outer regions of the deposit and condensed within the deposit region closer toward the steel, at lower local temperatures.

For a more detailed analysis of the Cl distribution within the probe

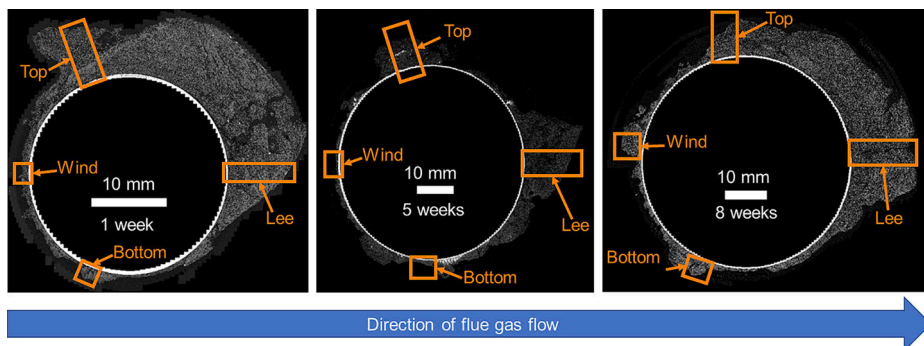


Fig. 3. SEM images of deposit cross-sections after exposure times of 1, 5, and 8 weeks indicating locations of detailed analysis on wind, lee, bottom, and top side of deposits.

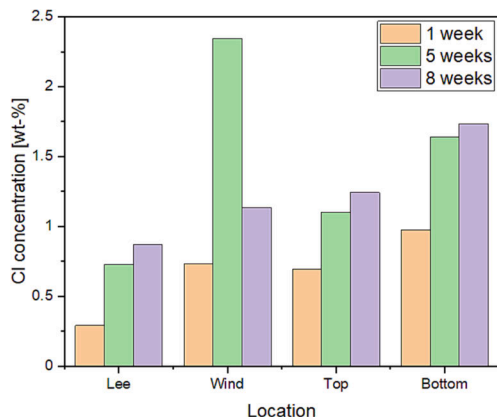


Fig. 4. Development of average mass-based Cl concentration with increased exposure time at lee, wind, top, and bottom side of the probe deposit.

deposits, the molar Cl/(Na + K) ratios over the cross-sections of the three deposits from the top side of the probe are shown in Fig. 5 together with their corresponding grey-scale images.

A clear difference was seen when comparing the 1-week deposit with the 5- and 8-week deposits. The Cl concentration throughout the cross-section of the 1-week sample was lower compared to the samples with longer exposure times. This overall enrichment in deposit Cl seen in the images in Fig. 5 was in line with the trend shown in Fig. 4. The deposit was enriched in Cl over time via condensation of Cl-rich vapours, diffusing into the deposit from the flue gas.

Furthermore, alkali chloride layers formed on the furnace-facing side of particles within all analysed deposits. For the 5- and 8-week samples, a chloride-rich layer was also observed directly on the steel surface. The presence of such alkali chloride layers is a characteristic of temperature gradient-induced deposit ageing via diffusional transport of alkali chloride vapours toward the steel [10]. This mechanism has been studied thoroughly in laboratory-scale tests [9,10,14] and has also been shown to take place in actual deposits collected directly from superheater tubes [8,15]. The results of the present probe measurements confirmed deposit ageing to form an alkali chloride layer directly on the steel surface. Such a Cl-layer was not found on the probe's steel surface after the 1-week experiment but after the 5-week and 8-week experiments. Thus, the layer likely formed due to deposit ageing rather than during initial deposit formation via condensation of alkali chlorides

directly on the steel surface.

However, in contrast to deposits obtained from the laboratory-scale experiments, chloride layers formed also on non-furnace facing sides of particles, especially surrounding larger dense agglomerates within the deposits, similar to those seen in the 1-week and 8-week deposits in Fig. 5. These larger agglomerates were predominantly seen on the wind side directly exposed to the flue gas stream during the experiment. The exact formation mechanism of the Cl-layers surrounding such larger particles is not known. It is believed that a mechanism other than the temperature gradient-induced diffusional transport of alkali chloride vapours resulted in the formation of the Cl-layers on the non-furnace-facing sides of particles.

An indication of a second mechanism involved in the formation of the non-furnace facing alkali-chloride layers was their presence already after an exposure time of one week. Despite the generally low Cl content within the 1-week sample and the lack of similar well-pronounced Cl layers on deposit particles of smaller size within the same sample, alkali chloride layers surrounded larger irregularly shaped particles within the sample. Such larger particles were believed to be either carryover particles or parts of deposits, which initially formed on superheater tubes upstream of the probe and were removed by sootblowing, got re-entrained in the flue gas, and re-deposited subsequently on the probe.

However, the Cl-layers appeared to be more pronounced on the furnace-facing side of particles, especially within the samples of 5 and 8 weeks of exposure. Thus, it was believed that also the Cl layers on the furnace-facing side of larger irregularly shaped particles were at least partially formed via temperature gradient-induced diffusional transport of alkali chloride vapours toward the steel. An example of a deposit where the Cl-layers were more pronounced on the furnace-facing side of the particles is given in Fig. 6.

Fig. 6 also shows an example of the general morphological complexity of the probe deposit samples. Within the 8-week sample on the left, particles of varying shapes and sizes appeared. The region closest to the steel contained predominantly larger, irregularly shaped particles with particle sizes ranging between 500 μm and 1 mm. Due to the prevailing steel temperature of the probe and the local flue gas temperature, deposition of re-entrained particles seemed probable. Carryover particles likely solidify almost completely when reaching the probe. Thus, they will not deform upon impact, resulting in a particle structure seen in Fig. 6. Due to the chosen steel temperature, neither extensive sintering nor partial particle melting was expected to be relevant in this deposit region.

The outer deposit region contained spherical particles ranging between 1 μm and 100 μm in diameter, classified as intermediate-sized particles (ISP) [7]. Additionally, some outer deposit regions had undergone partial sintering during boiler operation. However, the outermost region of the deposit had not sintered significantly. Therefore, it was believed to reflect best the shape and composition of particles

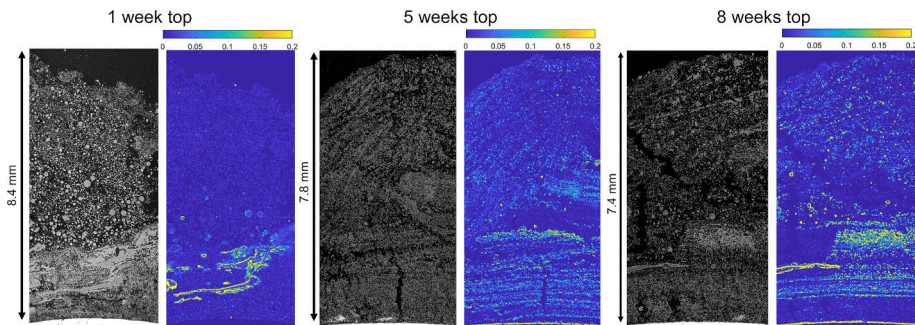


Fig. 5. Grey-scale SEM image and corresponding molar Cl/(Na + K) ratio of 1-week deposit (left), 5-week deposit (middle), and 8-week deposit (right).

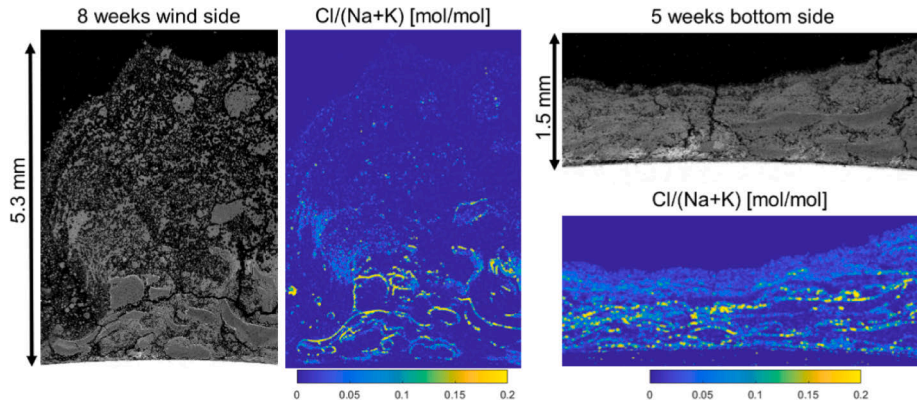


Fig. 6. 8-week wind side probe deposit and corresponding molar Cl/(Na + K) ratio and 5-week bottom side probe deposit and corresponding molar Cl/(Na + K) ratio.

initially deposited on the probe.

The morphology and thickness of deposits from the bottom side of the probe differed significantly from the other analysis locations. Bottom side deposits were typically the thinnest and appeared less porous compared to the other locations along the probe's circumference. The differences in morphology and deposit thickness were likely due to the bottom side directly facing a sootblower. Larger parts of the deposit were expected to have been removed during sootblowing, resulting in a thinner deposit on the bottom side. Furthermore, high water vapour concentrations possibly caused partial dissolution of the deposit followed by rapid recrystallisation, resulting in the observed less-porous, dense morphology.

Besides the general Cl enrichment with time, as shown in Fig. 4, local enrichment in K and S and concurrent depletion in Cl were observed within the analysed deposits. Regions of similar local composition have been analysed within deposit samples taken directly from the superheater tubes of the same boiler [15]. The enrichment in S and concurrent depletion in Cl in deposits obtained directly from the superheater tubes were reported to have formed when an initially alkali chloride-rich deposit was sulfated by SO_2 present in the flue gas. However, the enrichment in K could not be explained via the proposed sulfation mechanism; thus, a second unidentified mechanism has been believed to result in the observed concurrent K enrichment [15].

The local K and S enrichment within the probe deposits was not exclusively identified within the region closest to the steel but also in regions further away from the steel surface. Examples of two probe cross-sections showing signs of local sulfation within the deposit are given in Fig. 7.

An example of local depletion in Cl and concurrent enrichment in K and S, referred to as the sulfated region in the further discussion below, further away from the steel, is given in the top row of Fig. 7. The images in the bottom row give an example of a sulfated region directly above the steel surface. In further analyses of the probe deposit samples, similar sulfated regions were observed within the 5- and 8-week samples at other locations along the probe's circumference. Analogous to the cross-sections shown in Fig. 7 for the 5-week sample, the sulfated region was consistently observed at some distance to the steel surface. In contrast, the sulfated region was located right above the steel surface in the 8-week sample.

The sulfated regions analysed at different locations within the 5- and 8-week deposit samples were assumed to depend on temporal fluctuations in the flue gas' SO_2 concentration during boiler operation. Therefore, the measured SO_2 concentration in the flue gas stack of the

boiler was analysed in more detail. The SO_2 measurement data was provided by the boiler operator. Each data point represented a one-hour average of the measured SO_2 concentration. For both probe sampling periods, the overall measured SO_2 concentration in the stack was low, averaging 0.1 mg/Nm^3 SO_2 during the 5-week sampling period and 0.6 mg/Nm^3 SO_2 during the 8-week sampling period. However, the SO_2 concentration had been noticeably higher than the average during 12 h in both cases. For the 5-week exposure, this increased SO_2 concentration was identified on the 11th day after starting the experiment. For the 8-week exposure, a similar time interval of increased SO_2 concentration was seen on the 5th day. The increased SO_2 concentrations in the flue gas at different times during the experiment may explain the differences in the location of the sulfated regions between the 5-week and 8-week probe deposit samples.

Furthermore, the presence of a Cl-rich layer directly on the steel surface (Fig. 7) provided additional evidence for the sulfation of alkali chlorides to take place after the initial deposit formation. A sufficient amount of Cl within the inner region of the deposit is required for such a Cl layer to form directly on the steel surface via diffusional transport of alkali chloride vapours toward the steel. The results imply that the fraction of alkali chloride that remained within the initially deposited particles has subsequently been sulfated by reacting with SO_2 from the flue gas after the Cl layer on the steel surface has been formed.

Besides differences in the location of the sulfated region in the probe deposit cross-sections, differences in the degree of sulfation were identified when comparing the probe samples to the deposits collected directly from the superheater tubes of the same boiler [15]. The sulfation appeared to have advanced to a greater extent within the superheater deposits, resulting in a higher molar S/(Na + K) ratio. For better comparison, the molar S/(Na + K) ratios of the sulfated deposit regions and the remaining unsulfated regions of the two probe samples shown in Fig. 7 were calculated. The calculated ratios are summarised in Table 1 and compared to the equivalent ratios from an actual superheater deposit.

Table 1 shows that the difference in the molar S/(Na + K) ratio between the sulfated and non-sulfated regions of the probe deposits was less significant than in the superheater deposit sample. The higher degree of sulfation within the superheater deposit sample was likely due to the probe samples being collected during regular boiler operation. No major fluctuations in the flue gas composition were expected to occur during the probe sampling periods. In contrast, the superheater deposit samples started to build up during the start-up phase of the boiler, during which heavy fuel oil was used, causing significantly higher SO_2

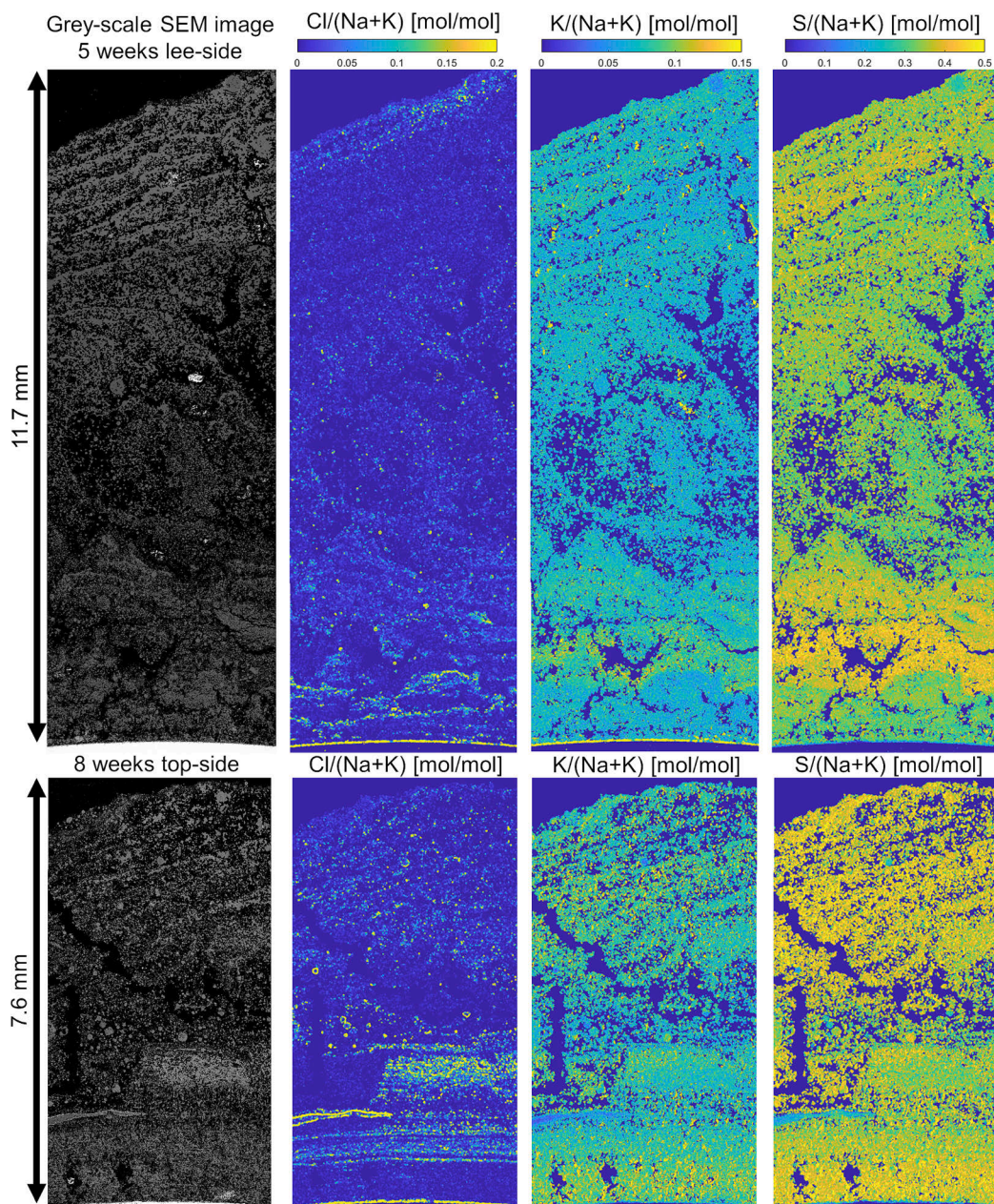


Fig. 7. Top row: SEM cross-sectional image and molar $\text{Cl}/(\text{Na} + \text{K})$, $\text{K}/(\text{Na} + \text{K})$, and $\text{S}/(\text{Na} + \text{K})$ ratios from the lee side of the 5- week deposit; bottom row: SEM cross-sectional image and molar $\text{Cl}/(\text{Na} + \text{K})$, $\text{K}/(\text{Na} + \text{K})$, and $\text{S}/(\text{Na} + \text{K})$ ratios from the top side of the 8-week deposit.

Table 1

Molar S/(Na + K) ratios of sulfated and non-sulfated probe deposit regions and actual superheater deposit [15] as reference.

Sample name	S/(Na + K) [mol/mol]
Probe 5-week lee sulfated	0.37
Probe 5-week lee non-sulfated	0.33
Probe 8-week wind sulfated	0.39
Probe 8-week wind non-sulfated	0.37
Superheater deposit sulfated	0.44
Superheater deposit non-sulfated	0.33

concentrations in the flue gas. Thus, higher sulfation rates can be expected during the start-up phase of the boiler [20], and sulfation of the innermost layer in the superheater deposits was more pronounced than in the probe deposit samples. However, the probe deposits suggest that sulfation of alkali chlorides within superheater deposits does not exclusively occur during the start-up phase of the boiler when SO₂ flue gas concentrations are significantly higher but might take place during regular boiler operation as well.

A more detailed analysis of the molar Cl/(Na + K) and K/(Na + K) ratios of the two probe deposit samples shown in Fig. 7 suggests differences in the composition of the Cl layer that had formed directly on the steel surface. As mentioned above, the Cl layers form because of temperature gradient-induced transport of alkali chloride vapours toward the steel. The most significant difference between the Cl layers of the two deposit samples was the lack of K within the Cl layer of the 8-week sample. In contrast, the 5-week sample was enriched in Cl and K in the layer adjacent to the steel surface.

The lack of K in the Cl-rich layer right above the steel surface after an exposure time of 8 weeks was attributed to alkali chloride-induced corrosion, often referred to as active oxidation. The Cl-rich layer formed directly on the steel surface due to deposit ageing contained initially NaCl and KCl. A similar layer of alkali chlorides was also formed in laboratory experiments studying deposit ageing mechanisms using synthetic ash deposits [9,14]. Alkali chlorides then initiated the corrosion reaction by adsorbing on the oxide layer of the steel, forming alkali hydroxides while releasing Cl ions [21,22]. The formed Cl ions diffuse through the oxide layer toward the steel surface, where FeCl₂, stable under reducing conditions, forms at the steel-oxide-scale interface. Of the formed alkali hydroxides, a large share volatilises, while smaller amounts, predominantly NaOH, react with the oxide layer to form Na₂Fe₂O₄. In contrast, only small amounts of potassium ferrates are expected to form [23]. Thus, as the corrosion reactions proceed with time, K volatilises from the steel surface in the form of KOH, resulting in the observed depletion in K of the Cl-rich layer attached to the steel surface shown in the 8-week deposit in Fig. 7.

3.2. Impact of observed enrichment patterns on local T₀

The impact of local enrichment patterns in the probe deposit samples on boiler operation was evaluated from the local first melting temperature profiles of selected deposit cross-sections in Fig. 8. The figure also shows the molar Cl/(Na + K), K/(Na + K), and S/(Na + K) ratios.

Two 1-week deposit samples are shown in the upper row of Fig. 8. The lee side deposit (top left in Fig. 8) had a uniform composition throughout the cross-section; thus, no variations were observed in the calculated T₀ profile. The 1-week top side deposit (top right in Fig. 8) contained several larger particles surrounded by a Cl layer within the region close to the steel, causing a decrease in the local T₀ values. The Cl layers surrounding these larger agglomerates were assumed to be due to some other mechanism than temperature gradient-induced diffusion of alkali chlorides. Therefore, the lee-side deposit of uniform composition and its corresponding linear T₀ profile were more representative of short-term deposits. Additional probe deposit samples of shorter exposure times (30 min to 3 h) had a similar uniform composition throughout the cross-section. Also, the calculated T₀ profiles were linear within the

same temperature range as those of the 1-week lee side deposit.

It should be noted that small variations of up to 5 °C in the calculated local T₀ values are insufficient to conclude whether the variations are due to compositional changes. The accuracy of SEM composition analysis might give variations of up to 5 °C in the calculated local T₀. However, the T₀ values in Fig. 8 provide a reasonable estimate of how specific enrichment patterns affect the local first melting temperature within a deposit.

The 5-week top side deposit (bottom left of Fig. 8) had a Cl and K-rich layer directly on the steel surface, followed by a region enriched in Cl and K when compared to the regions of the deposit further away from the steel. The calculated local T₀ reached values as low as 505 °C within the Cl and K-rich layer adjacent to the steel surface, corresponding to the global minimum of the system [17]. Throughout the inner deposit region, concurrently enriched in Cl and K, the local first melting temperature was lower compared to the outer regions of the deposit. When moving further away from the steel surface, the Cl and K content of the deposit was lower on average, while the S content was higher. Therefore, the local first melting temperature of the outermost regions of the deposit was the highest throughout the cross-section and did not show any significant variations.

Reeve et al. [12] have shown that an increase in the deposit Cl up to molar Cl/(Na + K) ratios of 5 % results in a decrease in T₀. As described above, alkali chloride from the flue gas was assumed to diffuse into the deposit, causing the overall deposit Cl content to increase over time. Thus, the lower local T₀ of the outer deposit region of the 5-week deposit sample compared to the 1-week samples is also due to an increase in the overall Cl content of the deposit (see Fig. 4), due to temperature gradient-induced deposit ageing. Besides higher Cl concentrations, the 5-week deposit sample contained also higher amounts of CO₃, further decreasing the first melting temperature [13] and thus contributing to the observed lower T₀ values in the outer region of the 5-week sample than the 1-week samples.

The deposit sample on the right of Fig. 8 consisted of a Cl-rich layer directly on the steel surface with no further enrichment in K. The Cl-rich layer was followed by a sulfated region depleted in Cl while concurrently enriched in K and S. The local T₀ of the Cl-rich layer adjacent to the steel surface was not significantly lower than the T₀ of the remaining parts of the deposit due to the lack of K. An increase in the Cl content lowers the deposit T₀, but not to the same extent as concurrent enrichment in Cl and K [12,13].

However, already small amounts of corrosion products, well below the detection limit of the SEM analysis, can significantly impact the deposit's first melting temperature and lower the local T₀ well below steam temperatures typical for kraft recovery boilers. For example, iron chlorides and KCl form a eutectic melt at 355 °C [22]. The calculated T₀ values in Fig. 8 were based on the deposits' Na, K, Cl, S, C, and O contents. The impact of corrosion products or other impurities on the local first melting temperature was not taken into account in the calculations.

The sulfated region in the deposit on the right of Fig. 8 showed no significant increase in the local T₀. The local enrichment in S compared to the outer deposit region was not pronounced, as the sulfation of the deposit had not progressed far enough to significantly affect the local first melting temperature. Increased calculated T₀ values have been reported for sulfated regions of superheater deposit samples taken from the same boiler [15]. Thus, further progress of the sulfation likely results in a local increase in T₀ with time, reducing the risk for melt formation close to the steel, and therefore, melt-induced corrosion. However, as a Cl and K-rich layer was analysed on the steel surface of the 5-week deposit sample, the sulfation reaction is not likely to prevent active oxidation of the superheater steel. In contrast, Cl-induced corrosion mechanisms initiate almost instantaneously after the alkali chlorides deposit on the steel surface [22]. In this work, a Cl-rich layer on the steel surface provided a source for alkali chloride-induced corrosion still after 8 weeks.

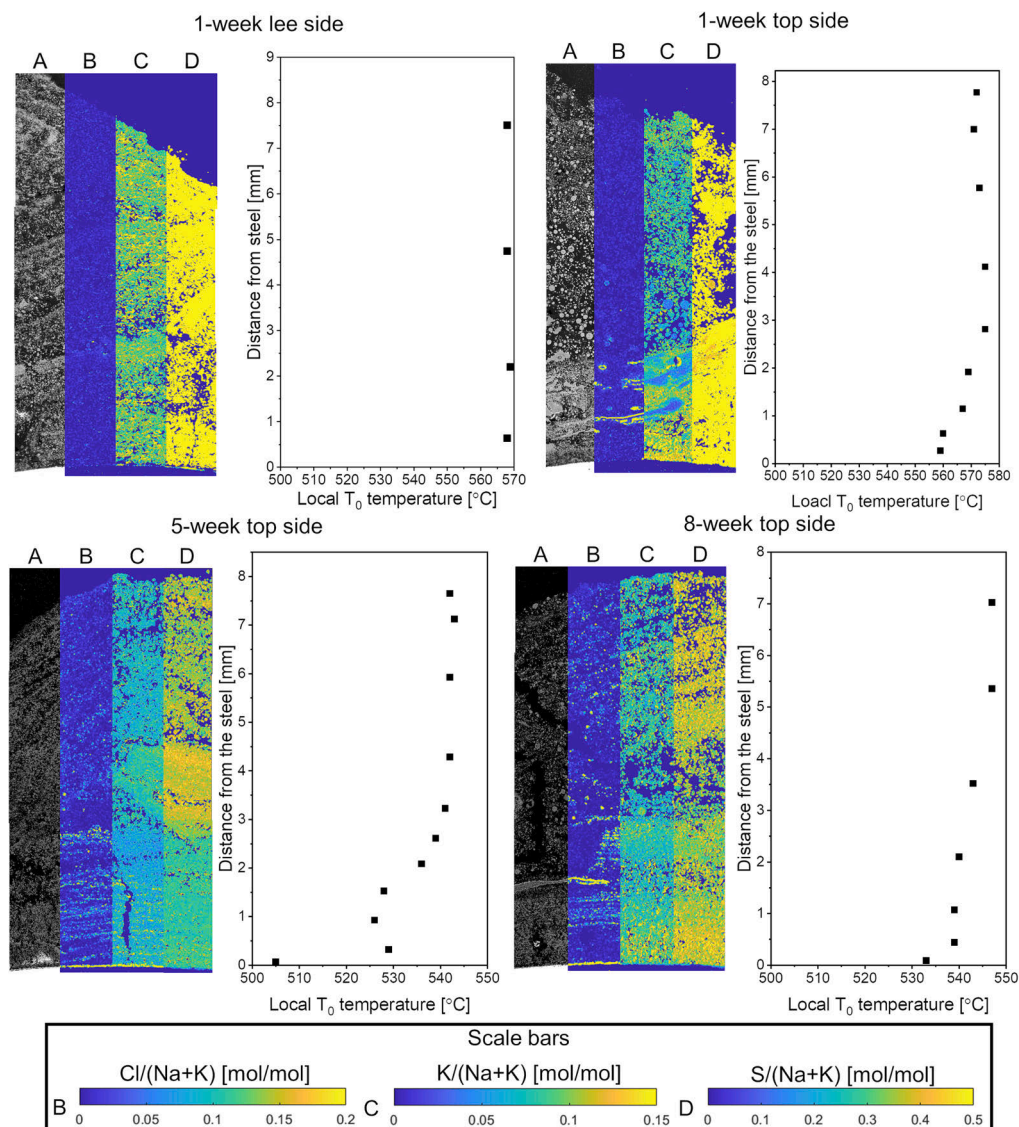


Fig. 8. Local T_0 profiles and molar B) Cl/(Na + K), C) K/(Na + K), and D) S/(Na + K) ratios of: 1-week lee side (top left); 1-week top side (top right); 5-week top side (bottom left); and 8-week top side deposit (bottom right).

4. Conclusions

A novel probe design was used to obtain ash deposit samples of 1-, 5-, and 8-week exposures from the superheater region of a Finnish kraft recovery boiler. The three probe deposit samples showed similarities in shape and morphology, indicating the suitability of the probe to study time-dependent changes within ash deposits and providing results of good reproducibility. Furthermore, the probe deposits showed similar morphological characteristics as deposits obtained directly from the

superheater tubes of the same boiler. Morphological differences along the probe's circumference likely depended on differences in locally prevailing deposition mechanisms and external influences such as sootblowing.

The Cl concentration in the deposit increased with exposure time. The analysed Cl-enrichment with time was assumed to be due to alkali chloride vapours from the flue gas diffusing into the initially formed porous deposit. Subsequently, Cl condensed within the deposit, resulting in an overall enrichment in deposit chlorine. Cl enriched locally as alkali

chloride layers on the furnace-facing side of particles through temperature gradient-induced concentration diffusion.

Additionally, a Cl-rich layer developed with time onto the steel surface of the 5-week and 8-week samples, but not the 1-week sample. Overall, the temperature gradient-induced deposit ageing mechanism resulted in the local enrichment of Cl and K of the deposits toward the steel.

Sulfation of alkali chlorides was observed within the 5 and 8-week deposit samples. Sulfation was limited to distinct regions within the deposits, most likely being formed as a result of temporarily elevated SO_2 concentrations in the flue gas. For deposits with sulfation, 12 h of elevated flue gas SO_2 were identified from process data at different points in time.

Within regions concurrently enriched in Cl and K, a decrease in the local T_0 was seen. A minimum in the local T_0 of 505 °C was reached within the Cl and K-rich layer adjacent to the steel surface, about 35 °C lower compared to T_0 at the outer deposit region. Furthermore, a decrease in the deposit T_0 due to the overall enrichment in alkali chloride caused by temperature gradient-induced diffusion of alkali chloride vapours from the flue gas into the deposits was seen. The local T_0 was typically 15–20 °C lower toward the steel as compared to the outer parts of the deposit. No major changes in the local T_0 were seen due to sulfation. The degree of sulfation within the probe deposit samples was too low for it to affect the local T_0 significantly. However, more extensive sulfation would result in locally increased T_0 values.

CRedit authorship contribution statement

Roland Balint: Investigation, Methodology, Data curation, Writing – original draft, Visualization. **Markus Engblom:** Supervision, Project administration, Writing – review & editing, Investigation, Validation. **Emil Vainio:** Investigation. **Tor Laurén:** Methodology, Investigation. **Jonne Niemi:** Validation, Investigation, Writing – review & editing. **Jaakko Rautala:** Resources. **Timo Saarinen:** Resources. **Mikko Hupa:** Validation, Writing – review & editing, Funding acquisition. **Leena Hupa:** Writing – review & editing, Funding acquisition.

Declaration of Competing Interest

The authors declare that they have no known competing financial interests or personal relationships that could have appeared to influence the work reported in this paper.

Data availability

Data will be made available on request.

Acknowledgements

This work was financed by Suomen Soodakattilayhdistys (The Finnish Recovery Boiler Committee) [Contract numbers: 16A0913/S144; 16A0913/S155]. Financing through a research grant awarded by the Fortum Foundation [Application number 20190123] and the Åbo Akademi University Graduate School in Chemical Engineering is highly acknowledged. This work has been partly carried out within the Åbo Akademi CLUE² Research Consortium (2017–2022). Support from ANDRITZ Oy, Valmet Technologies Oy, UPM-Kymmene Oyj, Metsä Fibre Oy, and International Paper Inc. is gratefully acknowledged. Additional support from the Academy of Finland project “New insights

on the effects of temperature gradients on high temperature corrosion” [Decision number 338322] is highly appreciated. We want to thank Linus Silvander for carrying out SEM/EDXA analyses and Jarno Toivanen for building the sampling probe.

References

- [1] KEY STATISTICS 2021 - European pulp & paper industry. Brussels: Confederation of European Paper Industries; n.d.
- [2] Vakkilainen EK. Kraft recovery boilers - Principles and practice. Suomen Soodakattilayhdistys ry 2005. ISBN: 952-91-8603-7.
- [3] Mikkonen P, Kauppinen EI, Pyykönen J, Jokiniemi JK, Aurela M, Vakkilainen EK, et al. Alkali salt ash formation in four Finnish industrial recovery boilers. *Energy Fuel* 1999;13(4):778–95.
- [4] Vakkilainen EK. In: *Steam Generation from Biomass*. Elsevier; 2017. p. 237–59.
- [5] Karlemo C. Non-process elements in the recovery cycle of six Finnish Kraft pulp mills. Master's Thesis. Åbo Akademi University, 2019.
- [6] Tran H. Chapter 9: Upper Furnace Deposition and Plugging. *Kraft Recovery Boilers*, Atlanta, GA: Tappi Press; 1997. p. 245–82. ISBN: 0-9625985-9-3.
- [7] Kochesfahani SH, Tran H, Jones AK, Grace TM, Lien SJ, Schmidl W. Particulate Formation During Black Liquor Char Bed Burning. *J Pulp Pap Sci* 2000;26:180–7.
- [8] Balint R, Engblom M, Niemi J, Silva da Costa D, Lindberg D, Yrjas P, et al. Temperature gradient induced changes within superheater ash deposits high in chlorine. *Energy* 2021;226:120439.
- [9] Lindberg D, Niemi J, Engblom M, Yrjas P, Laurén T, Hupa M. Effect of temperature gradient on composition and morphology of synthetic chlorine-containing biomass boiler deposits. *Fuel Process Technol* 2016;141:285–98. <https://doi.org/10.1016/j.fuproc.2015.10.011>.
- [10] Niemi J, Lindberg D, Engblom M, Hupa M. Simultaneous melt and vapor induced ash deposit aging mechanisms – Mathematical model and experimental observations. *Chem Eng Sci* 2017;173:196–207. <https://doi.org/10.1016/j.ces.2017.07.041>.
- [11] Niemi J, Engblom M, Laurén T, Yrjas P, Lehmusto J, Hupa M, et al. Superheater deposits and corrosion in temperature gradient – Laboratory studies into effects of flue gas composition, initial deposit structure, and exposure time. *Energy* 2021;228:120494.
- [12] Reeve DW, Tran HN, Barham D. The effluent-free bleached kraft pulp mill - Part XI Morphology, chemical and thermal properties of recovery boiler superheater fireside deposits. *Pulp & Paper Canada* 1981;82:T315–20.
- [13] Tran H, Gonsko M, Mao X. Effect of composition on the first melting temperature of fireside deposits in recovery boilers. *Tappi J* 1999;82:93–100.
- [14] Niemi J, Balint R, Engblom M, Lehmusto J, Lindberg D. Temperature-Gradient-Driven Aging Mechanisms in Alkali-Bromide- And Sulfate-Containing Ash Deposits. *Energy Fuel* 2019;33:5883–92. <https://doi.org/10.1021/acs.energyfuels.8b04199>.
- [15] Balint R, Engblom M, Niemi J, Lindberg D, Saarinen T, Rautala J, et al. Morphological and Chemical Differences within Superheater Deposits from Different Locations of a Black Liquor Recovery Boiler. *Energy* 2023;267:126576. <https://doi.org/10.1016/j.energy.2022.126576>.
- [16] Bale CW, Bélisle E, Chartrand P, Decterov SA, Eriksson G, Gheribi AE, et al. FactSage thermochemical software and databases, 2010–2016. *Calphad* 2016;54:35–53.
- [17] Lindberg D, Backman R, Chartrand P. Thermodynamic evaluation and optimization of the (NaCl + Na₂SO₄ + Na₂CO₃ + KCl + K₂SO₄ + K₂CO₃) system. *J Chem Thermodyn* 2007;39:1001–21. <https://doi.org/10.1016/j.jct.2006.12.018>.
- [18] Tran HN, Reeve DW, Barham D. Formation of Kraft Recovery Boiler Superheater Fireside Deposits. *Pulp Paper Canada* 1983;84:36–41.
- [19] Fakourian S, McAllister Z, Fry A, Wang Y, Li X, Wendt JOL, et al. Modeling ash deposit growth rates for a wide range of solid fuels in a 100 kW combustor. *Fuel Process Technol* 2021;217:106777. <https://doi.org/10.1016/j.fuproc.2021.106777>.
- [20] Boonsongsup L, Iisa K, Frederick WJ. Kinetics of the Sulfation of NaCl at Combustion Conditions. *Kinetics of the Sulfation of NaCl at Combustion Conditions* 1997;36(10):4212–6.
- [21] Folkesson N, Jonsson T, Halvarsson M, Johansson L-G, Svensson J-E. The influence of small amounts of KCl(s) on the high temperature corrosion of a Fe-2.25Cr-1Mo steel at 400 and 500 °C: KCl-induced corrosion of a Fe-2.25Cr-1Mo. *Mater Corros* 2011;62:606–15. <https://doi.org/10.1002/maco.201005942>.
- [22] Jonsson T, Folkesson N, Svensson J-E, Johansson L-G, Halvarsson M. An ESEM in situ investigation of initial stages of the KCl induced high temperature corrosion of a Fe-2.25Cr-1Mo steel at 400 °C. *Corros Sci* 2011;53:2233–46. <https://doi.org/10.1016/j.corsci.2011.03.007>.
- [23] Karlsson S, Pettersson J, Johansson L-G, Svensson J-E. Alkali Induced High Temperature Corrosion of Stainless Steel: The Influence of NaCl, KCl and CaCl₂. *Oxid Met* 2012;78:83–102. <https://doi.org/10.1007/s11085-012-9293-7>.

R. Balint, M. Engblom, J. Niemi, M. Hupa, L. Hupa (2024)

**Superheater ash deposit ageing – impact of melt fraction on morphology
and chemistry.**

Fuel



Contents lists available at ScienceDirect

Fuel

journal homepage: www.elsevier.com/locate/fuel

Full Length Article

Superheater ash deposit ageing – Impact of melt fraction on morphology and chemistry

Roland Balint^{*}, Markus Engblom, Jonne Niemi, Mikko Hupa, Leena Hupa

Faculty of Science and Engineering, Åbo Akademi University, Henrikinkatu 2, Turku, FI-20500 Finland



ARTICLE INFO

Keywords:

Ash deposits
Temperature gradient
Melting behavior
Ageing mechanisms

ABSTRACT

The initial melting behaviour of synthetic ash deposits, with a focus on how the amount of melt formed, affects the final deposit morphology, was studied. Binary and ternary reciprocal deposits were exposed to a temperature gradient with varying exposure time, steel temperature, and furnace temperature. Two different archetype deposit morphologies emerged. The final deposit morphology was identified to depend on the amount of melt formed during the experiment. A skeletal deposit morphology developed in systems with less than 30 wt-% melt. Short-term experiments proved that the formation of the skeletal structure is accelerated by the presence of melt, accumulating at contact points of distinct particles. If melt fractions exceeded 30 wt-%, a molten morphology developed, as the amount of melt present was sufficient to fill the pores within the deposit. For molten deposits of ternary reciprocal systems, enrichment of K in the formed melt and concurrent movement toward the steel was observed. The results confirmed a deposit ageing mechanism that has been proposed earlier, based on full-scale superheater deposit samples. The experiments showed that deposit melting and ageing behaviour are strongly connected, as the two identified morphologies differed in their ageing behaviour. The presented results improve the understanding of the initial melting behaviour of deposits and illustrate the connection between deposit morphology and deposit ageing. The results can be utilised as input data for deposition models and help in predicting the final deposit morphology and its associated ageing behaviour, aiding boiler operators and manufacturers dealing with deposit-related issues.

1. Introduction

Worldwide, the governing process used in the pulp and paper industry is kraft pulping. The black liquor recovery boiler is an essential part of the kraft pulp mill. Through the combustion of black liquor, the spent pulping chemicals are recovered to be reused. At the same time, heat and power, sufficient to cover the demand of the whole mill [1], are produced. An inevitable part of the combustion process is the release of inorganics in different physical states, which are subsequently entrained in the flue gas and form deposits on heat transfer surfaces via several pathways [2]. Such deposits reduce the electrical efficiency of the process [3] and can also cause corrosion of the heat transfer surfaces they form on [2].

The formation of ash deposits has been studied extensively over the last decades [4–7]. Several deposit formation mechanisms have been identified and studies on different aspects of deposit formation can be found in the literature [3,4,6–8]. The main components of kraft recovery

boiler deposits are Na, K, Cl, SO₄, and CO₃ [9]. Of these compounds, alkali chlorides are mainly responsible for superheater corrosion. For solid deposits, the dominating corrosion mechanism is active oxidation [10,11]. If the deposit adjacent to the steel surface is (partially) molten, the corrosion rate increases significantly [6,11,12]. Therefore, a good understanding of the melting behaviour of ash deposits is essential to avoid the presence of melt in the direct vicinity of the steel surface.

The first melting temperature (T_0) of an ash deposit depends on its chemical composition. For kraft recovery boiler deposits, T_0 can be as low as 501 °C when only considering its main components [13]. In addition, smaller amounts of various inorganics originating either from the raw wood [14] or introduced into the liquor during various process steps [14] can be found in the deposits, further affecting T_0 . In addition, corrosion products originally formed at the steel surface [15] can be found within deposits, which can form low melting eutectics and increase the risk of melt getting in direct contact with the steel. For kraft recovery boiler deposits, the melting behaviour is mainly influenced by

^{*} Corresponding author at: Laboratory of Molecular Sciences and Engineering, Faculty of Science and Engineering (FNT), Åbo Akademi University, Henriksgatan 2, Åbo, FI-20500 Finland.

E-mail address: roland.balint@abo.fi (R. Balint).

<https://doi.org/10.1016/j.fuel.2023.130386>

Received 28 April 2023; Received in revised form 31 October 2023; Accepted 11 November 2023

Available online 18 November 2023

0016-2361/© 2023 The Authors. Published by Elsevier Ltd. This is an open access article under the CC BY license (<http://creativecommons.org/licenses/by/4.0/>).

the deposit K and Cl content. An increase in the deposit's K content causes a decrease in T_0 [16]. An increase in the deposit's Cl content results in an increase in the amount of melt present within the deposit [17].

Several studies have reported local differences in the chemical composition and morphology of superheater deposits from kraft recovery boilers [17,18], and other biomass boilers [19–21]. Such differences in the local chemical composition of a deposit can also affect the local T_0 [18,22]. A commonly found explanation for why deposits form layered structures of varying chemical composition is a change in the deposition behaviour [21,23]. In literature, a generally accepted pathway of deposit formation is the initial formation of a sticky layer on the blank steel surface via condensation of inorganic vapours [23]. The sticky layer then enables further deposition of larger fly-ash particles which differ in their composition from the initially formed sticky layer [23]. Thus, distinct layers of varying compositions and T_0 can be found within a deposit's cross-section.

Recent studies carried out at Åbo Akademi University have shown that temperature gradient-induced processes can also cause changes in the local chemical composition and morphology of deposits [15,24,25]. Due to the temperature difference between the hotter flue gas and the cooler steel surface, deposits are exposed to a temperature gradient. In laboratory experiments utilising synthetic ash deposits, several temperature gradient-induced mechanisms affecting the local deposit chemistry and morphology have been identified [15,24,25]. Such mechanisms are commonly referred to as deposit ageing, as they take place after the deposit has formed. These mechanisms were later also confirmed to take place in actual kraft recovery boiler superheater deposits [26–28]. In addition, new observations were made within the full-scale deposits. Melt enriching in K and Cl was identified to result in a decrease in the local T_0 of deposits toward the steel [26]. The results are believed to have provided a reasonable explanation for the heavy corrosion, that has earlier been reported for the same boiler [18].

Besides differences in the local chemical composition, significant morphological differences have been observed among deposits from different recovery boilers. Deposits of a generally higher Cl content formed a dense morphology that appeared to have been completely molten. In these dense deposits, K and Cl-enriched melt had moved toward the steel locally lowering T_0 [26]. Deposits of lower Cl content formed a different morphology. The deposits were porous and particles formed a sintered skeletal structure. The porous morphology enabled the diffusion of flue-gas compounds into the deposit, altering the local chemical composition of the inner deposit region [27,28]. The observed differences in the final deposit morphology and therewith connected differences in the ageing behaviour were due to differences in the melting behaviour of the deposits. However, the exact parameters determining the final deposit morphology are not known. Based on the observations made in these earlier studies, the melting behaviour of deposits is believed to affect the final deposit morphology strongly.

The objective of this work was to get a better understanding of the initial melting behaviour of kraft recovery boiler deposits. The main goal was to identify the parameter determining whether the final morphology of a mature deposit is molten or skeletal. Therefore, the initial melting behaviour of synthetic ash deposits was studied in a laboratory setup. Various deposit compositions were exposed to a temperature gradient for short periods, to better understand the initial melt formation and further propagation of the melting processes. The melt fraction present during the experiment was determined by measuring the temperature right above the outer deposit surface. The maximum amount of melt formed during an experiment was identified as the decisive parameter for the final deposit morphology. A threshold value at which the morphology changes from skeletal to molten is proposed.

2. Material and methods

A laboratory setup was used to study the initial steps of the melting

behaviour of synthetic ash deposits exposed to a temperature gradient. Varying compositions of deposits containing Na, K, Cl and SO_4 were used. The setup consists of an air-cooled probe which is placed inside a tube furnace. The synthetic deposits were placed on two removable steel rings at the probe tip. Due to the temperature difference between the cooled probe surface and the hotter furnace, a temperature gradient builds up over the synthetic deposit. The synthetic deposits were placed in a mould of fire sealant paste to prevent the molten deposit from flowing off the probe during the experiment. The temperature of the probe was measured and controlled by a thermocouple placed inside one of the sampling rings. A PID regulator adjusted the flow of cooling air within the probe, maintaining a constant steel temperature during the experiment. During the experiment, a second thermocouple was placed inside the tube furnace, measuring and logging the temperature right above the outer deposit surface. The setup has been used earlier, to study the effect of a temperature gradient on synthetic deposits. A more detailed description of the experimental setup can be found in these earlier studies [24,25].

The compositions of the synthetic ash deposits and their corresponding calculated first melting temperatures (T_0) are summarised in Table 1.

The first three synthetic deposits in Table 1 contain only one alkali metal each (binary salt system). The $86\text{-Na}_2\text{SO}_4$ and $77\text{-K}_2\text{SO}_4$ compositions, which have also been used in earlier deposit ageing studies [25], form 20 wt-% melt at T_0 and were chosen to identify possible differences between K and Na-containing deposits. The $69\text{-K}_2\text{SO}_4$ mixture forms 30 wt-% melt at the same T_0 as the $77\text{-K}_2\text{SO}_4$ mixture. The three binary salt mixtures are eutectic systems, in which the local T_0 is not affected by local temperature gradient-induced element enrichment. The four other synthetic deposits are more complex. They contain Na and K salts simultaneously (ternary reciprocal salt system), hence more representative of actual black liquor kraft recovery boiler superheater deposits. The ternary reciprocal salt mixtures vary in their K and Cl content. The compositions were chosen to achieve variation in T_0 , T_{100} , and the amount of melt formed at T_0 . The ternary reciprocal mixtures aim to cover a variety of melting behaviours possibly occurring in actual recovery boiler deposits.

The salt mixtures were prepared by weighing the single compounds which were subsequently mixed, melted, and ground. This procedure provided a homogeneous distribution of all compounds in the mixture. By this, all local differences in the chemical composition of the deposits can be attributed to being temperature gradient-induced and do not originate from an initially inhomogeneous deposit. The ground particles were sieved to a particle size fraction ranging between 53 and 250 μm , which was used in the experiments. In one experiment, particles smaller than 53 μm were used to study the impact of smaller particles on the deposit melting behaviour. After sieving, the salt compositions were analysed using SEM/EDXA to take into account minor deviations of the used salts from the compositions shown in Table 1. The compositions determined using SEM/EDXA were then used to calculate the respective melting behaviour of the salts.

The melting behaviour of the used deposits was calculated using FactSage 8.1 [29] and the FTPulp database, optimized for compositions representing kraft recovery boiler deposits [13]. The used database contains data relevant to salt mixtures comprising NaCl, KCl, Na_2SO_4 ,

Table 1
Composition and first melting temperature of synthetic ash deposits.

Synthetic ash	Na [wt-%]	K [wt-%]	Cl [wt-%]	SO_4 [wt-%]	T_0 [°C]
86- Na_2SO_4	33	–	4	63	626
77- K_2SO_4	–	46	5	49	690
69- K_2SO_4	–	46	8	46	690
1 K 1 Cl	32	1	1	66	615
10 K 1 Cl	25	10	1	64	556
10 K 10 Cl	26	10	10	54	557
1 K 10 Cl	33	1	10	56	613

K_2SO_4 , Na_2CO_3 , K_2CO_3 , Na_2S , and K_2S . In the calculations the following phases were considered: FTpulp-MELTA (liquid phase), FTpulp-Hexa (hexagonal alkali sulfate-carbonate solution), FTpulp-KCO, FTpulp-NKCB, FTpulp-NKCA, FTpulp-OrtA, FTpulp-OrtB (all low-temperature alkali sulfate-carbonate solid solutions), FTpulp-ACL (alkali chloride solid solution), FTpulp-NAKS (alkali sulfide solid solution), and FTpulp-Gsrt ($K_3Na_2(SO_4)_2$ -based solid solution). In all calculated cases, FTpulp-Hexa and FTpulp-ACL were the solid stable phases at T_0 . The deposits' melting behaviour as a function of temperature is shown in Fig. 1.

The initial melting behaviour of deposits was studied using short-term experiments. The 0-minute experiment had the shortest exposure time, where the probe was removed from the furnace as soon as the furnace reached the temperature set point (see Fig. 2). However, for these short-term experiments, the outer deposit surface was exposed to temperatures higher than the probe set temperature for 30 – 50 min, depending on the chosen temperatures. A typical heating curve for the probe and tube furnace of a 0-minute experiment is shown in Fig. 2.

At point 1 in Fig. 2, the probe reached its set temperature of 450 °C. At this point, cooling of the probe was initiated, maintaining a stable steel temperature. Between points 1 and 2, the furnace temperature increased continuously, while the steel temperature remained at 450 °C. During this time interval, the temperature gradient over the deposit cross-section developed and the outer region of the deposit reached temperatures above its T_0 . At point 2, the furnace reached the target temperature of 980 °C. The furnace temperature shown in Fig. 2 represents the temperature right above the outer surface of the synthetic deposit, measured by a thermocouple. This temperature is assumed to correspond to the temperature of the outer deposit surface. The temperature measured by the thermocouple was then used to calculate the amount of melt formed during the experiment. The maximum temperature at the outer deposit surface depended on the chosen steel temperature. The lower the steel temperature, the stronger the cooling effect of the steel and the lower the maximum temperature at the outer deposit surface. A table summarising all experiments and their respective steel temperature, deposit surface temperature, and experimental duration is given in Appendix.

After the experiment, the probe was removed from the furnace and the flow of cooling air was increased to quench the synthetic deposit samples to room temperature. For analysis, the cooled steel rings with the deposits were cast in epoxy resin. The samples were then cut to obtain a cross-section, which was subsequently polished and carbon coated. The samples' morphology and chemical composition were analysed using scanning electron microscopy (SEM) and energy-dispersive X-ray analysis (EDXA).

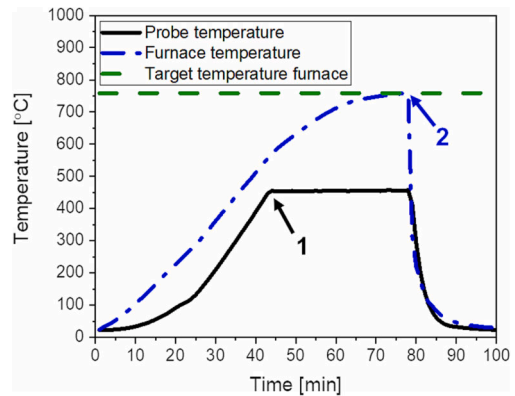


Fig. 2. Profiles of probe and furnace temperature of a 0-minute temperature gradient experiment with the horizontal line indicating the furnace target temperature.

3. Results and discussion

3.1. Differences in deposit morphology

After exposing the synthetic ash deposits to a temperature gradient, differences in their final morphology were observed. Two archetype deposit morphologies developed depending on the initial salt composition and chosen steel and furnace temperatures. Cross-sectional SEM images of the two deposit archetypes are shown in Fig. 3. The figure contains images of synthetic laboratory deposits as well as full-scale superheater deposits, presented in more detail elsewhere [26,27].

In Fig. 3, the steel surface is at the bottom of the images, corresponding to the lowest local temperature within the cross-section. During the exposure, the local deposit temperature increased with the distance from the steel toward the hotter furnace air (flue gas in the case of the superheater deposits). Thus, the local deposit temperature reached its maximum at the top of the image. All SEM images of deposit cross-sections in the present report are oriented the same way as those in Fig. 3. For greyscale SEM images, black represents voids within the deposit. Shades of dark grey correspond to alkali sulfate (and carbonate in the case of actual superheater deposits). Brighter shades of grey correspond to alkali chlorides.

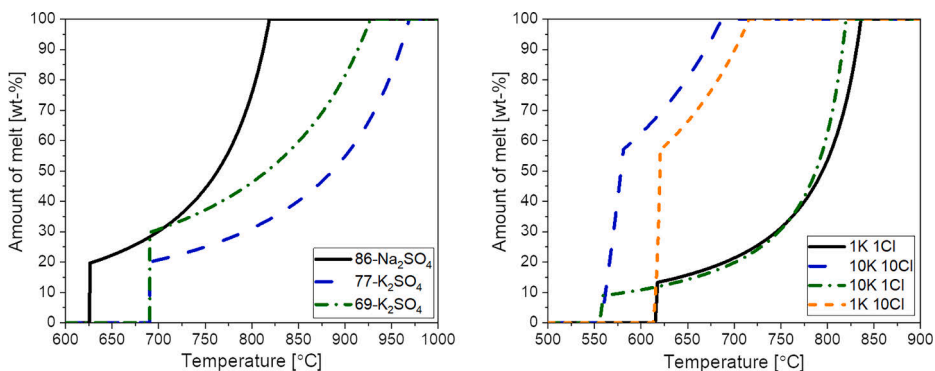


Fig. 1. Melting behaviour of synthetic ash deposits used in present study: binary salt system mixtures (left) and ternary reciprocal salt system mixtures (right).

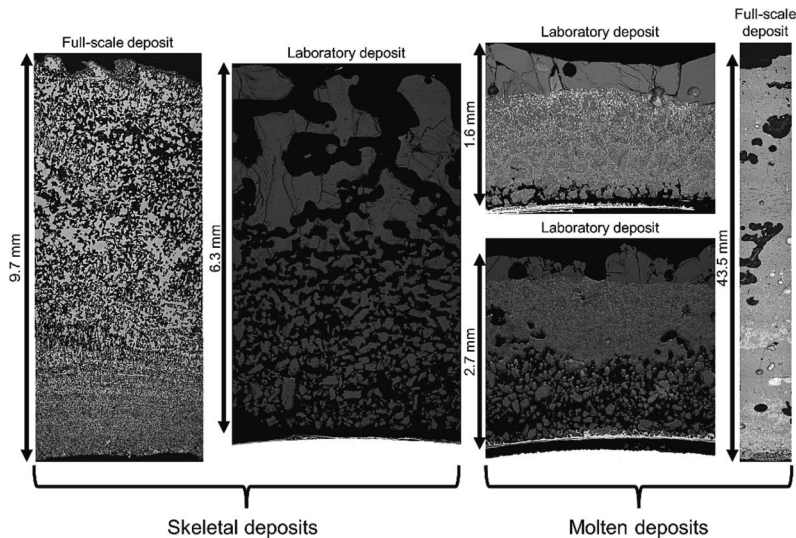


Fig. 3. Examples of laboratory and full-scale deposits for two morphological archetypes: Skeletal full-scale [27] and laboratory deposits on the left and molten full-scale [26] and laboratory deposits on the right.

All deposits in Fig. 3 have a porous region closest to the steel. Only for the low-Cl boiler deposit, sintering is observed throughout the whole cross-section even closest to the steel. The original distinct particles can still be identified in the innermost layer of the low-Cl boiler deposit. The local temperature within the deposit cross-section was the lowest closest to the steel. To avoid direct contact of molten deposit fractions with the steel, material/steam temperatures are typically kept well below the deposit's T_0 . Under such conditions, sintering processes are slow, due to the lack of melt. The presence of melt is known to accelerate sintering processes significantly [30]. Thus, no extensive sintering was observed in the low-Cl boiler deposit. However, the smaller particle size of the superheater deposit compared to the laboratory deposits shown in Fig. 3 has been reported to favour sintering [31]. Hence, the low-Cl boiler deposit formed a skeletal morphology throughout the cross-section, despite local temperatures having been below T_0 . In addition, single sub-micrometer-sized fume particles tend to agglomerate already in flight, before depositing on the heat transfer surface. Therefore, deposits consisting predominantly of fume particles can form a morphology similar to a sintered deposit. It should be mentioned here that material loss during boiler deposit sampling cannot be ruled out. For porous deposits, especially if unsintered as the local deposit temperature remained below T_0 [32,33], there is an increased risk for particles closest to the steel surface to get lost or destroyed during sampling.

The deposits have apparent morphological differences in the region further away from the steel surface (Fig. 3). The deposits on the left-hand side consist of a network of sintered particles, and the original individual particles can no longer be identified. For all deposits, the measured temperature at the outer surface was above their respective bulk T_0 . Thus, the outer deposit regions were partially molten during the exposure. Already small amounts of melt accelerate sintering processes significantly [30]; hence, the deposit morphology changes when local temperatures reach T_0 . This morphology will be referred to as "skeletal" and is characterised by a porous network of sintered particles, as seen in the outer region of the deposits on the left of Fig. 3. Depending on the degree of sintering, the original individual particles can no longer be identified, as in the laboratory deposits on the left of Fig. 3.

The local temperature at the outer surface of the deposits on the right

in Fig. 3 exceeded T_0 as well. However, the morphology suggests that the temperature was high enough for extensive melt formation. Thus, sufficient melt was present for pore filling, forming the dense morphology seen in Fig. 3. This kind of deposit is referred to as "molten" in further discussion. A molten deposit is characterised by a dense morphology where the original pores of the deposit have been filled by melt. Molten morphologies can still contain inclusions of air, as seen in the molten full-scale deposit in Fig. 3. The amount of melt formed within kraft recovery boiler deposits and the synthetic deposits used in this study depends mainly on their Cl content [17].

In this work, the shortest exposure time was zero minutes, calculated from when the furnace reached the set temperature. Already at such short exposure times, morphological changes in the deposit cross-sections were observed. The temperature logs showed that the outer deposit surface reached temperatures above T_0 already during the heating phase. The formed melt subsequently accelerated morphological changes and a skeletal or molten morphology could already be observed after 0-minute experiments.

A detailed analysis of the elemental composition of molten deposits of ternary reciprocal salts revealed local enrichment in K and Cl toward the steel. Similar observations have also been made in molten, high-Cl boiler deposits [26]. A cross-sectional SEM image of a synthetic deposit enriched in K and Cl toward the steel and the corresponding molar K/(Na + K) and Cl/(Na + K) ratios are given in Fig. 4. The figure also shows an SEM image and elemental molar ratios of a high-Cl deposit obtained directly from a superheater tube of a kraft recovery boiler [26].

The synthetic and boiler deposit has a maximum in the average K/(Na + K) ratio in the molten layer at the interface with the porous region closest to the steel. Each point in the graph gives the average molar ratio value over a horizontal line of pixels. The analysed maximum values were due to the local enrichment in K within the melt. This enrichment enabled the melt to move closer to the steel with time. The main constituent in kraft recovery boiler deposits is Na_2SO_4 . In such deposits, the increase in K content decreases the local first melting temperature. The enrichment in K within the melt enables movement of melt toward the steel, to regions where local temperatures are below T_0 of the initially deposited material. A detailed explanation of the mechanism resulting in

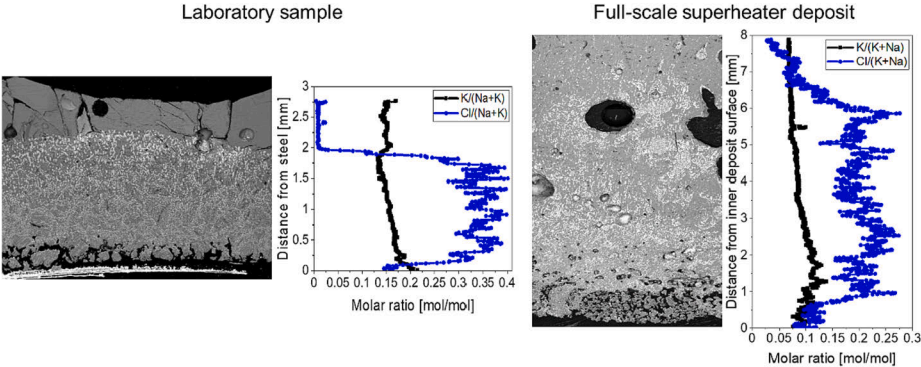


Fig. 4. Greyscale SEM images of molten deposits and corresponding molar K/(Na + K) and Cl/(Na + K) ratios showing local enrichment in K toward the steel; laboratory 10 K 10Cl deposit (left); full-scale superheater deposit (right).

melt movement is given elsewhere [26].

For the laboratory sample shown in Fig. 4, the steel temperature and initial bulk T_0 were 450 °C and 557 °C, respectively. Based on experiments using binary salts, the first estimate of the porous layer thickness for the laboratory sample was approximately 1 mm. However, due to the enrichment in K and the resulting local decrease in T_0 , the melt moved closer to the steel before solidifying. Hence the final porous layer thickness of 0.3 mm was significantly thinner than initially estimated. Thus, the experience from earlier experiments utilising binary systems was no longer applicable to more complex ternary reciprocal salt systems. The experiments using ternary reciprocal salts confirmed the observations made earlier in the actual boiler deposits.

For binary salts, a local change in deposit composition due to element enrichment does not affect T_0 due to their eutectic nature. Nevertheless, local element enrichment within the molten phase has also been reported for binary systems [15,24,25]. The composition of the

molten phase approaches the eutectic composition toward the interface between the molten and porous layer [15,24,25]. However, this does not change the local first melting temperature and no significant decrease in the thickness of the porous layer has been reported when using binary salts.

A molten phase moving closer toward the steel can significantly increase the risk for corrosion [34], as melt getting in direct contact with the steel surface causes severe melt-induced corrosion. Furthermore, due to the deposit melting, the location of T_0 within the deposit cross-section moves closer toward the steel and the steepness of the temperature gradient over the porous region underneath increases. The steeper temperature gradient over the porous deposit region subsequently accelerates deposit ageing via diffusional transport of alkali chloride vapours toward the steel [35].

No local element enrichment in K or Cl toward the steel took place in the skeletal deposit regions. The amount of melt present was insufficient

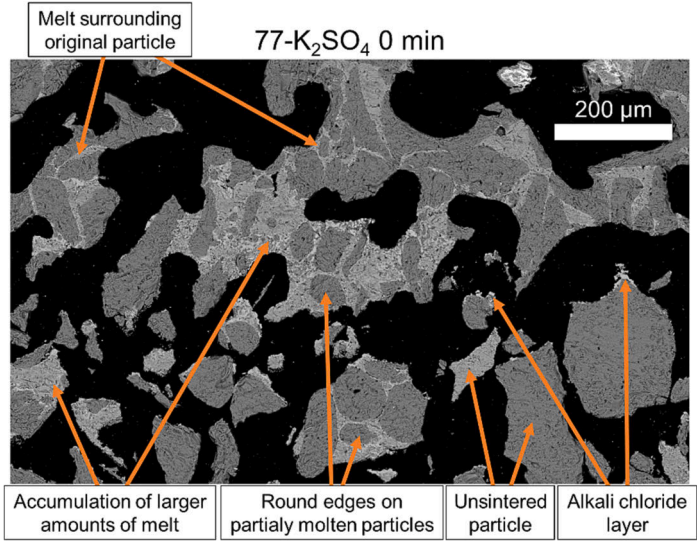


Fig. 5. Detailed view on skeletal region of a 0-minute experiment highlighting its main features.

for pore filling and movement of melt toward the steel. However, the outer part of skeletal deposits experienced temperatures above T_0 , and the formed melt accelerated sintering, hence the formation of the skeletal region. The impact of melt on the formation of the skeletal deposit morphology is highlighted in Fig. 5.

The sintering of salt systems proceeds predominantly via two main mechanisms. In the first, volatile compounds in the deposit evaporate and condense at contact points or close contact areas between distinct particles within the deposit [36]. The second mechanism involves solid-state diffusion within the deposit particles [36]. Both mechanisms result in the formation of necks between the single deposit particles. These necks then grow further, up to a point at which the original particles can no longer be identified. The presence of melt greatly accelerates the sintering process [30], as it accumulates at contact points and supports neck formation. In this case, the mechanism is referred to as liquid phase sintering. For the skeletal region, seen in the short-term deposits in this work, the sintering process and formation of the skeletal morphology were accelerated by the presence of melt. Thus, as explained above, a skeletal layer formed already during the 0-minute experiment.

In the deposit shown in Fig. 5, locally high concentrations of alkali

chloride were observed in the skeletal region. These Cl-rich regions are an indicator for partial melting of the deposit to have taken place. For all synthetic deposit compositions used in this work, and recovery boiler deposits in general, all Cl present in the deposit is incorporated in the molten phase as soon as T_0 is reached. For the skeletal deposit in Fig. 5, the amount of melt formed was insufficient to fill the pores. Thus no molten morphology formed. Instead, the formed melt accumulated at contact points of distinct particles, where it accelerated the sintering process. In some cases, Cl-rich melt seemed to surround deposit particles. The round edges of these melt-surrounded particles were an additional indicator of partial melting of the deposit.

With increasing exposure time, alkali chlorides within the melt are prone to evaporate. Alkali chloride vapours diffuse either into the furnace/flue gases or toward the colder region in the deposit, closer to the steel. Diffusion toward the steel is driven by the gas-phase concentration gradient [24,25]. At lower local temperatures, the alkali chlorides form typical layers on the furnace-facing sides of particles via condensation [24,25]. Thin layers of alkali chloride were identified after the 0-minute experiments, as shown in Fig. 5. With increasing exposure time, the alkali chloride layers grew in thickness and the skeletal deposit

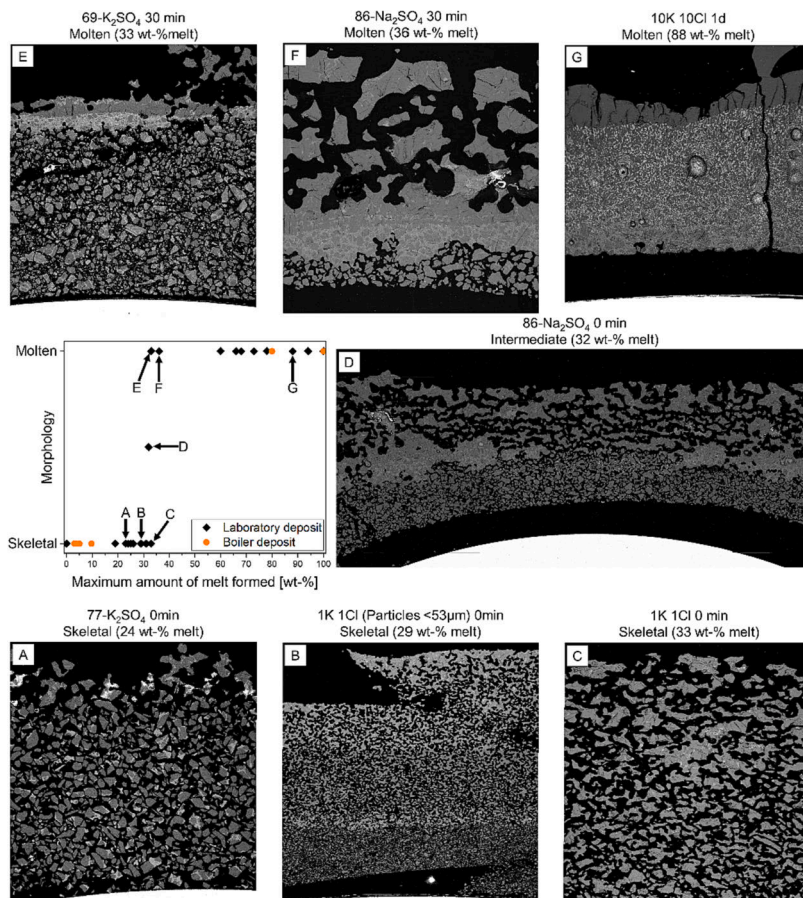


Fig. 6. Summary of available data on final deposit morphology as a function of the amount of melt. Selected SEM images depicting skeletal (A, B, and C); intermediate (D); molten deposits (E, F, and G). The orange dots are for kraft recovery boiler deposits.

was depleted in Cl.

The differences in morphology and ageing behaviour of the two deposit archetypes have a significant impact on the corrosivity and removability of the deposits. Therefore, being able to predict the final deposit morphology can help significantly in predicting and preventing operational issues caused by deposits. In the following, the decisive parameter causing a change in deposit morphology, as well as a threshold for when the change in deposit morphology takes place will be identified.

3.2. Transition from skeletal to molten morphology

The results presented above imply that the final deposit morphology depends on the amount of melt formed within the deposit. SEM images of 33 deposit cross-sections were analysed to identify the threshold for the melt fractions, at which a molten deposit morphology forms. The samples comprise short- and long-term temperature gradient laboratory experiments, using binary and ternary reciprocal salt systems. In addition, actual superheater deposits from two kraft recovery boilers were analysed. Based on the deposit morphology, the results were classified into three categories: skeletal, molten, and intermediate. The graph showing the morphology as a function of the maximum amount of melt in Fig. 6 summarises the deposit classification. The figure also shows SEM images of selected deposit cross-sections illustrating the changes in deposit morphology with changing melt fractions. SEM images of all studied laboratory deposit cross-sections are given in the supplementary material.

The maximum amount of melt in the deposits was calculated based on the highest temperature measured by the thermocouple at the outer deposit surface. For deposits with an initial low Cl content (1 wt-%), SEM analysis revealed evaporation of a significant share of Cl into the furnace during the heating phase which affects the deposit's melting behaviour. Hence, for deposits of a low initial Cl content, the maximum amount of melt was determined based on SEM analysis data instead of its initial composition. For deposits of a higher initial Cl content, evaporation of Cl did not have a similar impact on the melting behaviour.

The parameters varied in the laboratory deposits summarised in the graph in Fig. 6 were exposure time, set temperatures of probe and furnace, and deposit composition. Furthermore, the impact of different initial particle sizes on the final deposit morphology was studied. Fig. 6 also contains data from boiler deposits. The superheater deposits are marked with orange circles in the graph. All skeletal superheater deposits were obtained from a Finnish kraft recovery boiler [27], while all superheater deposits of a molten morphology were obtained from a Brazilian kraft recovery boiler [26]. The Brazilian deposits formed a molten morphology due to a significantly higher Cl content compared to the Finnish deposits.

The amount of melt formed in the skeletal deposits increased from A to C (Fig. 6). No molten layer formed in these deposits. The deposit in Image A had the lowest melt fraction of the selected deposits. Only a thin skeletal layer formed at its outer surface and most of the deposit remained porous. The results imply that the thickness of the skeletal layer did not depend on the amount of melt but on the differences in T_{steel} , deposit T_0 , and $T_{\text{outer surface}}$. Only the region of the deposit where the local temperature exceeded T_0 formed a skeletal morphology. For the deposit in image A, the maximum temperature during the experiment was only 50 °C above T_0 ; thus, only a thin layer on the outer deposit surface experienced temperatures above T_0 .

Image B in Fig. 6 shows a deposit consisting of a smaller particle size fraction. Niemi et al. [35] reported a decrease in particle size to have resulted in the formation of a molten deposit morphology, with all other parameters unchanged. Reducing the particle size decreases the pore size of void areas but does not affect the deposit's overall porosity. Further, liquid phase sintering eliminates smaller pores more efficiently due to higher capillary forces [30,37]. As a reduction of the particle size affects the sintering process, the formation of a molten morphology does

not exclusively depend on the amount of melt in the deposit. The threshold amount of melt required to form a molten morphology can vary. Deposit melting is a highly complex process and is affected by several parameters simultaneously. Furthermore, deposit densification can take place via pathways other than pore filling by melt [38], which can eventually result in a morphology similar to molten deposits. However, these mechanisms are typically much slower and of no relevance for the short-term experiments presented here.

In this work, only reducing the particle size did not change the deposit morphology. The increase in capillary forces due to smaller particles has a lesser impact on the final deposit morphology than the amount of melt [37]. Therefore, no change in the final deposit morphology was observed for deposit B.

Image C in Fig. 6 shows sporadically distributed, larger agglomerates of particles throughout the outer region of the cross-section. The analysis suggests that these agglomerates consist of several particles sintered together by a small amount of melt, rather than formed by a larger amount of melt in the outer deposit.

Significant differences were identified between deposits C and D in Fig. 6. Larger accumulations of melt were observed in the middle of deposit D. Within these melt accumulations, phase separation and enrichment in Cl toward the steel was identified, a mechanism that was earlier associated with the formation of larger amounts of melt. A similar phase separation was not seen for the agglomerates in deposit C. Therefore, the areas of molten morphology in deposit D were assumed to have formed due to the accumulation of melt. However, the amount of melt was not sufficient to form a molten morphology, covering the whole cross-section of the deposit. The outer region still resembled a skeletal structure. As the deposit showed properties of both morphological archetypes it was classified as an intermediate morphology between skeletal and molten.

Images E, F, and G in Fig. 6 are examples of molten deposit morphologies. Image E shows the deposit with the lowest calculated melt fraction of all molten deposits. Only a thin molten layer formed on the outer deposit surface, and most of the deposit underneath the molten layer remained porous. The relatively thin molten layer indicates that the amount of melt formed during the experiment was just above the threshold to form a molten deposit morphology. Phase separation and Cl-enrichment in the melt toward the steel surface were identified. As deposit E was a binary salt, no decrease in T_0 due to local element enrichment and subsequent movement of melt toward the steel took place. Hence only a thin molten layer formed on the outer deposit surface.

The molten layer of deposit F is significantly thicker compared to deposit E. Furthermore, a skeletal region above the molten layer suggests that melt, initially formed at the outer part of the deposit, moved toward the steel where it accumulated and formed a molten morphology. Two conditions must be met for the melt to move toward the steel. First, the amount of melt formed must be sufficient to move toward the steel due to capillary and gravitational forces. Second, the temperature closer to the steel must be above the melt's solidification temperature. A temperature profile develops over the cross-section with prolonged exposure. Accordingly, T_0 in the deposit moves closer toward the steel. Furthermore, the sintering and melting of the deposit increase the thermal conductivity [39] in the outer deposit region, additionally moving T_0 closer to the steel.

The experimental conditions for deposits D and F were identical, except for the longer exposure time for deposit F. The experimental setup did not allow a precise temperature adjustment at the outer deposit surface. Therefore a slightly higher temperature was recorded for deposit F than D. The melt fraction in the molten deposit F was 4 wt-% higher than in deposit D. The slight increase in melt fraction resulted in a significant change in the deposit morphology. The morphology of deposit F supports the classification of deposit D as intermediate since the small increase in the melt fraction from D to F caused a molten morphology to form. Deposits D and F gave additional proof of the

amount of melt to be the decisive parameter affecting the final deposit morphology. Already a small increase in the melt fraction, under the same experimental conditions, resulted in a significant change in the deposit morphology.

In deposit G in Fig. 6, a significantly larger amount of melt (88 wt-%) formed during the experiment. The synthetic salt used in this experiment was of a ternary reciprocal system. Temperature gradient-induced local enrichment in K enabled the melt to move closer toward the steel before solidifying. Therefore, melt was present in regions where local temperatures were well below the initial bulk T_0 . The pores in the deposit closer to the steel were filled by melt and eliminated. The gap between the steel and the molten region seen in deposit G is due to the sample preparation after the exposure. The epoxy resin used to fix the deposit detached and separated it from the steel surface. This issue was observed for several of the laboratory experiments. However, a loss of the porous layer during sample preparation, especially cutting the deposit to obtain a cross-section, cannot be ruled out to have resulted in the formation of the gap between the molten deposit and the steel.

The data summarized in the graph in Fig. 6 indicates that the morphology changed from skeletal to molten when approximately 30 wt-% melt had formed within the deposit. A melt fraction of 30 wt-% was sufficient for the liquid to fill the void areas within the deposit, resulting in a molten morphology. This melt fraction agrees with the general understanding of liquid phase sintering: approximately 30 vol-% liquid is typically required to fill all voids of a porous structure [30]. Furthermore, when considering various packing models of spheres, the identified melt fraction of about 30 wt-% lies within the void area range of ordered close packings (26 vol-%) and random close packings (36 vol-%) [40]. The packing models are based on spheres of equal size, whereas the deposit particle size ranged between 53 and 250 μm , and the particles were of non-uniform shape. However, the suggested amount of approximately 30 wt-% melt for a molten deposit to form is still in good agreement with the packing models of spheres and the liquid phase sintering theory.

As mentioned in the discussion above, several other parameters such as deposit particle size, deposit porosity, the viscosity of the molten phase, or morphological changes affecting the deposit temperature profile influence the melting behaviour of deposits. However, based on the observations made in the present study, all these other parameters were identified as having only a minor impact on the final deposit morphology. Thus, the maximum amount of melt formed in a deposit is identified as the decisive parameter determining its final morphology.

As a continuation of this work, the influence of other parameters on the melting behaviour and thus the final deposit morphology can be studied in more detail. A possible next step can be the extension of the experimental matrix into utilising deposits of compositions other than those relevant to kraft recovery boilers. Furthermore, the impact of the presence of SO_2 or H_2O in the gas phase can be studied to identify to which extent interactions of the deposit and compounds present in the gas phase affect the final deposit morphology.

The results presented above can help in predicting the ageing behaviour of deposits more accurately. The identified threshold amount of melt can be utilised as an additional input for deposition models, that also take subsequent deposit ageing into account. By distinguishing between a skeletal and molten deposit morphology, the ageing behaviour and changes in the local chemical composition of deposits and therewith associated operational problems can be modelled more accurately. This is valuable data for both boiler operators and manufacturers and can help in preventing severe melt-induced corrosion. Furthermore, information on the evolution of the deposit morphology can be utilised when scheduling sootblowing. The better the knowledge of deposits and how they change in their local chemistry and morphology during boiler operation, the more efficiently sootblowing cycles can be scheduled.

4. Conclusions

In short-term laboratory experiments, synthetic ash deposits of compositions characteristic for kraft recovery boilers were exposed to a temperature gradient to study the initial melting behaviour of deposits. Two archetype deposit morphologies with differences in their ageing behaviour emerged. The main findings can be summarised as follows.

- The governing parameter determining the final deposit morphology was identified to be the maximum amount of melt formed within the deposit, with other parameters investigated having only a minor impact on the final deposit morphology. The threshold for a change in the final deposit morphology is at about 30 wt-% melt formed in the deposit.
- A skeletal morphology forms if the amount of melt remains below 30 wt-%. Skeletal deposits are characterized by a sintered, but still porous morphology. If small amounts of melt are formed in the deposit, a skeletal morphology can already form after very short exposure times as the sintering process is accelerated significantly by the presence of melt.
- A molten morphology forms when the maximum amount of melt exceeds 30 wt-%. Molten deposits are characterized by a dense, non-porous layer that forms due to melt filling the voids of the initially porous deposit.
- Differences in the ageing behaviour of the two morphological archetypes were identified. The governing ageing mechanism for skeletal deposits is the diffusional transport of vapours toward the steel, induced by a temperature gradient. In molten deposits, movement of melt toward the steel coupled with element enrichment was seen, causing a decrease in the local first melting temperature.
- The presented results provide new information on deposit ageing mechanisms and their impact on superheater corrosion and deposit removability. The new insights aim to help in identifying the governing deposit ageing mechanisms based on deposit morphology, which facilitates the identification of regions in a boiler at an increased risk for deposit-induced problems to occur. This in turn helps to better predict and avoid deposit-induced issues in boilers.

CRedit authorship contribution statement

Roland Balint: Writing – original draft, Investigation, Data curation, Conceptualization. **Markus Engblom:** Writing – review & editing, Validation, Supervision, Project administration, Investigation, Funding acquisition, Conceptualization. **Jonne Niemi:** Writing – review & editing, Validation, Supervision, Conceptualization. **Mikko Hupa:** Writing – review & editing, Validation, Funding acquisition. **Leena Hupa:** Writing – review & editing, Funding acquisition.

Declaration of Competing Interest

The authors declare that they have no known competing financial interests or personal relationships that could have appeared to influence the work reported in this paper.

Data availability

SEM images of the analysed deposits are provided as supplementary material and were uploaded at the attach file step

Acknowledgements

This work was financed by a research grant awarded by the Fortum Foundation, Finland [Application number 20190123] and the Åbo Akademi University Graduate School in Chemical Engineering. This work has been partly carried out within the Åbo Akademi CLUE2 Research Consortium (2017–2022). Support from ANDRITZ Oy, Valmet

Technologies Oy, UPM-Kymmene Oyj, Metsä Fibre Oy, and International Paper Inc. is gratefully acknowledged. Additional support from the Research Council of Finland project “New insights on the effects of

temperature gradients on high temperature corrosion” [Decision number 338322] is highly appreciated. We want to thank Linus Silvander for carrying out SEM/EDXA analyses.

Appendix

A) Summary of laboratory temperature gradient experiments containing deposit name, steel temperature, maximum temperature at outer deposit surface, and exposure time

Salt name	Steel temperature [°C]	Maximum deposit temperature [°C]	Exposure time [h]
1 K 1Cl	450	753	72
1 K 1Cl	450	685	120
77-K ₂ SO ₄	450	726	0.5
77-K ₂ SO ₄	450	737	0
1 K 1Cl	500	767	0
1 K 10Cl	400	618	24
10 K 1Cl	450	731	120
10 K 1Cl	450	732	168
1 K 1Cl (<53 μm)	500	767	0
77-K ₂ SO ₄	500	796	24
86-Na ₂ SO ₄	450	712	0
69-K ₂ SO ₄	450	731	0.5
1 K 1Cl	550	780	0
69-K ₂ SO ₄	450	749	0
86-Na ₂ SO ₄	450	725	0.5
10 K 10Cl	400	593	336
10 K 10Cl	400	611	120
10 K 10Cl	400	617	168
1 K 10Cl	400	666	240
10 K 10Cl	400	631	4
10 K 10Cl	400	643	120
10 K 10Cl	400	666	24
10 K 10Cl	400	677	4
1 K 10Cl	450	735	72
1 K 10Cl	450	737	168
10 K 10Cl	450	747	0
10 K 10Cl	450	757	72

Appendix A. Supplementary data

Supplementary data to this article can be found online at <https://doi.org/10.1016/j.fuel.2023.130386>.

references

[1] Vakkilainen EK. Kraft recovery boilers - Principles and practice. Suomen Soodakattilayhdistys ry 2005.

[2] Mikkonen P, Kauppinen EI, Pyykönen J, Jokiniemi JK, Aurela M, Vakkilainen EK, et al. Alkali salt ash formation in four Finnish industrial recovery boilers. *Energy Fuel* 1999;13:778–95. <https://doi.org/10.1021/ef980189a>.

[3] Capablo J. Formation of alkali salt deposits in biomass combustion. *Fuel Process Technol* 2016;153:58–73. <https://doi.org/10.1016/j.fuproc.2016.07.025>.

[4] Tran HN, Reeve DW, Barham D. Formation of kraft recovery boiler superheater fireside deposits. *Pulp and Paper Canada* 1983;84:36–41.

[5] Kleinhans U, Wieland C, Frandsen FJ, Spliethoff H. Ash formation and deposition in coal and biomass fired combustion systems: Progress and challenges in the field of ash particle sticking and rebound behavior. *Prog Energy Combust Sci* 2018;68: 65–168. <https://doi.org/10.1016/j.pecs.2018.02.001>.

[6] Niu Y, Tan H, Hui S. Ash-related issues during biomass combustion: Alkali-induced slagging, silicate melt-induced slagging (ash fusion), agglomeration, corrosion, ash utilization, and related countermeasures. *Prog Energy Combust Sci* 2016;52:1–61. <https://doi.org/10.1016/j.pecs.2015.09.003>.

[7] Baxter LL. Ash Deposit Formation and Deposit Properties 2000. <https://doi.org/10.2172/760515>.

[8] Wessel RA, Baxter L, Shaddix C, Verrill C, Frederick WJJ, Lien S, et al. Particle formation and deposition in recovery boilers. TAPPI Fall Technical Conference and Trade Fair 2002:315–28.

[9] P. Mikkonen Fly ash particle formation in kraft recovery boilers. 2000.

[10] Grabke HJ, Reese E, Spiegel M. The effects of chlorides, hydrogen chloride, and sulfur dioxide in the oxidation of steels below deposits. *Corros Sci* 1995;37: 1023–43. [https://doi.org/10.1016/0010-938X\(95\)00011-8](https://doi.org/10.1016/0010-938X(95)00011-8).

[11] Uusitalo MA, Vuoristo PMJ, Mäntylä TA. High temperature corrosion of coatings and boiler steels below chlorine-containing salt deposits. *Corros Sci* 2004;46: 1311–31. <https://doi.org/10.1016/j.corsci.2003.09.026>.

[12] Karlsson A, Moller PJ, Johansen V. IRON and steel corrosion in a system of O₂, SO₂, and alkali chloride. The formation of low melting point salt mixtures. *Corros Sci* 1990;30:153–8. [https://doi.org/10.1016/0010-938X\(90\)90069-H](https://doi.org/10.1016/0010-938X(90)90069-H).

[13] Lindberg D, Backman R, Chartrand P. Thermodynamic evaluation and optimization of the (NaCl + Na₂SO₄ + Na₂CO₃ + KCl + K₂SO₄ + K₂CO₃) system. *J Chem Thermodyn* 2007;39:1001–21. <https://doi.org/10.1016/j.jct.2006.12.018>.

[14] Karlemo C. Non-process elements in the recovery cycle of six Finnish Kraft pulp mills. Åbo Akademi University; 2019. Master’s Thesis.

[15] Niemi J, Balint R, Engblom M, Lehmusto J, Lindberg D. Temperature-gradient-driven aging mechanisms in alkali-bromide- And sulfate-containing ash deposits. *Energy Fuel* 2019;33:5883–92. <https://doi.org/10.1021/acs.energyfuels.8b04199>.

[16] Tran H, Gonsko M, Mao X. Effect of composition on the first melting temperature of fireside deposits in recovery boilers. *Tappi J* 1999;82:93–100.

[17] Reeve DW, Tran HN, Barham D. The effluent-free bleached kraft pulp mill - Part XI Morphology, chemical and thermal properties of recovery boiler superheater fireside deposits. *Pulp & Paper Canada* 1981;82:T315–20.

[18] A. Costa D, Silva F, Abella Cenibra CNSA. EXPERIENCE OF RECOVERY BOILER SUPERHEATER CORROSION AT CENIBRA. International Chemical Recovery Conference - ICRC, Halifax, Canada; 2017.

[19] Jensen PA, Frandsen FJ, Hansen J, Dam-Johansen K, Henriksen N, Hörlyck S. SEM investigation of superheater deposits from biomass-fired boilers. *Energy Fuel* 2004; 18:378–84. <https://doi.org/10.1021/ef030097l>.

[20] Tang X, Liu Q, Wang T. Ash deposition characteristics during oxy-fuel combustion of biomass in a drop tube furnace. *Biomass Convers Biorefin* 2023. <https://doi.org/10.1007/s13399-023-04020-3>.

[21] Hansen LA, Nielsen HP, Frandsen FJ, Dam-Johansen K, Hörlyck S, Karlsson A. Influence of deposit formation on corrosion at a straw-fired boiler. *Fuel Process Technol* 2000;64:189–209. [https://doi.org/10.1016/S0378-3820\(00\)00063-1](https://doi.org/10.1016/S0378-3820(00)00063-1).

- [22] Lapuerta M, Acosta A, Pazo A. Fouling deposits from residual biomass with high sodium content in power plants. *Energy Fuel* 2015;29:5007–17. <https://doi.org/10.1021/acs.energyfuels.5b00356>.
- [23] Zhou H, Jensen PA, Frandsen FJ. Dynamic mechanistic model of superheater deposit growth and shedding in a biomass fired grate boiler. *Fuel* 2007;86:1519–33. <https://doi.org/10.1016/j.fuel.2006.10.026>.
- [24] Lindberg D, Niemi J, Engblom M, Yrjas P, Laurén T, Hupa M. Effect of temperature gradient on composition and morphology of synthetic chlorine-containing biomass boiler deposits. *Fuel Process Technol* 2016;141:285–98. <https://doi.org/10.1016/j.fuproc.2015.10.011>.
- [25] Niemi J, Lindberg D, Engblom M, Hupa M. Simultaneous melt and vapor induced ash deposit aging mechanisms – Mathematical model and experimental observations. *Chem Eng Sci* 2017;173:196–207. <https://doi.org/10.1016/j.ces.2017.07.041>.
- [26] Balint R, Engblom M, Niemi J, da Costa DS, Lindberg D, Yrjas P, et al. Temperature gradient induced changes within superheater ash deposits high in chlorine. *Energy* 2021;226:120439. <https://doi.org/10.1016/j.energy.2021.120439>.
- [27] Balint R, Engblom M, Niemi J, Lindberg D, Saarinen T, Rautala J, et al. Morphological and chemical differences within superheater deposits from different locations of a black liquor recovery boiler. *Energy* 2023;267:126576. <https://doi.org/10.1016/j.energy.2022.126576>.
- [28] Balint R, Engblom M, Vainio E, Laurén T, Niemi J, Rautala J, et al. Changes in chlorine content over time – Probe deposit sampling in a Finnish kraft recovery boiler. *Fuel* 2023;340:127599. <https://doi.org/10.1016/j.fuel.2023.127599>.
- [29] CW, Bale E, Bélsle P, Chartrand SA, Decterov G, Eriksson AE, Gheribi et al. FactSage thermochemical software and databases, 2010–2016. *Calphad: Computer Coupling of Phase Diagrams and Thermochemistry* 54 2016 35 53 10.1016/j.calphad.2016.05.002.
- [30] German RM, Suri P, Park SJ. Review: Liquid phase sintering. *J Mater Sci* 2009;44:1–39. <https://doi.org/10.1007/s10853-008-3008-0>.
- [31] Skrifvars B-J, Hupa M, Hyöty P. Composition of recovery-boiler dust and its effect on sintering. *Tappi J* 1991;74:185–9.
- [32] Laxminarayan Y, Nair AB, Jensen PA, Wu H, Frandsen FJ, Sander B, et al. Tensile adhesion strength of biomass ash deposits: Effect of the temperature gradient and ash chemistry. *Energy Fuel* 2018;32:4432–41. <https://doi.org/10.1021/acs.energyfuels.7b03114>.
- [33] Mao X, Tran H, Cormack DE. Effects of chemical composition on the removability of recovery boiler fireside deposits. *TAPPI JOURNAL* 2001;84.
- [34] Hupa M, Karlström O, Vainio E. Biomass combustion technology development – It is all about chemical details. *Proc Combust Inst* 2017;36:113–34. <https://doi.org/10.1016/j.proci.2016.06.152>.
- [35] Niemi J, Engblom M, Laurén T, Yrjas P, Lehmusto J, Hupa M, et al. Superheater deposits and corrosion in temperature gradient – Laboratory studies into effects of flue gas composition, initial deposit structure, and exposure time. *Energy* 2021;228. <https://doi.org/10.1016/j.energy.2021.120494>.
- [36] Frederick WJ, Ling A, Tran HN, Lien SJ. Mechanisms of sintering of alkali metal salt aerosol deposits in recovery boilers. *Fuel* 2004;83:1659–64. <https://doi.org/10.1016/j.fuel.2004.02.005>.
- [37] Lee SM, Kang SJL. Theoretical analysis of liquid-phase sintering: Pore filling theory. *Acta Mater* 1998;46:3191–202. [https://doi.org/10.1016/S1359-6454\(97\)00489-8](https://doi.org/10.1016/S1359-6454(97)00489-8).
- [38] Techakijakajorn U, Frederick WJ, Tran HN. Sintering and densification of recovery boiler deposits: Laboratory data and a rate model. *J Pulp Pap Sci* 1999;25:73–80.
- [39] Zbogor A, Frandsen FJ, Jensen PA, Glarborg P. Heat transfer in ash deposits: A modelling tool-box. *Prog Energy Combust Sci* 2005;31:371–421. <https://doi.org/10.1016/j.pecs.2005.08.002>.
- [40] Berryman JG. Random close packing of hard spheres and disks. *Phys Rev A* 1983;27:1053–61. <https://doi.org/10.1103/PhysRevA.27.1053>.

J. Niemi, R. Balint, M. Engblom, J. Lehmusto, D. Lindberg (2019)
**Temperature-Gradient-Driven Aging Mechanisms in Alkali-Bromide-
and Sulfate-Containing Ash Deposits.**

Energy & Fuels

V



Temperature-Gradient-Driven Aging Mechanisms in Alkali-Bromide- and Sulfate-Containing Ash Deposits

Jonne Niemi,^{*,†} Roland Balint,^{‡,§} Markus Engblom,[†] Juho Lehmusto,[†] and Daniel Lindberg^{†,§}

[†]Johan Gadolin Process Chemistry Centre, Laboratory of Inorganic Chemistry, Åbo Akademi University, Piispankatu 8, FI-20500 Turku, Finland

[‡]Department of Mechanical Engineering, Institute for Energy Systems, TU München, Boltzmannstraße 15, 85747 Garching, Germany

[§]Department of Chemical and Metallurgical Engineering, School of Chemical Engineering, Aalto University, Kemistintie 1, FI-00076 Aalto, Finland

ABSTRACT: The aging of alkali-bromide-containing ash deposits was studied by applying premixed alkali bromide–alkali sulfate mixtures on a laboratory-scale temperature gradient probe. The probe temperature was kept at 500 °C, while the furnace air temperature was measured to be 800 °C, simulating a heat exchanger ash deposit temperature profile. Deposits of ~5 mm thick were aged in the furnace for 2–8 h and subsequently rapidly cooled to room temperature. The deposit cross-sections were analyzed and characterized using SEM/EDX. The deposits were observed to form multilayered structures, where the furnace-facing region was dense and sintered, while the steel-facing region was porous. Within the porous region, a gas phase migration of alkali bromides toward the colder temperature was observed. The alkali bromide migration toward the colder steel temperature observed in the experiments was quantified and compared to modeling results. The modeling results were calculated by modifying an existing temperature-gradient-driven alkali chloride intradeposit migration model for alkali bromides. The model is in agreement with the experimental results, validating an enrichment mechanism for alkali bromides. Because of their relatively high saturation pressures, alkali bromide migration was observed to be significantly faster than the earlier reported migration of alkali chlorides. Enrichment of alkali bromides in colder temperatures in boiler deposits could lead to significant changes in the local composition of the deposit, possibly leading to an enhanced corrosion rate of the tube material and/or densification of the deposit structure.

1. INTRODUCTION

Waste-derived fuels and cheap biomass fuels have become increasingly interesting for energy conversion applications. Waste-derived fuels are cheap compared to pristine biomass, and firing waste is a good alternative to landfilling.¹ Although waste firing is a lucrative alternative from the economic and environmental point of view, there exist a number of technical challenges associated with waste-derived fuels. Especially when trying to attain higher electrical efficiency by raising the final steam temperature, and as a result, the superheater material temperature, corrosion-related challenges in the boiler increase.²

One major challenge is the heterogeneity of the waste-derived fuels. Different waste fractions have different chemical compositions, particle sizes, etc., and the estimation of the ash chemistry and its effects on boiler design and operation is challenging. Waste fractions can include high amounts of alkali metals (Na, K), heavy metals (Pb, Zn), and halides (Cl, Br), all of which are often connected to rapid corrosion of boiler materials.^{3–9} Alkali-chloride-induced high-temperature corrosion has been studied extensively, and it is recognized as one of the prominent reasons for corrosion in biomass-fired boilers. However, the detailed corrosion mechanisms are still being discussed.² Heavy metals in combination with Cl have also been studied to some extent, and several studies discussing the corrosion effects and mechanisms have been published.^{3,4,8–11} The existing corrosion results with alkali bromides are similar

to those with alkali chlorides. While high-temperature corrosion of alkali bromides has been considered in the literature,^{6,7} the research on the topic is still scarce. To the best of our knowledge, alkali bromide corrosion has not been studied in the presence of a temperature gradient across the ash deposit.

One of the main sources of Br in waste-derived fuels is brominated flame-retardants, which can be found, e.g., in municipal solid waste and solid recovered fuel. Plastics treated with brominated flame-retardants can contain several mass percent Br. Brominated biocides are another important source of Br in waste-derived fuels.¹² In addition to waste, even some biomass fractions can include high amounts of Br. Naturally occurring Br mainly originates from seawater; therefore, the biomass fractions containing the most amounts of Br are some selected marine algae and coastal peat.¹³

The amount of Br in the fuel is often relatively low, e.g., in comparison to the amount of Cl. In spite of the low concentrations in the fuel, Br has been observed in the corrosion front of waterwall tubes in a BFB boiler firing a

Special Issue: 27th International Conference on Impact of Fuel Quality on Power Production and Environment

Received: December 3, 2018

Revised: February 21, 2019

Published: March 11, 2019

mixture of bark, solid recovered fuel, and wastewater sludge from a paper mill.¹⁴ In addition, Br has been observed to enrich in waterwall deposits. Vainikka et al.¹⁵ observed several mass percent of Br locally in waterwall deposits, while the fuel fed into the boiler contained only tens of mg kg⁻¹ of Br.

Ash deposits and heat exchanger tubes experience temperature gradients during boiler operation. The temperature difference from the flue gas to the process steam/water is several hundreds of °C. Temperature gradients are known to affect the deposition behavior.¹⁶ In addition, temperature gradients have been shown to affect corrosion of steel and the chemistry and morphology of ash deposits. Corrosion rates of the heat exchanger tube have been shown to increase with higher flue gas temperature even if the tube temperature is kept constant.^{17,18} Temperature gradients have been shown to induce diffusion within oxide layers¹⁹ and to induce penetration of corrosive chloride species through unstable oxide layers to the unaffected steel surface.²⁰

The effects of temperature gradients on ash deposit chemistry and morphology have been studied mainly in laboratory scale. The main observations have so far been the formation of distinct regions within the deposit, distinguishable by either composition or structure, and migration of species due to temperature gradients.^{10,21–24} Depending on the deposit composition, temperature gradients have been observed to affect the adhesion of deposits to the tube material.²⁵ The effect on adhesion was concluded to be mainly due to the formation of a melt, subsequent liquid phase sintering, and melt movement toward the steel surface, where it glues the deposit to the tube surface.

The temperature-gradient-induced gas phase migration of alkali chlorides has been reported and modeled earlier.^{22,23} As a result of the migration, an enrichment of alkali chlorides is observed in the lower temperatures within the deposit. The alkali chlorides form pure cubical structures within the deposits and even enrich on the steel surface as pure alkali chloride crystals. Similar results have been observed in biomass-fired boilers,^{26–28} and the effect has been suggested to be due to the intradeposit gas phase migration of alkali chlorides.²⁹

Alkali chlorides and bromides are similar in their molecular structure, melting characteristics, and chemistry. The similarities make bromides interesting from another point of view; i.e., alkali bromides can be used to test vaporization–condensation mechanisms observed with alkali chlorides. Alkali bromides can be utilized to find out whether the phenomena, e.g., the temperature-gradient-induced alkali chloride migration, are alkali-chloride-specific or more general in nature. This paper focuses on studying the effects of temperature gradient on alkali bromide and alkali sulfate mixtures. The aim of this paper is to recognize fundamental phenomena prevailing in synthetic ash deposits, and to test the hypothesis that alkali bromide–alkali sulfate mixtures behave in a similar fashion as alkali chloride–alkali sulfate mixtures when exposed to temperature gradients. In addition, the aim is to modify and test the applicability of an existing alkali chloride migration model for alkali bromides, to further validate the understanding of the enrichment phenomena and its implications for boiler applications.

2. EXPERIMENTAL SECTION

The main experimental setup consists of a laboratory-scale air-cooled probe, which is inserted into a tube furnace. Synthetic ash deposits are applied on top of the probe. The furnace temperature is higher than

the probe temperature, creating a temperature gradient over the deposit. The temperature gradient simulates a real boiler situation where a temperature gradient is present over the deposit, from the flue gas to the steam. A detailed description of the setup can be found in Lindberg et al.²² and Niemi et al.²³

Binary mixtures of NaBr–Na₂SO₄ and KBr–K₂SO₄ were studied in this paper. The compositions were chosen so that the melt formed at the first melting temperature is ~60 wt % of the total mass and that the remaining solid phase is either Na₂SO₄ or K₂SO₄. The compositions of the deposit materials are shown in Table 1, together

Table 1. Deposit Compositions and Their Calculated and Measured (in Parentheses) Characteristic Melting Temperatures, as Well as Premelt Temperatures

deposit composition [wt %]				temperature [°C]		
NaBr	Na ₂ SO ₄	KBr	K ₂ SO ₄	solidus	liquidus	premelt
31.5	68.5			622 (617)	719 (n.a. ^a)	850
		40.6	59.4	670 (668)	845 (n.a.)	950

^an.a.: not available.

with their calculated and measured characteristic melting temperatures. Factsage thermodynamics software³⁰ was used to calculate the melting behavior and vapor pressure of the volatile species. The FTSalt database is one of the largest thermodynamic databases for higher-order nonideal salt systems, and contains the nonideal interaction parameters for binary (e.g., NaCl–KCl), common-ion ternary (e.g., NaCl–KCl–ZnCl₂), and reciprocal ternary salt systems (e.g., NaCl–KCl–Na₂SO₄–K₂SO₄). However, the thermodynamic interaction parameters for the NaBr–Na₂SO₄ and KBr–K₂SO₄ systems have not been published previously and are not included in the FTSalt database. However, the phase equilibria of NaBr–Na₂SO₄ and KBr–K₂SO₄ have been studied experimentally by Rea,³¹ Palkin et al.,³² Gromakov,³³ Flood et al.,³⁴ and Nyankovskaya.³⁵ The two binary systems are simple eutectic systems, similar to the corresponding NaCl–Na₂SO₄ and KCl–K₂SO₄ systems. On the basis of the experimental studies, the nonideal binary interaction parameters for the liquid phase were optimized using the same liquid phase solution model, the modified quasichemical model in the quadruplet approximation,³⁶ as Lindberg et al.³⁷ used for the multicomponent NaCl–Na₂SO₄–Na₂CO₃–KCl–K₂SO₄–K₂CO₃ system. The details of the assessed thermodynamic parameters will be published in a separate publication. The calculated binary phase diagrams together with experimental data are shown in Figure 1.

In addition, the melting behavior of the mixtures was studied with DSC/TGA (differential scanning calorimetry/thermogravimetric analysis), conducted with a TA Instruments SDT Q600 device. The mixtures were heated above the solidus temperature and cooled down in multiple cycles. Heating and cooling rates of 20 °C min⁻¹ and a gas flow of 100 mL min⁻¹ of N₂ were applied. The solidus temperatures for the mixtures were extracted from the data. The liquidus temperatures were not extracted as the vaporization of alkali bromides was kept at a minimum.

For the deposit preparation, the salt components were mixed, melted together for 20 min, quenched to room temperature, ground, and sieved to the desired size fraction (53–250 μm). The mixture preparation was conducted to obtain homogeneous salt mixtures.

The deposits were applied on the probe. The applied deposit thickness was approximately 5 mm, postexposure. The probe was inserted into a furnace where it was heated up. Once the probe reached the designated steel temperature (500 °C), cooling was initiated, and the experiment was considered to start. The furnace temperature was raised to the target temperature, which was set to 980 °C and measured ~800 °C above the deposit. The deposits were aged in the furnace for 2, 4 or 8 h, and subsequently rapidly cooled to room temperature. The solidified deposits, together with the steel sample rings, were cast in epoxy resin, cut for a cross-section, and

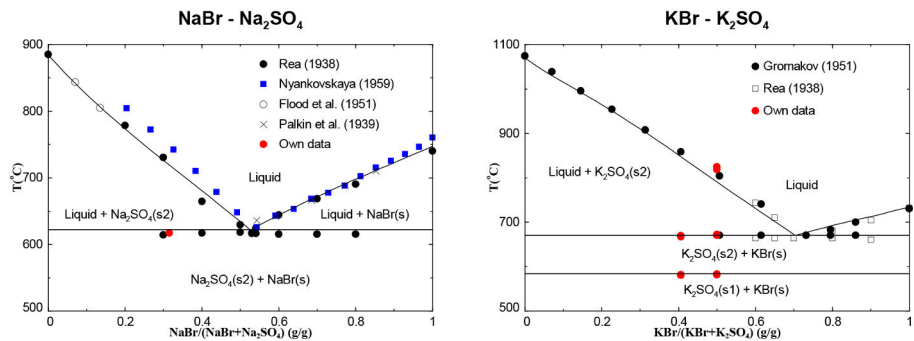


Figure 1. Calculated phase diagrams of NaBr–Na₂SO₄ and KBr–K₂SO₄ on mass basis together with the experimental data of the systems.

Table 2. Standard Chemical Compositions of EN10216-2, 10CrMo9-10, and P235GH Steels in wt %: The Rest Is Fe

steel	C	Si	Mn	P	S	Cr	Mo	N	Cu	Cr + Cu + Mo + Ni
10CrMo9-10	0.08–0.14	≤0.5	0.4–0.8	≤0.02	≤0.01	2.0–2.5	0.9–1.1	≤0.012	≤0.3	
P235GH	≤0.16	≤0.35	≤1.20	≤0.025	≤0.010					≤0.70

analyzed using SEM/EDX. All of the experiments were conducted in ambient air.

The probe houses two steel sample rings, which were both covered with the same deposit material in a given experiment, but two different steel materials were used. A low-alloyed 10CrMo9-10 steel was used as the temperature control ring (Ring 1), and a P235GH carbon steel ring was used as the temperature measurement ring (Ring 2). The standard steel compositions are shown in Table 2. The temperature control and measurement were conducted using thermocouples housed within the rings. Because of the nonuniform temperature across the probe, the measured temperature was always slightly higher than the controlled temperature. The experimental matrix is shown in Table 3.

Table 3. Experimental Matrix Showing the Steel Ring Temperatures during Experiments, with Distinct Deposit Materials and Exposure Times

temperature [°C]		deposit material	exposure time [h]
Ring 1, 10CrMo9-10	Ring 2, P235GH		
500	507	NaBr–Na ₂ SO ₄	2
500	505	NaBr–Na ₂ SO ₄	4
500	506	NaBr–Na ₂ SO ₄	8
500	523	KBr–K ₂ SO ₄	2
500	504	KBr–K ₂ SO ₄	4
500	506	KBr–K ₂ SO ₄	8

3. RESULTS

3.1. Above the First Melting Temperature. The SEM/EDX results for all of the experiments show a multilayered deposit morphology (Figure 2). The uppermost layer is dense and enriched in alkali sulfates. The next layer consists mainly of a mixture of alkali bromides and alkali sulfates in a ratio that is close to the eutectic composition of a NaBr–Na₂SO₄ or KBr–K₂SO₄ mixture, i.e., enriched in alkali bromides in comparison to the original composition. The eutectic composition surrounds alkali sulfate crystals (see Figure 3). Close to the steel, there is a porous region, in which the particles display similar structure to the original deposit particles; i.e., the

particles do not show signs of melting during the experiment. The deposit morphology is similar to the deposit morphologies observed by Lindberg et al.²² and Niemi et al.²³ with mixtures of alkali chlorides and alkali sulfates.

The structure of the deposits was observed to evolve as a function of time. The 2 h experiments showed, in general, more alkali bromides in the uppermost region. The amount of alkali bromides in the uppermost region decreased in 4 and 8 h experiments (Figure 3). In general, already the 2 h experiments displayed a dense upper layer, indicating that the densification occurs within a short time span.

The overall deposit structure was concluded to be similar to that observed in the alkali chloride–alkali sulfate systems, suggesting that the mechanisms responsible for the deposit structure are similar. Above the first melting temperature, the deposit aging mechanism with binary eutectic systems has been concluded to be mainly due to liquid phase sintering and temperature gradient zone melting (TGZM) phenomena.^{23,24} The liquid phase sintering is supported by the fast sintering and by the holes observed in the dense deposit structure. The holes are characteristic for structures affected by liquid phase sintering occurring by the pore filling mechanism.³⁸

TGZM³⁹ was observed to occur in all of the experiments. A distinctive feature for the mechanism is the sharp interphase between the primary crystallizing phase (alkali sulfate) and the eutectic region, mixed with alkali bromides and sulfates (see Figures 2 and 3). The pockets containing a mixture of alkali bromides and sulfates within the dense alkali sulfate structure further indicate TGZM. The phenomenon is described schematically in Figure 4. The liquid phase composition of a binary mixture, with a eutectic melting behavior, e.g., NaBr–Na₂SO₄ or KBr–K₂SO₄, depends on the temperature. In the case of NaBr–Na₂SO₄ and KBr–K₂SO₄, when the temperature of the system is between the solidus temperature and the liquidus temperature, the system will form a two-phase system. The two phases are the primary crystallizing phase, which in this case is the alkali sulfate phase, and a melt phase, which has a composition following the liquidus line of the phase diagram according to the lever rule (see Figure 4, step 2). All of the

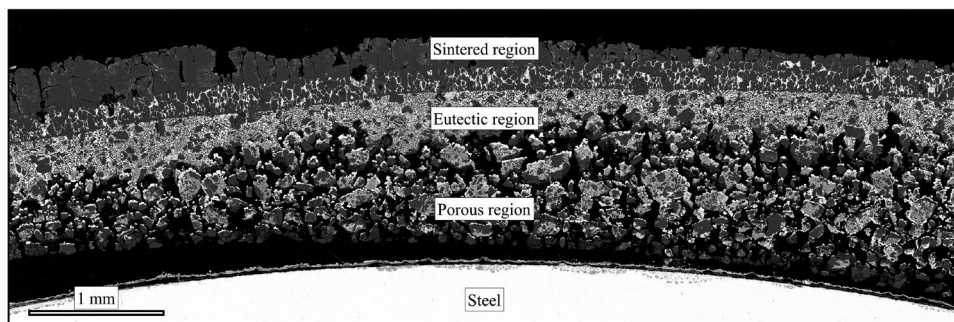


Figure 2. SEM backscatter image of the overall deposit structure of the NaBr–Na₂SO₄ deposit after 4 h of exposure. The image shows the porous, eutectic, and sintered regions. The light, dark gray, and black shades represent NaBr, Na₂SO₄, and epoxy, respectively.

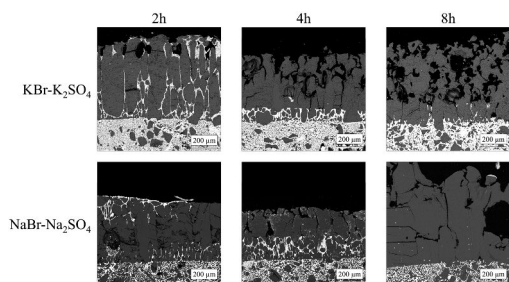


Figure 3. Evolution of the uppermost layer in the K system and in the Na system. The light, dark gray, and black shades represent (Na/K)Br, (Na/K)₂SO₄, and epoxy, respectively.

alkali bromide in that temperature region will be included in the melt phase.

When subjected to a temperature gradient, the melt composition differs between temperatures, creating a concen-

tration gradient across the melt. The concentration gradient induces diffusion within the melt to balance the concentration difference. As a result, the alkali bromide migrates toward the hotter temperature; subsequently, at the lower temperature, the alkali sulfate crystallizes from the melt. The increased concentration of the alkali bromide at the higher temperature enables that more of the alkali sulfate is being incorporated into the melt phase, resulting in a bulk movement of the melt, and alkali bromide, toward the hotter temperature. At the top of the deposit, the alkali bromides vaporize into the furnace and leave behind a refined alkali sulfate structure.

In addition to the movement of alkali bromides, TGZM was observed to affect also the corrosion products. In the 8 h experiments, the upper part of the deposit cross-section and the top of the deposit were observed to have a red hue. The SEM/EDX results showed a presence of Fe within the upper part of the deposit and on the outer edge (facing the furnace air). The results from the outer edge of the 8 h experiment with 10CrMo9-10 exposed to the Na mixture are shown in Figure 5. In addition, some Fe was observed in the lower part

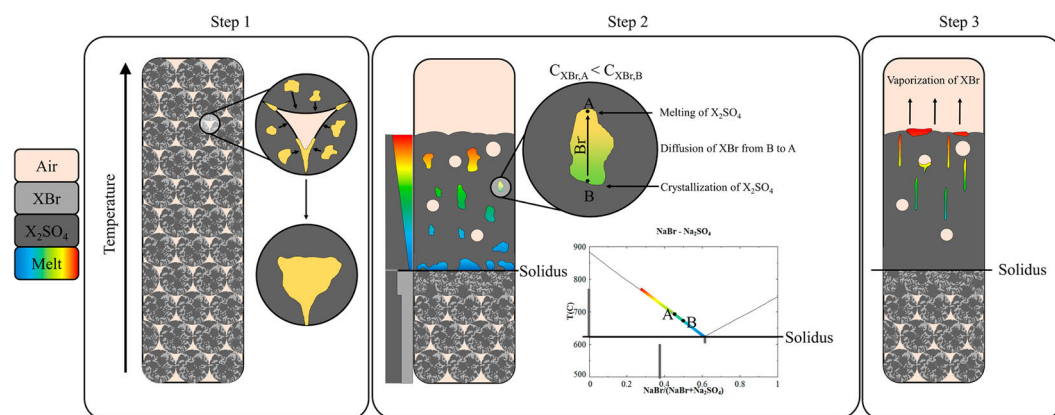


Figure 4. Schematic image explaining the deposit morphology and chemistry evolution due to liquid phase sintering and temperature gradient zone melting (TGZM) phenomena. Step 1 shows the initial deposit densification by liquid phase sintering. Step 2 shows how the TGZM induces alkali bromide migration toward the outer surface of the deposit. Step 3 shows a refined alkali sulfate structure and the sharp interface between the eutectic layer and the refined alkali sulfate.

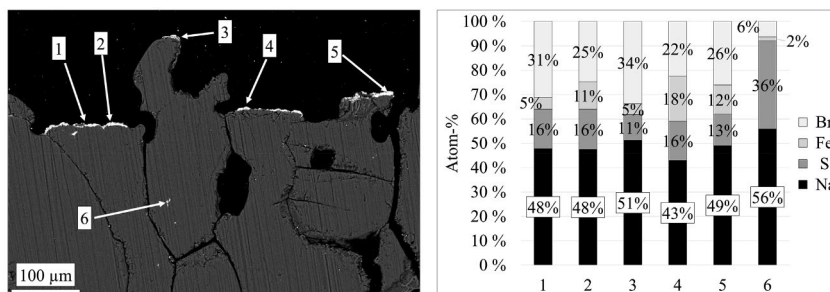


Figure 5. SEM backscatter image showing the corrosion products in the upper part of the deposit in an 8 h experiment with 10CrMo9-10 steel exposed to the NaBr–Na₂SO₄ mixture. The oxygen and carbon results are excluded from the data, because these elements are present in the epoxy.

of the eutectic layer in the 4 h experiments with P235GH steel exposed to the NaBr–Na₂SO₄ deposit. A similar behavior has been observed with alkali chloride and alkali sulfate mixtures.^{21,40} However, the behavior has not been observed with alkali bromide–alkali sulfate mixtures before.

The migration of corrosion products due to TGZM is more complicated compared to the relatively simple binary mixtures (NaBr–Na₂SO₄ and KBr–K₂SO₄). With binary mixtures, the roles of the liquid phase and the primary crystallizing phase are clear, and the concentration gradient within the liquid phase is easy to concern from the phase diagram. With the inclusion of corrosion products (e.g., FeBr₂, FeBr₃, CrBr₃, and metal oxides), the melting properties and, consequently, the prediction of the TGMZ phenomenon become more complicated. In addition, the corrosion products are prone to oxidation with high enough O₂ partial pressures, which alters the composition and makes the system even more complicated.

Although detailed predictions of migration of corrosion products due to TGZM remain an unresolved issue and lie outside of the scope of this study, the mechanism is a plausible cause for the Fe presence at the top of the deposits exposed to temperature gradients.

3.2. Below the First Melting Temperature. Below the first melting temperature, pure alkali bromide layers were observed on the furnace-facing side of particles and on the oxide layer. In addition, on the steel-facing side of the particles, alkali-bromide-depleted areas were observed. An example of a pure alkali bromide layer and an alkali-bromide-depleted area is shown in Figure 6.

The phenomenon has been studied earlier with alkali chlorides, and it is caused by Fickian diffusion that occurs because of a temperature-gradient-induced concentration gradient in the gas phase.^{22,23} Alkali bromides vaporize from the steel-facing side of the particle, leaving behind an alkali sulfate scaffold. The vaporized alkali bromides migrate toward the colder temperature, i.e., toward the steel surface. Subsequently, the alkali bromides condense on a colder surface because of supersaturation in the gas phase. The colder surface can be either the furnace-facing side of an ash particle below the particle of origin, or the steel surface. The vaporization–condensation mechanism results in a bulk migration of alkali bromides toward the colder temperature, i.e., toward the steel surface.

The alkali bromide migration layer thicknesses were quantified as described by Lindberg et al.,²² and the results,

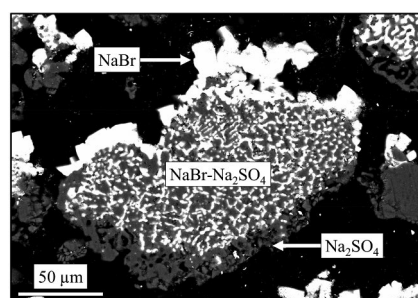


Figure 6. SEM backscatter image showing NaBr enrichment on the top of a NaBr–Na₂SO₄ particle and NaBr depletion at the bottom of the particle.

as a function of temperature, are shown in Figure 7. An existing migration model for alkali chlorides²³ was modified to predict the alkali bromide migration. The species-specific values were modified (see Table 4), and the differences in the densities of the alkali bromides and sulfates were taken into account. The values shown in Table 4 are utilized for partial pressure calculations and for diffusion coefficient estimation, according to the kinetic theory of gases.

The model describes the Fickian diffusion of volatile species due to the temperature-gradient-induced concentration gradient. The concentration gradient, and therefore the diffusion flux, is directly proportional to the temperature gradient across the gas phase. The temperature gradient across the gas phase was estimated from the bulk temperature gradient across the porous layer, and from the estimated porosity of the deposit. The temperature gradients across the porous layers in individual experiments were estimated from the SEM images. The temperature gradient (dT/dx) values were estimated to be 65–90 °C mm^{−1} for the KBr–K₂SO₄ mixtures and 70–115 °C mm^{−1} for the NaBr–Na₂SO₄ mixtures, and they are shown in Figure 7. In the model calculations, the bulk temperature gradient was multiplied by a correction factor of 3.7 to account for the steeper temperature gradient across the gas phase than across the solid phase (for additional information, see Niemi et al.²³). In addition, the logarithm of the alkali bromide saturation pressure is linearly proportional to the inverse absolute temperature, ergo the logarithm of the concentration gradient is linearly proportional to the inverse absolute

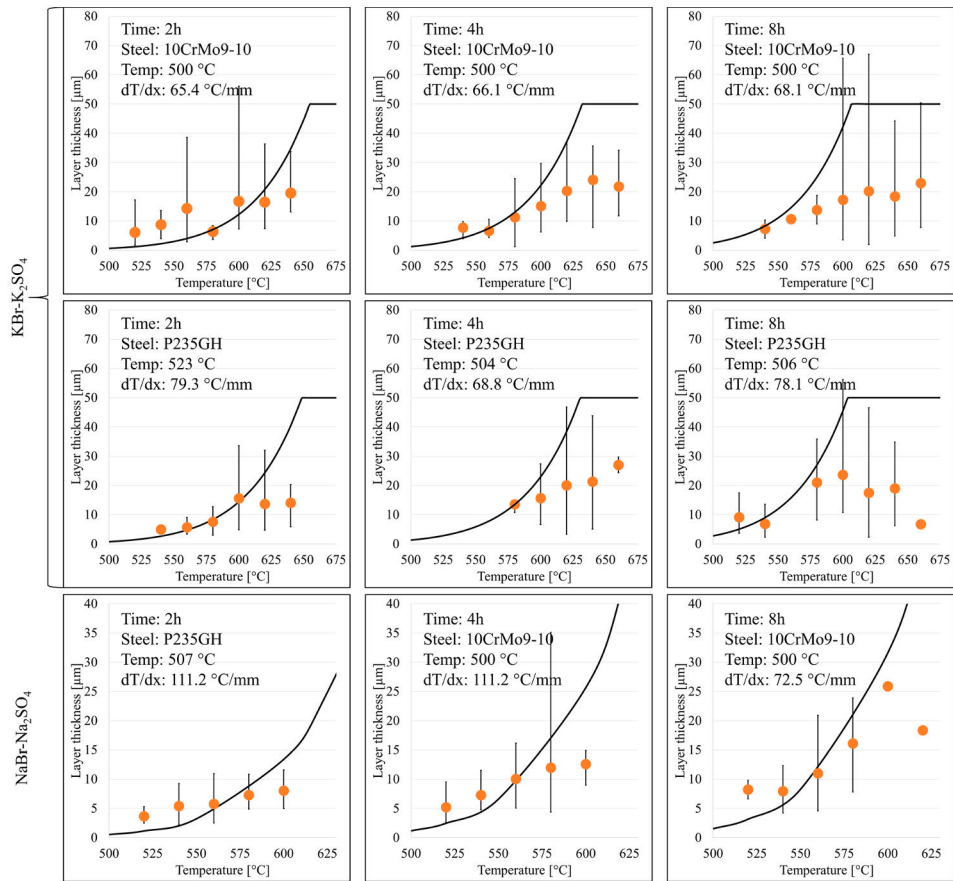


Figure 7. Average measured alkali bromide layer thicknesses (dots) together with modeled results (continuous line) as a function of temperature in individual experiments. The error bars show the maximum and minimum thickness values measured in the temperature interval (20 °C) in question.

Table 4. Molecule-Dependent Constants for Determining the Saturation Pressures (A_i and B_i) of Alkali Bromides, Effective Molecular Diameters in the N_2 Atmosphere ($d_{i,eff}$), Effective Mass in the N_2 Atmosphere (μ_i), and Density at Room Temperature (ρ_i)^{30,41,42}

component, i	A_i [K]	B_i [–]	$d_{i,eff}$ [m]	μ_i [kg]	ρ_i [kg m ^{–3}]
KBr	–24 298	16.07	3.68×10^{-10}	3.77×10^{-26}	2750
(KBr) ₂	–27 388	18.08	4.74×10^{-10}	4.16×10^{-26}	2750
NaBr	–24 850	16.19	3.41×10^{-10}	3.66×10^{-26}	3210
(NaBr) ₂	–26 308	17.25	4.54×10^{-10}	4.10×10^{-26}	3210

temperature, which results in an exponential increase in the diffusion flux as a function of the absolute temperature.

The model estimates a decrease in the diffusion flux as a function of time. The effective diffusion coefficient decreases, as the gaseous species need to travel longer within the particle of origin as it is depleted of the alkali bromides as a function of time. A similar decrease in the migration rate was observed also in the experimental results. The initial particle-to-particle distance in the model was chosen to be 50 μm , corresponding to the experimental observations and to the solids fraction of

close-packing structures (0.74) in one dimension when a particle size of 150 μm is applied. The initial particle-to-particle distance was also used as a boundary condition for the model; i.e., the maximum alkali bromide layer thickness was limited to 50 μm . The modeled values are plotted together with the corresponding experimental results in Figure 7.

The model values agree reasonably well with the experimental values in lower temperatures and with short exposure times. The deviations in the higher temperatures and with longer exposure times are understandable as the predicted

layer thicknesses are unreasonably thick for the experimental setup, which results in pronounced deviations with longer experiments and in higher temperatures. In the experiment with $\text{KBr}-\text{K}_2\text{SO}_4$ on the P235GH steel with 4 h of exposure, where no layer data is reported for low temperatures, the lower temperature part of the porous layer was missing. The loss of deposit material is due to the deposit preparation in the cutting stage. The loss of deposit material after the cutting phase of the sample preparation was observed as a lack of deposit material and epoxy resin. The 2 h exposure of 10CrMo9-10, and the 4 and 8 h exposures of P235GH to $\text{NaBr}-\text{Na}_2\text{SO}_4$, showed a missing porous layer, which is why no layer growth data is available for those experiments.

Regardless of the deviation of the modeled values from the experimental values in the higher temperatures, the results imply that the underlying phenomenon, i.e., the temperature-gradient-induced gas phase migration, is successfully recognized for the alkali bromides. The model results are in reasonably good agreement with the experimental values, which indicates that the model can be utilized for deposit aging calculations if some limitations are considered. The limitations include space limitations for the layer growth, lower activity for the gaseous species due to solid or liquid solutions, and mass balance limitations. The results of this paper confirm the hypothesis that the temperature-gradient-induced diffusion mechanism observed with alkali chlorides also applies for other volatile compounds found in ash deposits.

Compared to alkali chlorides, the alkali bromide migration was observed to occur at a higher rate in the same temperature range and with the same temperature gradient. The calculated saturation pressure of alkali halides at a set temperature increases when the size of either the cation or the anion increases ($\text{KCl} > \text{NaCl} > \text{LiCl}$, $\text{NaBr} > \text{NaCl} > \text{NaF}$). The saturation pressure of alkali halides increases exponentially as a function of temperature. In a set temperature and temperature gradient, the partial pressure gradient is steeper for the species with the higher saturation pressure ($\text{KCl} > \text{NaCl} > \text{LiCl}$, $\text{NaBr} > \text{NaCl} > \text{NaF}$), resulting in a higher diffusion flux.

3.3. Corrosion. Significant corrosion was observed in all of the experiments. With P235GH, the corrosion layer consisted typically of alkali bromides, iron oxide, iron bromides, and a combination of all of the aforementioned. 10CrMo9-10 produced a similar oxide layer but included also Cr species. Already the 2 h experiments resulted in oxide layer thicknesses of $\sim 10 \mu\text{m}$, but the oxide layer growth rate seemed to slow down rapidly after the initial oxide layer formation.

Figure 8 shows a typical corrosion layer of P235GH from the 4 h experiment, with the $\text{KBr}-\text{K}_2\text{SO}_4$ mixture. Just above the steel surface, Br was observed, but little to no alkali metals were observed, indicating a formation of metal bromides. A similar distribution of elements was observed also with the other experiments. With P235GH, Br was observed together with Fe, while with 10CrMo9-10, Br was observed together with Fe and Cr. FeBr_2 , FeBr_3 , NiBr_2 , and CrBr_3 have been observed to form at steel surfaces exposed to Br_2 and high temperatures.⁴³

Above the metal bromides, a dense oxide layer was observed. For P235GH, the oxide layer contained mainly iron oxides. With 10CrMo9-10, the oxide layer consisted of a mixture of iron and chromium oxides. The dense oxide layer did not contain Br with either of the tested steels and regardless of the exposure time.

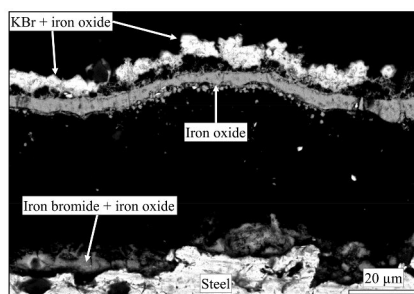


Figure 8. Corrosion layer of P235GH steel after 4 h of exposure to $\text{KBr}-\text{K}_2\text{SO}_4$.

On top of the dense oxide layer, pure crystals of alkali bromides were detected for all of the experiments. The crystals are a result of the vaporization–condensation of alkali bromides within the deposit. The mechanism can be clearly seen to enrich alkali bromides at the oxide layer.

In the experiment with P235GH exposed to $\text{NaBr}-\text{Na}_2\text{SO}_4$ for 4 h, in addition to the dense oxide layer, a more porous oxide layer was observed to grow on top of and around the salt particles near the steel surface. In addition, indications of iron bromides were observed above the dense oxide layer, close to salt particles (Figure 9). In the same experiment and in the 8 h experiment with 10CrMo9-10 steel exposed to the $\text{NaBr}-\text{Na}_2\text{SO}_4$ mixture, corrosion products were found in the upper parts of deposits, which indicates vaporization of corrosion products and condensation within the deposit. This occurs due to an oxygen potential gradient from the metal surface, where it is buffered by the metal–metal oxide equilibrium, to the air in the furnace. With low oxygen potential, volatile metal halide species (e.g., FeCl_2 , FeCl_3 , FeBr_2 , FeBr_3) can vaporize close to the metal–metal oxide interface and subsequently react to metal oxides when they reach a location within the deposit with higher oxygen potential.

Similar corrosion behavior, where the oxide layer grows around the deposit salt particles, has been observed with 10CrMo9-10 steel exposed to KBr ⁶ and to NaCl or KCl ⁴⁴ at high temperatures in isothermal conditions. Enestam et al.⁴⁴ proposed that the porous oxide layer formation in NaCl and KCl deposits is due to the formation and subsequent vaporization of metal halides, which then react to metal oxides and condense on the salt particles above the steel surface. Wu et al.⁶ reported analogous behavior with KBr . To the best of our knowledge this is the first study showing similar corrosion behavior of steel exposed to NaBr .

4. IMPLICATIONS

Deposit aging has direct effects on the deposit removability and chemistry. The results of Laxminarayan et al.²⁵ show that liquid phase sintering of deposits and liquid movement toward the steel surface increase the adhesion strength of deposits to the heat exchanger surfaces. They also note that gas phase migration of alkali chlorides plays a role in the evolution of the deposit adhesion strength. The results of this study show that even alkali bromides migrate within ash deposits and can potentially enrich on heat exchanger surfaces, affecting both corrosion and deposit adhesion strength. Already low Br

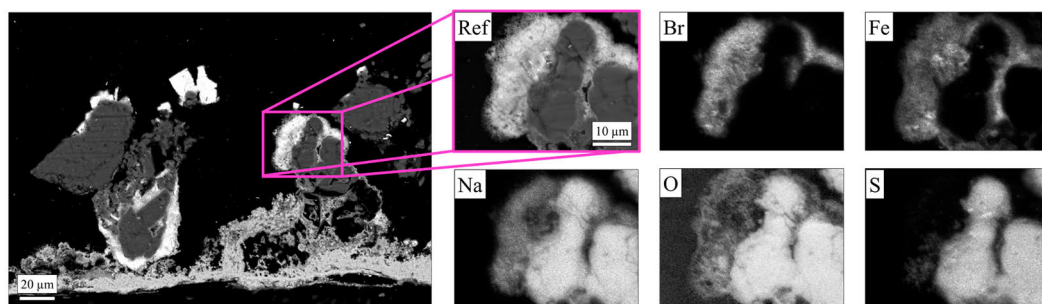


Figure 9. SEM image showing the porous oxide layer of P235GH steel after 4 h of exposure to NaBr–Na₂SO₄.

concentrations in the fuel have been shown to result in enrichment of Br in waterwall deposits.¹⁵

The results of Costa and Paoliello⁴⁵ show that the deposit composition in a black liquor recovery boiler can vary greatly from the inner to the outer part of the deposit. They observed high concentrations of K and Cl close to the steel surface, which could be due to the enrichment of K and Cl in the melt phase, which has migrated to the steel surface. Similar results have been reported by Reeve et al.⁴⁶ Although alkali bromides are not commonly found in recovery boilers, the results of this study further indicate which mechanisms are responsible for the enrichment of alkali chlorides in cold temperatures, i.e., gas phase migration and liquid phase sintering.

In the present work, migration of gaseous alkali bromides toward the colder temperatures was shown to occur due to temperature gradients. The migration rate increases as a function of both the local temperature and the temperature gradient. This implies that, in boiler design, in addition to the absolute temperature of the heat exchanger material, the temperature gradient from the flue gas to the steel also affects the corrosion risk. Others have reported results, which support this view.^{17,18}

The temperature-gradient-induced gas phase migration model has been shown to qualitatively work with alkali chlorides and alkali bromides. The model relies on Fick's first law of diffusion and on the kinetic theory of gases, which makes it also easily applicable for other volatile species within deposits and for other applications where temperature gradients are present. For technically relevant detailed results, the migration model would probably need to be used in combination with thermodynamic modeling, as the partial pressures of volatile species are connected to the solid and liquid phases locally present in the deposit. In turn, the gas phase migration affects the local compositions within the deposit, resulting in a highly dynamic system, where the phase composition would need to be re-evaluated continuously.

The synthetic deposits used in this study differ from actual boiler deposits in a number of ways. The compositions of the deposits used in this study are simple binary eutectics, with relatively high alkali bromide concentration compared to boiler environments. The boiler deposit contains many different components, depending on the fuel. For biomass fuels, the main ash-forming elements are Ca, K, Si, and Mg.⁴⁷ With waste-derived fuels, the ash composition is even more complicated, and the deposit can in addition contain, e.g., high amounts of Pb and Zn.⁸

Boiler ash deposits are often heterogeneous in nature, with different compositions and structures across the deposit, mainly due to the way of the deposit formation. The deposit formation in a boiler occurs by several different mechanisms that occur simultaneously, condensation, thermophoresis, eddy impaction, and inertial impaction being the most common deposit formation mechanisms.⁴⁸ The deposit formation mechanisms, as well as the ash composition, affect the deposit structure. Deposits vary greatly in nature between boilers and locations within the boiler. Contrary to boiler deposits, the deposits used in this study are homogeneous both in composition and in structure at the beginning of the experiments. However, the synthetic deposits were observed to become increasingly heterogeneous because of the exposure to temperature gradients. This indicates that even deposit aging can contribute to the deposit structure and composition. There are indications that deposit aging also affects the local composition and structure of ash deposits.^{28,29}

The vaporization–condensation mechanism of volatile species can only occur if there are volatile species present within the deposit, and the deposit structure is porous; i.e., there are void spaces available for the volatile species to condense to. Several studies have shown that boiler deposits are indeed porous;^{28,49,50} however, parameters, such as the fuel, the location in the boiler, and the temperature profile, affect the porosity and the pore size. The pore size will most likely limit the migration rate of the volatile species within the deposits. The vaporization–condensation mechanism is expected to occur at a slower pace in boiler deposits than in the synthetic deposits in question. There are additional limiting factors that are present in boiler deposits; e.g., the volatile species might be part of a solid or liquid solution, which results in their lower partial pressure. In addition, the amount of the volatile species is likely to be fairly low within the deposits, which also limits the potential for enrichment in lower temperatures. However, alkali bromides have been observed to enrich at lower temperatures within deposits, i.e., close to the steel surface.¹⁵ The enrichment is likely to be caused by both the deposit build-up mechanisms (i.e., alkali bromide condensation from the flue gas) and the deposit aging mechanisms (i.e., intradeposit vaporization–condensation and liquid phase sintering).

The liquid phase sintering and TGZM both require a melt phase present to occur. In addition, liquid phase sintering can only occur in a porous deposit, while TGZM requires a continuous solid phase in order to occur. Liquid phase sintering is likely to occur in boiler deposits, but the extent of it

is still unclear. The sintering tendency has been shown to be connected to the amount of melt present.²³ The amount of melt in a boiler deposit is likely to be significantly lower than in the synthetic ash deposits studied in this paper, which will result in lesser deposit densification. In addition, boiler deposits may contain molten phases with high viscosity, with which the sintering effects are expected to be slower. However, in boilers the deposits have a longer time to mature.

The industrial relevance of TGZM in boiler deposits remains unclear. TGZM could potentially alter the corrosion rate of heat exchanger tubes. On one hand, with optimal conditions, TGZM can induce migration of corrosive halide species toward the fuel gas, i.e., away from the steel surface. On the other hand, TGZM can induce migration of corrosion products or parts of the protective oxide layer toward the hotter temperature, resulting in an exposed steel surface and rapid corrosion.

5. CONCLUSIONS

Steel samples were covered with mixtures of alkali bromides and alkali sulfates and exposed to industrially relevant temperature gradients to study the corrosion of steel and aging mechanisms occurring in ash deposits. The results show similar behavior to alkali chloride and alkali sulfate mixtures. Both display liquid phase sintering and temperature gradient zone melting in supersolidus temperatures. In subsolidus temperatures, gas phase migration toward the colder temperatures was observed to occur for alkali bromides. An existing one-dimensional alkali chloride migration model was modified to predict the alkali bromide migration. The predicted amount of alkali bromides (layer thickness) is correctly predicted for short exposure times in low temperatures (<600 °C). The predictions deviate for longer exposure times and in locations of the deposit where the migration rate is the fastest. The most likely reason for the deviation is that the alkali bromide migration is limited in the experimental deposit by the limited void space available for layer growth. The corrosion results show the formation of metal bromides at the steel surface.

■ AUTHOR INFORMATION

Corresponding Author

*E-mail: joniemi@abo.fi.

ORCID

Jonne Niemi: 0000-0002-7840-7658

Notes

The authors declare no competing financial interest.

■ ACKNOWLEDGMENTS

This work was conducted within the Academy of Finland project "Understanding the dynamics of intradeposit chemistry and morphology for control of corrosion in high temperature processes" (Decision 310266) as part of the activities of the Johan Gadolin Process Chemistry Centre at Åbo Akademi University. Additional funding from the Graduate School in Chemical Engineering (GSCE) and from the Academy of Finland (Decisions 266384 and 296435) for three of the authors (J.N., D.L., and J.L., respectively) is greatly appreciated. The authors would like to thank Linus Silvander for operating the SEM apparatus, Peter Backman for operating the DSC/TGA apparatus, and Jaana Paananen for her help with the experimental setup and sample preparation.

■ REFERENCES

- (1) Cucchiella, F.; D'Adamo, I.; Gastaldi, M. Sustainable waste management: Waste to energy plant as an alternative to landfill. *Energy Convers. Manage.* **2017**, *131*, 18–31.
- (2) Hupa, M.; Karlström, O.; Vainio, E. Biomass combustion technology development – It is all about chemical details. *Proc. Combust. Inst.* **2017**, *36* (1), 113–134.
- (3) Bankiewicz, D.; Enestam, S.; Yrjas, P.; Hupa, M. Experimental studies of Zn and Pb induced high temperature corrosion of two commercial boiler steels. *Fuel Process. Technol.* **2013**, *105*, 89–97.
- (4) Kinnunen, H.; Hedman, M.; Engblom, M.; Lindberg, D.; Uusitalo, M.; Enestam, S.; Yrjas, P. The influence of flue gas temperature on lead chloride induced high temperature corrosion. *Fuel* **2017**, *196*, 241–251.
- (5) Sánchez Pastén, M.; Spiegel, M. High temperature corrosion of metallic materials in simulated waste incineration environments at 300–600 °C. *Mater. Corros.* **2006**, *57* (2), 192–195.
- (6) Wu, H.; Yrjas, P.; Hupa, M. Laboratory Studies of Potassium-Halide-Induced High-Temperature Corrosion of Superheater Steels. Part 1: Exposures in Dry Air. *Energy Fuels* **2015**, *29* (2), 1186–1195.
- (7) Wu, H.; Bankiewicz, D.; Yrjas, P.; Hupa, M. Laboratory Studies of Potassium-Halide-Induced High-Temperature Corrosion of Superheater Steels. Part 2: Exposures in Wet Air. *Energy Fuels* **2015**, *29* (4), 2709–2718.
- (8) Sorell, G. The Role of Chlorine in High Temperature Corrosion in Waste to Energy Plants. *Mater. High Temp.* **1997**, *14* (3), 207–220.
- (9) Niemi, J.; Kinnunen, H.; Lindberg, D.; Enestam, S. Interactions of PbCl₂ with Alkali Salts in Ash Deposits and Effects on Boiler Corrosion. *Energy Fuels* **2018**, *32* (8), 8519–8529.
- (10) Kinnunen, H.; Lindberg, D.; Laurén, T.; Uusitalo, M.; Bankiewicz, D.; Enestam, S.; Yrjas, P. High-temperature corrosion due to lead chloride mixtures simulating fireside deposits in boilers firing recycled wood. *Fuel Process. Technol.* **2017**, *167*, 306–313.
- (11) Enestam, S.; Backman, R.; Mäkelä, K.; Hupa, M. Evaluation of the condensation behavior of lead and zinc in BFB combustion of recovered waste wood. *Fuel Process. Technol.* **2013**, *105*, 161–169.
- (12) Vainikka, P.; Hupa, M. Review on bromine in solid fuels - Part 2: Anthropogenic occurrence. *Fuel* **2012**, *94* (1), 34–51.
- (13) Vainikka, P.; Hupa, M. Review on bromine in solid fuels. Part 1: Natural occurrence. *Fuel* **2012**, *95* (1), 1–14.
- (14) Vainikka, P.; Enestam, S.; Silvennoinen, J.; Taipale, R.; Yrjas, P.; Frantsi, A.; Hannula, J.; Hupa, M. Bromine as an ash forming element in a fluidised bed boiler combusting solid recovered fuel. *Fuel* **2011**, *90* (3), 1101–1112.
- (15) Vainikka, P.; Bankiewicz, D.; Frantsi, A.; Silvennoinen, J.; Hannula, J.; Yrjas, P.; Hupa, M. High temperature corrosion of boiler waterwalls induced by chlorides and bromides. Part 1: Occurrence of the corrosive ash forming elements in a fluidised bed boiler co-firing solid recovered fuel. *Fuel* **2011**, *90* (5), 2055–2063.
- (16) Baxter, L. L. Ash Deposition during Biomass and Coal Combustion: A Mechanistic Approach. *Biomass Bioenergy* **1993**, *4* (2), 85–102.
- (17) Brossard, J. M.; Diop, I.; Chaucherie, X.; Nicol, F.; Rapin, C.; Vilasi, M. Superheater fireside corrosion mechanisms in MSWI plants: Lab-scale study and on-site results. *Mater. Corros.* **2011**, *62*, 543–548.
- (18) Brossard, J. M.; Lebel, F.; Rapin, C.; Mareche, J.-F.; Chaucherie, X.; Nicol, F.; Vilasi, M. Lab-scale study on fireside superheaters corrosion in MSWI plants. In *NAWTEC17, Proceedings of the 17th annual North American waste to energy conference*, Chantilly, Virginia, United States, 2009; pp 63–69.
- (19) Covino, B. S., Jr.; Holcomb, G. R.; Cramer, S. D.; Bullard, S. J.; Ziomek-Moroz, M.; White, M. L. Corrosion in a temperature gradient. In *17th Annual Conference on Fossil Energy Materials* 2003.
- (20) Kawahara, Y. Evaluation of high-temperature corrosion life using temperature gradient corrosion test with thermal cycle component in waste combustion environments. *Mater. Corros.* **2006**, *57*, 60–72.

- (21) Lagerbom, J.; Lepistö, T.; Backman, R.; Hupa, M. Behavior of alkaline sulfate-chloride salts in temperature gradient corrosion test furnace. In *VTT Symp.*, 2001; pp 541–551.
- (22) Lindberg, D.; Niemi, J.; Engblom, M.; Yrjas, P.; Lauren, T.; Hupa, M. Effect of temperature gradient on composition and morphology of synthetic chlorine-containing biomass boiler deposits. *Fuel Process. Technol.* **2016**, *141*, 285–298.
- (23) Niemi, J.; Lindberg, D.; Engblom, M.; Hupa, M. Simultaneous melt and vapor induced ash deposit aging mechanisms – Mathematical model and experimental observations. *Chem. Eng. Sci.* **2017**, *173*, 196–207.
- (24) Niemi, J.; Lindberg, D.; Engblom, M.; Tran, H. A Fundamental Study on the Change in Composition of Fireside Deposits with Time in Kraft Recovery Boilers. *J. Sci. Technol. For. Prod. Processes* **2018**, *7* (2), 45–52.
- (25) Laxminarayan, Y.; Nair, A. B.; Jensen, P. A.; Wu, H.; Frandsen, F. J.; Sander, B.; Glarborg, P. Tensile Adhesion Strength of Biomass Ash Deposits: Effect of the Temperature Gradient and Ash Chemistry. *Energy Fuels* **2018**, *32* (4), 4432–4441.
- (26) Michelsen, H. P.; Frandsen, F.; Dam-Johansen, K.; Larsen, O. H. Deposition and high temperature corrosion in a 10 MW straw fired boiler. *Fuel Process. Technol.* **1998**, *54* (1–3), 95–108.
- (27) Hansen, L. A.; Nielsen, H. P.; Frandsen, F. J.; Dam-Johansen, K.; Hörlyck, S.; Karlsson, A. Influence of deposit formation on corrosion at a straw-fired boiler. *Fuel Process. Technol.* **2000**, *64* (1–3), 189–209.
- (28) Jensen, P. A.; Frandsen, F. J.; Hansen, J.; Dam-Johansen, K.; Henriksen, N.; Hörlyck, S. SEM investigation of superheater deposits from biomass-fired boilers. *Energy Fuels* **2004**, *18* (2), 378–384.
- (29) Wu, D.; Dahl, K. V.; Madsen, J. L.; Christiansen, T. L.; Montgomery, M.; Hald, J. Effects of Different Fuel Specifications and Operation Conditions on the Performance of Coated and Uncoated Superheater Tubes in Two Different Biomass-Fired Boilers. *ACS Appl. Energy Mater.* **2018**, *1* (4), 1463–1475.
- (30) Bale, C. W.; Belisle, E.; Chartrand, P.; Decterov, S. A.; Eriksson, G.; Gheribi, A. E.; Hack, K.; Jung, I. H.; Kang, Y. B.; Melancon, J.; Pelton, A. D.; Petersen, S.; Robelin, C.; Sangster, J.; Spencer, P.; Van Ende, M. A. FactSage thermochemical software and databases, 2010–2016. CALPHAD: CALPHAD: Comput. Coupling Phase Diagrams Thermochem. **2016**, *54*, 35–53.
- (31) Rea, R. F. Temperature-measuring cones. *J. Am. Ceram. Soc.* **1938**, *21*, 98–101.
- (32) Palkin, A. P.; Gromakov, S. D.; Reshetnikov, P. F.; Semenov, N. I.; Turusov, M. G. Ternary fusibility systems. *Acta Univ. Voronegiensis (U. S. S. R.)* **1939**, *10* (4), 5–39.
- (33) Gromakov, S. D. Some rules pertaining to the determination of the type of phase diagrams of binary systems. *Zh. Fiz. Khim.* **1951**, *25*, 1014–1025.
- (34) Flood, H.; Forland, T.; Nesland, A. Cryoscopic measurements in fused salts at elevated temperatures. *Acta Chem. Scand.* **1951**, *5*, 1193–1198.
- (35) Nyankovskaya, R. N. Fusion diagram for the system of the sulfates and bromides of sodium and potassium. *Zh. Neorg. Khim.* **1959**, *4*, 2591–2595.
- (36) Pelton, A. D.; Chartrand, P.; Eriksson, G. The modified quasi-chemical model: Part IV. Two-sublattice quadruplet approximation. *Metall. Mater. Trans. A* **2001**, *32* (6), 1409–1416.
- (37) Lindberg, D.; Backman, R.; Chartrand, P. Thermodynamic evaluation and optimization of the (NaCl+Na₂SO₄+Na₂CO₃+KCl+K₂SO₄+K₂CO₃) system. *J. Chem. Thermodyn.* **2007**, *39* (7), 1001–1021.
- (38) German, R. M.; Suri, P.; Park, S. J. Review: liquid phase sintering. *J. Mater. Sci.* **2009**, *44* (1), 1–39.
- (39) Pfann, W. G. Temperature Gradient Zone Melting. *JOM* **1955**, *7* (9), 961–964.
- (40) Lindberg, D.; Niemi, J.; Engblom, M.; Laurén, T.; Yrjas, P.; Hupa, M. Experimental and modeling approaches to simulate temperature-gradient induced intradeposit chemical processes with implications for biomass boiler corrosion. 23rd International Conference on FBC, Grand Ambassador Seoul, Seoul, South Korea, May 13–17, 2018; C9–1, pp 1124–1134.
- (41) Shannon, R. D. Revised Effective Ionic-Radii and Systematic Studies of Interatomic Distances in Halides and Chalcogenides. *Acta Crystallogr., Sect. A: Cryst. Phys., Diffraction, Theor. Gen. Crystallogr.* **1976**, *32* (SEP1), 751–767.
- (42) Topping, T.; Biermann, S.; Hoeft, J.; Mawhorter, R.; Cave, R. J.; Szemenyei, C. The structure of alkali halide dimers: A critical test of ionic models and new ab initio results. *J. Chem. Phys.* **1996**, *104* (20), 8032–8042.
- (43) Lee, S.; Tsujikawa, S. Corrosion behavior of Fe-Cr and Fe-Ni-base commercial alloys in flowing Ar-42.6%O₂-14.7%Br-2 gas mixture at 700 degrees C. *Mater. Corros.* **1997**, *48* (6), 364–371.
- (44) Enestam, S.; Bankiewicz, D.; Tuiremo, J.; Mäkelä, K.; Hupa, M. Are NaCl and KCl equally corrosive on superheater materials of steam boilers? *Fuel* **2013**, *104*, 294–306.
- (45) Costa, D. S.; Paoliello, F. A. Experience of recovery boiler superheater corrosion at Cenibra. In *International Chemical Recovery Conference*; Halifax, Nova Scotia, 2017.
- (46) Reeve, D. W.; Tran, H. N.; Barham, D. Superheater Fireside Deposits and Corrosion in Kraft Recovery Boilers. *Tappi J.* **1981**, *64* (5), 109–113.
- (47) Vassilev, S. V.; Baxter, D.; Andersen, L. K.; Vassileva, C. G. An overview of the chemical composition of biomass. *Fuel* **2010**, *89* (5), 913–933.
- (48) Kleinhans, U.; Wieland, C.; Frandsen, F. J.; Spliethoff, H. Ash formation and deposition in coal and biomass fired combustion systems: Progress and challenges in the field of ash particle sticking and rebound behavior. *Prog. Energy Combust. Sci.* **2018**, *68*, 65–168.
- (49) Zhou, H.; Zhou, B.; Zhang, H.; Li, L.; Cen, K. Investigation of Slagging Characteristics in a 300 kW Test Furnace: Effect of Deposition Surface Temperature. *Ind. Eng. Chem. Res.* **2014**, *53* (17), 7233–7246.
- (50) Zbogor, A.; Frandsen, F. J.; Jensen, P. A.; Glarborg, P. Heat transfer in ash deposits: A modelling tool-box. *Prog. Energy Combust. Sci.* **2005**, *31* (5–6), 371–421.

